DISCOVERY AND TOTAL SYNTHESIS OF BIO-FUNCTIONAL NATURAL PRODUCTS FROM TRADITIONAL MEDICINAL PLANTS

EDITED BY: Tao Wang, Satoru Tamura and Toshio Morikawa

frontiers Research Topics

About Frontiers

Frontiers is more than just an open-access publisher of scholarly articles: it is a pioneering approach to the world of academia, radically improving the way scholarly research is managed. The grand vision of Frontiers is a world where all people have an equal opportunity to seek, share and generate knowledge. Frontiers provides immediate and permanent online open access to all its publications, but this alone is not enough to realize our grand goals.

Frontiers Journal Series

The Frontiers Journal Series is a multi-tier and interdisciplinary set of open-access, online journals, promising a paradigm shift from the current review, selection and dissemination processes in academic publishing. All Frontiers journals are driven by researchers for researchers; therefore, they constitute a service to the scholarly community. At the same time, the Frontiers Journal Series operates on a revolutionary invention, the tiered publishing system, initially addressing specific communities of scholars, and gradually climbing up to broader public understanding, thus serving the interests of the lay society, too.

Dedication to Quality

Each Frontiers article is a landmark of the highest quality, thanks to genuinely collaborative interactions between authors and review editors, who include some of the world's best academicians. Research must be certified by peers before entering a stream of knowledge that may eventually reach the public - and shape society; therefore, Frontiers only applies the most rigorous and unbiased reviews.
Frontiers revolutionizes research publishing by freely delivering the most outstanding research, evaluated with no bias from both the academic and social point of view. By applying the most advanced information technologies, Frontiers is catapulting scholarly publishing into a new generation.

What are Frontiers Research Topics?

Frontiers Research Topics are very popular trademarks of the Frontiers Journals Series: they are collections of at least ten articles, all centered on a particular subject. With their unique mix of varied contributions from Original Research to Review Articles, Frontiers Research Topics unify the most influential researchers, the latest key findings and historical advances in a hot research area! Find out more on how to host your own Frontiers Research Topic or contribute to one as an author by contacting the Frontiers Editorial Office: researchtopics@frontiersin.org

DISCOVERY AND TOTAL SYNTHESIS OF BIO-FUNCTIONAL NATURAL PRODUCTS FROM TRADITIONAL MEDICINAL PLANTS

Topic Editors:
Tao Wang, Tianjin University of Traditional Chinese Medicine, China
Satoru Tamura, Iwate Medical University, Japan
Toshio Morikawa, Kindai University, Japan

Table of Contents

Editorial: Discovery and Total Synthesis of Bio-functional Natural Products From Traditional Medicinal Plants

Toshio Morikawa[1]*, Satoru Tamura[2] and Tao Wang[3]

[1] *Pharmaceutical Research and Technology Institute, Kindai University, Osaka, Japan,* [2] *School of Pharmacy, Iwate Medical University, Iwate, Japan,* [3] *Institute of TCM, Tianjin University of Traditional Chinese Medicine, Tianjin, China*

Editorial on the Research Topic

Discovery and Total Synthesis of Bio-functional Natural Products From Traditional Medicinal Plants

The term "natural product" refers to any naturally occurring substance, but it generally refers to a secondary metabolite (Morikawa, 2019; Sicker et al., 2019). Secondary metabolites, which are isolated from plants, animals, and microorganisms, are classified as polyketides, isoprenoids, steroids, aromatics, and alkaloids. Research into the discovery and synthesis of novel bio-functional natural products is a challenging, expensive, and time-consuming process (Pagare et al., 2015; Seca and Pinto, 2019). However, research on natural products stimulates the development of novel separation techniques, spectroscopic approaches to structure elucidation, and synthetic methodologies. The chemical diversity and variety of bio-functional properties of natural products thus attracts attention from chemists, biochemists, and biologists (Morikawa, 2018a,b). The Research Topic on "Discovery and Total Synthesis of Bio-Functional Natural Products from Traditional Medicinal Plants" is intended to promote bio-functional natural products as candidates and/or leads for pharmaceuticals, nutraceuticals, dietary supplements, cosmetics, and food additives. The field of this Research Topic includes natural products chemistry, phytochemistry, pharmacognosy, organic chemistry, food chemistry, bioorganic chemistry, chemical biology, molecular pharmacology, molecular nutritional sciences, and related fields of bio-functional natural products.

The review by Grynkiewicz and Demchuk discussed new perspectives for fisetin, a naturally occurring flavonol, which has distinct antioxidant properties along with a plethora of other plant polyphenols. In particular, they described the potential applications and demand for fisetin in healthcare, methods for its preparation, and its suitability for pharmaceutical use. Wang, Song et al. reviewed the phytochemical, structural modification, and relevant bioactivities, such as anticancer, lipid-regulating, anti-inflammatory, antibacterial, antiviral, and diuretic activities of triterpenoids, especially those obtained from *Alisma* species and their derivatives. Harada et al. summarized the chemistry and neurotrophic activities of (−)-talaumidin and its derivatives. They achieved the first enantioselective total synthesis of (−)-talaumidin *via* a flexible and reliable synthetic pathway involving an Evans asymmetric aldol reaction, as well as stereo-controlled

hydroboration and Friedel-Crafts arylation, to construct the four contiguous chiral centers on the tetrahydrofuran ring. To investigate the structure-activity relationships, a systematic synthesis of all diastereomers and syntheses of several related derivatives was reported along with an evaluation of neurite outgrowth promotion and neuroprotection in primary cultured rat cortical neurons and in nerve growth factor-differentiated PC12 cells. Candidates including (–)-talaumidin for the regeneration of mouse optic nerves *in vivo* were discovered. Nakamura et al. developed a practical and reproducible method for total synthesis of hydroxy-α-sanshool, α-sanshool, and spilanthol, which is a characteristic polyunsaturated fatty acid amide obtained from *Zanthoxylum* species. Notably, a highly selective Wittig reaction using a newly synthesized phosphonium salt with low deliquescence and long-term stability created the desired *Z*-form polyenes. This improved methodology was shown to be applicable to the efficient synthesis of other sanshool derivatives. Regarding the structure determination of novel naturally occurring compounds from traditional medicinal plants, four picrotoxane-type sesquiterpenes, dendroterpene A–D, were isolated from the stems of *Dendrobium nobile* (Wang, Chen et al.). Six highly oxidized lanostane- and cycloartane-type triterpenes, xuetongalactones A–F, were obtained from the stems of *Kadsura heteroclita* (Shehla et al.). Six new limonoids, dictamlinonol A, dictamlimonoside B, and dictamlimonols C–F, were isolated from the root bark of *Dictamnus dasycarpus* (*Cortex Dictamni*) (Chen et al.). Three new geranylated coumarins, kayeassamin I and mammeasins E and F, were obtained from the flowers of *Mammea siamensis* (Morikawa et al.). Five new cyclic organosulfer compounds, foliogarlic disulfanes A_1-A_3 and foliogarlic trisulfanes A_1 and A_2, were isolated from the leaves of *Allium sativa* (Fukaya et al.). Their structures, including the stereochemistry, were elucidated by NMR, MS, X-ray diffraction, and electronic circular dichroism spectroscopic analyses. Various bio-functional activities including; α-glucosidase inhibitory (Wang, Chen et al.), cytotoxicic (Wang, Chen et al.; Shehla et al.), anti-inflammatory (Shehla et al.; Chen et al.), and 5α-reductase inhibitory activities (Morikawa et al.) were also reported. A limonoid fraxinellon was a noteworthy compound obtained as a main constituent of *Cortex Dictamni* in a yield of ∼0.15% with

remarkable anti-inflammatory activity. Fraxinellon inhibited lipopolysaccharide (LPS)-induced nitric oxide production and reduced the LPS-induced expression of inducible nitric oxide synthase and cyclooxigenase-2 at the mRNA and protein levels in a dose-dependent manner by regulating the nuclear factor kappa-light-chain-enhancer of activated B cells in RAW 264.7 macrophage-like cells (Chen et al.). In addition, a geranylated coumarin surangin C obtained from *M. siamensis* flowers exhibited 5α-reductase inhibitory activity (IC_{50} = 5.9 μM). Although the intensity of the 5α-reductase inhibitory activity of these coumarins is moderate compared to the positive control with a steroid skeleton finasteride (IC_{50} = 0.12 μM), there are few reports of 5α-reductase inhibitors with non-steroidal skeletons. These active coumarins may therefore be useful candidates for seed compounds of new non-steroidal 5α-reductase inhibitors (Morikawa et al.).

Exploratory research using naturally occurring products with diverse chemical and bio-functional properties remains a promising tool for discovering new bio-functional principles. The isolation and structural elucidation of the constituents from a wide variety of medicinal resources, including traditional medicinal plants, as well as synthetic research and biological evaluation are therefore being performed. Fortunately, in this Research Topic, researchers who are active in this field have reported on recent promising research. We hope that the articles collected within this Research Topic will help inspire readers to embrace future opportunities in the field.

AUTHOR CONTRIBUTIONS

All authors listed have made a substantial, direct and intellectual contribution to the work, and approved it for publication.

ACKNOWLEDGMENTS

REFERENCES

Morikawa, T. (ed.). (2018a). *Biological Activity of Natural Secondary Metabolite Products*. Basel: MDPI. doi: 10.3390/books978-3-03897-175-7

Morikawa, T. (ed.). (2018b). *The Molecular Aspect of Natural Secondary Metabolite Products in Health and Disease*. Basel: MDPI. doi: 10.3390/books978-3-03897-177-1

Morikawa, T. (2019). Recent research in bioactive natural products from traditional medicinal plants. *Chem. Pharm. Bull.* 67, 632–633. doi: 10.1248/cpb.c19-ctf6707

Pagare, S., Bhatla, M., Tripathi, N., Pagare, S., and Bansal, Y. K. (2015). Secondary metabolites of plants and their role: overview. *Curr. Trends Biotechnol. Pharm.* 9, 293–304.

Seca, A. M. L., and Pinto, D. C. G. A. (2019). Biological potential and medical use of secondary metabolite. *Medicines* 6:66. doi: 10.3390/medicines6020066

Sicker, D., Zeller, K.-P., Siehl, H.-U., Berger, S. (eds.). (2019). *Natural Products: Isolation, Structure Elucidation, History*. Weinheim: Wiley-VCH Verlag GmbH & Co.

New Perspectives for Fisetin

Grzegorz Grynkiewicz* and Oleg M. Demchuk*

Pharmaceutical Research Institute, Warszawa, Poland

Fisetin is a flavonol that shares distinct antioxidant properties with a plethora of other plant polyphenols. Additionally, it exhibits a specific biological activity of considerable interest as regards the protection of functional macromolecules against stress which results in the sustenance of normal cells cytoprotection. Moreover, it shows potential as an anti-inflammatory, chemopreventive, chemotherapeutic and recently also senotherapeutic agent. In view of its prospective applications in healthcare and likely demand for fisetin, methods for its preparation and their suitability for pharmaceutical use are discussed herein.

Keywords: fisetin, flavon-3-ols, synthesis of flavonols, biological activity of flavonols, anti-cancer, anti-aging

INTRODUCTION

The first record of fisetin as an isolate from venetian sumach (*Rhus cotinus* L.) dates back to 1833. A basic chemical characteristics of the compound was provided several decades later by Schmidt (1886), while its structure was elucidated and eventually confirmed by synthesis by S. Kostanecki, who in 1890s started a massive investigation of yellow plant pigments and coined new group names for their sub-categories, presently known as "flavones," "chromones," "chalcones," etc. (Kostanecki et al., 1904). The flavonol fisetin (CAS No. [528-48-3]), conventionally described as: 2-(3,4-dihydroxyphenyl)-3,7-dihydroxy-4H-1-benzopyran-4-one; 3,3′,4′,7-tetrahydroxyflavone; or 5-deoxyquercetin, and represented by the **structural formula 1**, has by now been identified as a secondary metabolite of many plants, occurring in their green parts, fruits, as well as in barks and hardwood (Panche et al., 2016; Hostetler et al., 2017; Verma, 2017; Wang et al., 2018). It was Roux, who in a series of meticulous studies conducted before the advent of modern spectral tools of structural analysis, explained the origin and stereochemistry of oligomeric tannins which contain flavon-3-olic structures closely related to fustin, fisetidinol, fisetin, and similar structures present in various African trees (Roux and Paulus, 1961, 1962; Roux et al., 1961; Drewes and Roux, 1965) (**Figure 1**). Although condensed tannins used by the leather industry have retained some of their technical significance, today more attention is paid to the presence of fisetin in vegetable constituents of human diet and their role as important epigenetic factors in modulating the state of human health. Fisetin is present in strawberries, apples, persimmons, grapes, onions, kiwi, kale, etc., albeit in low concentration, up to hundreds of micrograms per 1 gram of fresh biomass. The reason for this interest stems from relatively recent observations that compound 1 is not only particularly efficient as an antioxidant agent, but also exhibits remarkable selectivity as regards influencing multiple biological processes considered crucial for biological homeostasis.

These findings naturally raise some questions concerning the general availability of fisetin. Thus far, the natural substance of high chemical purity—high-melting yellow needles, soluble in polar organic solvents and practically insoluble in water—has been available for research purposes as an isolate from plants and as a biochemical reagent which has already become an important molecular probe in human physiology. The question of fisetin's availability naturally arises with the surge in the number of pharmacological studies. Ensuring a uniform quality of the investigated active substance is required when preparing a CTD (Common Technical Document) document necessary before the substance is approved for clinical trials. This question is further discussed in more details.
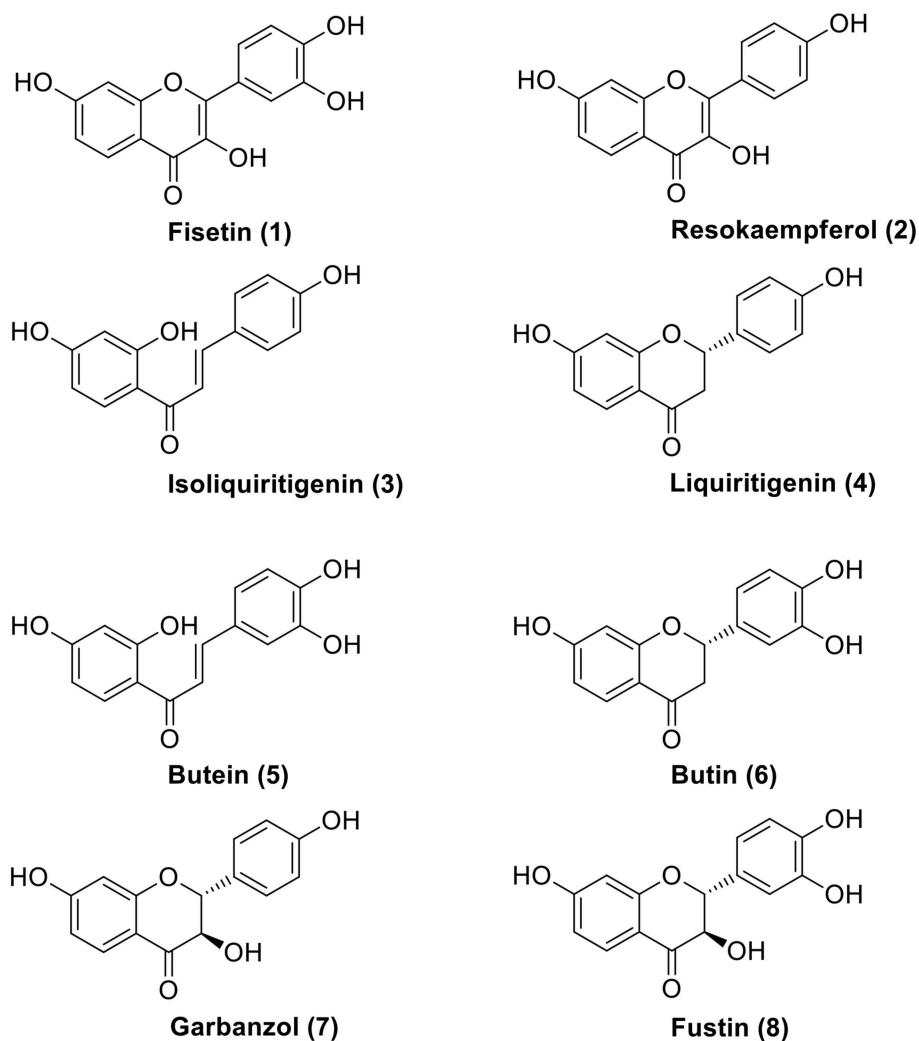
FIGURE 1 | Fisetin (**1**) and biogenetic precursors of the 5-deoxy flavonoid series: chalcones (**3** and **5**), flavanones (**4** and **6**), and dihydroflavonols (**7** and **8**).

Almost all natural phenylpropanoids tend to occur in glycosylated forms, but the glycosides of **1** are seldom mentioned in phytochemical literature, unlike sugar derivatives of its analogs presented in **Figure 1**. Compounds **2**–**8** are closely related to fisetin: during plant biogenesis chalcones and their isomeric flavanones are subject to two different kinds of hydroxylations (aromatic in the ring B of **4** and alicyclic in the ring C of **6**), both performed by the CYP450 type enzymes. Finally, flavan-ol-3-on-4 (**8**) is oxidized, losing both centers of chirality and affording **1**. The development of a protein fold for the chalcone synthase (CHS, EC 2.3.1.74; and its isomerase CHI, EC 5.5.1.6) constituted a great evolutionary achievement which allowed plants to master a stereoselective phenylpropanoid synthesis and attain many new functions as far as signaling, defense and allelopathy are concerned (Austin and Noel, 2003; Dao et al., 2011; Ngaki et al., 2012; Yin et al., 2018). However, in the abiotic world of chemical synthesis, the position of the isomeric equilibrium between chalcones and their racemic flavanone counterparts can be controlled by a mere change of the pH value (**Figure 2**) (Pramod

et al., 2012; Bhattacharyya and Hatua, 2014; Masesane, 2015). Thus, an interaction of a dietary plant metabolome with human physiology may require special care in interpreting nutritional phenomena, traditionally based on selected marker compounds.

CHEMICAL BASIS FOR THE SELECTIVE BIOLOGICAL ACTIVITY OF FISETIN

Ample experimental evidences existed to support a simple generalization that practically all plant phenolics exhibit pronounced antioxidant properties (Halliwell, 2006; Galleano et al., 2010; Prior and Wu, 2013). Very complicated chemistry of simple phenolics, comprising the reactivity of free radicals, iono-radicals and organic ionic structures resulting from the proton transfer is in considerable part reflected in their biological activity and pharmacology (Cicerale et al., 2008; Pereira et al., 2009; Baruah, 2011; Adeboye et al., 2014). Polyphenolic structures extended by the inclusion of a catechol ring are particularly
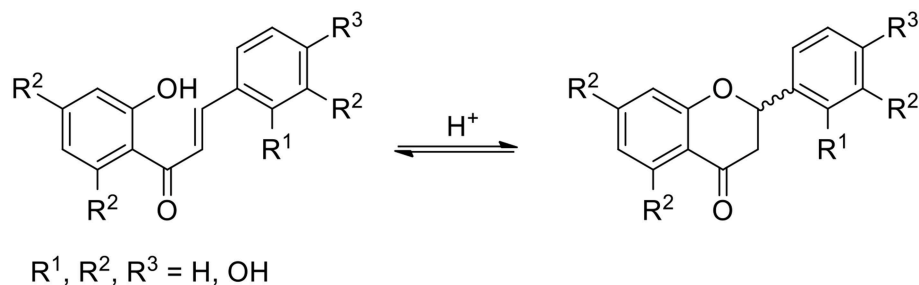
FIGURE 2 | Equilibrium between the chalcone and flavanone counterparts.
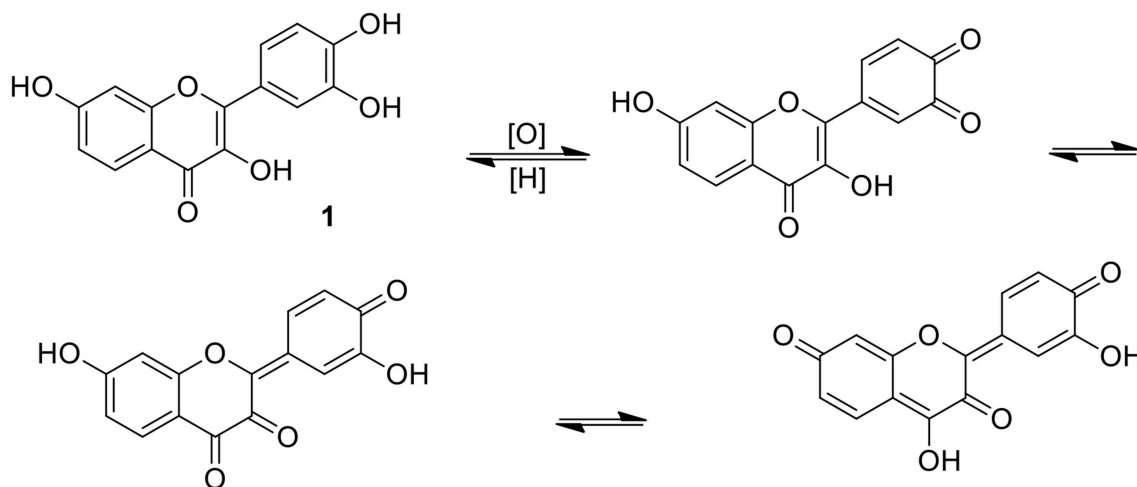
FIGURE 3 | Isomerism of fisetin involving quinone/quinone methide structures; justification of a strongly electrophilic character of the catecholic ring (Awad et al., 2001).

susceptible to specific aromatic electron delocalization which may involve, as a result of contact with the hydrogen acceptors, quinone, and vicinal diketone structures, as exemplified for 1 in **Figure 3** (Awad et al., 2001). Apparently, such intermediates are less prone to flavonoid oligomerization, but can be active as acceptors of a variety of cellular nucleophiles.

CELLULAR SENESCENCE AND FISETIN

Nearly six decades ago the phenomenon of a finite proliferation capacity of human fibroblasts was discovered (Hayflick, 1965, 1974) initiating a period of extensive studies on cell growth arrest mechanisms, particularly in connection to the causes of the aging process. According to the recent findings, cellular senescence which is essentially permanent, appears to play distinct roles both: in normal physiology and various pathologies. Senescent cell phenotypes, which normally secrete inflammatory proteins (SASP) and aim at apoptosis, can undergo certain modes of pharmacologically induced intervention leading to the cell fate reversal (Kuilman et al., 2010, p. 92). Essentially, senescence and cancerogenesis (oncogenesis) direct cell fate into opposite directions, which is of crucial importance when it comes

to understanding the mechanisms of chemotherapy during which tumor regression can result from the induced senescence response (Campisi, 2013; van Deursen, 2014; Mendelsohn et al., 2015). Despite the fact that the senescent cells can also undergo cancer promotion and progression, influence of pharmacological agents on both reverse processes will remain an important field of research for a long time. At present both: the idea of senescence eliciting stimuli under a variety of stressful conditions and the ability to counteract and/or reverse the senescence-associated secretory phenotype are strongly interconnected. This is based on the theories of aging which point to the detrimental effects of reactive oxygen species (ROS), either of mitochondrial origin or generated by an environmental impact (Gil del Valle, 2011, p. 102; Liochev, 2013). While the notion of natural products, particularly those ingested with diet, as protectors against ROS, is already well-established on the cellular level, it seems too general to explain in detail particular selective activities of a myriad of plant secondary metabolites for whom claims of beneficiary medicinal effects have already been formulated.

Apart from the antibiotical activity (Manjolin et al., 2013; Borsari et al., 2016), fisetin shares a distinct antioxidating activity with many other polyphenolic compounds, which was confirmed

FIGURE 4 | Kostanecki's synthesis of fisetin.

FIGURE 5 | Robinson's synthesis of fisetin.
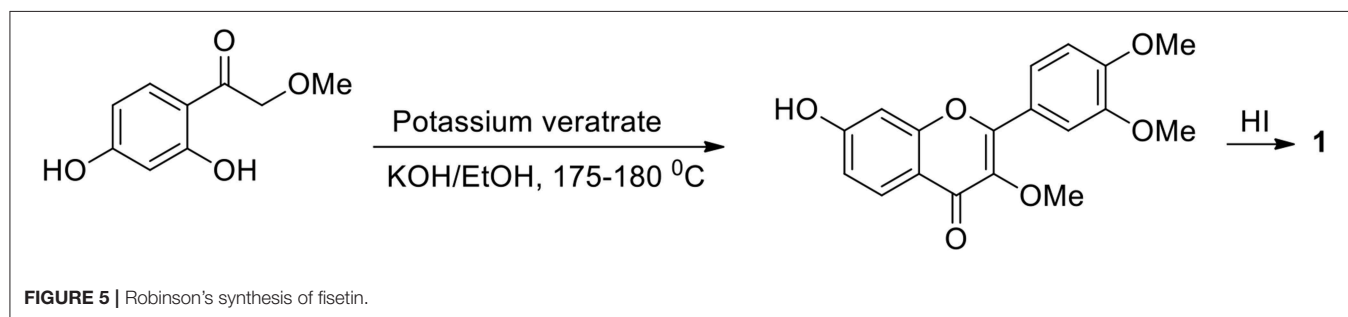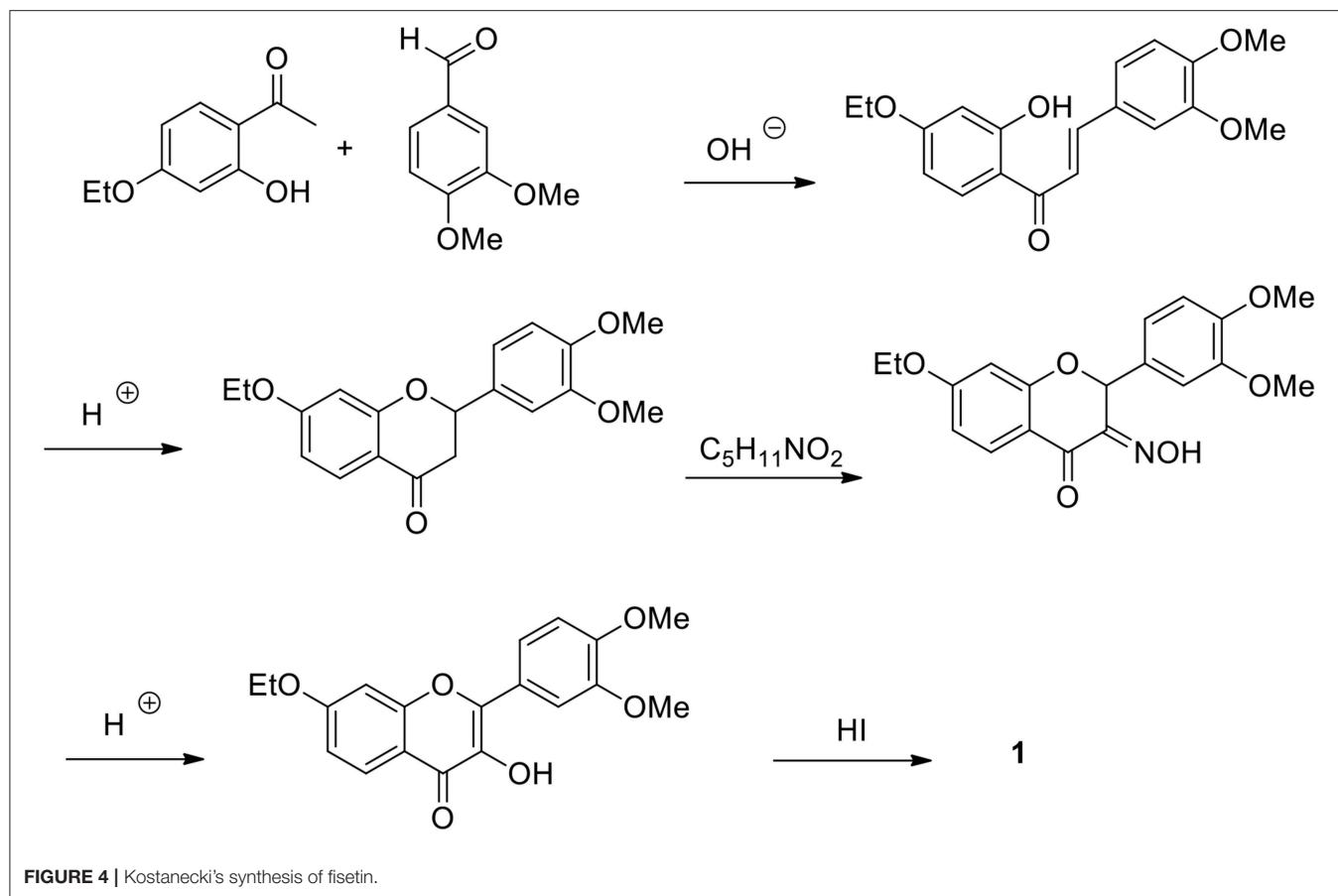
by various *in vitro* as well as *in vivo* models (Khan et al., 2013; Lall et al., 2016; Jiang et al., 2018; Kashyap et al., 2018). Additionally, antioxidant effects of **1** and in particular the induction of the glutathione synthesis are considered important as far as neuroprotection is concerned.

Also, much attention has been paid to the anticancer activity of **1**. *In vitro* studies were performed which offer a panoramic view of the target organ selectivities, as well as an overview of the macromolecular targets. The latter include: AMP-activated protein kinase (AMPK); cyclooygensae (COX); epidermal growth factor receptor (EGFR); extracellular signal-regulated kinase (ERKI1/2); matri metalloproteinase (MMP); nuclear factor-kappa B (NF-κB); prostate-specific antigen (PSA)

transcription factor T-cell factor (TCF); TNF-related apoptosis-inducing ligand (TRAIL); Wnt inhibitory factor (WIF-1); X-linked inhibitor of apoptosis (XIAP), among others (Lall et al., 2016; Hostetler et al., 2017; Kashyap et al., 2018; Wang et al., 2018).

The anticancer activity of fisetin can be enhanced by some auxiliary substances. For example, fisetin significantly impairs carcinoma cell growth in the presence of ascorbic acid, which results in a 61% inhibition of cell growth, in 72 h; the treatment with ascorbic acid alone had no effect on cellular proliferation (Kandaswami et al., 1993). It was also shown that flavonols of the fisetin type extracted from Allium Vegetables, may play a role of such an auxiliary in combination with well-defined
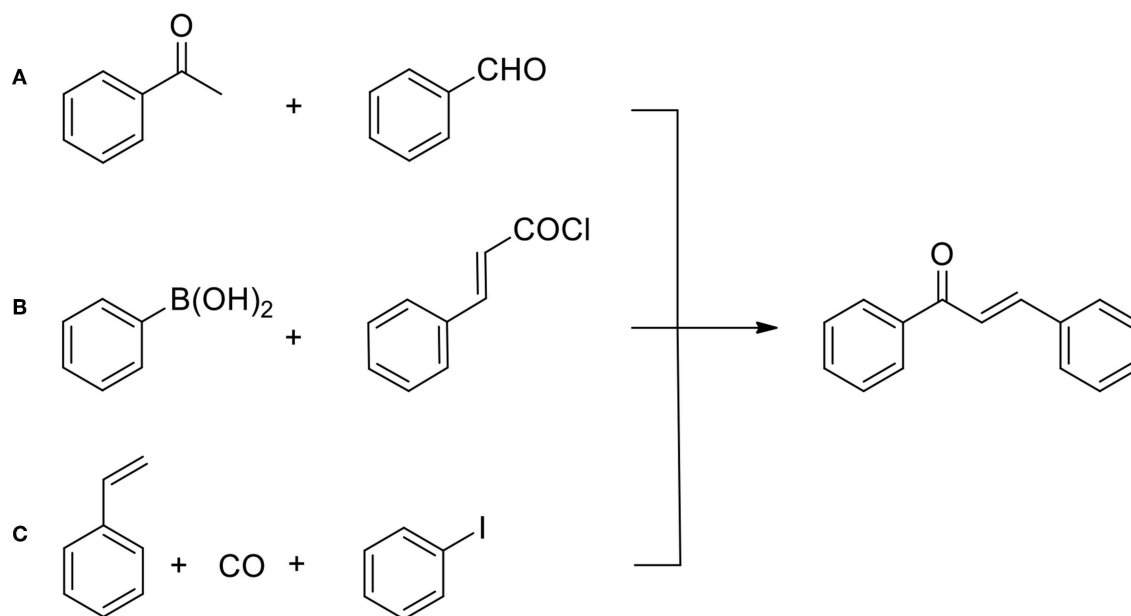
FIGURE 6 | General methods for the chalcone preparation: **(A)** Claisen-Schmidt condensation (base catalyzed); **(B)** Suzuki cross-coupling (Pd catalyzed); **(C)** carbonylative Heck olefin arylation (catalyzed by Pd complexes).

anticancer drugs and enhance the antiproliferative activity of cis-diamminedichloroplatinum(II), nitrogen mustard, and busulphan in human tumor cell culture systems. The analysis of the chemical composition of the flavonol extracts from different kinds of Allium Vegetables and their effects on the neoplastic transformation of NIH/3T3 cells has already been presented (Leighton et al., 1992).

Other activities along this line include: enhancement of the long-term memory, antidepressant effects, inhibition of ischemic reperfusion injury and amelioration of behavioral deficits following a stroke (Khan et al., 2013; Maher, 2015; Currais et al., 2018; Kashyap et al., 2018).

Perhaps the most promising of the documented fisetin biological activities resides in the anticipated possibility of targeting fundamental aging mechanisms. Although the senescent cells resist apoptosis through upregulation of the senescent-cell anti-apoptotic pathways (SCAP), it has been demonstrated that some combination of pharmacological agents (called senolitics or senotherapeutics; e.g., Dasatinib with Quercetin) can overcome this resistance. A follow-up screening of the flavonoids revealed that 1 was even more effective than quercetin and could accomplish the task of reducing senescence markers as a single agent (Yousefzadeh et al., 2018). Model experiments that started with S. cerevisiae and proceeded through D. melanogaster all the way to vertebrate animals clearly demonstrate that fisetin is able to extend the lifespan of investigated organisms of both sexes (Wood et al., 2004; Si et al., 2011; Wagner et al., 2015). As a result of these findings J. L. Kirkland's team at the Mayo Clinic has recently designed and begun a clinical trial aimed at the "Alleviation by Fisetin of Frailty, Inflammation, and Related Measures in

Older Adults" (AFFIRM-LITE) with fisetin administered orally in doses up to 20 mg per kilogram of patient body weight[1]. In view of poor solubility (10.45 µg/mL), relatively low oral bioavailability (44%) and rapid metabolism, such a development warrants interest in the prospective fisetin sources for suitable pharmaceutical formulations.

Recent *in vitro* studies have given a mechanistic insight into how fisetin inhibits the target of the rapamycin pathway in various cell models and therefore influences cellular pathways that are known to affect aging (Syed et al., 2013; Pallauf et al., 2016).

It has also been found that fisetin in combination with other epigenetically active molecules which are able to cross the blood-aqueous and blood-retina barriers exhibit synergistic beneficial effects. This applies for a low dose red wine polyphenols, as well as for vitamin D3 and some other compounds of small molecular weight, synergistically improving visual acuity in patients with advanced atrophic age-related muscular degeneration, including the older ones with advanced stages of the disease for whom very few options remained (Ivanova et al., 2017).

Taking into account moderate international market availability of natural fisetin on the one hand and its high biological activity on the other hand, food supplementation of that compound is still rare. On the market there are several dietary supplements containing fisetin which according to the producers have "apparent brain-health benefits." They are advertised as seno-therapeutic (Yousefzadeh et al., 2018), anticarcinogenic, dietary antioxidants for Health Promotion (Khan et al., 2013), as neurotrophic, anti-inflammatory agents

---

[1]ClinicalTrials.gov Identifier: NCT03675724.

that "may help fine-tune your mind," as well as "help promote cognition and overall brain health," or "help patients with Alzheimer's and Parkinson's disease." At the same time the producers shake off all responsibility for the product by adding a disclosure to the effect: "These statements have not been evaluated by the Food and Drug Administration. This product is not intended to diagnose, treat, cure or prevent any disease." Since the majorities of studies on biological activity of fisetin are mainly academic, clinical trials evaluating its activity are still rare. Recent clinical trials[2] have provided a detailed evaluation of fisetin's anti-oxidative, anti-apoptotic, hyperglycemia alleviating, kidney function enhancing effects. Studies on altering biologic markers of inflammation, insulin resistance, and bone resorption and frailty in older postmenopausal women (AFFIRM) have also been performed.

Recently, in connection with the pharmacokinetic study of 1 performed on Sprague-Dawley rats the presence of 3′-O-methylated metabolite (geraldol) was recorded along with sulfates and glucuronides. Subsequently, a suggestion was advanced that this transformation is advantageous, since it renders 1 more stable, as evidenced by higher AUC concentrations and better distribution to distal organs, including the brain, when compared to other metabolites (Mehta et al., 2018).

In addition to age and oncology related diseases it was also indicated that iron complexes with fisetin derivatives have a biological effect similar to that of desferrioxamine available on the market in oral applications for the treatment of β-thalassemia (Yildiz et al., 2010).

QUEST FOR THE FISETIN API

According to current estimates, strawberries, with 160 μg/g, are the richest source of fisetin, which makes the prospect of its isolation in the technical manufacturing process poor, despite the fact that the fruits belong to industrial scale agricultural crops. In order to recover 1 from a fruit a very selective solid phase extraction process using appropriate synthetic resins would be required, producing significant amounts of processing water waste. As we have learned in the past decades from Active Pharmaceutical Ingredient (API) manufacturing, their processes evolve continuously. Thus, medicinal products of natural origin often undergo a semi-synthetic or synthetic process, before they are defined as a biotechnological product. Such transitions stem from current general indications which strongly advocate green chemistry and environmental protection in technical process design, while complete development of biotechnological process usually require long period of time (Fox et al., 2007; Sheldon, 2008, p. 193; Patel, 2018; Sun et al., 2018). Some efforts toward designing a biosynthetic pathway to fisetin from L-tyrosine present in Escherichia coli and Saccharomyces cerrevisiae have already been reported (Jendresen et al., 2015; Stahlhut et al., 2015; Jones et al., 2016; Pandey et al., 2016; Rodriguez et al., 2017). Nevertheless, in the case of a molecule so small and simple as 1, the synthetic stage of API manufacturing is imminent, which

_____
[2]ClinicalTrials.gov Identifier: NCT03430037.

calls for a critical evaluation of the already described syntheses, especially in view of the current requirements for pharmaceutical GMP and quality assurance.

The first synthesis of 1, completed in 1904 (Kostanecki et al., 1904), involved the preparation of partially protected chalcone which could be cyclized to flavanone under acidic conditions. The next step in the advancement of phenylpropanoid intermediate oxidation was achieved by amyl nitrate which served as an oxidation agent. Stepwise oxime hydrolysis and alkylated phenol groups deprotection by HI afforded fisetin identical with the authentic sample isolated from the plant source (**Figure 4**). This method has several recent modifications mostly devoted to the oxidation and demethylation steps (Hasan et al., 2010; Borsari et al., 2016).

The next attempt at preparing 1 was made by Robinson in 1926 (Allan and Robinson, 1926). The treatment of ω-methoxyresacetophenone with veratric anhydride in the presence of potassium veratrate in ethanol in a sealed glass tube at 180°C afforded required chromen-4-one which was converted to 1 by hydrogen iodide (**Figure 5**).

Recently, more friendly methods have been developed for flavonoids in general and flavonols in particular. It should be pointed out that currently, as illustrated on **Figure 6**, there exists a wide selection of synthetic methods used to prepare chalcones which remain principal intermediates for cyclization to chromanones (Zhuang et al., 2017). In particular, with the aid of modern transition metal catalysts, the formation of carbon—carbon bonds between two aromatic synthons can take place in a variety of ways, as discovered by Heck, Suzuki and Negishi (Johansson-Seechurn et al., 2012).

Chalcones hydroxylated in the ortho- position to the ketone group are of special interest here, because they can easily undergo cyclization leading to the flavone precursors and flavones (**Figure 7**), much more seldom to aurones (not shown) (Krohn et al., 2009; Megens and Roelfes, 2012; Nising and Bräse, 2012; Zhang et al., 2013; Masesane, 2015).

Considering facile availability of chalcones (easily transformable to flavones, for example by iodine promoted cyclization conducted in DMSO), their epoxidation followed by an intramolecular oxirane ring opening could be considered as the method of choice for flavonol preparation. Indeed, such a pathway was developed into a practical synthetic method by successive efforts of Irish and Japanese researchers and their followers. Currently known as the Algar-Flynn-Oyamada reaction (AFO), it uses the basic solution of hydrogen peroxide as a crucial reagent (Oyamada, 1935; Gunduz et al., 2012; Bhattacharyya and Hatua, 2014; Shen et al., 2017). Its general scheme, indicating typical substitution patterns, is presented below (**Figure 8**). This reaction offers a possibility of the aurone product formation by the α-oxirane ring opening, with only moderate yields of flavonols usually reported. It should be mentioned that flavones which are more readily available than flavonols by a variety of preparative procedures can be easily halogenated in position 3 using reagents that generate positively charged halogen atoms, such as NCS (N-chlorosuccinimid), NBS (N-bromosuccinimid), or iodine in the presence of CAN (cerium-ammonium nitrite). Apparently, this seemingly
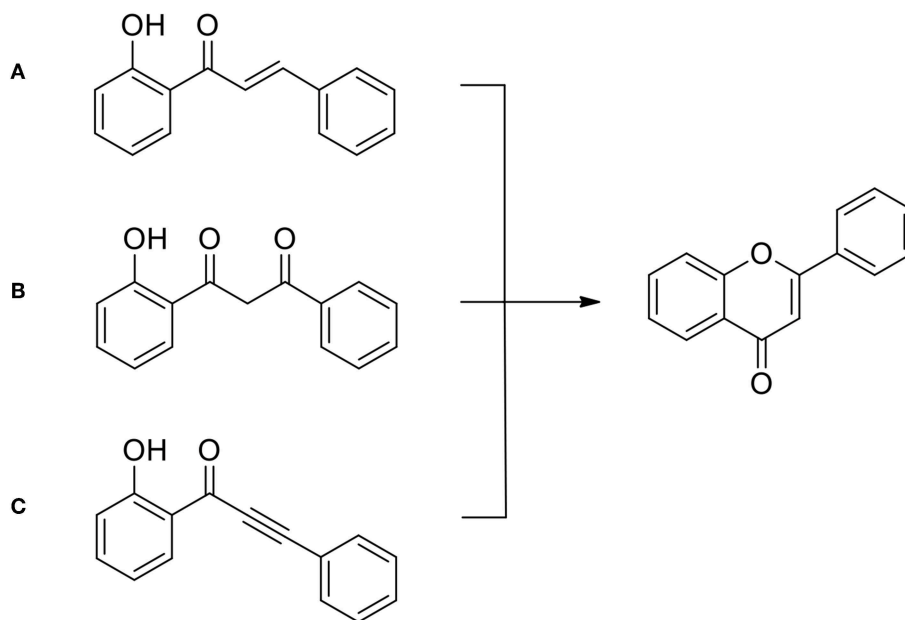
FIGURE 7 | General approaches to flavone syntheses: **(A)** from chalcones (following Kostanecki's synthesis); **(B)** from 1,3-diaryl propandiones (following Kostanecki—Robinson—Venkataraman ideas); **(C)** from phenylalkenyl ketones, according to Lee (2017).
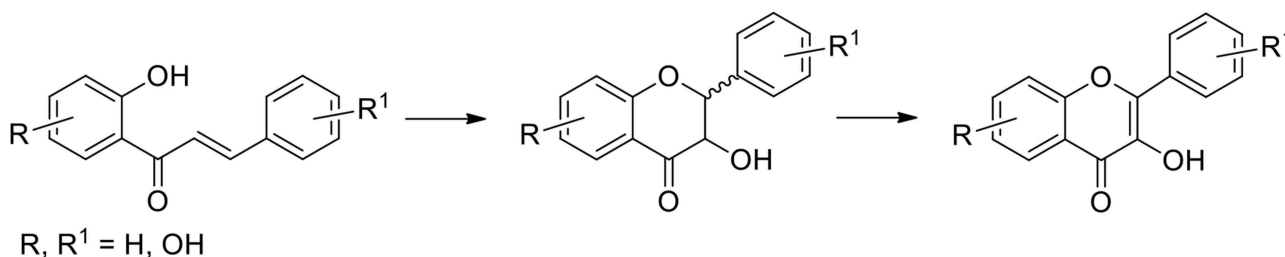
FIGURE 8 | General scheme for the AFO synthesis of flavonols upon chalcone epoxidation with H_2O_2.
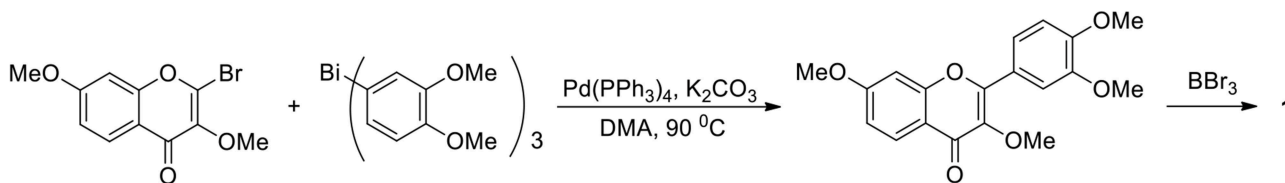
FIGURE 9 | Synthesis of fisetin by arylation of the 2-bromochromone derivative.

obvious avenue has not been exploited as a practical method for preparing flavonols.

In a more recent attempt at the preparation of flavonols organometallic chemistry was applied to the 2-bromochromanone Pd catalyzed arylation step, as illustrated below (**Figure 9**). In the case of fisetin two crucial steps of synthesis were completed in 75% of the overall yield (Rao and Kumar, 2014). In principle, three equivalents of

the bromochromone substrate could be arylated by one equivalent of an appropriate phenylbismuth reagent in such a reaction.

It seems that the initial idea of Kostanecki, where flavanones were chosen as the principal substrates for the transformation, has not been fully exploited yet, although it has already been demonstrated that precursors such as flavones can be directly oxidized to flavanols, for example by 3,3-dimethyldioxirane

(Maloney and Hecht, 2005). In this connection, a semi-synthesis should be mentioned as more than a theoretical possibility. The example of hesperidin's (abundant citrus flavanone easily recoverable from orange peels) transformation into methoxylated 3-flavonol in the 5 synthetic steps clearly indicates that some natural products can be treated as suitable substrates toward the required flavonoid material (Garg et al., 2001; Lewin et al., 2010).

While the above list of reactions seems to exhaust the chemical synthetic means for prospective fisetin API availability (Molga et al., 2019), current industrial trends indicate that biotransformations are to be considered an ultimate resource of chemical entities for human use in food and medicine supplements. To this end, substantial knowledge concerning fisetin biosynthesis exists: chalcone isoliquiritigenin is cyclized to flavanone liquiritigenin, hydroxylased to catechin garbanzol, flavone resokaempferol, and oxidized to **1**. All the biocatalysts for this chain of transformations are known, moreover, they have been successfully expressed in microorganisms for the preparation of both quercetin and fisetin (Jendresen et al., 2015; Stahlhut et al., 2015; Jones et al., 2016; Pandey et al., 2016; Rodriguez et al., 2017).

CONCLUSIONS AND OUTLOOK

The average daily intake of fisetin from various vegetable sources is estimated to be at the level of 0.4 mg (Kashyap et al., 2018). In view of recent findings concerning its beneficial antioxidant, anti-inflammatory, antitumor, neuroprotective, and anti-aging biological activities, a growing need for a high purity substance fit for pharmaceutical development can be forecasted. The quest for the medicinal status of 1 may be slow and difficult, as the history of flavonoids' retraction from the vitamin status shows. Nevertheless, current demand for natural products such as fisetin may come from the less regulated markets, as in the case of functional food or dietary supplements. There is no uniform legal concept for functional food and its current definition: "natural or processed foods that contain biologically-active compounds; which, in defined, effective, non-toxic amounts, provide a clinically proven and documented health benefit utilizing specific biomarkers, for the prevention, management, or treatment of a chronic disease or its symptoms" (Danik and Jaishree, 2015; Martirosyan, 2015) may not sound ideal. Nevertheless, it serves the purpose in terms of health claim use, and it can certainly promote new market entries, provided good science is used to support the presence of new constituents in the food products. Chemical synthesis seems to be an obvious first aid solution, with the process design based on chalcone intermediates, along the AFO route. However, this simple chemistry requires considerable optimization efforts aimed at minimalization or even elimination of the protective group chemistry input. Alternatively, availability of suitable (i.e., 5-deoxy) intermediate raw materials should be carefully examined, since flavon-3-ols can be obtained by chemical transformation from their structural relatives such as flavan-4-ones, flavones, catechins and chalcones. In any case, care should be taken to enhance poor solubility and bioavalability of 1. Some technical solutions have already been proposed (DeCorte, 2016; Chadha et al., 2019). The issue of fisetin's low solubility could be overridden by way of its complexation with cyclosophoroase dimer and cyclodextrins which also significantly improves the cytotoxicity of fisetin against HeLa cells (Jeong et al., 2013; Zhang et al., 2015). Such studies may well serve to extend the medicinal chemistry capacity of 1 as well as its analogs and derivatives, following numerous examples of secondary metabolites exploited as drug leads. Finally, it is likely that the future of fisetin manufacturing as an API (or its precursor) might lie in the realm of biotechnology (Wu et al., 2018; Huccetogullari et al., 2019; Mark et al., 2019). In any case, it should be pointed out that a single agent (such as **1**) supplementation may bring about different overall pharmacological effects than a vegetable diet rich in the same substance, since in the latter case a whole 5-deoxy flavonoid segment of a plant metabolome (which comprises many related individual chemicals) collides with human system biology, leading to a considerably more complex network of mutual interactions.

AUTHOR CONTRIBUTIONS

The authors have an equal contribution in the conceptualisation, data collection, and manuscript preparation.

REFERENCES

Adeboye, P. T., Bettiga, M., and Olsson, L. (2014). The chemical nature of phenolic compounds determines their toxicity and induces distinct physiological responses in Saccharomyces cerevisiae in lignocellulose hydrolysates. *AMB Express* 4:046. doi: 10.1186/s13568-014-0046-7

Allan, J., and Robinson, R. (1926). CCCIX—A new synthesis of fisetin and of quercetin. *J. Chem. Soc.* 129, 2334–2336. doi: 10.1039/JR9262902334

Austin, M. B., and Noel, J. P. (2003). The chalcone synthase superfamily of type III polyketide synthases. *Nat. Prod. Rep.* 20, 79–110. doi: 10.1039/b100917f

Awad, H. M., Boersma, M. G., Boeren, S., van Bladeren, P. J., Vervoort, J., and Rietjens, I. M. C. M. (2001). Structure–activity study on the quinone/quinone methide chemistry of flavonoids. *Chem. Res. Toxicol.* 14, 398–408. doi: 10.1021/tx000216e

Baruah, J. B. (2011). *Chemistry of Phenolic Compounds: State of the Art*. New York, NY: Nova Science Publishers. ISBN 9781617613357.

Bhattacharyya, S., and Hatua, K. (2014). Computational insight of the mechanism of Algar–Flynn–Oyamada (AFO) reaction. *RSC Adv.* 4, 18702–18709. doi: 10.1039/c3ra46623j

Borsari, C., Luciani, R., Pozzi, C., Poehner, I., Henrich, S., Trande, M., et al. (2016). Profiling of flavonol derivatives for the development of antitrypanosomatidic drugs. *J. Med. Chem.* 59, 7598–7616. doi: 10.1021/acs.jmedchem.6b00698

Campisi, J. (2013). Aging, cellular senescence, and cancer. *Annu. Rev. Physiol.* 75, 685–705. doi: 10.1146/annurev-physiol-030212-183653

Chadha, R., Bhalla, Y., Chadha, K., and Karan, M. (2019). Crystal engineering of fisetin: a step towards improved biopharmaceutical parameters. *SDRP J. Food Sci. Technol.* 4, 597–613. doi: 10.25177/JFST.4.2.RA.461

Cicerale, S., Conlan, X. A., Sinclair, A. J., and Keast, R. S. J. (2008). Chemistry and health of olive oil phenolics. *Crit. Rev. Food Sci. Nutr.* 49, 218–236. doi: 10.1080/10408390701856223

Currais, A., Farrokhi, C., Dargusch, R., Armando, A., Quehenberger, O., Schubert, D., et al. (2018). Fisetin reduces the impact of aging on behavior and

physiology in the rapidly aging SAMP8 mouse. *J Gerontol. Ser. A* 73, 299–307. doi: 10.1093/gerona/glx104

Danik, M. M., and Jaishree, S. (2015). A new definition of functional food by FFC: what makes a new definition unique? *Funct. Foods Health Dis.* 5, 209–223. doi: 10.31989/ffhd.v5i6.183

Dao, T. T. H., Linthorst, H. J. M., and Verpoorte, R. (2011). Chalcone synthase and its functions in plant resistance. *Phytochem. Rev.* 10, 397–412. doi: 10.1007/s11101-011-9211-7

DeCorte, B. L. (2016). Underexplored opportunities for natural products in drug discovery. *J. Med. Chem.* 59, 9295–9304. doi: 10.1021/acs.jmedchem.6b00473

Drewes, S. E., and Roux, D. G. (1965). Natural and synthetic diastereoisomeric (-)-3',4',7-trihydroxyflavan-3,4-diols. *Biochem. J.* 96, 681–687. doi: 10.1042/bj0960681

Fox, R. J., Davis, S. C., Mundorff, E. C., Newman, L. M., Gavrilovic, V., Ma, S. K., et al. (2007). Improving catalytic function by ProSAR-driven enzyme evolution. *Nat. Biotechnol.* 25, 338–344. doi: 10.1038/nbt1286

Galleano, M., Verstraeten, S. V., Oteiza, P. I., and Fraga, C. G. (2010). Antioxidant actions of flavonoids: thermodynamic and kinetic analysis. *Arch. Biochem. Biophys.* 501, 23–30. doi: 10.1016/j.abb.2010.04.005

Garg, A., Garg, S., Zaneveld, L. J. D., and Singla, A. K. (2001). Chemistry and pharmacology of the citrus bioflavonoid hesperidin. *Phytother. Res.* 15, 655–669. doi: 10.1002/ptr.1074

Gil del Valle, L. (2011). Oxidative stress in aging: theoretical outcomes and clinical evidences in humans. *Biomed. Aging Pathol.* 1, 1–7. doi: 10.1016/j.biomag.2011.03.001

Gunduz, S., Goren, A. C., and Ozturk, T. (2012). Facile syntheses of 3-hydroxyflavones. *Org. Lett.* 14, 1576–1579. doi: 10.1021/ol300310e

Halliwell, B. (2006). Reactive species and antioxidants. Redox biology is a fundamental theme of aerobic life. *Plant Physiol.* 141, 312–322. doi: 10.1104/pp.106.077073

Hasan, A., Sadiq, A., Abbas, A., Mughal, E., Khan, K. M., and Ali, M. (2010). Isolation and synthesis of flavonols and comparison of their antioxidant activity. *Nat. Prod. Res.* 24, 995–1003. doi: 10.1080/14786410902847302

Hayflick, L. (1965). The limited *in vitro* lifetime of human diploid cell strains. *Exp. Cell Res.* 37, 614–636. doi: 10.1016/0014-4827(65)90211-9

Hayflick, L. (1974). The strategy of senescence. *Gerontologist* 14, 37–45. doi: 10.1093/geront/14.1.37

Hostetler, G. L., Ralston, R. A., and Schwartz, S. J. (2017). Flavones: food sources, bioavailability, metabolism, and bioactivity. *Adv. Nutr.* 8, 423–435. doi: 10.3945/an.116.012948

Huccetogullari, D., Luo, Z. W., and Lee, S. Y. (2019). Metabolic engineering of microorganisms for production of aromatic compounds. *Microbial Cell Factories* 18:041. doi: 10.1186/s12934-019-1090-4

Ivanova, D., Richer, S., and Bhandari, A. (2017). Improved visual acuity and retinal integrity with resveratrol based supplementation in patients with macular degeneration. *Int. J. Ophthalmol. Clin. Res.* 4:082. doi: 10.23937/2378-346X/1410082

Jendresen, C. B., Stahlhut, S. G., Li, M., Gaspar, P., Siedler, S., Förster, J., et al. (2015). Highly active and specific tyrosine ammonia-lyases from diverse origins enable enhanced production of aromatic compounds in bacteria and *Saccharomyces cerevisiae. Appl. Environ. Microbiol.* 81, 4458–4476. doi: 10.1128/AEM.00405-15

Jeong, D., Choi, J. M., Choi, Y., Jeong, K., Cho, E., and Jung, S. (2013). Complexation of fisetin with novel cyclosophoroase dimer to improve solubility and bioavailability. *Carbohydr. Polym.* 97, 196–202. doi: 10.1016/j.carbpol.2013.04.066

Jiang, Y., Dong, G., and Song, Y. (2018). Nucleus pulposus cell senescence is alleviated by resveratrol through regulating the ROS/NF-κB pathway under high-magnitude compression. *Biosci. Rep.* 38:BSR20180670. doi: 10.1042/BSR20180670

Johansson-Seechurn, C., Kitching, M. O., Colacot, T. J., and Snieckus, V. (2012). Palladium-catalyzed cross-coupling: a historical contextual perspective to the 2010 Nobel Prize. *Angew. Chem. Int. Ed.* 51, 5062–5085. doi: 10.1002/anie.201107017

Jones, J. A., Vernacchio, V. R., Sinkoe, A. L., Collins, S. M., Ibrahim, M. H. A., Lachance, D. M., et al. (2016). Experimental and computational optimization of an Escherichia coli co-culture for the efficient production of flavonoids. *Metab. Eng.* 35, 55–63. doi: 10.1016/j.ymben.2016.01.006

Kandaswami, C., Perkins, E., Soloniuk, D. S., Drzewiecki, G., and Middleton, E. (1993). Ascorbic acid-enhanced antiproliferative effect of flavonoids on squamous cell carcinoma *in vitro. Anticancer. Drugs* 4, 91–96. doi: 10.1097/00001813-199302000-00012

Kashyap, D., Sharma, A., Sak, K., Tuli, H. S., Buttar, H. S., and Bishayee, A. (2018). Fisetin: a bioactive phytochemical with potential for cancer prevention and pharmacotherapy. *Life Sci.* 194, 75–87. doi: 10.1016/j.lfs.2017.12.005

Khan, N., Syed, D. N., Ahmad, N., and Mukhtar, H. (2013). Fisetin: a dietary antioxidant for health promotion. *Antioxid. Redox Signal.* 19, 151–162. doi: 10.1089/ars.2012.4901

Kostanecki, S., Lampe, V., and Tambor, J. (1904). Synthese des Fisetins. *Chem. Ber.* 37, 784–791. doi: 10.1002/cber.190403701128

Krohn, K., Ahmed, I., and John, M. (2009). Enantioselective synthesis of Flavan-3-ols using a Mitsunobu cyclization. *Synthesis* 2009, 779–786. doi: 10.1055/s-0028-1083361

Kuilman, T., Michaloglou, C., Mooi, W. J., and Peeper, D. S. (2010). The essence of senescence. *Genes Dev.* 24, 2463–2479. doi: 10.1101/gad.1971610

Lall, R. K., Adhami, V. M., and Mukhtar, H. (2016). Dietary flavonoid fisetin for cancer prevention and treatment. *Mol. Nutr. Food Res.* 60, 1396–1405. doi: 10.1002/mnfr.201600025

Lee, J. I. (2017). Novel synthesis of flavones by regioselective cyclization of 1-(2-hydroxyphenyl)-3-phenyl-2-propyn-1-ones derived from 2-hydroxybenzoic acids. *Bull. Korean Chem. Soc.* 38, 675–678. doi: 10.1002/bkcs.11134

Leighton, T., Ginther, C., Fluss, L., Harter, W. K., Cansado, J., and Notario, V. (1992). Molecular characterization of quercetin and quercetin glycosides in Allium vegetables. *ACS Symp. Ser.* 507, 220–238. doi: 10.1021/bk-1992-0507.ch016

Lewin, G., Maciuk, A., Thoret, S., Aubert, G., v., Dubois, J., et al. (2010). Semisynthesis of natural flavones inhibiting tubulin polymerization, from hesperidin. *J. Nat. Prod.* 73, 702–706. doi: 10.1021/np100065v

Liochev, S. I. (2013). Reactive oxygen species and the free radical theory of aging. *Free Radical Biol. Med.* 60, 1–4. doi: 10.1016/j.freeradbiomed.2013.02.011

Maher, P. (2015). How fisetin reduces the impact of age and disease on CNS function. *Front. Biosci.* 7, 58–82. doi: 10.2741/s425

Maloney, D. J., and Hecht, S. M. (2005). Synthesis of a potent and selective inhibitor of p90 Rsk. *Org. Lett.* 7, 1097–1099. doi: 10.1021/ol0500463

Manjolin, L. C., dos Reis, M. B. G., Maquiaveli, C., d,. C., Santos-Filho, O. A., and da Silva, E. R. (2013). Dietary flavonoids fisetin, luteolin and their derived compounds inhibit arginase, a central enzyme in Leishmania (Leishmania) amazonensis infection. *Food Chem.* 141, 2253–2262. doi: 10.1016/j.foodchem.2013.05.025

Mark, R., Lyu, X., Lee, J. J. L., Parra-Saldívar, R., and Chen, W. N. (2019). Sustainable production of natural phenolics for functional food applications. *J. Funct. Foods* 57, 233–254. doi: 10.1016/j.jff.2019.04.008

Martirosyan, D. M. (2015). *Introduction to Functional Food Science: Textbook.* Scotts Valley, CA: CreateSpace Independent Publishing Platform. ISBN 9781512023947.

Masesane, I. B. (2015). A comprehensive review of the oxidative cyclisation of 2'-hydroxychalcones to aurones and flavones. *Int. J. Chem. Stud.* 3, 53–59.

Megens, R. P., and Roelfes, G. (2012). DNA-based catalytic enantioselective intermolecular oxa-Michael addition reactions. *Chem. Commun.* 48, 6366–6368. doi: 10.1039/c2cc31854g

Mehta, P., Pawar, A., Mahadik, K., and Bothiraja, C. (2018). Emerging novel drug delivery strategies for bioactive flavonol fisetin in biomedicine. *Biomed. Pharmacother.* 106, 1282–1291. doi: 10.1016/j.biopha.2018.07.079

Mendelsohn, J., Howley, P. M., Israel, M. A., Gray, J. W., and Thompson, C. (2015). *The Molecular Basis of Cancer, 4th Edn.* Philadelphia, PA: Saunders/Elsevier. ISBN 9781455740666.

Molga, K., Dittwald, P., and Grzybowski, B. A. (2019). Navigating around patented routes by preserving specific motifs along computer-planned retrosynthetic pathways. *Chem* 5, 460–473. doi: 10.1016/j.chempr.2018.12.004

Ngaki, M. N., Louie, G. V., Philippe, R. N., Manning, G., Pojer, F., Bowman, M. E., et al. (2012). Evolution of the chalcone-isomerase fold from fatty-acid binding to stereospecific catalysis. *Nature* 485, 530–533. doi: 10.1038/nature11009

Nising, C. F., and Bräse, S. (2012). Recent developments in the field of oxa-Michael reactions. *Chem. Soc. Rev.* 41, 988–999. doi: 10.1039/C1CS15167C

Oyamada, T. (1935). A new general method for the synthesis of the derivatives of flavonol. *Bull. Chem. Soc. Jpn.* 10, 182–186. doi: 10.1246/bcsj.10.182

Pallauf, K., Duckstein, N., and Rimbach, G. (2016). A literature review of flavonoids and lifespan in model organisms. *Proc. Nutr. Soc.* 76, 145–162. doi: 10.1017/S0029665116000720

Panche, A. N., Diwan, A. D., and Chandra, S. R. (2016). Flavonoids: an overview. *J. Nutr. Sci.* 5:e47. doi: 10.1017/jns.2016.41

Pandey, R. P., Parajuli, P., Koffas, M. A. G., and Sohng, J. K. (2016). Microbial production of natural and non-natural flavonoids: pathway engineering, directed evolution and systems/synthetic biology. *Biotechnol. Adv.* 34, 634–662. doi: 10.1016/j.biotechadv.2016.02.012

Patel, R. N. (2018). Biocatalysis for synthesis of pharmaceuticals. *Bioorg. Med. Chem.* 26, 1252–1274. doi: 10.1016/j.bmc.2017.05.023

Pereira, D., Valentão, P., Pereira, J., and Andrade, P. (2009). Phenolics: from Chemistry to Biology. *Molecules* 14, 2202–2211. doi: 10.3390/molecules14062202

Pramod, K., Pradip, W., and Pudukulathan, Z. (2012). An improved and eco-friendly method for the synthesis of flavanone by the cyclization of 2'-hydroxy chalcone using methane sulphonic acid as catalyst. *Chem. J.* 2, 106–110.

Prior, R. L., and Wu, X. (2013). Diet antioxidant capacity: relationships to oxidative stress and health. *Am. J. Biomed. Sci.* 5, 126–139. doi: 10.5099/aj130200126

Rao, M. L. N., and Kumar, A. (2014). Pd-catalyzed atom-economic couplings of triarylbismuth reagents with 2-bromo- and 2,6-dibromochromones and synthesis of medicinally important fisetin. *Tetrahedron Lett.* 55, 5764–5770. doi: 10.1016/j.tetlet.2014.08.081

Rodriguez, A., Strucko, T., Stahlhut, S. G., Kristensen, M., Svenssen, D. K., Forster, J., et al. (2017). Metabolic engineering of yeast for fermentative production of flavonoids. *Bioresour. Technol.* 245, 1645–1654. doi: 10.1016/j.biortech.2017.06.043

Roux, D. G., Maihs, E. A., and Paulus, E. (1961). Condensed tannins. 9. Distribution of flavonoid compounds in the heartwoods and barks of some interrelated wattles. *Biochem. J.* 78, 834–839. doi: 10.1042/bj0780834

Roux, D. G., and Paulus, E. (1961). Condensed tannins. 7. Isolation of (−)-7:3′:4′-trihydroxyflavan-3-ol [(−)-fisetinidol], a naturally occurring catechin from black-wattle heartwood. *Biochem. J.* 78, 120–123. doi: 10.1042/bj0780120

Roux, D. G., and Paulus, E. (1962). Condensed tannins. 13. Interrelationships of flavonoid components from the heartwood of Robinia pseudacacia. *Biochem. J.* 82, 324–330. doi: 10.1042/bj0820324

Schmidt, J. (1886). Ueber das Fisetin, den Farbstoff des Fisetholtzes. *Chem. Ber.* 19, 1734–1749. doi: 10.1002/cber.18860190223

Sheldon, R. A. (2008). E factors, green chemistry and catalysis: an odyssey. *Chem. Commun.* 2008, 3352–3365. doi: 10.1039/b803584a

Shen, X., Zhou, Q., Xiong, W., Pu, W., Zhang, W., Zhang, G., et al. (2017). Synthesis of 5-subsituted flavonols via the Algar-Flynn-Oyamada (AFO) reaction: the mechanistic implication. *Tetrahedron* 73, 4822–4829. doi: 10.1016/j.tet.2017.06.064

Si, H., Fu, Z., Babu, P. V. A., Zhen, W., LeRoith, T., Meaney, M. P., et al. (2011). Dietary epicatechin promotes survival of obese diabetic mice and *Drosophila melanogaster*. *J. Nutr.* 141, 1095–1100. doi: 10.3945/jn.110.134270

Stahlhut, S. G., Siedler, S., Malla, S., Harrison, S. J., Maury, J., Neves, A. R., et al. (2015). Assembly of a novel biosynthetic pathway for production of the plant flavonoid fisetin in *Escherichia coli*. *Metab. Eng.* 31, 84–93. doi: 10.1016/j.ymben.2015.07.002

Sun, H., Zhang, H., Ang, E. L., and Zhao, H. (2018). Biocatalysis for the synthesis of pharmaceuticals and pharmaceutical intermediates. *Bioorg. Med. Chem.* 26, 1275–1284. doi: 10.1016/j.bmc.2017.06.043

Syed, D. N., Adhami, V. M., Khan, M. I., and Mukhtar, H. (2013). Inhibition of Akt/mTOR signaling by the dietary flavonoid fisetin. *Anticancer. Agents Med. Chem.* 13, 995–1001. doi: 10.2174/18715206113139990129

van Deursen, J. M. (2014). The role of senescent cells in ageing. *Nature* 509, 439–446. doi: 10.1038/nature13193

Verma, R. K. (2017). A taxonomical review of Butea Monosperma (Lam.) Kuntze- a dye yielding plant. *World J. Pharm. Res.* 6, 284–295. doi: 10.20959/wjpr20179-9256

Wagner, A. E., Piegholdt, S., Rabe, D., Baenas, N., Schloesser, A., Eggersdorfer, M., et al. (2015). Epigallocatechin gallate affects glucose metabolism and increases fitness and lifespan in *Drosophila melanogaster*. *Oncotarget* 6, 30568–30578. doi: 10.18632/oncotarget.5215

Wang, T.-y., Li, Q., and Bi, K.-s. (2018). Bioactive flavonoids in medicinal plants: structure, activity and biological fate. *Asian J. Pharm. Sci.* 13, 12–23. doi: 10.1016/j.ajps.2017.08.004

Wood, J. G., Rogina, B., Lavu, S., Howitz, K., Helfand, S. L., Tatar, M., et al. (2004). Sirtuin activators mimic caloric restriction and delay ageing in metazoans. *Nature* 430, 686–689. doi: 10.1038/nature02789

Wu, F., Cao, P., Song, G., Chen, W., and Wang, Q. (2018). Expanding the repertoire of aromatic chemicals by microbial production. *J. Chem. Technol. Biotechnol.* 93, 2804–2816. doi: 10.1002/jctb.5690

Yildiz, E., Karabulut, S., Pinar, S. N., Karatas, Y., and Doran, F. (2010). Trivalent iron chelator with flavone moiety: synthesis and pharmacological properties. *Wuji Huaxue Xuebao Chin. J. Inorg. Chem.* 26, 1743–1749.

Yin, Y.-c., Zhang, X.-d., Gao, Z.-q., Hu, T., and Liu, Y. (2018). The Research Progress of Chalcone Isomerase (CHI) in plants. *Mol. Biotechnol.* 61, 32–52. doi: 10.1007/s12033-018-0130-3

Yousefzadeh, M. J., Zhu, Y., McGowan, S. J., Angelini, L., Fuhrmann-Stroissnigg, H., Xu, M., et al. (2018). Fisetin is a senotherapeutic that extends health and lifespan. *EBio Med.* 36, 18–28. doi: 10.1016/j.ebiom.2018.09.015

Zhang, J., Fu, X.-L., Yang, N., and Wang, Q.-A. (2013). Synthesis and cytotoxicity of chalcones and 5-deoxyflavonoids. *Sci. World J.* 2013, 1–6. doi: 10.1155/2013/649485

Zhang, J., Jiang, K., An, K., Ren, S., Xie, X., Jin, Y., et al. (2015). Novel water-soluble fisetin/cyclodextrins inclusion complexes: preparation, characterization, molecular docking and bioavailability. *Carbohydr. Res.* 418, 20–28. doi: 10.1016/j.carres.2015.09.013

Zhuang, C., Zhang, W., Sheng, C., Zhang, W., Xing, C., and Miao, Z. (2017). Chalcone: a privileged structure in medicinal chemistry. *Chem. Rev.* 117, 7762–7810. doi: 10.1021/acs.chemrev.7b00020

Four New Picrotoxane-Type Sesquiterpenes From *Dendrobium nobile* Lindl

Pei Wang[1], Xin Chen[1,2], Hao Wang[1], Shengzhuo Huang[1], Caihong Cai[1], Jingzhe Yuan[1], Guoliang Zhu[3], Xinglian Xu[2], Wenli Mei[1]* and Haofu Dai[1]*

[1] *Hainan Key Laboratory of Research and Development of Natural Product From Li Folk Medicine, Institute of Tropical Bioscience and Biotechnology, Chinese Academy of Tropical Agricultural Sciences, Haikou, China,* [2] *Nanjing Agricultural University, Nanjing, China,* [3] *East China University of Science and Technology, Shanghai, China*

Four picrotoxane-type sesquiterpenes, dendroterpene A–D (**1–4**), together with four known compounds (**5–8**), were isolated from the stems of *Dendrobium nobile* Lindl. Their structures were elucidated by spectroscopic analysis, X-ray diffraction analysis, analysis of the ECD data according to the Klyne's lactone sector rule, and quantum ECD calculation. Compounds **1** and **2** are two new picrotoxane-type sesquiterpenes with a new carbon skeleton containing a formamide group, which may be derived from the previously reported dendrobiumane B skeleton by the C(9)-C(11) carbon bond cleavage. Compounds **3**, **5**, **6**, and **8** exhibited inhibitory activity against α-glycosidase. Compounds **5** and **6** were cytotoxic against SGC-7901, K562, A549, BEL-7402, and Hela cell lines.

Keywords: *Dendrobium nobile* Lindl, picrotoxane, sesquiterpenes, α-glycosidase inhibitor, cytotoxicity

INTRODUCTION

Dendrobium nobile Lindl, the plant belongs Orchidaceae family, is one of three major plant sources of the traditional Chinese medicine "Shi Hu" in Chinese (edition 2005), which are used as a tonic to nourish the stomach and promote the production of body fluid recorded in the Chinese Pharmacopeia (Jiangsu New Medical College, 1986). The previous reports showed a series of chemical constituents isolated from *D. nobile* including sesquiterpenes (Zhang et al., 2007a), alkaloids (Liu and Zhao, 2003; Meng et al., 2017), bibenzyls derivatives (Zhang et al., 2007b), and glucosides (Zhao et al., 2001), some of which exhibited antitumor (Zhou et al., 2016), anti-inflammatory (Hwang et al., 2010), and immunomodulatory activities (Zhao et al., 2001).

Picrotoxane-type sesquiterpenes were one of main constituents of *D. nobile*, which exhibited the angiogenesis effect against sunitinibinduced damage (Meng et al., 2017) and inhibitory activity of nerve growth factor mediated neurite outgrowth (Leon et al., 2019). Our phytochemical investigation on the EtOAc extract of the stems of *D. nobile* led to the isolation of four new picrotoxane-type sesquiterpenes, dendroterpene A–D (**1–4**), along with four known compounds, nobilin E (**5**) (Zhang et al., 2007b), dendrocandin V (**6**) (Xiao et al., 2017), S(+)-dehydrovomifoliol (**7**) (Kato et al., 1977) and di-[2-(4-hydroxyphenyl)] ethyl ether (**8**) (Krysin et al., 2010). Compounds **1** and **2** are two new picrotoxane-type sesquiterpenes with a new carbon skeleton containing a formamide group, which may be derived from the previously reported dendrobiumane B skeleton by the C(9)-C(11) carbon bond cleavage. In this report, the isolation, structure elucidation and bioactivities of these compounds are described.

MATERIALS AND METHODS

General Experimental Procedures

Optical rotations were measured on a MCP 5100 modular compact polarimeter (Anton Paar, America). IR spectra were taken on a Nicolet 380 FT-IR instrument (Thermo, USA) as KBr discs. NMR spectra were recorded on a Bruker Avance III 500 MHz NMR spectrometer (Bruker, German). ESIMS and HRESIMS were recorded with amaZon SL (Bruker) or Compact QqTOF (Bruker). ECD spectra were measured by APL Chiascan (Applied Photophysics Ltd., England). Semi-preparative HPLC was carried out using a C_{18} column (Cosmosil-pack, 10 × 250 mm, 5 μm, 4 mL/min, Nacalai Tesque). C_{18} gel (20–45 μm, Fuji SilysiSa Chemical Co., Ltd., Greenville, NC, UA), Silica gel (60–80, 200–300 mesh, Qingdao Marine Chemical Co., Ltd., Qingdao, China), Sephadex LH-20 (Merck, Kenilworth, NJ, USA) were used for column chromatograghy. α-glycosidase (Sigma-Aldrich, UA) used for the bioactivity was derived from yeast and its EINECS (EC) unmber is 3.2.1.20.

Plant Material and Extraction

The fresh stems of *D. nobile* were collected from Shishan town in May 2018, Hainan, China. After drying, the dried stems (13.0 kg) were shattered. Then, the samples were extracted by 95% ethyl alcohol three times and for 5 days each time. The EtOH extract (716.2 g) was dissolved in H_2O and extracted three times by petroleum ether (8.0 L), EtOAc (8.0 L), and n-butyl alcohol (8.0 L) successively.

Isolation

The EtOAc extract (87.9 g) was separated into 16 fractions (Fr.1–Fr.16) by a silica gel column (200–300 mesh) using a gradient of petroleum ether-EtOAc (v/v, 20:1– 0:1) and then acetone. Fr.9 (10.0 g) was further separated into 20 fractions (Fr.9-1–Fr.9-20) by ODS column. Fr.9-1 (30.0 mg) was purified by semipreparative HPLC (20% MeOH/H_2O) to yield **8** (1.4 mg; t_R 12.1 min). Fr.9-6 (112.0 mg) was purified by semipreparative TLC eluting with petroleum ether-acetone (v/v 3:1) to obtain compound **7** (2.7 mg). Fr.9-7 (372.0 mg) was purified by a silica gel column eluting with petroleum ether-CHCl₃-MeOH (v/v/v 200:50:1) to yield compound **3** (4.2 mg). Compound **4** (2.0 mg) was obtained by recrystallization from Fr.9-8 (580.3 mg). Fr.9-10 (103.0 mg) was further purified by a silica gel column eluting with petroleum ether-acetone (v/v 8:1) to give **1** (13.0 mg). Fr.10 (9.0 g) was separated by ODS column to get 50 fractions (Fr.10-1–Fr.10-50). Compound **2** (100.2 mg) was obtained by recrystallization from Fr.10-14 (326.0 mg). Fr.10-38 (184.0 mg) was purified by Sephadex LH-20 eluting with MeOH to give **5** (15.0 mg). Fr.11 (9.0 g) was separated into three fractions (Fr.11-1–Fr.11-3) by Sephadex LH-20 eluting with MeOH. Fr.11-3 (80.1 mg) was purified by ODS column eluting with 65% MeOH/H_2O to yield compound **6** (20.9 mg).

ECD Calculation

The calculations were performed by using the density functional theory (DFT) as carried out in the Gaussian 03 (Frisch et al., 2004). The preliminary conformational distributions search was performed by Sybyl-X 2.0 software. All ground-state geometries were optimized at the B3LYP/6-31G(d) level. Solvent effects of methanol solution were evaluated at the same DFT level by using the SCRF/PCM method (Cammi and Tomasi, 1995). TDDFT at B3LYP/6-31G(d) was employed to calculate the electronic excitation energies and rotational strengths in methanol (Gross et al., 1996).

Characterization of Compounds 1–4

Dendroterpene A (**1**): Colorless crystals; $[\alpha]_D^{25}$ +149.9 (c 0. 1, MeOH); ECD (MeOH) λ_{max} ($\Delta\varepsilon$) 223 (+2.28); IR (KBr) ν_{max} 3350, 2927, 2856, 1761, 1683, 1118, 1024 cm^{-1}; m.p. 185–186 °C; ^{1}H and ^{13}C NMR (see **Table 1**); HRESIMS m/z 286.1417 [M + Na]$^+$ (calcd. for $C_{15}H_{21}NO_3Na$: 286.1414).

Dendroterpene B (**2**): Colorless crystals; $[\alpha]_D^{25}$ +10.0 (c 0.1, MeOH); ECD (MeOH) λ_{max} ($\Delta\varepsilon$) 207 (+4.77); IR (KBr) ν_{max} 3414, 2964,2926, 2861, 1764, 1666, 1223, 1021 cm^{-1}; m.p. 200–201°C; ^{1}H and ^{13}C NMR (see **Table 1**); HRESIMS m/z 302.1376 [M + Na]$^+$ (calcd. for $C_{15}H_{21}NO_4Na$: 302.1363).

Dendroterpene C (**3**): White powder; $[\alpha]_D^{25}$ +16.0 (c 0.1, MeOH); ECD (MeOH) λ_{max} ($\Delta\varepsilon$) 225 (+ 1.16), IR (KBr) ν_{max} 3447, 2928, 1777, 11276, 1111, 1036 cm^{-1}; ^{1}H and ^{13}C NMR (see **Table 1**); HRESIMS m/z 287.1281 [M + Na]$^+$ (calcd. for $C_{15}H_{20}O_4Na$:287.1254).

Dendroterpene D (**4**): Colorless crystals; $[\alpha]_D^{25}$ +139.9 (c 0.1, MeOH); IR (KBr) ν_{max} 3414, 2930, 1629, 1108, 1028 cm^{-1}; m.p. 167–168 °C; ^{1}H and ^{13}C NMR (see **Table 1**); HRESIMS m/z 303.1228 [M + Na]$^+$ (calcd. for $C_{15}H_{20}O_5$ Na: 303.1203).

X-Ray Crystallographic Data of 1, 2, and 4

Compound **1** was obtained as colorless crystals with molecular formula of $C_{15}H_{21}NO_3$ from MeOH. Space group $P2_12_12_1$, a = 7.7078(5) Å, b = 10.1533 (7) Å, c = 17.8721(12) Å, α = 90.00°, β = 90.00(10)°, γ = 90.00°, V = 1398.66 (16) Å^3, Z = 4, D_{calcd} = 1.251 g/cm^3, μ(CuKα) = 0.7000 mm^{-1}, and F(000) = 568, T = 293(2) K, crystal size 0.32 × 0.20 × 0.12 mm, R_1 = 0.0445(I>2sigma(I), wR_2 = 0.1054 (all data), Flack parameter = 0.0(4). 3147 reflections measured, 2119 unique (R_{int} = 0.0213, R_{sigma} = N/A) which were used in all calculations. The structure was solved by direct methods (SHELXS-97) and expanded using Fourier techniques (SHELXL-97). Crystallographic data (excluding structure factors) for structure **1** in this paper have been deposited in the Cambridge Crystallographic Data Center as supplementary publication number CCDC 1943060.

Compound **2** was obtained as colorless crystals with molecular formula of $C_{15}H_{21}NO_4$ from MeOH. Space group $P2_1$, a = 7.7610(4) Å, b = 8.8111 (4) Å, c = 10.3388(6) Å, α = 90.00°, β = 104.463(5)°, γ = 90.00°, V = 684.59 (6) Å^3, Z = 2, D_{calcd} = 1.300 g/cm^3, μ(CuKα) = 0.771 mm^{-1}, F(000) = 300, crystal size 0.34 × 0.27 × 0.13 mm, R_1 = 0.0390(I>2sigma(I), wR_2 = 0.1028 (all data), Flack parameter = 0.0(4). 3304 reflections measured, 2070 unique (R_{int} = 0.0259, R_{sigma} = N/A) which were used in all calculations. The structure was solved by direct methods (SHELXS-97) and expanded using Fourier techniques (SHELXL-97). Crystallographic data (excluding structure factors) for structure **2** in this paper have been deposited in the Cambridge Crystallographic Data Center as supplementary publication number CCDC 1943062.

TABLE 1 | ^{1}H (500 MHz) and ^{13}C (125 MHz) NMR Data of compounds **1–4**.

No.	1[a] δ_C	1[a] δ_H, mult. (J in Hz)	2[b] δ_C	2[b] δ_H, mult. (J in Hz)	3[c] δ_C	3[c] δ_H, mult. (J in Hz)	4[c] δ_C	4[c] δ_H, mult. (J in Hz)
1	52.5, C	–	53.3, C	–	47.8, C	–	50.4, C	–
2	51.2, CH	4.24, s	49.0, CH	4.18, d, (9.7)	81.5, CH	4.28,d, (3.6)	81.6, CH	4.25, d, (3.6)
3	84.5, CH	4.34, brd, (5.5)	83.2, CH	4.33, brd, (5.6)	77.9, CH	4.75,dd, (3.6, 5.6)	77.5, CH	4.79, dd, (3.6, 5.1)
4	52.5, CH	2.02, m	52.3, CH	2.01, ddd, (4.7, 4.7, 11.2)	50.9, CH	2.29,ddd, (5.0,5.0,11.7)	51.1, CH	2.27, m
5	46.1, CH	2.28, t, (4.3)	51.0, CH	2.47, d, (4.7)	43.4, CH	2.57, dd, (4.3,5.6)	43.2, CH	2.57, dd, (4.3, 5.8)
6	42.5, CH	2.33, m	80.6, C	–	43.6, CH	2.20, m	44.9, CH	2.31, m
6-OH	–	–	–	5.40, brs	–	–	–	–
7	36.9, CH$_2$	2.69, ddd, (2.3, 2.3, 7.3,17.1) 2.35, m	46.1, CH$_2$	2.64, brd, (15.1) 2.52, brd, (15.1)	32.4, CH$_2$	2.15, m	29.7, CH$_2$	2.07, m; 2.36, m
8	130.3, CH	5.51, dd, (2.3, 5.5)	137.3, CH	5.79, brd, (6.3)	27.8, CH$_2$	2.01, m; 2.14, m	38.5, CH$_2$	1.82, m; 2.28, m
9	136.6, CH	5.63, m	127.7, CH	5.47, d, (6.3)	55.2, CH	2.77,t, (9.4)	85.1, C	–
10	27.3, CH$_3$	1.04, s	22.3, CH$_3$	0.96, s	31.3, CH$_3$	1.52, s	24.3, CH$_3$	1.43, s
11	163.7, CH	8.09, s	161.7, CH	8.12, s	177.1, C	–	177.2, C	–
12-NH	–	–	–	8.51, d, (9.6)	–	–	–	–
13	26.4, CH	1.84, m	26.4, CH	2.36, m	24.8, CH	1.75, m	24.8, CH$_3$	1.84, m
14	20.1, CH	0.95, d, (6.6)	22.2, CH$_3$	1.00, d, (6.1)	20.6, CH$_3$	1.04, d, (6.5)	20.7, CH$_3$	1.04, d, (6.5)
15	21.0, CH$_3$	0.93, d, (6.6)	20.3, CH$_3$	0.89, d, (6.6)	21.4, CH$_3$	1.02, d, (6.5)	21.5, CH$_3$	1.02, d, (6.6)
16	180.3, C	–	176.5, C	–	177.5, C	–	177.5, C	–

^{a}measured in CD$_3$OD; ^{b}measured in DMSO-d$_6$; ^{c}measured in CDCl$_3$.

Compound **4** was obtained as colorless crystals with molecular formula of C$_{15}$H$_{21}$NO$_3$ from MeOH. Space group $P2_1$, $a = 7.5120(3)$ Å, $b = 13.6611(7)$ Å, $c = 13.9060(5)$ Å, $\alpha = 90.00°$, $\beta = 90.00(10)°$, $\gamma = 90.00°$, $V = 1427.06(11)$ Å^3, $Z = 4$, $D_{calcd} = 1.360$ mg/m^3, $\mu(CuK\alpha) = 0.842$ mm^{-1}, $F(000) = 600$, crystal size $0.327 \times 0.22 \times 0.15$ mm. $R_1 = 0.0368(I>2sigma(I))$, $wR_2 = 0.0938$ (all data), Flack parameter = 0.1(3). 2227 reflections measured, 1628 unique ($R_{int} = 0.0204$, $R_{sigma} = N/A$) which were used in all calculations. The structure was solved by direct methods (SHELXS-97) and expanded using Fourier techniques (SHELXL-97). Crystallographic data (excluding structure factors) for structure **4** in this paper have been deposited in the Cambridge Crystallographic Data Center as supplementary publication number CCDC 1943065.

Bioassay for α-Glycosidase Inhibitory Activity

The method optimized by Jong et al. (2007) was performed *in vitro* to test the α-glucosidase inhibitory activity of compounds **1–8**. Acarbose was used as positive control.

Bioassay for Cytotoxicity

The MTT method optimized by Mosmann (1983) was performed *in vitro* to test the cytotoxic activity of compounds **1–8**. Cisplatin was used as a positive control.

RESULTS AND DISCUSSION

Identification of Compounds 1-4

Compound **1** was obtained as colorless crystals with the molecular formula as C$_{15}$H$_{21}$NO$_3$, which was determined based on the pseudo-molecular ion peak at *m/z* 286.1417 [M + Na]$^+$ (calcd. for C$_{15}$H$_{21}$NO$_3$Na: 286.1414) in the HRESIMS spectrum. Analysis of its 1D and HSQC NMR spectra (see **Supplementary Figures 1**, **2**, and **4** in the Supplementary Material) revealed two olefinic methines ($\delta_{C/H}$ 136.6/5.63 and $\delta_{C/H}$ 130.3/5.51), three methyls ($\delta_{C/H}$ 27.3/1.04, 21.0/0.93 and 20.1/0.95), one methylene ($\delta_{C/H}$ 36.9/2.69, 2.35), six sp^3 methines ($\delta_{C/H}$ 84.5/4.34, 52.5/2.02, 51.2/4.24, 46.1/2.28, 42.5/2.33, and 26.4/1.84) with one oxygenated, one quaternary carbon (δ_C 52.5) and two ester or amide carbonyl groups (δ_C 180.3 and δ_C 163.7). The above data and sequential COSY correlations (**Figure 2** and **Supplementary Figure 3** in the Supplementary Material) from H-2 to H-9, as well as from H-4 to H$_3$-14 and H$_3$-15 through H-13, along with the HMBC correlations (**Figure 2** and **Supplementary Figure 5** in the Supplementary Material) from H$_3$-10 to C-2, C-6 and C-9, from H-2 to C-6 and C-9, from H-3 and H-6 to C-16, and from H-5 to C-1, revealed a picrotoxane-type sesquiterpene skeleton (Zhao et al., 2003). A detailed comparison of the above data with those of the previously reported dendrobiumane C (Zhao et al., 2003) disclosed high similarity. The differences between them were that the hydroxymethyl group CH$_2$-11 ($\delta_{C/H}$ 59.8/4.04, 4.27) and the oxymethine group CH-2 ($\delta_{C/H}$ 73.1/3.67) in dendrobiumane C

were replaced by a hydrogen atom H-9 (δ_H 5.51) and a methine CH-2 ($\delta_{C/H}$ 51.2/4.24) linked with a formamide group in **1**, respectively, as evidence by COSY correlation from H-9 to H-8, along with the HMBC correlations from H-2 to C-9 and C-11, from H-9 to C-6 and C-10, as well as from H$_3$-10 to C-2 and C-6. The ROESY correlations (**Figure 3** and **Supplementary Figure 6** in the Supplementary Material) from H$_3$-10 to H-2, H-6 and H-13, and from H-2 and H-6 to H-13 suggested that H-2, H-6 and H$_3$-10 were on the same face of the six-member ring, while H-4 was on the face opposite to them. Due to the complex bridge-ring lactone skeleton, the chemical structure models analysis of **1** displayed the only possibility of the relative configurations of C-3 and C-5 is that H-3 and H-5 were on the same face of six-member ring with H-2, H-6, and H$_3$-10 when the relative configurations of C-1, C-2, C-4 and C-6 were confirmed. To support the above structure elucidation and determine the absolute configuration of **1**, a single-crystal X-ray diffraction pattern was obtained using the anomalous scattering of Cu Kα radiation (**Figure 4**), allowing an explicit assignment of the absolute configuration of **1** as 1*S*, 2*S*, 3*R*, 4*S*, 5*R*, and 6*S*. In order to confirm the absolute configuration assignment, Lactone sector rule (Jexkings et al., 1965) based on ECD data was used. The molecule was viewed from the line on the plane of the ester group along the bisectrix of the O–C=O angle, i.e., as shown in **Figure 5** for 4*S*. The functional group at C-4 lying in the back upper right sector was responsible for the positive CD Cotton effect resulted from n–π* transition of lactone, which was well in accordance with the positive Cotton effect at

λ_{max} 223 nm of **1** (**Supplementary Figure 24** in Supplementary Material). Hence, compound **1**, named as dendroterpene A, was determined to be a picrotoxane-type sesquiterpene.

Compound **2** was also isolated as colorless crystals. The HRESIMS (*m/z* 302.1376 [M + Na]$^+$, calcd. for $C_{15}H_{21}NO_4Na$: 302.1363) indicated a molecular formula of $C_{15}H_{21}NO_4$. The 1D and 2D NMR data of **2** (**Table 1** and **Figure 2**) were very similar to those of **1**, except that an oxygenated quaternary carbon C-6 (δ_C 80.6) in **2** replaced signals corresponding to CH-6 in **1** ($\delta_{C/H}$ 42.5/2.33). In the HMBC spectrum (**Figure 2** and **Supplementary Figure 11** in the Supplementary Material) of **2**, correlations from H-2, H-4, H-8, H-9, 6-OH, and H$_3$-10 to the oxygenated quaternary carbon C-6, together with the molecular formula, suggested that the H-6 in **1** was oxygenated to

FIGURE 2 | Key HMBC (——▶) and ^{1}H–^{1}H COSY (—) correlations of compounds **1–4**.

FIGURE 1 | The structures of compounds **1–8**.
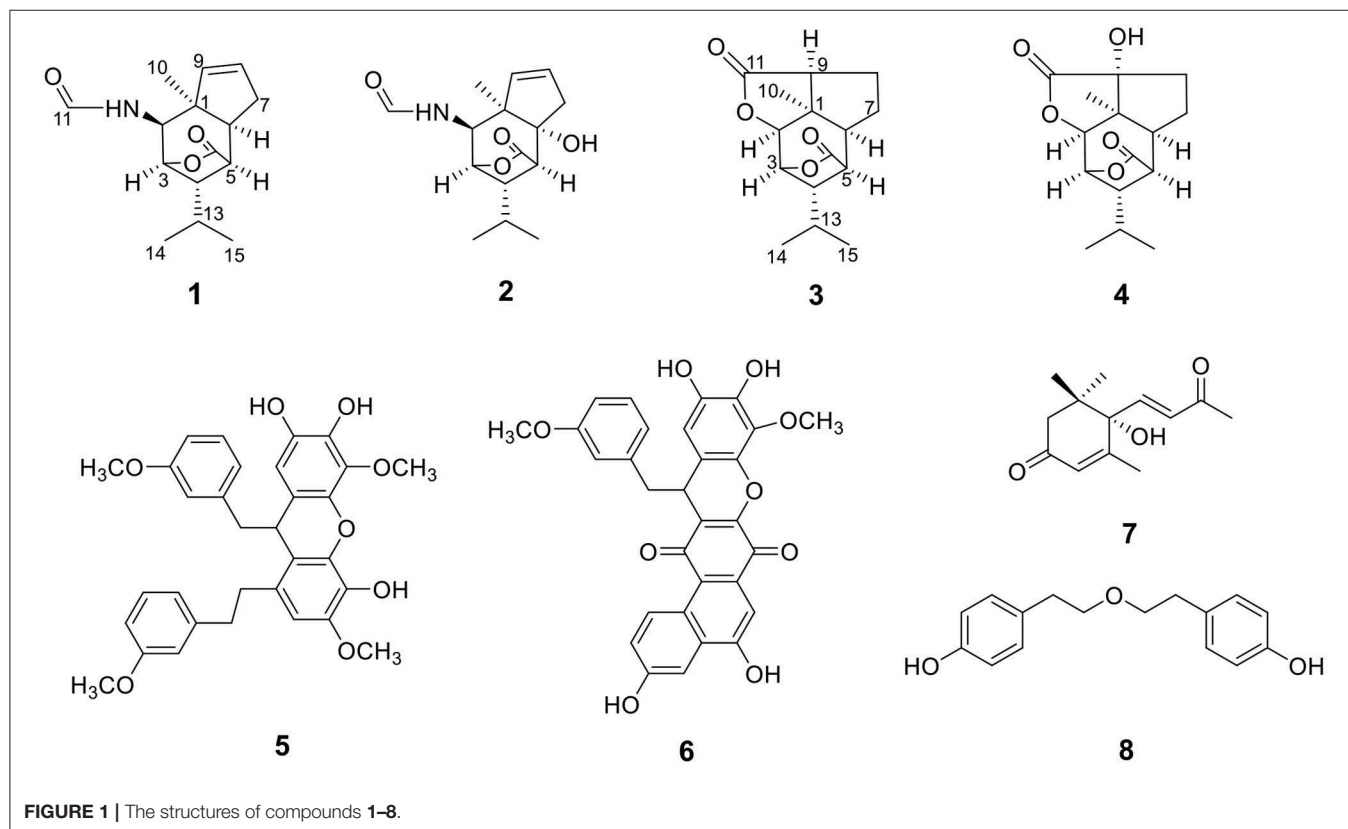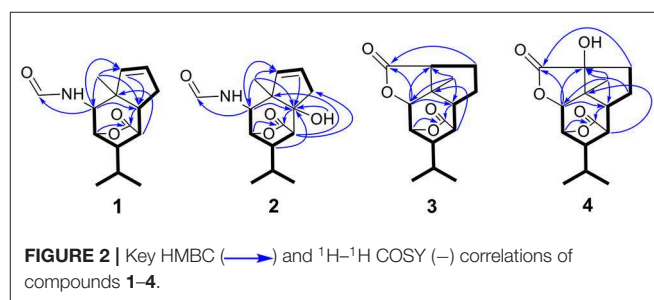
a hydroxylated quaternary carbon in **2**. The H-2, 6-OH and H_3-10 were on the same face of the six-member ring, and the H-4 was on the opposite face in **2**, as evidence by the ROESY correlations (**Figure 3** and **Supplementary Figure 12** in the Supplementary Material) of H_3-10 with H-2, H-13 and 6-OH, and of H-2 and 6-OH with H-13. The relative configurations of C-3 and C-5 in **2** were identical with those of **1** according to the chemical structure models analysis of **2.**

The above assignment was further confirmed by a single-crystal X-ray diffraction pattern obtained using the anomalous scattering of Cu Kα radiation (**Figure 4**), which also led to an unambiguous assignment of the absolute configuration of **2** as 1*R*, 2*S*, 3*R*, 4*S*, 5*S*, and 6*R*. The absolute configuration of **2** was also confirmed by Lactone sector rule based on ECD data (Jexkings et al., 1965) (**Figure 5** and **Supplementary Figure 24** in Supplementary Material). Therefore, compound **2** was also identified as a picrotoxane-type sesquiterpene, and named as dendroterpene B.

Compound **3** has the molecular formula of $C_{15}H_{20}O_4$ based on HRESIMS (*m/z* 287.1281 [M + Na]$^+$, calcd for $C_{15}H_{20}O_4$Na:287.1254), suggesting six degrees of unsaturation. 1D NMR and HSQC data displayed three methyls ($\delta_{C/H}$ 31.3/1.52, 21.4/1.02 and 20.6/1.04), two methylenes, seven methines including two oxygenated ones ($\delta_{C/H}$ 81.5/4.28 and 77.9/4.75), three quaternary carbons including two ester carbonyl

carbons (δ_C 177.5 and 177.1). The above data of **3** were very similar to those of the previously reported dedrobiumane E (Zhao et al., 2003). Their structural differences were that two oxygenated quaternary carbons C-6 (δ_C 76.8) and C-9 (δ_C 83.8) and two oxygenated methine groups CH-7 ($\delta_{C/H}$ 65.2/4.05) and CH-8 ($\delta_{C/H}$ 60.1/3.86) in dedrobiumane E were replaced by two sp^3 methines ($\delta_{C/H}$ 43.6/2.20 and $\delta_{C/H}$ 55.2/2.77) and two sp^3 methylenes ($\delta_{C/H}$ 32.4/2.15 and $\delta_{C/H}$ 27.8/2.01, 2.14) in **3**, as proved by the sequential COSY correlations of H-5/H-6/H-7/H-8/H-9, along with the detail interpretation of the HMBC correlations from H-2 to C-6, C-9, and C-11, from H_3-10 to C-2, C-6, and C-9, from H-3 and H-6 to C-16, from H-5 to C-1, as well as from H-8 to C-11 (**Figure 2**). The ROESY experiments (**Figure 3** and **Supplementary Figure 18** in the Supplementary Material) displayed the correlations from H_3-10 to H-2, H-6, and H-9, as well as the correlations between H-2 and H-13, indicating H-2, H-6, H-9, and H_3-10 were on the same face, while H-4 was on the face opposite to them. The relative configurations of C-3 and C-5 in **3** were also determined to be consistent with those of **1** and **2** through the same method. The calculated ECD curve for **3** matched well with the experimental one (**Figure 6**), assigning the absolute configurations of **3** as 1*R*, 2*S*, 3*R*, 4*S*, 5*R*, 6*S*, and 9*S* (Wang et al., 2014). Thus, the structure of **3** was established as picrotoxane-type sesquiterpene shown in **Figure 1**, and named as dendroterpene C.
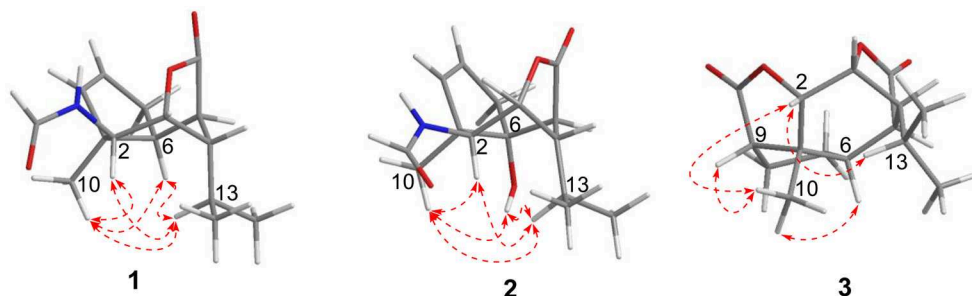
FIGURE 3 | ROESY (◄– –►) correlations of compounds **1–3**.

FIGURE 4 | Molecular plots of compounds **1**, **2**, and **4**.

FIGURE 5 | Application of lactone sector rule to compounds **1** and **2**.

FIGURE 6 | Measured ECD and TD-DFT calculated ECD curves of compound **3**.
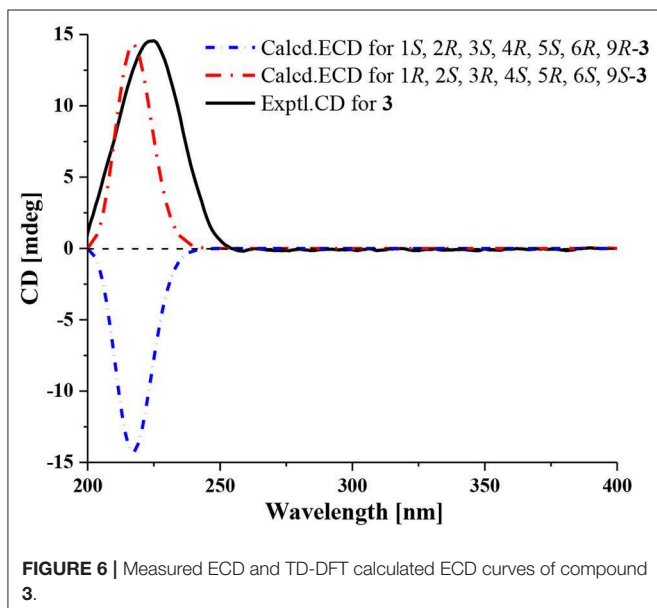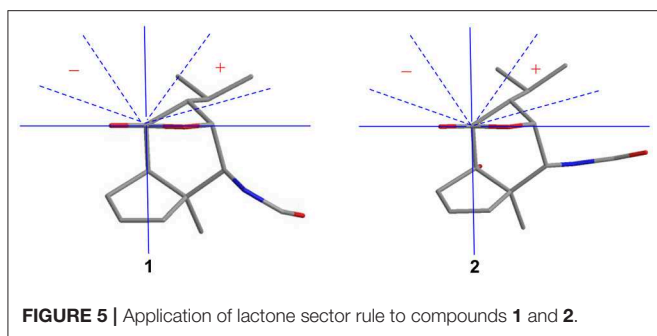
Compound **4**, colorless crystals, the molecular formula of which was established to be $C_{15}H_{20}O_5$ according to the pseudo-molecular ion peak at m/z 303.1228 [M + Na]$^+$ (calcd. for $C_{15}H_{20}O_5Na$: 303.1203) in the HRESIMS spectrum. The similarity of NMR data (**Table 1** and **Figure 2**) between **3** and **4** indicated that they have the same picrotoxane-type sesquiterpene skeleton. The only structural difference between them was CH-9 ($\delta_{C/H}$ 55.2/2.77) in **3** was oxygenated to a hydroxylated quaternary carbon (δ_C 85.1) in **4**, as supported by sequential COSY correlations of H-2/H-3/H-4/H-5/H-6/H-7/H-8, together with the HMBC correlations from H-2, H-6, H-7, and H$_3$-10 to C-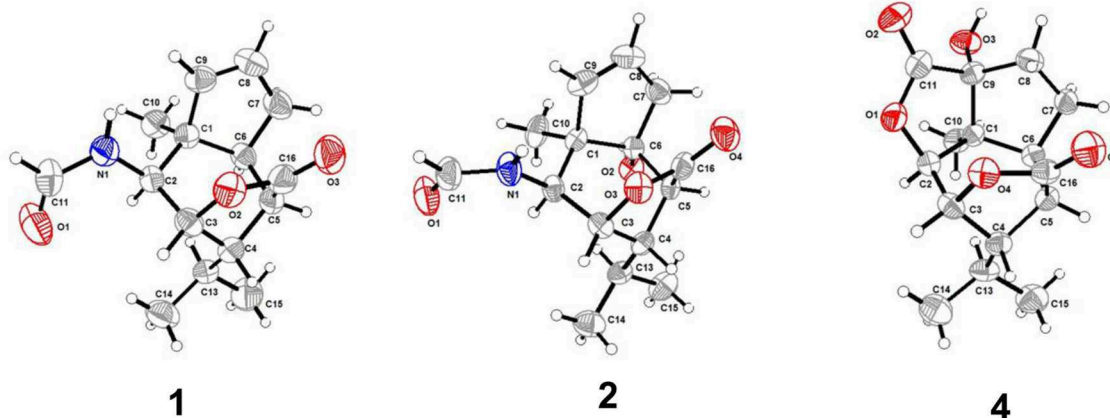9. The stereochemical structure of **4** (1*S*, 2*S*, 3*R*, 4*S*, 5*R*, 6*S*, and 9*R*), was determined by a single-crystal X-ray diffraction pattern obtained using the anomalous scattering of Cu Kα radiation (**Figure 4**). From a biosynthetic consideration, the absolute configurations of **4** were deduced be identical to those of **1**-**3**. Hence, compound **4** was also identified as a picrotoxane sesquiterpene as shown in **Figure 1**, named as dendroterpene D.

The Postulated Biosynthesis Pathway of Compounds 1–4

The carbon skeletons of previously reported picrotoxane-type sesquiterpenes are highly conserved.

The main skeletal changes are that one is the C-11-O-C-2 ring or the C-11-N-C-2 ring closure exemplified by dendrobiumane E and the other is the C-11-O-C-2 ring or the C-11-N-C-2 ring opening illustrated by dedrobiumane B. In our present study, the discovery of **1** and **2** with a new carbon skeleton containing a formamide group, which was derived from unprecedented carbon bond cleavage pattern prompted us to study its plausible biosynthetic pathways (**Figure 7**). Dendrobiumane B was assumed to be the biosynthetic precursor of **1**–**4**. Dendrobiumane **B** underwent oxidation to produce the intermediate (**A**). **A** underwent esterification and the C-11-O-C-2 ring closure produced compound **3**, which underwent oxidation to afford compound **4**. Dendrobiumane **B** underwent transamination to give the intermediate (**B**), which underwent oxidation to form intermediate (**C**). **C** underwent cyclization to produce intermediate (**D**), and **D** underwent dehydration to yield intermediate (**E**). **E** underwent oxidation to give intermediate (**F**), which underwent reduction and dehydration to produce compound **1**. Then, **1** underwent oxidation to get **2**.

Biological Activity

Compounds **1**–**8** were tested for inhibitory activity against α-glycosidase using the PNPG method and for cytotoxic effects on SGC-7901, K562, A549, BEL-7402, and Hela cell lines using the MTT method (See **Supplementary Table 1** in the Supplementary Material). The result showed that compounds **3**, **5**, **6**, and **8** exhibited potent inhibitory activity against α-glycosidase with IC$_{50}$ values of 0.97, 0.03, 0.68, and 0.30 mM, respectively (Acarbose as positive control with IC$_{50}$ value of 0.72 mM). Compound **5** displayed weak cytotoxic effects against SGC-7901, K562, A549, BEL-7402, and Hela cell lines with the IC$_{50}$ values of 17.30, 10.39, 29.03, 20.13, and 22.19 μM, respectively (Cisplatin as positive control with IC$_{50}$ values of 4.11, 3.08, 1.93, 4.02, and 11.29 μM), in addition, compound **6** showed cytotoxic effects against K562 with the IC$_{50}$ value of 28.23 μM.

CONCLUSIONS

In conclusion, four new picrotoxane-type sesquiterpenes (**1**–**4**), together with four known compounds (**5**–**8**), were isolated from the stems of *D. nobile*. Compounds **1** and **2** are two new picrotoxane-type sesquiterpenes with a new carbon skeleton containing a formamide group, which may be derived from the previously reported dendrobiumane B skeleton by the C(9)-C(11) carbon bond cleavage. In the previously report, picrotoxane sesquiterpenes exhibited the angiogenesis effect against sunitinibinduced damage (Meng et al., 2017) and inhibitory activity of nerve growth factor mediated neurite outgrowth (Leon et al., 2019). Compound **3** exhibited inhibitory activity against α-glycosidase with IC$_{50}$ values of 0.97 mM. However, compound **4** is inactive (IC$_{50}$ > 1 mM) against α-glycosidase, indicating that the hydroxyl at C-9 may reduce the activity. In addition, the known bibenzyl derivative nobilin E (**5**) exhibited inhibitory effects on NO production in activated murine macrophage-like cell line RAW 264.7 in the previously

FIGURE 7 | Hypothetical biogenetic pathway of compounds **1**–**4**.
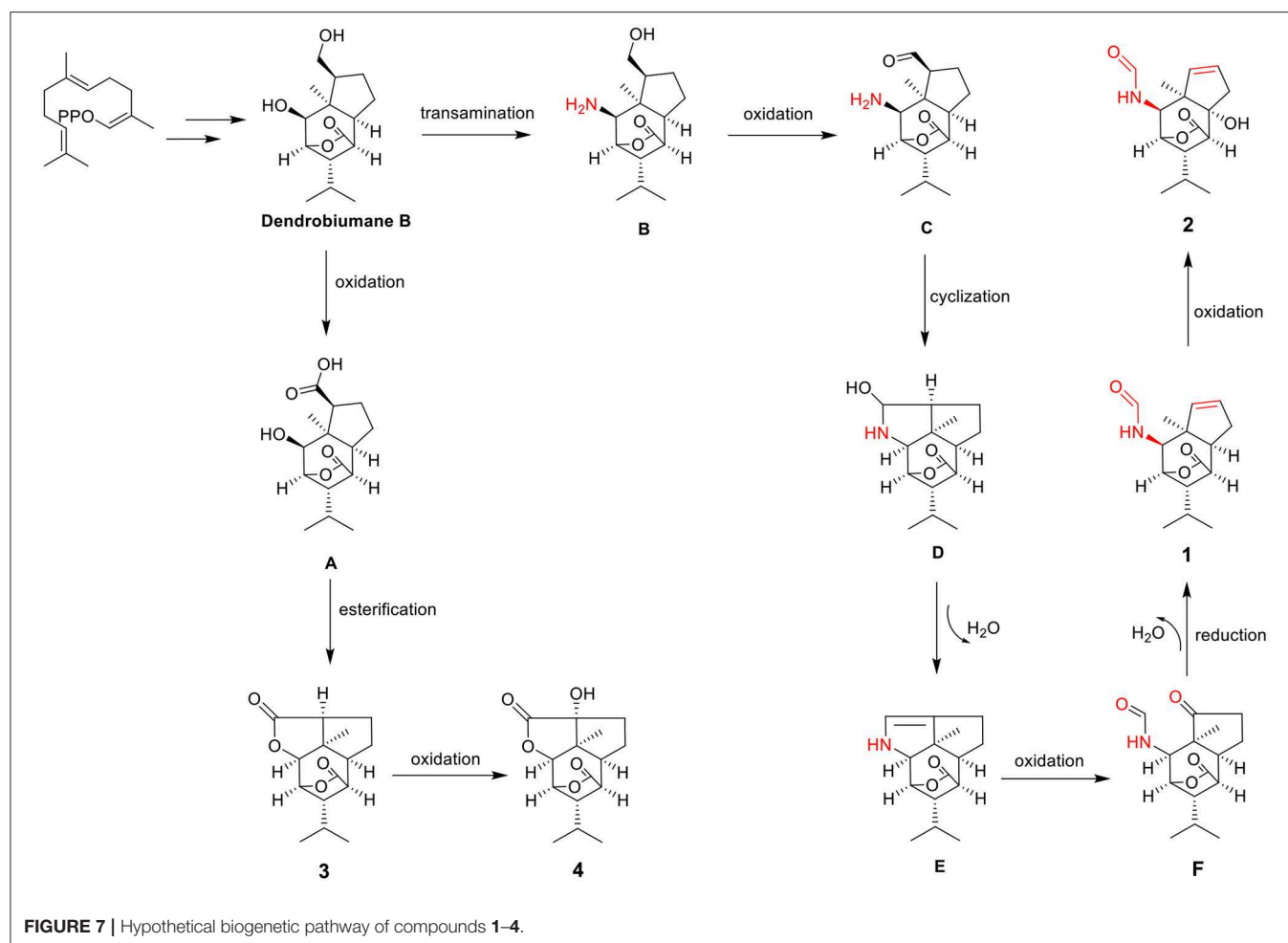
report (Zhang et al., 2007b). The bioactivities of the known bibenzyl derivative dendrocandin V (**6**) have not been reported. In this report, compounds **5** and **6** both exhibited inhibitory activity against α-glycosidase with IC$_{50}$ values of 0.03 and 0.68 mM, respectively. In addition, Compound **5** displayed weak cytotoxic effects against SGC-7901, K562, A549, BEL-7402 and Hela cell lines with the IC$_{50}$ values of 17.30, 10.39, 29.03, 20.13, and 22.19 μM, respectively. Compound **6** showed cytotoxic effect against K562 with the IC$_{50}$ value of 28.23 μM.

DATA AVAILABILITY STATEMENT

All datasets generated for this study are included in the article/**Supplementary Material**.

AUTHOR CONTRIBUTIONS

PW, XC, HW, CC, JY, and XX performed the experiments. PW and XC identified the structures. GZ performed ECD calculation. PW, HD, and WM conceived and designed the experiments. SH collected the fresh stems of *D. nobile*. PW wrote the paper. All authors have approved the final version of the manuscript.

FUNDING

SUPPLEMENTARY MATERIAL

The Supplementary Material for this article can be found online at: https://www.frontiersin.org/articles/10.3389/fchem.2019.00812/full#supplementary-material

These data include 1D and 2D NMR spectra of compounds **1**–**4**, CD spectra of **1** and **2**, and cytotoxic and α-glycosidase inhibitory activities of compounds **1**–**8**.

REFERENCES

Cammi, R., and Tomasi, J. (1995). Remarks on the use of the apparent surface charges (ASC) methods in solvation problems: Iterative versus matrix-inversion procedures and the renormalization of the apparent charges *J. Comput. Chem.* 16, 1449–1458. doi: 10.1002/jcc.540161202

Frisch, M. J., Trucks, G. W., Schlegel, H. B., Scuseria, G. E., Robb, M. A., Cheeseman, J. R., et al. (2004). *Gaussian 03, Revision C.01*. Wallingford, CT: Gaussian Inc.

Gross, E. K.U., Dobson, J.F., and Petersilka, M. (1996). Density functional theory of time-dependent phenomena. *Dens. Func. Theory II.* 81–172. doi: 10.1007/BFb0016643

Hwang, J. S., Lee, S. A., Hong, S. S., Han, X. H, Lee, C., Kang, S. J., Lee, D., et al. (2010). Phenanthrenes from *Dendrobium nobile* and their inhibition of the LPS-induced production of nitric oxide in macrophage RAW 264.7 cells. *Bioorg. Med.Chem.Lett.* 20, 3785–3787. doi: 10.1016/j.bmcl.2010.04.054

Jexkings, J. P., Klyne, W., and Scope, P. M. (1965). Optical rotatory dispersion. *Part XXIV. Lactones. J. Chem. Soc.* 7211–7229. doi: 10.1039/jr9650007211

Jiangsu New Medical College (1986). *Dictionary of Chinese Herb Medicines.* Shanghai: Shanghai Scientific and Technologic Press.

Jong, A. N., Bhandari, M. R., and Kawabata, J. (2007).α-Glucosidase inhibitors from Devil tree. *Food Chem.* 103. 1319–1323. doi: 10.1016/j.foodchem.2006.10.043

Kato, T., Tsunakawa, M., Sasaki, N., Aizawa, H., Fujita, K., Kitahara, Y., et al. (1977). Growth and germination inhibitors in rice husks. *Phytochemistry* 16, 45–48. doi: 10.1016/0031-9422(77)83010-0

Krysin, A. P., Egorova, T. G., and Vasil'ev, V. G. (2010). Thermolysis of 4-(ω- hydroxyl alkyl)-2,6-di-tert-butylphenols. *Russ. J. Gen. Chem.* 80, 275–283. doi: 10.1134/S1070363210020167

Leon, R. M., Ravi, D., An, J. S., Genio, C. L. D., Rheingold, A. L., Gaur, A.B., et al. (2019). Synthesis of C14-desmethylene corialactone D and discovery of inhibitors of nerve growth factor mediated neurite outgrowth. *Org. Lett.* 21, 3193–3197. doi: 10.1021/acs.orglett.9b00921

Liu, Q. F., and Zhao, W. M. (2003). A new dendrobine-type alkaloid from *Dendrobium nobile. Chinese Chem. Lett.* 14, 278–279.

Meng, C. W., He, Y. L., Peng, C., Ding, X. J., Guo, L., and Xiong, L. (2017). Picrotoxane sesquiterpenoids from the stems of *Dendrobium nobile* and their absolute configurations and angiogenesis effect. *Fitoterapia* 121, 206–211. doi: 10.1016/j.fitote.2017.07.017

Mosmann, T. (1983). Rapid colorimetric assay for cellular growth and survival: Application to proliferation and cytotoxicity assays. *J. Immunol. Methods* 65, 55–63. doi: 10.1016/0022-1759(83)90303-4

Wang, P., Kong, F. D., Wei, J. J., Wang, Y., Wang, W., Hong, K., et al. (2014). Alkaloids from the mangrove-derived actinomycete *Jishengella endophytica* 161111. *Mar. Drugs* 12, 477–490. doi: 10.3390/md12010477

Xiao, S. J., Weng, Q. H., Zhang, M. S., Nie, X. Q., Chen, Y. Z., He, Y. Q., et al. (2017). Dendrocandin V, a new compound separation from *Dendrobium nobile* and its extraction and separation method. Chinese Patent. 107021947A.

Zhang, X., Liu, H. W., Gao, H., Han, H. Y., Wang, N. L., Wu, H. M., et al. (2007a). Nine New Sesquiterpenes from *Dendrobium nobile. Helvetica Chimica Acta* 90, 2386–2394. doi: 10.1002/hlca.200790245

Zhang, X., Xu, J. K., Wang, J., Wang, N. L., Kurihara, H., Kitanaka, S., et al. (2007b). Bioactive Bibenzyl derivatives and fluorenones from *Dendrobium nobile. J. Nat. Prod.* 70, 24–28. doi: 10.1021/np060449r

Zhao, W., Ye, Q., Tan, X., Jiang, H., Li, X., Chen, K., et al. (2001). Three new sesquiterpene glycosides from *Dendrobium nobile* with immunomodulatory activity. *J. Nat. Prod.* 64, 1196–1200. doi: 10.1021/np0102612

Zhao, W. M., Ye, Q. H., Dai, J. Q., Martin, M. T., and Zhu, J.P. (2003). Allo-aromadendrane- and picrotoxane-type sesquiterpenes from *Dendrobium moniliforme. Planta. Med.* 69, 1136–1140. doi: 10.1055/s-2003-818005

Zhou, X. M., Zheng, C. J., Gan, L. S., Chen, G. Y., Zheng, X. P., Song, X. P., et al. (2016). Bioactive phenanthrene and bibenzyl derivatives from the stems of *Dendrobium nobile. J. Nat. Prod.* 79, 1791–1797. doi: 10.1021/acs.jnatprod.6b00252

Xuetonglactones A–F: Highly Oxidized Lanostane and Cycloartane Triterpenoids From *Kadsura heteroclita* Roxb. Craib.

Nuzhat Shehla [1,2†], Bin Li [1,2†], Liang Cao [1], Jianping Zhao [3], Yuqing Jian [1], Muhammad Daniyal [1], Atia-tul Wahab [4], Ikhlas A. Khan [3], Duan-fang Liao [1], Atta-ur Rahman [2], M. Iqbal Choudhary [1,2,4]* and Wei Wang [1,2]*

[1] TCM and Ethnomedicine Innovation and Development International Laboratory, Academician Atta-ur-Rahman Belt and Road Traditional Medicine Research Center, School of Pharmacy, Hunan University of Chinese Medicine, Changsha, China, [2] International Center for Chemical and Biological Sciences, H. E. J. Research Institute of Chemistry, University of Karachi, Karachi, Pakistan, [3] National Center for Natural Products Research, Research Institute of Pharmaceutical Sciences, University of Mississippi, Oxford, MS, United States, [4] Dr. Panjwani Center for Molecular Medicine and Drug Research, International Center for Chemical and Biological Sciences, University of Karachi, Karachi, Pakistan

Xuetonglactones A–F (**1**–**6**), six unreported highly oxidized lanostane- and cycloartane-type triterpenoids along with 22 known scaffolds (**7**–**28**) were isolated from the stems of *Kadsura heteroclita* (Roxb.) Craib. Compared with previous congeners, xuetonglactone A (**1**), possesses an unprecedented 20,21-α-epoxide, and xuetonglactone D (**4**) features an unusual 19-α-hydroperoxyl moiety. The structures and the absolute configurations of the compounds were established by extensive one- and two-dimensional NMR, and electronic circular dichroism (ECD) spectroscopic analysis, with those of **1** and **5** confirmed by single-crystal X-ray diffraction technique. Compounds **1** and **2** exhibited inhibition of iNOS activity in LPS-induced macrophages with IC$_{50}$ values of 22.0, and 17.0 μg/mL, respectively. While compounds **6**, **7**, **8**, and **24** showed potent cytotoxic activities against human cervical cancer cell lines (HeLa) with the IC$_{50}$ values of 4.0, 5.8, 5.0, and 6.4 μM, and against human gastric cancer cells (BGC 823) with the IC$_{50}$ values of 2.0, 5.0, 2.5, and 2.0 μM, respectively. Moreover, plausible biogenetic pathways of (**1**–**6**) were also proposed.

Keywords: xuetonglactones, highly oxidized, lanostane triterpenoids, *Kadsura heteroclita*, cytotoxicity

INTRODUCTION

Schisandraceae family has contributed to the novel chemical scaffolds with an array of biological activities in past three decades. The family comprises of around fifty plant species belongs to genus *Kadsura* and *Schisandra* that are widely distributed in East, and Southeast Asia. The family has derived significant interest due to its highly oxygenated lanostane- and cycloartane-type triterpenoids, and dibenzocyclooctadiene lignans, along with schinortriterpenoids which are the characteristics isolates (Xiao et al., 2008; Shi et al., 2015). These constituents demonstrated potential pharmacological effects e.g., anti-hepatitis, anti-HIV, anti-inflammatory, anti-cancer, and inhibitory effect in cholesterol biosynthesis (Pu et al., 2008; Liu et al., 2014; Hu et al., 2015; Su et al., 2015).

GRAPHICAL ABSTRACT | Structures of **1–6**.
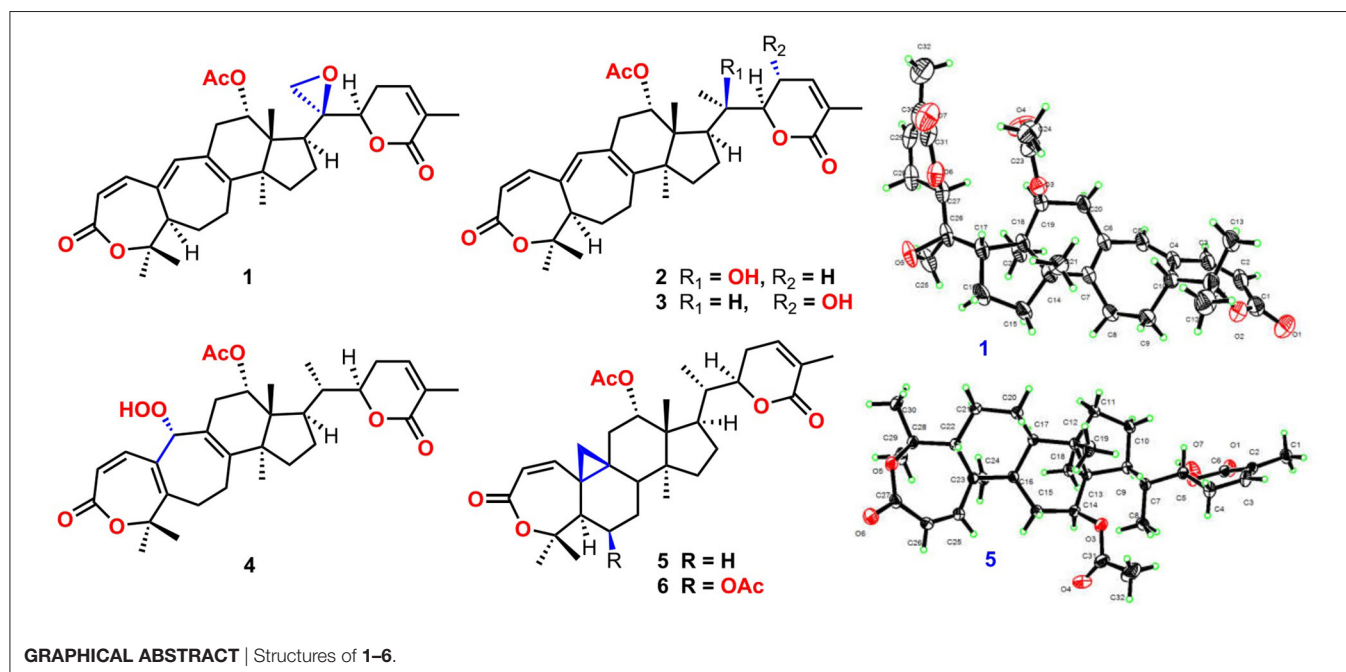
Kadsura heteroclita (Roxb.) Craib. of the genus *Kadsura* is a climbing species primarily grows in Southwestern China, has a long history of its folk use in Traditional Chinese Medicine (TCM) (Pu et al., 2008; Liu et al., 2014). The stems of *K. heteroclita* traditionally known as "Xuetong" has long been consumed for the treatment of rheumatoid arthritis, traumatic injuries, deudenal ulcers, and cancers, particularly by Tujia people living in Wulin mountains area. In "Tujia" dialect "Xue" (blood) herbs are commonly used for the treatment of these diseases by activating the blood circulation, relieving pain and eliminating dampness for centuries (Liu et al., 2016, 2018; Cao et al., 2019). This study aimed to trace back the biologically active chemical constituents responsible for its clinical application contained within the plant species. Recently, we reported the identification of several new sesquiterpenoids, and lignanoids from *K. heteroclita* and other species of the same genus (Liu et al., 2018; Cao et al., 2019). Our previous pharmacological studies displayed this plant has very good anti-rheumatoid arthritis, anti-inflammatory, and analgesic effects (Yu H. et al., 2019; Yu H. H. et al., 2019).

In course of our continuous efforts to crack the immense diversity in structural frameworks with untapped biological potential, herein four new lanostane-type triterpenoids xuetonglactones A–D (**1–4**), and two cycloartane-type triterpenoids xuetonglactones E–F (**5–6**) possessing differently highly oxidized sites, were reported from *K. heteroclita*. Structurally, xuetonglactones A and D (**1**, **4**) exhibited unique oxidized functionalities, featuring unprecedented 20,21-α-epoxy group in xuetonglactone A, and rare 19-α hydroperoxyl moiety in xuetonglactone D skeletons. The compounds were also evaluated for their cytotoxicity and anti-inflammatory activities. Hence, in this report, the details of isolation, structure

elucidation, biological evaluation, and possible biosynthetic pathways of (**1–6**) were described. The spectroscopic data of **1–6** is presented in the Supplementary Material (**Figures S1–S48**).

RESULTS AND DISCUSSION

Compound **1** was purified as a white crystalline solid, and the molecular formula was deduced to be $C_{32}H_{40}O_7$ from HRESI-MS spectrum (positive ion mode) on the basis of $[M + Na]^+$ ion at m/z 559.2671 (559.2672 calculated for $C_{32}H_{40}O_7 + Na$) indicating 13 degrees of unsaturation. A 3,4-secocycloanostane skeleton was deduced from the ^1H- and ^{13}C-NMR chemical shifts data with two α, β-unsaturated lactone rings, one of them being a seven membered ring in this triterpenoidal skeleton. This deduction was also supported by IR absorptions at 1,720, and 1,685 cm^{-1} for six- and seven-membered unsaturated lactone carbonyls and by UV absorptions (λ_{max}) at 202, and 329 nm, respectively. The ^1H-NMR data of **1** (**Table 1**) showed the presence of six tertiary methyl singlets (3H each, δ_H 0.71, 1.90, 1.53, 1.41, 1.39, and 2.12), four olefinic methines at δ_H 6.65 (d, $J_{1, 2} = 12.3$ Hz, H-1), 5.82 (d, $J_{2, 1} = 12.0$ Hz, H-2), 6.14 (s, H-19), and 6.51 (broad d, $J_{24, 23} = 4.8$ Hz, H-24), and two oxygenated methines at δ_H 5.14 (d, $J_{12\beta, 11} = 7.4$, H-12), and 4.49 (dd, $J_{22, 23\beta} = 12.7$ Hz; $J_{22,23\alpha} = 3.7$ Hz, H-22). The ^{13}C-NMR data (**Table 2**) displayed 32 carbon signals attributed to six tertiary methyls (δ_C 18.6, 16.9, 26.2, 29.3, 27.9, and 21.6), eight methines including four olefinic (δ_C 143.2, 118.3, 141.7, and 137.6), and two oxygenated methines (δ_C 71.9, and 78.3), seven methylenes, and eight quaternary carbons, including four olefinic (δ_C 151.1, 126.4, 140.4, and 128.2), and two oxygenated (δ_C 80.3, and 58.1) quaternary carbons. Furthermore, it also showed the presence

TABLE 1 | ^{1}H NMR data of **1–6** in CDCl$_3$ (δ_H in ppm, J in Hz within the parenthesis).

No.	1[a]	2[a]	3[b]	4[b]	5[b]	6[a]
1	6.65, d (12.3)	6.66, d (12.3)	6.68, d (12.3)	6.58, d (12.2)	6.05, d (12.7)	6.00, d (12.8)
2	5.82, d (12.0)	5.81, d (12.0)	5.83, d (12.1)	6.21, d (12.0)	5.94, d (12.6)	5.93, d (12.7)
3	–	–	–	–	–	–
4	–	–	–	–	–	–
5	2.44, m	2.48, m	2.47, m	–	2.42, dd (13.0, 4.7); 1.62, m	2.54, d (3.5)
6	2.27, m	2.25, m	3.12, 2.59 m	3.20, t (13.4, 1); 2.34, m	1.90, m; 0.76, m	5.31, brs
7	1.92, m	1.91, m	2.13, 1.94 m	2.04, m; 2.40, m	1.18, m	1.84, m
8	–	–	–	–	1.62, m	1.78, dd (13.5, 4.0)
9	–	–	–	–	–	–
10	–	–	–	–	–	–
11	2.10, m	2.10, m	2.81, m; 2.13, m	2.80, dd (19.6, 8.0); 2.49 d (19.6)	2.00, dd (15.2, 5.2); 2.32, m	2.01, m
12	5.14, d (7.4)	5.31, d (7.2)	5.03, d (7.5)	4.94, d (7.9)	4.85, dd (8.8, 5.3)	4.87, dd (9.2, 5.7)
13	–	–	–	–	–	–
14	–	–	–	–	–	–
15	1.45, m	1.44, m	1.74, 1.44 m	1.67, m; 131, m	1.39, m	1.30, m
16	1.25, m	1.71, m	2.15, 1.53, m	1.89, m; 1.51, m	1.46, m	1.25, m
17	3.55, dd (10.9, 7.5)	2.70, m	2.66, m	2.11, m	2.22, m	2.23, m
18	0.71, s	0.96, s	0.75, s	0.76, s	1.01, s	1.05, s
19	6.14, s	6.16, s	6.18, s	4.61, s	1.15, d (2.6), 1.38 (overlapped)	1.30, dd (4.7)
20	–	–	2.04, m	2.10, m	2.01, m	2.02, m
21	2.75, dd (3.3)	1.33, s	0.98, d (7.0)	0.89, d (6.5)	0.85, d (6.7)	0.86, d (6.7)
22	4.49, dd (12.7, 3.7)	4.14, dd (12.7, 3.8)	4.34, dd (9.4, 2.5)	4.46, d (13.1)	4.48, dt (13.0, 3.2)	4.48, dd (9.8, 3.3)
23	2.03, m	2.32, m	4.56, br. d (7.7)	2.36, m; 2.11, m	2.11, m	2.14, m
24	6.51, dd (4.8, 1.6)	6.60, dd (4.6, 1.7)	6.480, s	6.60, s	6.61, d (6.0)	6.61, d (6.0)
25	–	–	–	–	–	–
26	–	–	–	–	–	–
27	1.90, s	1.91, s	1.93, s	–	1.92, s	1.92, s
28	1.53, s	1.54, s	126, s	1.13, s	1.35, s	1.47, s
29	1.41, s	1.41, s	1.54, s	1.64, s	1.38, s	1.42, s
30	1.39, s	1.32, s	1.41, s	1.67, s	1.01, s	1.03, s
OCOCH$_3$-12	2.12, s	2.13, s	2.09, s	2.05, s	2.04, s	2.04, s
OCOCH$_3$-6	–	–	–	–	–	2.05, s

[a] *Recorded at 500 MHz.*
[b] *Recorded at 600 MHz.*
Internal standard: TMS; In ^{1}H-NMR s, brs, d, dd, and m represent singlet, broad singlet, doublet, double doublet, and multiplet or overlapped signals, respectively.

of three carbonyl signals (δ_C 171.0, δ_C 166.3, and δ_C 165.0) corresponding to an acetoxy (C-12), and two lactone (C-3, and C-26) moieties, respectively. The ^{1}H- and ^{13}C-NMR chemical shifts data of **1** showed resemblances with that of known compound heteroclitalactone D (**17**) (Wang et al., 2006b) with obvious distinctions observed for resonances at C-17, C-20, and C-21. The detailed analysis of the NMR data established the structure of compound **1** bearing unprecedented oxirane in the structure at C-20. The NMR data revealed the presence of an extra methylene (δ_C 46.88, C-21) with a characteristic proton doublet (δ_H 2.75; and 2.96, dd, $J_{21a, 21b}$ = 3.3 Hz each, H-21) which supported the presence of additional ring at C-20 as epoxide to fulfill the

unsaturation demand in skeleton of **1**. Furthermore, the up-field shift of quaternary carbon (δ_C 58.12) at C-20 suggested the presences of epoxide at this junction, which could be attributed to the steric shielding effect of the strained ring at this position. These assignments were unambiguously confirmed by HMBC experiments, in which the epoxide methylene protons appeared at δ_H 2.75, and 2.96 (dd, $J_{21a, 21b}$ = 3.3 Hz each, H-21) were correlated with C-20 and C-22, while C-17 methine proton at δ_H 3.55 (dd, $J_{17, 16a}$ = 10.9, $J_{17, 16b}$ = 7.5 Hz) was correlated with C-12, C-14, C-16, C-18, C-20, and C-21 (**Figure 2**). This oxidized strained ring along with the presence of three conjugated double bonds, and other oxygenated moieties in the skeleton further

TABLE 2 | ^{13}C-NMR data of **1–6** in CDCl$_3$ (δ in ppm).

No.	1[a]	2[a]	3[b]	4[b]	5[b]	6[a]
1	143.2, d	143.5, d	143.5, d	142.8, d	150.0, d	149.4, d
2	118.3, d	118.1, d	118.1, d	123.7, d	120.9, d	120.5, d
3	166.3, s	167.0, s	167.1, s	167.0, s	167.3, s	166.4, s
4	80.3, s	80.3, s	80.4, s	81.5, s	84.5, s	83.4, s
5	49.2, d	49.2, d	49.2, d	153. 1, s	46.7, d	48.1, d
6	39.5, t	39.7, t	37.4, t	26.6, t	24.8, t	70.3, d
7	28.0, t	28.0, t	27.2, t	26.9, t	25.0, t	28.7, t
8	151.1, s	150.9, s	151.4, s	147.5, s	46.8, d	40.7, d
9	126.4, s	126.6, s	126.7, s	121.2, s	27.1, s	29.7, s
10	140.7, s	140.3, s	140.4, s	133.7, s	33.0, s	31.7, s
11	35.4, t	35.2, t	35.2, t	39.2, t	37.5, t	37.4, t
12	71.9, d	74.0, d	73.8, d	74.1, d	75.0, d	74.6, d
13	52.3, s	51.2, s	51.6, s	51.1, s	48.4, s	47.8, s
14	48.5, s	49.3, s	48.2, s	47.8, s	48.8, s	48.5, s
15	31.9, t	32.3, t	32.0, t	30.6, t	36.2, t	36.6, t
16	20.9, t	23.5, t	27.9, t	26.3, t	26.8, t	26.8, t
17	35.5, d	41.2, d	39.4, d	39.3, d	40.1, d	40.0, d
18	18.6, q	18.5, q	16.3, q	16.3, q	16.7, q	16.6, q
19	141.7, d	142.1, d	142.2, d	90.3, d	32.9, t	35.6, t
20	58.1, s	75.9, s	39.7, d	38.9, d	39.1, d	39.0, d
21	46.9, t	21.5, q	13.7, q	12.5, q	12.1, q	120, q
22	78.3, d	84.3, d	84.6, d	80.0, d	80.3, d	80.1, d
23	24.3, t	24.4, t	64.0, d	23.4, t	23.4, t	23.3, t
24	137.8, d	139.0, d	143.7, d	139.0, d	139.3, d	139.0, d
25	128.2, s	128.3, s	127.8, s	128.5, s	128.6, s	128.5, s
26	165.0, s	165.3, s	165.0, s	166.3, s	166.5, s	166.2, s
27	16.9, q	17.0, q	16.7, q	17.0, q	17.2, q	17.0, q
28	26.2, q	26.2, q	27.6, q	28.2, q	22.4, q	24.0, q
29	29.3, q	29.2, q	26.3, q	24.6, q	29.2, q	28.0, q
30	27.9, q	28.2, q	29.2, q	24.6, q	20.5, q	20.6, q
OCOCH$_3$-12	171.0, s	171.4, s	170.2, s	170.0, s	170.1, s	169.8, s
OCOCH$_3$-12	21.6, q	21.8, q	21.4, q	21.3, q	21.5, q	21.1, q
OCOCH$_3$-6	–	–	–	–	–	169.5, s
OCOCH$_3$-6	–	–	–	–	–	21.3, q

[a] Recorded at 500 MHz.
[b] Recorded at 600 MHz.
Internal standard: TMS; In ^{13}C-NMR d, t, q, and s represent methine, methylene, methyl, quaternary carbons; Chemical shifts assignments based on DEPT, HSQC, and HMBC data.

supported the structure of **1** is based on a highly oxidized cyclolanostane type triterpenoidal skeleton (Chen et al., 2001; Wang et al., 2006a). Chemical shifts assignments were made on the basis of HSQC, HMBC, and ^{1}H-^{1}H COSY experiments to get the planner structure of **1**. The α-configuration of the C-12 (acetoxy group) was concluded based on the ROESY cross peaks between H-12 and CH$_3$-18 (**Figure 3**). In the ECD spectrum, compound **1** showed a positive Cotton effect at 255 nm ($\Delta\varepsilon$ = + 5.64) which was similar to that of schiglausin A (Zou et al., 2012), indicating an *R* configuration of C-22. Combining the observed ROESY correlations of H-5 with CH$_3$-30, CH$_3$-30 with H-17, H-17 with H-22, the ECD spectrum, and the X-ray diffraction using Cu Kα radiation (**Figure 4**), the absolute
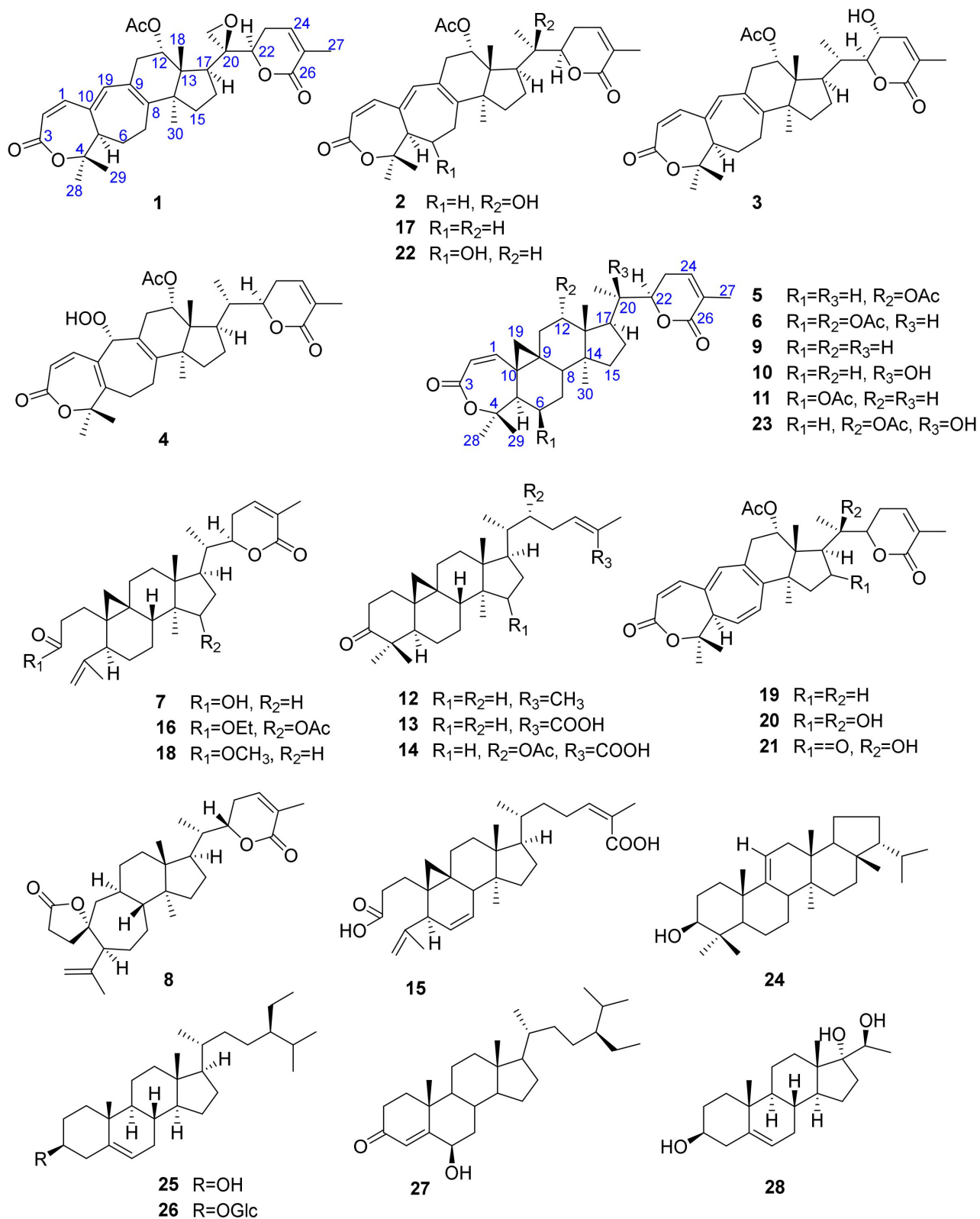
stereochemistry of the seven chiral centers, were determined as 5*S*, 12*S*, 13*R*, 14*S*, 17*R*, 20*S*, and 22*R*. Thus, the structure of **1** was fully established as shown (**Figure 1**) and named xuetonglactone A.

Compound **2** was obtained as a white amorphous solid. Its molecular formula was determined to be C$_{32}$H$_{42}$O$_7$ based on [M + Na]$^+$ ion at *m/z* 561.2828 (561.2829 calculated for C$_{32}$H$_{42}$NaO$_7$) and [M + Cl]$^-$ peak at *m/z* 573.2612 (573.2619 calculated for C$_{32}$H$_{42}$O$_7$ + Cl) from its HRESI-MS spectra (positive ion and negative ion modes), corresponding 12 degrees of unsaturation. The ^{1}H-NMR chemical shifts data (**Table 1**) of **2** showed the presence of seven tertiary methyl singlets (3H each, δ_H 0.96, 1.32, 1.33, 1.41, 1.54, 1.91, and 2.13). By comparing the NMR chemical shifts data of compound **2** with that of **1** which has a methylene at position C-21, hence the presence of a tertiary methyl (δ_H 1.33, s, C-21) instead of epoxide, in the skeleton of **2** was inferred. Furthermore, relative configuration on ring C was same as of **1**, based on similar ROESY correlations. While the absence of ROESY cross peaks between CH$_3$-21 and CH$_3$-18 thus appearance of cross peaks between CH$_3$-21 and H-17/H-22 (**Figure 3**) suggested the β-orientation of OH-20. The assignment of the absolute configuration at C-22 was concluded to be *R* by the similar ECD measurement as that of **1**. Therefore, the structure of **2** was established as shown (**Figure 1**) and named xuetonglactone B accordingly.

Compound **3** was obtained as a white amorphous solid and possess the same molecular formula with **2** as C$_{32}$H$_{42}$O$_7$ based on [M + Na]$^+$ ion at *m/z* 561.2836 (561.2828 calculated for C$_{32}$H$_{42}$O$_7$ + Na) from its HRESI-MS spectrum (positive ion mode). The spectroscopic data of **3** (**Tables 1, 2**) was quite similar with those of **2** except for a secondary methyl (δ_H 0.98, $J_{21,20}$ = 7.0 Hz, H-21) instead of tertiary, and a broad doublet of oxymethine (δ_H 4.56, $J_{23, 22}$ = 7.7 Hz, δ_C 64.0, H-23) instead of methylene protons in the skeleton of **3**. These observations were also confirmed by HMBC cross peaks of H-20 with C-23, and that of H-22 with C-17, C-23, and C-21, and C-24. Furthermore, α-configuration of the acetoxy group was determined by the similar cross peaks between H-12 and CH$_3$-18 in NOESY spectrum (**Figure 3**). A strong negative Cotton effect at 273 nm [$\Delta\varepsilon$ (273) = +0.41, MeOH] was observed in the experimental ECD spectrum of **3**. The absolute configuration at C-22 was established as *S* by comparison of its ECD spectrum with analog colossolactone VIII (El Dine et al., 2008). Furthermore, the large coupling constant (9.4 Hz) between H-23 and H-22 indicated an anti-conformation of these two protons (Lakornwong et al., 2014), hence the absolute configuration of these two chiral centers were found to be 22*S*, and 23*R*. Consequently, compound **3** was determined and given the trivial name xuetonglactone C.

Compound **4** was isolated as yellow, amorphous solid. Its molecular formula was deduced as C$_{32}$H$_{42}$O$_8$ on the basis of [M + Na]$^+$ ion peak at *m/z* 577.2772 in the HRESI-MS (577.2777 calculated for C$_{32}$H$_{42}$O$_8$ + Na), suggesting 12 degrees of unsaturation. Since the NMR resonances of **4** were similar to those of known compound **17** (Wang et al., 2006b) with some obvious discrepancies, therefore detailed comparison of the chemical shifts data revealed that both compounds have similar C/D/E rings system in the skeleton. However, different

FIGURE 1 | Structures of 1–28.

FIGURE 2 | Key HMBC and ^{1}H-^{1}H COSY correlations of **1**–**6**.

FIGURE 3 | Key ROESY/NOESY correlations of **1**–**6**.
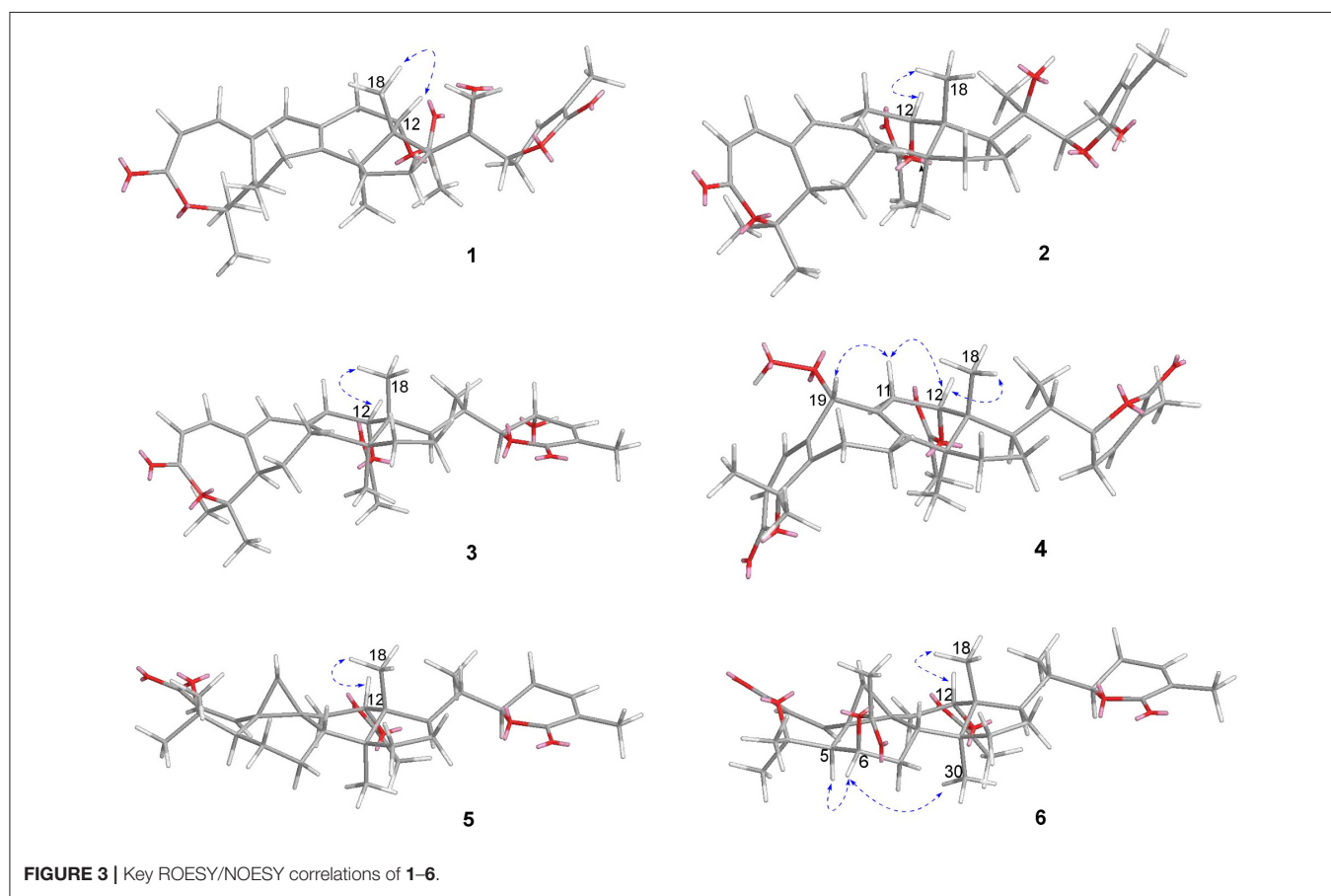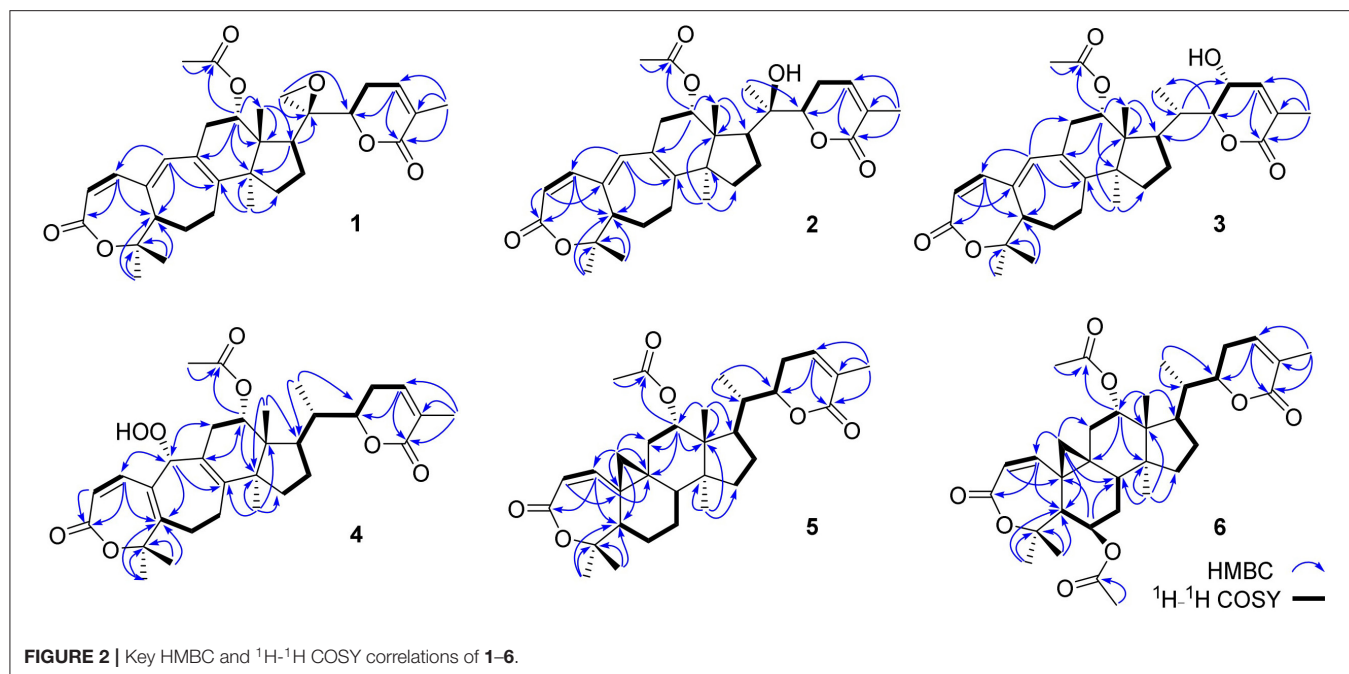
^{1}H- and ^{13}C-NMR chemical shifts were observed for C-5, C-6, C-10, and C-19 suggesting the major skeletal difference of **4** corresponds to the rings A/B. The double bond between C-10 and C-19 in **17** shifted in between C-5 (δ_C 153.1) and C-10 (δ_C 133.7) in **4**. This inference was further supported by the HMBC correlation of H-1 (δ_H 6.58, d, $J_{1,2}$ = 12.2 Hz), H-19 (δ_H 4.61, s), H$_3$-29 (δ_H 1.64, s), and H$_3$-30 (δ_H 1.67, s) with C-5, and of H-2 (δ_H 6.21, d, $J_{2,1}$ = 12.0 Hz) and H-19 with C-10. Furthermore, C-19 was connected with an unusual hydroperoxyl group, which was supported by the carbon resonance observed at δ_C 90.3 and the methine proton signal at δ_H 4.61 (1H, s) (Song et al., 2013), which was also confirmed by HMBC cross peaks of H-1 and H-11 to C-19, and H-19 to C-1, C-5, C-8, C-9, C-10, and C-11. α oriented 12-acetoxyl group was ascertained on the basis of NOESY cross peak between H $_\beta$-12 and CH$_3$-18, the significant NOESY correlations between H$_\beta$-12 /H$_\beta$-11 (δ_H 2.82, $J_{H\beta-11/H\alpha-11}$ = 19.6, $J_{H\beta-11/H\beta-12}$ 8.0 Hz), and H$_\beta$-11/H$_\beta$-19 indicated that the hydroperoxyl group should be α-orientated (**Figure 3**). The absolute configuration 22*R* could be delineated by similar ECD relationship (Wang et al., 2006b). Hence the structure of **4** was determined and given a trivial name xuetonglactone D accordingly.

Compound **5** was obtained as white crystalline. The HRESI-MS spectrum of **5** displayed [M + Na]$^+$ ion peak at *m/z* 547.3047 (547.3036 calculated for C$_{32}$H$_{44}$O$_6$ + Na), corresponding to the molecular formula of C$_{32}$H$_{44}$O$_6$ indicative of 11 degrees of unsaturation. The IR spectrum showed absorptions at 1,721, and 1,679 cm^{-1} suggesting two lactone moieties in the skeleton. A 3,4-secocycloartane skeleton was deduced from ^{1}H- and ^{13}C-NMR chemical shifts data (**Tables 1, 2**). The ^{1}H-NMR spectrum of **5** showed characteristic signals for the cyclopropyl methylene protons at δ_H 1.15 (d, $J_{19a, 19b}$ = 2.6 Hz), and 1.38 (overlapped), but unlike the known compound **7** (Liu and Huang, 1991), the downfield shift of cyclopropane protons was due to the deshielding effect of conjugated double bond in ring A. The ^{1}H-NMR also displayed six tertiary methyl singlets (δ_H 1.01, 1.92, 1.35, 1.38, 1.01, and 2.04), and a secondary methyl proton at δ_H 0.85 (d, $J_{21, 20\beta}$ = 6.7 Hz, H-21). In ^{13}C-NMR spectrum presence of 32 carbon signals (**Table 2**) could be assigned to six tertiary (δ_C 16.7, 17.2, 22.4, 29.2, 20.5, and 21.5), and a secondary methyl (δ_C 12.1), ten methines, seven methylenes, and nine quaternary carbons including three carbonyl (δ_C 167.3, 166.5, and 170.1), an oxygenated (δ_C 84.5), and an olefinic quaternary carbons (δ_C 128.6), as well as two oxygenated (δ_C 75.0, and 80.3), and three olefinic methine (δ_C 150.0, 120.9, and 139.3) signals. In comparison of **3**, the major difference in ^{1}H- and ^{13}C-NMR chemical shifts data of **5** was obvious owing to absence of a pair of olefinic carbons and a proton in ring B, thus appearance of a C-19 cyclopropane ring proton doublets (δ_H 1.15, d, $J_{19a, 19b}$ = 2.6 Hz), and 1.38 (overlapped) corresponding to δ_C 32.9 instead in the structure. These distinctions were confirmed by the key correlations observed in ^{1}H-^{1}H COSY, and HMBC spectra. In HMBC spectrum CH$_2$-19 protons correlated with C-1, C-10, C-5, C-8, C-9, and C10. Additionally, the ^{1}H-^{1}H COSY interactions between H-11/H12, H-20/H-21, H-20/H-22, H-22/H-23, and H-23/H-24 spin systems were consistent with the unambiguous spectral assignments based on HSQC, and

1 (a)

5 (b)

7 (c)

FIGURE 4 | X-ray structures of **1**(a), **5**(b), and **7**(c).

HMBC interactions (**Figure 2**). Moreover, α-configurations of 12-OCOCH$_3$ was determined by ROESY spectrum (**Figure 3**). Since a strong positive cotton effect at 272 nm ($\Delta\varepsilon$ = +3.31, MeOH) was observed, the absolute configuration at C-22 in **5** was consequently assigned as *R*-configuration by ECD measurement. The absolute configuration at C-22 in **5**, named xuetonglactone

FIGURE 5 | Plausible biosynthetic pathway for **1–6**.

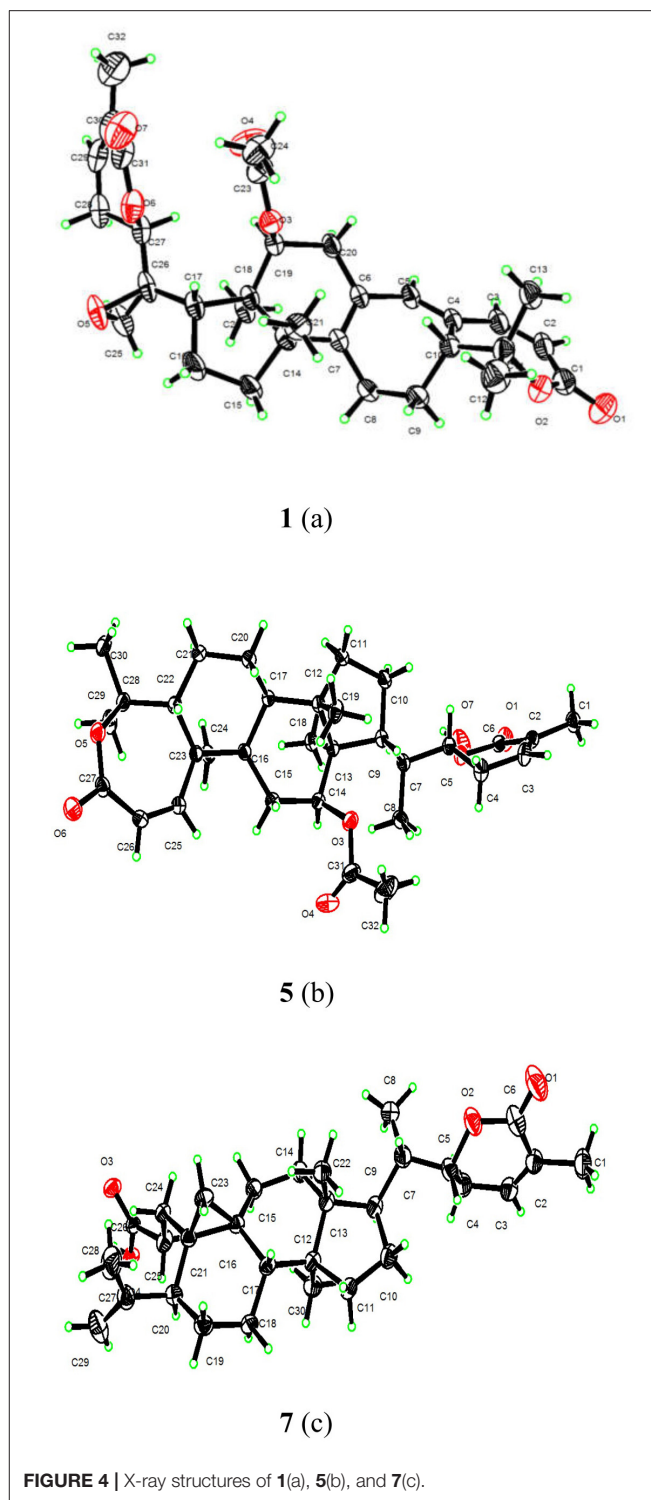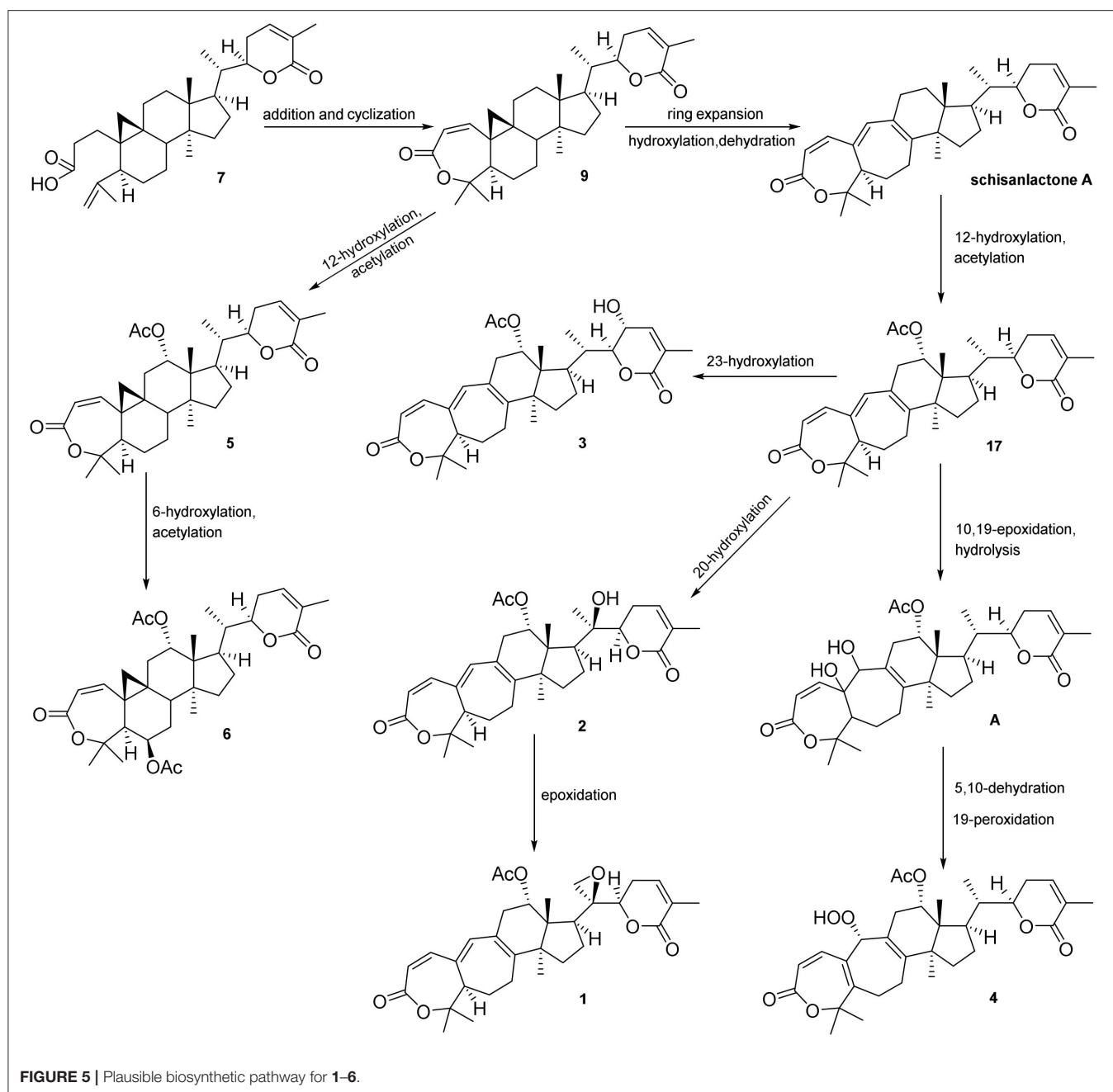E was also further confirmed by single crystal X-ray diffraction technique (**Figure 4**).

Compound **6** was purified as white amorphous solid. The molecular formula was assigned as $C_{34}H_{46}O_8$ based on molecular ion peak at 617.2884 m/z $[M + Cl]^-$ (617.2881 calculated for $C_{34}H_{46}O_8 + Cl$) in the HRESI-MS spectrum, which was indicative of 12 unsaturation degrees. The ^{13}C-NMR spectrum of **6** exhibited 34 carbon resonances, attributed to seven tertiary, and a secondary methyls, 10 methines, 6 methylenes, and 10 quaternary carbons. Four ester carbonyls (δ_C 166.4, 166.2, 169.5, 169.8, and) corresponding to C-3, C-26, OCOCH$_3$-6, and

OCOCH$_3$-12, respectively were observed in **6**. The ^1H- and ^{13}C-NMR chemical shifts data of **6** (**Tables 1**, **2**) were extremely similar to those of **5**, and the major difference embodied in the chemical shift of C-6 (δ_H 5.31, δ_C 70.3) suggesting the appearance of an additional acetyl group at C-6 [δ_H 2.05 (δ_C 21.3, 169.5)], thus absence of a methylene, and appearance of an oxygenated methine in **6**. Furthermore, configurations of 6-OCOCH$_3$ and 12-OCOCH$_3$ were determined based on the ROESY cross peaks of H-5/H-6/CH$_3$-30/ and H-12/CH$_3$-18, so β- 6-OCOCH$_3$ and α-12-OCOCH$_3$ were inferred (**Figure 3**). The ECD spectrum of **6** was the same with that of **5**, hence C-22 was assigned to the

R-configuration, thus the absolute structure was determined as shown (**Figure 1**), and named xuetonglactone F accordingly.

Xuetongsu (schisanlactone E, **7**) (Liu and Huang, 1991) was isolated as colorless crystal. The X-ray diffraction data of **7** was reported for the first time in this report (**Figure 4**). It was the major compound in "Xuetong" (Wang et al., 2006c). Biosynthetically, it might be the precursor of compounds **1–6**, through series of oxidative cleavage *via* Baeyer-Villiger oxidation, ring expansion, hydroxylation, cyclization, acetoxylation, and epoxidation steps yielded compounds **1–6**. A plausible biogenetic route for **1–6** was proposed as shown in **Figure 5**.

Twenty-two known analogous (**7–28**) were identified by analysis of their spectroscopic data with the reported data for xuetongsu (schisanlactone E, **7**) 10.8 g (Liu and Huang, 1991), kadnanolactone A (**8**) 5.0 mg (Yang et al., 2010), schisanlactone B (**9**) 25.0 mg (Liu et al., 1983), kadsuphilactone B (**10**) 6.8 mg (Shen et al., 2005), schisanbilactone A (**11**) 4.0 mg (Ma et al., 2009), cycloartenone (**12**) 2.5 g (Pavanasisivam and Sultanbawa, 1973), schisandronic acid (**13**) 18.2 mg (Li et al., 2003), heteroclic acid (**14**) 5.6 mg (Wang et al., 2006b), changnanic acid (**15**) 18.0 mg (Liu and Huang, 1991), heteroclitalactone C (**16**) 5.5 mg (Wang et al., 2006b), heteroclitalactone D (**17**) 42.0 mg (Wang et al., 2006b), heteroclitalactone F (**18**) 7.0 mg (Wang et al., 2006b), heteroclitalactone G (**19**) 22.0 mg (Wang et al., 2007), heteroclitalactone I (**20**) 6.5 mg (Wang et al., 2007), heteroclitalactone K (**21**) 12.5 mg (Wang et al., 2007), heteroclitalactone L (**22**) 15.3 mg (Wang et al., 2007), heteroclitalactone M (**23**) 17.3 mg (Wang et al., 2007), sorghumol (**24**) 12.9 mg (Han et al., 2008), β-sitosterol (**25**) 100 mg (Chaturvedula and Prakash, 2012), daucosterol (**26**) 10.0 mg (Rahmana et al., 2009), 6β-hydoxysitostenone (**27**) 7.6 mg (Liang et al., 2015), and a steroid, trihydoxy pregnene (**28**) 13.0 mg (Deng et al., 2010). Their structures are presented in **Figure 1**.

Anti-inflammatory activity of the compounds **1–6** were evaluated for their inhibitory effects against iNOS, and NF-κB activation. Compounds **1** and **2** showed inhibition of iNOS activity in LPS-induced macrophages with the IC_{50} values of 22.0, and 17.0 μg/mL (**Table 3**), respectively, while parthenolide was used as control drug (**Table 3**), unfortunately no inhibitory effects found against NF-κB expression (Zhao et al., 2014). Additionally, cytotoxic activities of all the compounds against HeLa and BGC-823 cancer cell lines were also evaluated (**Table 4**). Compounds **6**, **7**, **8**, and **24** showed strong cytotoxicities against HeLa cancer cell lines with the IC_{50} values of 4.0, 5.8, 5.0, and 6.4 μM, and against BGC 823 with the IC_{50} values of 2.0, 5.0, 2.5, and 2.0 μM, respectively, while compared with paclitaxel as positive control (**Table 4**; Hayon et al., 2003).

MATERIALS AND METHODS

General Experimental Procedure

Optical rotations were measured on a PerkinElmer 341-MC digital polarimeter, UV spectra were recorded on a TU-1900 spectrophotometer; A Hitachi 260-30 spectrometer was used for scanning IR spectroscopy; Experimental ECD spectra were recorded on a JASCO J-815 Circular Dichroism (CD) Spectropolarimeter; NMR

TABLE 3 | Inhibition of iNOS activities of the tested compounds.

Compounds	IC_{50} (μM)
1	22.0
2	17.0
6	NA
Parthenolide	3.2

NA, Not active.

TABLE 4 | Cytotoxicities of the tested compounds on HeLa and BCG-823 cancer cell lines.

Compounds	HeLa IC_{50} (μM)	BCG-823 IC_{50} (μM)
2	48.22	24.38
5	38.92	33.28
6	4.0	2.0
7	5.8	5.0
8	5.0	2.5
10	35.25	25.98
14	34.56	22.93
15	38.89	27.17
20	33.23	20.22
21	45.87	21.032
22	29.89	18.47
23	50.23	21.51
24	6.4	2.0
Paclitaxel	0.0026	0.010

spectra were performed on Bruker ARX-600 spectrometers, and on Agilent DD2-500 NMR spectrometer (500) MHz; HRESIMS were performed on a UPLC/xevo G2 Qtof spectrometer.

Preparative RP-HPLC was conducted on Agilent 1260 Infinity Series equipped with quaternary pump with Eclipse XDB-C18 (5 μm 9.4 × 250 mm) column at flow rate of 2.5 mL/min, at 210 nm UV detection using single wavelength detector. While the separation conditions were optimized on semi-preparative Agilent 1260 HPLC equipped with DAD detector by using Eclipse XDB-C18 (5 μm 4.6 × 250 mm) at flow rate of 1 mL/min. Thin layer Chromatography was performed on TLC aluminum sheets pre-coated with silica gel GF254 (EMD Chemicals, Merck KGaA, Dermstadt, Germany), visualized under UV light of 254 and 365 nm followed by 5% vanilline-H_2SO_4 reagent, and heat.

Plant Material

The stems of *K. heteroclita* (Roxb.) Craib. were collected from Hupingshan mountainous region at elevation of 5,971 ft in Shimen County, Hunan, P. R. China, and identified by Prof. Wei Wang from School of Pharmacy, Hunan University of Chinese Medicine. The voucher specimen number (CEL 1280-KH) was deposited to TCM and Ethnomedicine Innovation & Development International Laboratory, School of Pharmacy, Hunan University of Chinese Medicine, Changsha, Hunan, P. R. China.

Extraction and Isolation

Air dried plant material (100 kg) was extracted three times by using 80% ethanol in water under refluxed condition for 3 h each to produce viscous extract. This whole extract was then sequentially partitioned by liquid-liquid extraction (LLE) using non-polar, moderate to high polar organic solvents (pet-ether, chloroform, and *n*-butanol) against water to obtain wide range of metabolites.

Chloroform extract (353 g) was then subjected to silica gel column chromatography (CC) by gradient elution of solvent system PE-EtOAc (100% PE, 25% EtOAc in PE, 50% EtOAc/PE, 75% EtOAc in PE, 100% EtOAc) followed by EtOAc-MeOH elution. Subsequently the collected fractions were compiled, under the continuous guidance of TLC monitoring system to afford 12 final fractions (Kh-A to Kh-L).

Fraction Kh-C (54.7 g) was subjected to a series of silica gel column chromatography by gradient elution of PE-EtAcO v/v% to afford Kh-C-I to Kh-C-VIII. Fraction Kh-C-I yielded needle like crystals of **12** (35 mg) eluted with 10% EtAcO/PE on silica gel column. Compound **18** (9.0 mg) was isolated as white scaly crystals by silica gel CC using 4% EtAcO/PE mobile phase from Kh-C-III. Fraction Kh-C-V after successive separation afforded white solid of **13** (18.2 mg) eluted with 10% acetone, and **16** (6.0 mg) eluted with 15% acetone in PE, respectively on silica gel column. While Kh-C-VII yielded **25** (150 mg), and **24** (13 mg) by 6% and 10% EtAcO/PE, respectively, thorough silica gel CC.

Fraction Kh-D (42.5 g) after successive chromatography on silica column afforded 10 fractions. Fraction Kh-D-VI was separated on silica gel column and eluted by acetone/PE to give **14** (7.5 mg), and yielded **15** (18.0 mg) as transparent crystals by 6% acetone/CHCl$_3$, furthermore, compound **8** (5.0 mg) was also separated on sephadex LH-20 CC by 1:1 MeOH/CHCl$_3$ from the same sub-fraction. White crystals of **7** (4.0 g) was isolated as major compound by 15% EtAcO/PE on silica gel column.

Fraction Kh-E (25.5 g) was eluted by PE and EtAcO by gradient system. After series of separation **27** (7.6 mg) was isolated on sephadex column by 1:1 MeOH/CHCl$_3$ solvent system from fraction Kh-E-V. While fraction Kh-E-VI yielded compound **19** (22.0 mg) by 50% EtAcO/DCM silica gel CC, and compound **9** (25.0 mg) was purified as feathery substance on sephadex LH-20 by 1:1 MeOH/CHCl$_3$ solvent system from resulting fraction Kh-E-VI-e.

Fraction Kh-F (48.5 g) was subjected to series of silica gel CC using DCM/EtAc followed by EtAc/MeOH solvent system of increasing polarity. Compounds **11** (5.0 mg), and **17** (28.00 mg) were isolated on silica gel columns by 30% DCM/PE, and 20% acetone/PE, respectively, from sub-fraction. The resulting fraction Kh-F-X-e was separated on sephadex LH-20 CC using 50% MeOH in CHCl$_3$ to yield sub-fraction Kh-F-X-e-2 (88 mg), which was then further purified by semi-preparative RP-HPLC. The separation conditions were optimized on analytical HPLC equipped with DAD detector. Compound **2** (20.0 mg, retention time = t_R 14.03 min), **10** (12.0 mg, retention time = t_R 17.52 min), and compound **5** (6.2 mg, retention time = t_R 20.53 min) were purified by 75% MeOH in H$_2$O at flow of 2.5 mL/min using 210 nm

of UV detection by using Eclipse XDB-C18 (5 μm 9.4 × 250 mm) column. While compound **28** (13.0 mg) was isolated from Kh-F-X-h eluted with 30% EtAcO/DCM on silica gel column.

Fraction Kh-G (42.8 g) was fractionated gradiently, and compound **26** (8.0 mg) was purified as precipitates during fraction collection of 15% EtAcO/DCM.

Fraction Kh-H (55.4 g) was subjected to silica gel CC by gradient elution with PE/EtOAc, and EtOAc/MeOH to yield sub fraction. Further silica gel CC was carried out for sub-fraction Kh-H-IX (6.37 g) using DCM/EtOAc and EtOAc/MeOH solvent system of increased polarity to yield fractions Kh-H-IX-a to Kh-H-IX-f. Compound **1** (10.0 mg), and compound **6** (9.5 mg) were separated on sephadex LH-20 CC eluted with 50% MeOH in CHCl$_3$ from sub-fraction Kh-H-IX-c (155.78 mg), and Kh-H-IX-d-3 (85.70 mg), respectively. While fraction Kh-IX-e (2.4 g) was subjected to successive separations and ultimately compound **21** (12.5 mg, retention time = t_R 11.66 min), **22** (15.3 mg, retention time = t_R 20.10 min), **23** (10.0 mg, retention time = t_R 23.57 min), and compound **20** (6.5 mg, retention time = t_R 33.12 min) were purified by preparative HPLC by 55% MeOH//H$_2$O at flow rate of 2.5 mL/min using Zorbax SB-C18 (5 μm 9.4 × 150 mm) column at 210 nm UV detection.

Finally, Fraction I (35.0 g) was chromatographed on silica gel CC eluted with a DCM/MeOH gradient system (99.5:0.5–0:100) to obtain 10 fractions. Kh-I-X (3.0 g) was subjected to silica gel CC eluted with PE/EtOAc (80:20 to 0:100) to give 12 fractions. Fraction Kh-I-X-k was purified on semi-preparative RP-HPLC, with a solvent of MeOH/H$_2$O (3 mL/min, 75:25) at 225 nm, to afford compounds **3** (6.7 mg) and compounds **4** (6.7 mg).

Spectroscopic Data
Xuetonglactone A (1)
Colorless prismatic crystals; $[\alpha]_D^{25}$ + 186.9 (*c* 2.44, MeOH); ECD 255 nm ($\Delta\varepsilon$ = + 5.64); IR ν_{max} 2,967, 1,720, 1,684, 1,599, 1,569, 1,375, 1,291, 1,246, 1,127, 1,101, 1,053, 1,028, 987, 851, 821 cm^{-1}; ^{1}H-NMR (500 MHz, CDCl$_3$) and ^{13}C-NMR (125 MHz, CDCl$_3$) data, see **Tables 1, 2**, respectively; (+)-HRESIMS *m/z* 559.2671 [M + Na]$^+$ (calcd for C$_{32}$H$_{40}$O$_7$ + Na, 559.2672).

Xuetonglactone B (2)
White amorphous; $[\alpha]_D^{25}$ + 242.7 (*c* 3.94, MeOH); ECD 255 nm ($\Delta\varepsilon$ = + 5.80); IR ν_{max} 3,449, 2,952, 1,720, 1,686, 1,669, 1,597, 1,567, 1,373, 1,289, 1,248, 1,127, 1,049, 1,026, 987, 853, 821 cm^{-1}; ^{1}H-NMR (500 MHz, CDCl$_3$) and ^{13}C-NMR (125 MHz, CDCl$_3$) data, see **Tables 1, 2**, respectively; (+)-HRESIMS *m/z* 561.2828 [M + Na]$^+$ (calcd for C$_{32}$H$_{42}$NaO$_7$ + Na, 561.2829), and (–)-HRESIMS *m/z* 573.2612 (calcd for C$_{32}$H$_{42}$O$_7$ + Cl, 537.2619).

Xuetonglactone C (3)
White amorphous solid; $[\alpha]_D^{25}$ 108.1 (*c* 2.44, MeOH); ECD 273 nm ($\Delta\varepsilon$ = + 0.41); IR ν_{max} 3,446, 2,929, 1,724, 1,687, 1,656, 1,375, 1,291, 1,249, 1,131, 1,024, 990, 825 cm^{-1}; ^{1}H-NMR (600 MHz, CDCl$_3$) and ^{13}C-NMR (150 MHz, CDCl$_3$) data, see

Tables 1, 2, respectively; (+)-HRESIMS *m/z* 561.2836 [M + Na]$^+$ (calcd for $C_{32}H_{42}O_7$ + Na, 561.2828).

Xuetonglactone D (4)

White amorphous; $[\alpha]_D^{25}$ 41.8 (*c* 1.67, MeOH); ECD 258 nm ($\Delta\varepsilon = +$ 5.53); IR ν_{max} 3,449, 2,988, 2,923, 2,850, 1,724, 1,465, 1,381,1,243, 1,125, 1,032, 988 cm^{-1}; ^{1}H-NMR (600 MHz, CDCl$_3$) and ^{13}C-NMR (150 MHz, CDCl$_3$) data, see **Tables 1, 2,** respectively; (+)-HRESIMS *m/z* 577.2772 [M + Na]$^+$ (calcd for $C_{32}H_{42}O_8$ + Na, 577.2777).

Xuetonglactone E (5)

White prismatic crystals; mp 235.1–236.6°C (MeOH); $[\alpha]_D^{25}$ −8.8 (*c* 0.1, MeOH); ECD 272 nm ($\Delta\varepsilon = +$ 3.31); IR ν_{max} 2,946, 1,721, 1,679, 1,558, 1,457, 1,381, 1,243, 1,106, 1,035, 914 cm^{-1}; ^{1}H-NMR (600 MHz, CDCl$_3$) and ^{13}C-NMR (150 MHz, CDCl$_3$) data, see **Tables 1, 2,** respectively; (+)-HRESIMS *m/z* 547.3047 [M + Na]$^+$ (calcd for $C_{32}H_{44}O_6$ + Na, 547.3036).

Xuetonglactone F (6)

White amorphous; $[\alpha]_D^{25}$ + 66.7 (*c* 1.56, MeOH); ECD 266 nm ($\Delta\varepsilon = +$ 2.41); IR ν_{max} 2,916, 2,849, 1,736, 1,718, 1,684, 1,459, 1,377, 1,289, 1,239, 1,120, 993, 915, 825 cm^{-1}; ^{1}H-NMR (500 MHz, CDCl$_3$) and ^{13}C-NMR (125 MHz, CDCl$_3$) data, see **Tables 1, 2,** respectively; (−)-HRESIMS *m/z* 617.2884 [M + Cl]$^-$ (calcd for $C_{34}H_{46}O_8$ + Cl, 617.2881).

X-Ray Crystallographic Analysis

X-ray crystallographic data of **1, 5,** and **7** were obtained using a Bruker APEX-II CCD diffractometer with Cu *K* radiation, = 1.54178 Å The CCDC numbers for **1, 5,** and **7** contain the supplementary crystallographic data, which can be obtained free of charge via http://www.ccdc.cam.ac.uk/conts/retrieving.html.

Crystal Data for Xuetonglactone A (1)

$C_{32}H_{40}O_7$, M = 536.64, colorless crystals, Orthorhombic, a = 7.1986 (3) Å, b = 13.9377 (6) Å, c = 28.5609 (13) Å, α = 90.00°, β = 90.00°, γ = 90.00°, V = 2865.6 (2) Å^3, s $P2_12_12_1$, T = 296 K, Z = 4, μ(Cu Kα) = 0.70 mm^{-1}, 22,617 reflections measured, 5,112 independent reflections (R_{int} = 0.073). Final R indices [I >2σ(I)]: R1 = 0.052, wR2 = 0.164. Flack parameter: −0.10 (13). CCDC number: 1859825.

Crystal Data for Xuetonglactone E (5)

$C_{32}H_{44}O_6 \cdot H_2O$, M = 542.69, colorless crystal, Orthorhombic, a = 10.9410 (7) Å, b = 14.5893 (9) Å, c = 18.2354 (11) Å, α = 90.00°, β = 90.00°, γ = 90.00°, V = 2910.8 (3) Å^3, space group $P2_12_12_1$, T = 296 K, Z = 4, μ(Cu Kα) = 0.69 mm^{-1}, 31,389 reflections measured, 5,410 independent reflections (Rint = 0.040). Final R indices [I > 2σ(I)]: R1 = 0.036, wR2 = 0.109. Flack parameter: 0.06 (4). CCDC number: 1859823.

Crystal Data for Xuetongsu (7)

4($C_{30}H_{44}O_4$)·O, M =1,890.60, colorless crystal, Monoclinic, a = 46.638 (2) Å, b = 7.4805 (4) Å, c = 7.8525 (4) Å, α = 90.00°, β = 91.597(2)°, γ = 90.00°, V = 2738.5 (2) Å^3, space group C2, T = 296.15 K, Z = 1, μ(Cu Kα) = 0.59 mm^{-1}, 10,267 reflections measured, 3,797 independent reflections (Rint = 0.098). Final R

indices [I > 2s(I)]: R1 = 0.040, wR2 = 0.140. Flack parameter: 0.09 (13). CCDC number: 1859822.

Biological Activity Evaluation

Inhibition of iNOS Activity

The assay was performed in mouse macrophages (RAW264.7) cultured in phenol red-free RPMI medium with 10% bovine calf serum, 100 U/mL penicillin G sodium, and 100 μg/mL streptomycin. The cells were seeded in 96-well plates at the density of 1 × 10^5 cells/well, and incubated for 24 h for a confluency of 75% or more. The cells were treated with the test compounds, and after 30 min of incubation, lipopolysaccharide (LPS, Sigma-Aldrich, St. Louis, MO, USA) (5 μg/mL) was added and further incubated for 24 h. The activity of iNOS was determined in terms of the concentration of NO by measuring the level of nitrite in the cell culture supernatant using Griess reagent (Sigma-Aldrich, St. Louis, MO, USA). Percent inhibition of nitrite production by the test compound was calculated in comparison to the vehicle control. IC$_{50}$ values were obtained from dose response curves. Parthenolide was used as the positive control (Zhao et al., 2014).

Cytotoxicity Assay

Cell viability was determined by a MTT assay (Roche Diagnosis, Indianapolis, IN). Briefly, BGC-823 and HeLa cell lines were seeded at 6 × 10^3 cells/well in 96-well plates. Cells were allowed to adhere for overnight, and then the cells were changed to fresh medium containing various concentrations natural compound dissolved in DMSO. After 48 h incubation, the growth of cells was measured. The effect on cell viability was assessed as the percent cell viability compared with untreated control group, which were arbitrarily assigned 100% viability. The compound concentration required to cause 50% cell growth inhibition (IC$_{50}$) was determined by interpolation from dose–response curves. All experiments were performed in triplicate, and paclitaxel was used as the positive control (Hayon et al., 2003).

CONCLUSIONS

To sum up, four new highly oxygenated lanostane-type triterpenoids xuetonglactones A–D (**1–4**) and two highly oxygenated cycloartane-type triterpenoids xuetonglactones E–F (**5–6**), along with 22 known compounds (**7–28**) were isolated from stems of *K. heteroclita*. To the best of our knowledge xuetonglactones A (**1**) endowed with unprecedented 20,21-α-epoxide functionality, and xuetonglactones D (**4**) possessed rare 19-α hydroperoxyl moiety, their absolute configurations were determined by X-ray diffraction and ECD data analysis. Moreover, bioassays indicated that **1** and **2** showed inhibition of iNOS activity in LPS-induced macrophages, **6**, **7**, **8**, and **24** showed potent cytotoxicities against HeLa and BGC 823 cancer cell lines. Notably, this study has further enriched the chemical diversity of highly oxygenated triterpenoidal skeletons, which might trigger research rigor among synthetic and medicinal chemistry community.

DATA AVAILABILITY STATEMENT

The raw data supporting the conclusions of this article will be made available by the authors, without undue reservation, to any qualified researcher.

AUTHOR CONTRIBUTIONS

WW and DL conceived and designed the idea of the study. NS performed the isolation work. BL performed physical data analysis. NS and BL prepared the first draft of the manuscript. LC helped in collection of literature and assisting in crystallization. JZ performed the NMR data acquisition. YJ and AW contributed in analysis of NMR data. MD performed the bioassays of the compounds. MC and AR contributed in revision and final data analyses. IK provided the core facility to acquire NMR and other spectroscopic data. All authors read and approved the final manuscript.

FUNDING

SUPPLEMENTARY MATERIAL

The Supplementary Material for this article can be found online at: https://www.frontiersin.org/articles/10.3389/fchem.2019.00935/full#Supplementary-Material

REFERENCES

Cao, L., Shehla, N., Tasneem, S., Cao, M., Sheng, W., Jian, Y., et al. (2019). New cadinane sesquiterpenes from the stems of *Kadsura heteroclita*. *Molecules* 24:1664. doi: 10.3390/molecules24091664

Chaturvedula, V. S. P., and Prakash, I. (2012). Isolation of stigmasterol and β-sitosterol from the dichloromethane extract of *Rubus suavissimus*. *Int. Curr. Pharm. J.* 1, 239–242. doi: 10.3329/icpj.v1i9.11613

Chen, Y. G., Qin, G. W., and Xie, Y. Y. (2001). Triterpenoids from medicinal plants of Schisandraceae and their spectroscopic characteristics. *Chem. Res. Appl.* 13, 363–367.

Deng, Y. R., Wei, Y. P., Yin, F., Yang, H., and Wang, Y. (2010). A new cardenolide and two new pregnane glycosides from the root barks of *Periploca sepium*. *Hel. Chim. Acta.* 93, 1602–1609. doi: 10.1002/hlca.200900320

El Dine, R. S., El Halawany, A. M., Ma, C. M., and Hattori, M. (2008). Anti-HIV-1 protease activity of lanostane triterpenes from the Vietnamese mushroom *Ganoderma colossum*. *J. Nat. Prod.* 71, 1022–1026. doi: 10.1021/np8001139

Han, M. H., Yang, X. W., and Jin, Y. P. (2008). Novel triterpenoid acyl esters and alkaloids from *Anoectochilus roxburghii*. *Phytochem. Anal.* 19, 438–443. doi: 10.1002/pca.1070

Hayon, T., Dvilansky, A., Shpilberg, O., and Nathan, I. (2003). Appraisal of the MTT-based assay as a useful tool for predicting drug chemosensitivity in leukemia. *Leuk Lymphoma* 44, 1957–1962. doi: 10.1080/1042819031000116607

Hu, Z. X., Shi, Y. M., Wang, W. G., Li, X. N., Du, X., Liu, M., et al. (2015). Kadcoccinones A–F, new biogenetically related lanostane-type triterpenoids with diverse skeletons from *Kadsura coccinea*. *Org. Lett.* 17, 4616–4619. doi: 10.1021/acs.orglett.5b02360

Lakornwong, W., Kanokmedhakul, K., Kanokmedhakul, S., Kongsaeree, P., Prabpai, S., Sibounnavong, P., et al. (2014). Triterpene lactones from cultures of *Ganoderma* sp. KM01. *J. Nat. Prod.* 77, 1545–1553. doi: 10.1021/np400846k

Li, R. T., Han, Q. B., Zhao, A. H., and Sun, H. D. (2003). Micranoic acids A and B: two new octanortriterpenoids from *Schisandra micrantha*. *Chem. Pharm. Bull.* 51, 1174–1176. doi: 10.1248/cpb.51.1174

Liang, X. U., Wang, X. H., Luo, R. Y., Lu, S. Q., Gou, Z. J., Wang, M. A., et al. (2015). Secondary metabolites of rice sheath blight pathogen *Rhizoctonia solani* Kühn and their biological activities. *J Integr. Agric.* 14, 80–87. doi: 10.1016/S2095-3119(14)60905-9

Liu, J., Qi, Y., Lai, H., Zhang, J., Jia, X., Liu, H., et al. (2014). Genus *Kadsura*, a good source with considerable characteristic chemical constituents and potential bioactivities. *Phytomedicine* 21, 1092–1097. doi: 10.1016/j.phymed.2014.01.015

Liu, J. S., and Huang, M. F. (1991). Isolation and structures of schisanlactone E and changnanic acid. *Acta. Chim. Sin.* 49, 502–506.

Liu, J. S., Huang, M. F., Ayer, W. A., and Bigam, G. (1983). Schisanlactone B, a new triterpenoid from a *Schisandra* sp. *Tetrahedron Lett.* 24, 2355–2358. doi: 10.1016/S0040-4039(00)81923-1

Liu, Y., Yang, Y., Tasneem, S., Hussain, N., Daniyal, M., Yuan, H., et al. (2018). Lignans from Tujia ethnomedicine Heilaohu: chemical characterization and evaluation of their cytotoxicity and antioxidant activities. *Molecules* 23:2147. doi: 10.3390/molecules23092147

Liu, Y., Zhao, J., Chen, Y., Li, W., Li, B., Jian, Y., et al. (2016). Polyacetylenic oleanane-type triterpene saponins from the roots of *Panax japonicus*. *J. Nat. Prod.* 79, 3079–3085. doi: 10.1021/acs.jnatprod.6b00748

Ma, W., He, J., Li, L., and Qin, L. (2009). Two new triterpenoids from the stems of *Schisandra bicolor*. *Helv. Chim. Acta.* 92, 2086–2091. doi: 10.1002/hlca.200900245

Pavanasisivam, G., and Sultanbawa, M. U. S. (1973). Cycloartenyl acetate, cycloartenol and cycloartenone in the bark of *Artocarpus* species. *Phytochemistry* 12, 2725–2726. doi: 10.1016/0031-9422(73)85088-5

Pu, J. X., Yang, L. M., Xiao, W. L., Li, R. T., Lei, C., Gao, X. M., et al. (2008). Compounds from *Kadsura heteroclita* and related anti-HIV activity. *Phytochemistry* 69, 1266–1272. doi: 10.1016/j.phytochem.2007.11.019

Rahmana, S. M. M., Muktaa, Z. A., and Hossainb, M. A. (2009). Isolation and characterization of β-sitosterol-D-glycoside from petroleum extract of the leaves of *Ocimum sanctum* L. *Asn. J. Food, Agro-Industry*. 2, 39–43.

Shen, Y. C., Lin, Y. C., Chiang, M. Y., Yeh, S. F., Cheng, Y. B., and Liao, C. C. (2005). Kadsuphilactones A and B, two new triterpene dilactones from *Kadsura philippinensis*. *Org. Lett.* 7, 3307–3310. doi: 10.1021/ol051155k

Shi, Y. M., Xiao, W. L., Pu, J. X., and Sun, H. D. (2015). Triterpenoids from the Schisandraceae family: an update. *Nat. Prod. Rep.* 32, 367–410. doi: 10.1039/C4NP00117F

Song, Q. Y., Jiang, K., Zhao, Q. Q., Gao, K., Jin, X. J., and Yao, X. J. (2013). Eleven new highly oxygenated triterpenoids from the leaves and stems of *Schisandra chinensis*. *Org. Biomol. Chem.* 11, 1251–1258. doi: 10.1039/c2ob27115j

Su, W., Zhao, J., Yang, M., Yan, H. W., Pang, T., Chen, S. H., et al. (2015). A coumarin lignanoid from the stems of *Kadsura heteroclita*. *Bioorg. Med. Chem. Lett.* 25, 1506–1508. doi: 10.1016/j.bmcl.2015.02.022

Wang, W., Liu, J., Han, J., Xu, Z., Liu, R., Liu, P., et al. (2006b). New triterpenoids from *Kadsura heteroclita* and their cytotoxic activity. *Planta Med.* 72, 450–457. doi: 10.1055/s-2005-916263

Wang, W., Liu, J., Yang, M., Sun, J., Wang, X., Liu, R., et al. (2006c). Simultaneous determination of six major constituents in the stems of *Kadsura heteroclita* by LC-DAD. *Chromatographia* 64, 297–302. doi: 10.1365/s10337-006-0031-7

Wang, W., Liu, J. Z., Ma, X. C., Yang, M., Wang, W. X., Xu, Z. R., et al. (2006a). Three new cyclolanostane triterpenoids from the ethanol extract of the stems of *Kadsura heteroclita*. *Helv. Chim. Acta.* 89, 1888–1893. doi: 10.1002/hlca.200690180

Wang, W., Xu, Z., Yang, M., Liu, R., Wang, W., Liu, P., et al. (2007). Structural determination of seven new triterpenoids from *Kadsura heteroclita* by NMR techniques. *Magn. Reson. Chem.* 45, 522–526. doi: 10.1002/mrc.2000

Xiao, W. L., Li, R. T., Huang, S. X., Pu, J. X., and Sun, H. D. (2008). Triterpenoids from the Schisandraceae family. *Nat. Prod. Rep.* 25, 871–891. doi: 10.1039/b719905h

Yang, J. H., Wen, J., Du, X., Li, X. N., Wang, Y. Y., Li, Y., et al. (2010). Triterpenoids from the stems of *Kadsura ananosma. Tetrahedron.* 66, 8880–8887. doi: 10.1016/j.tet.2010.09.059

Yu, H., Zeng, R., Lin, Y., Li, X., Tasneem, S., Yang, Z., et al. (2019). *Kadsura heteroclita* stem suppresses the onset and progression of adjuvant-induced arthritis in rats. *Phytomedicine* 58:152876. doi: 10.1016/j.phymed.2019.152876

Yu, H. H., Lin, Y., Zeng, R., Li, X., Zhang, T., Tasneem, S., et al. (2019). Analgesic and anti-inflammatory effects and molecular mechanisms of *Kadsura heteroclita* stems, an anti-arthritic Chinese Tujia ethnomedicinal herb. *J. Ethnopharmacol.* 238:111902. doi: 10.1016/j.jep.2019.111902

Zhao, J., Khan, S. I., Wang, M., Vasquez, Y., Yang, M. H., Avula, B., et al. (2014). Octulosonic acid derivatives from Roman chamomile (*Chamaemelum nobile*) with activities against inflammation and metabolic disorder. *J. Nat. Prod.* 77, 509–515. doi: 10.1021/np 400780n

Zou, J., Yang, L. B., Jiang, J., Diao, Y. Y., Li, X. N., Huang, J., et al. (2012). Lanostane triterpenoids from the stems of *Schisandra glaucescens. Planta Med.* 78, 472–479. doi: 10.1055/s-0031-12 98214

Anti-inflammatory Limonoids From *Cortex Dictamni*

Yue Chen[1†], Jingya Ruan[1†], Fan Sun[2], Huimei Wang[3,4], Shengcai Yang[1], Ying Zhang[1], Jiejing Yan[2], Haiyang Yu[2], Yuanqiang Guo[3,4], Yi Zhang[1,2]* and Tao Wang[1,2]*

[1] Tianjin Key Laboratory of TCM Chemistry and Analysis, Tianjin University of Traditional Chinese Medicine, Tianjin, China, [2] Institute of TCM, Tianjin University of Traditional Chinese Medicine, Tianjin, China, [3] State Key Laboratory of Medicinal Chemical Biology, College of Pharmacy, Nankai University, Tianjin, China, [4] Tianjin Key Laboratory of Molecular Drug Research, Nankai University, Tianjin, China

The root barks of perennial herb *Dictamnus dasycarpus* (*Cortex Dictamni*) were reported to be rich in anti-inflammation activity constituents, limonoids. Then, the investigation of anti-inflammation therapeutic limonoids from this plant was developed in the present study. Through the combination of various chromatographies isolation, six new limonoids, named dictamlimonol A (**1**), dictamlimonoside B (**2**), and dictamlimonols C–F (**3–6**), along with seven known ones (**7–13**), were obtained. Their structures were ascertained based on the extensive spectroscopic methods and ECD data analysis. Among them, compound **1** was the first 7,19-epoxy limonoid found in natural products. The anti-inflammatory effects of all limonoids were evaluated in lipopolysaccharide (LPS)-treated RAW 264.7 cell lines. Compounds **5**, **7–11**, and **13** were found to inhibit LPS-induced nitric oxide (NO) production. Moreover, dictamlimonol D (**5**), fraxinellone (**11**), and dasylactone A (**13**) were found to reduce the LPS-induced expressions of interleukin-6 (IL-6), tumor necrosis factor (TNF-α), inducible nitric oxide synthase (iNOS), nuclear factor kappa-light-chain-enhancer of activated B cells (NF-κB), and cyclooxygenase-2 (COX-2) at the protein levels in a dose-dependent manner. These findings support that the administration of *Cortex Dictamni* may be beneficial for inflammation.

Keywords: *Cortex Dictamni*, dictamlimonoside, dictamlimonol, tumor necrosis factor, interleukin-6, inducible nitric oxide synthase, nuclear factor kappa-light-chain-enhancer of activated B cells, cyclooxygenase-2

INTRODUCTION

Limonoids are highly oxygenated tetranorterpenoids derived from a precursor with a 4,4,8-trimethyl-17-furanyl steroid skeleton (Lv et al., 2015). Until now, they are reported to distribute mainly in Rutaceae and Meliaceae plant resources. Previous studies suggested that limonoids exhibited strong anti-inflammatory activity (Akihisa et al., 2017; Hu et al., 2018; Sun et al., 2018).

The natural plants of *Dictamnus* genus (Rutaceae family) are main resources of limonoids. The limonoids obtained from them could be subdivided as limonoid aglycones, degraded limonoids, and limonoid glucosides (Lv et al., 2015). *Dictamnus dasycarpus* Turcz is a perennial herb belonging to *Dictamnus* genus, widely distributed in China. Its root barks (*Cortex Dictamni*) have been used to treat inflammation, scabies, rheumatic pain, jaundice, and other symptoms (Yang et al., 2017, 2018). Though limonoids were reported as one of the major constituents in *Cortex Dictamni*, only fraxinellone obtained from it has been proved to possess *in vitro* anti-inflammatory effect (Kim et al., 2009; Lee et al., 2009; Wu et al., 2014) to date.

This study aims to clarify anti-inflammation limonoids in *Cortex Dictamni* by phytochemistry and bioactivity screening. Multiple chromatographies and spectral techniques were combined to isolate and identify limonoids. Then, the inhibitory activities of all obtained limonoids against nitric oxide (NO) production in RAW 264.7 cell lines induced by lipopolysaccharide (LPS) were evaluated. Furthermore, the anti-inflammatory mechanism of activity compounds was studied by using Western blot assay.

RESULTS AND DISCUSSION

Identification of New Compounds

Cortex Dictamni was extracted by 70% ethanol–water and then partitioned in EtOAc-H_2O to afford EtOAc and H_2O layer extract, respectively. The H_2O layer extract was eluted with H_2O and 95% EtOH, successively. After subjecting to D101 macroporous resin column chromatography (CC), the silica gel, ODS, Sephadex LH-20 CC, and preparative high-performance liquid chromatography (pHPLC) were used to isolate the 95% EtOH eluate from D101 macroporous resin CC. As a result, six new limonoids, dictamlimonol A (**1**), dictamlimonoside B (**2**), and dictamlimonols C–F (**3–6**), as well as seven known ones, limonin (**7**) (Guo, 2011), limonin diosphenol (**8**) (Du et al., 2005), obacunon (**9**) (Dong et al., 2010), 7α-obacunyl acetate (**10**) (Bennett and Hasegawa, 1982), fraxinellone (**11**) (Wang et al., 2006), 9β-hydroxyfraxinellone (**12**) (D'Ambrosio and Guerriero, 2002), and dasylactone A (**13**) (Yang et al., 2011), were obtained (**Figure 1**).

Dictamlimonol A (**1**) was obtained as an optically active [[α]$_D^{25}$ −100.0, MeOH] white powder. The molecular formula, $C_{26}H_{30}O_9$, of **1** was established by negative-ion ESI-Q-Orbitrap MS analysis [*m/z* 485.17969 [M–H]$^-$; calcd for $C_{26}H_{29}O_9$, 485.18061]. Its ^1H, ^{13}C NMR (**Table 1**, C_5D_5N), ^1H ^1H COZY, HSQC, and HMBC spectra indicated the presence of one furan ring at δ$_H$ 6.60 (1H, t like, *ca. J* = 1 Hz, H-22), 7.68 (1H, t like, *ca. J* = 1 Hz, H-23), 7.77 (1H, t like, *ca. J* = 1 Hz, H-21), and four methyl groups at δ$_H$ 0.91, 1.24, 1.40, 1.48 (3H each, all s, H$_3$-30, 28, 18, 29). According to the chemical shifts and the correlations observed in its ^1H ^1H COZY spectrum, "–O–CH–CH$_2$-," "–CH$_2$-CH$_2$-," and "–CH=CH–O–" moieties were deduced. The planar structure of it was determined based on the key HMBC correlations from H-1 to C-3–5; H$_2$-2 to C-3, C-10; H-5 to C-6; H-7 to C-6, C-9, C-14; H-15 to C-16; H-17 to C-14, C-20–22; H$_3$-18 to C-12–14, C-17; H$_2$-19 to C-1, C-5, C-7, C-10; H$_3$-28 to C-4, C-5, C-29; H$_3$-29 to C-4, C-5, C-28; H$_3$-30 to C-7–9, C-14, which was a derivative of limonin (**7**). The relative configurations of C-13 and C-17 of **1** should be the same as those of **7** on the basis of biogenetic consideration, which indicated both 13-methyl and 17-furan ring presented α-orientations. Meanwhile, the NOE correlations between δ$_H$ 1.40 (H$_3$-18) and δ$_H$ 2.89 (H-9), 4.72 (H-15); δ$_H$ 2.89 (H-9); and δ$_H$ 1.24 (H$_3$-28), 4.61 (H-1), 4.72 (H-7); δ$_H$ 1.24 (H$_3$-28); and δ$_H$ 4.61 (H-1) observed in its NOESY spectrum suggested that H-1, H-7, H-9, H-15, and H$_3$-28 were α-oriented; on the other hand, δ$_H$ 1.48 (H$_3$-29) and δ$_H$ 3.40 (H-5); δ$_H$ 3.40 (H-5) and δ$_H$ 4.62 (Hb-19); and δ$_H$ 4.62 (Hb-19) and δ$_H$ 0.91 (H$_3$-30) (**Figure 3**) indicated that H-5, H$_2$-19, H$_3$-29, and H$_3$-30 were β-oriented. Finally, the absolute configuration of **1**

was clarified by comparison of experimental and calculated ECD data, which was recorded at the B3LYP/SVP level with the CPCM model (Frisch et al., 2009; Shi et al., 2019). The calculated ECD spectrum of **1** (**Figure 4A**) was consistent with the experimental data closely. The result indicated that the absolute configuration of **1** was 1*S*,5*S*,7*R*,8*S*,9*R*,10*R*,13*S*,14*R*,15*S*,17*S*. Thus, its structure was finally established and named dictamlimonol A. It was the first 7,19-epoxy limonoid found in natural products.

Dictamlimonoside B (**2**) was a white powder with negative optical rotation [[α]$_D^{25}$ −72.1, MeOH]. Its molecular formula was determined to be $C_{20}H_{26}O_9$ [*m/z* 455.15375 [M + COOH]$^-$, calcd for $C_{21}H_{27}O_{11}$, 455.15479] by negative-ion ESI-Q-Orbitrap MS. D-glucose was detected from its acid hydrolysis product by HPLC analysis (Zhang et al., 2015). The ^1H, ^{13}C NMR (**Table 2**, CD$_3$OD) spectra showed signals of two methyl groups at δ$_H$ 0.84, 2.25 (3H each, both s, H$_3$-18 and 30), two methylene groups at δ$_H$ [1.58 (1H, dt like, *ca. J* = 4, 13 Hz), 1.78 (1H, dt like, *ca. J* = 3, 13 Hz), H$_2$-12], [1.91, 2.39 (1H each, both m, H$_2$-11)], two oxygenated methylene groups at δ$_H$ 4.11 (1H, br. d, *ca. J* = 4 Hz, H-9), 4.97 (1H, br. s, H-17), one furan ring at δ$_H$ 6.44 (1H, br. s, H-22), 7.55 (2H, m, overlapped, H-21 and 23), one β-D-glucopyranosyl at δ$_H$ 4.53 (1H, d, *J* = 7.5 Hz, H-1'), together with one α, β-unsaturated ketone group at δ$_C$ 131.9 (C-14), 147.1 (C-8), 171.8 (C-16). The ^1H ^1H COZY spectrum of **2** suggested the presence of three partial structures written in bold lines (**Figure 2**). Moreover, the abovementioned three partial structures and relative functional groups were connected together by the long-range correlations from H-9 to C-8, C-14; H$_2$-11 to C-8, C-13; H-17 to C-14, C-20–22; H$_3$-18 to C-12–14, C-17; H$_3$-30 to C-8, C-9, C-14, C-16; H-1' to C-9 displayed in the HMBC spectrum. Meanwhile, the NOE correlations (determined in DMSO-d_6) (**Figure 3**) between δ$_H$ 0.77 (H$_3$-18) and δ$_H$ 6.52 (H-22), 7.72 (H-21), as well as biogenetic law suggested that 13-methyl and 17-furan ring were α-oriented. The correlation between δ$_H$ 0.77 (H$_3$-18) and δ$_H$ 1.80 (H-11α) indicated that both 13-methyl and the proton with signal at δ$_H$ 1.80 were in axial bond. Moreover, the coupling constant of H-9 was about 4 Hz, which suggested that the proton was presented in equatorial bond (one α-H in compound **2**). Furthermore, the aglycone of it, 9β-hydroxyfraxinellone (**12**), was obtained when it was hydrolyzed with β-glucosidase. The calculated ECD spectrum of **2** (**Figure 4B**) matched the experimental data closely, which indicated that its absolute configuration was 9*S*,13*R*,17*R*. The structure of **2** was therefore clarified and named dictamlimonoside B.

Dictamlimonol C (**3**) was isolated as white powder with negative optical rotation ([α]$_D^{25}$ −74.6, MeOH). The molecular formula, $C_{16}H_{20}O_5$, of **3** was established by negative-ion ESI-Q-Orbitrap MS [*m/z* 337.12790 [M + COOH]$^-$, calcd for $C_{17}H_{21}O_7$, 337.12818]. Comparing its ^1H and ^{13}C NMR spectroscopic data (**Table 3**, CDCl$_3$) with those of **2** indicated that they possessed the same substituent groups [two methyl groups at δ$_H$ 0.95, 1.90 (3H each, both s, H$_3$-18 and 30), one furan ring at δ$_H$ 6.40, 7.38, 7.45 (1H each, all t like, *ca. J* = 2 Hz, H-22, 23, 21), and a "—CH$_2$–CH$_2$–CH(O)—"moiety]. At the same time, there were one more oxygenated methine proton at δ$_H$ 4.90 (1H, s, H-15) and one more methoxy at δ$_H$ 3.41 (3H, s, 9-OCH$_3$) in **3**. The long-range correlations from H-9
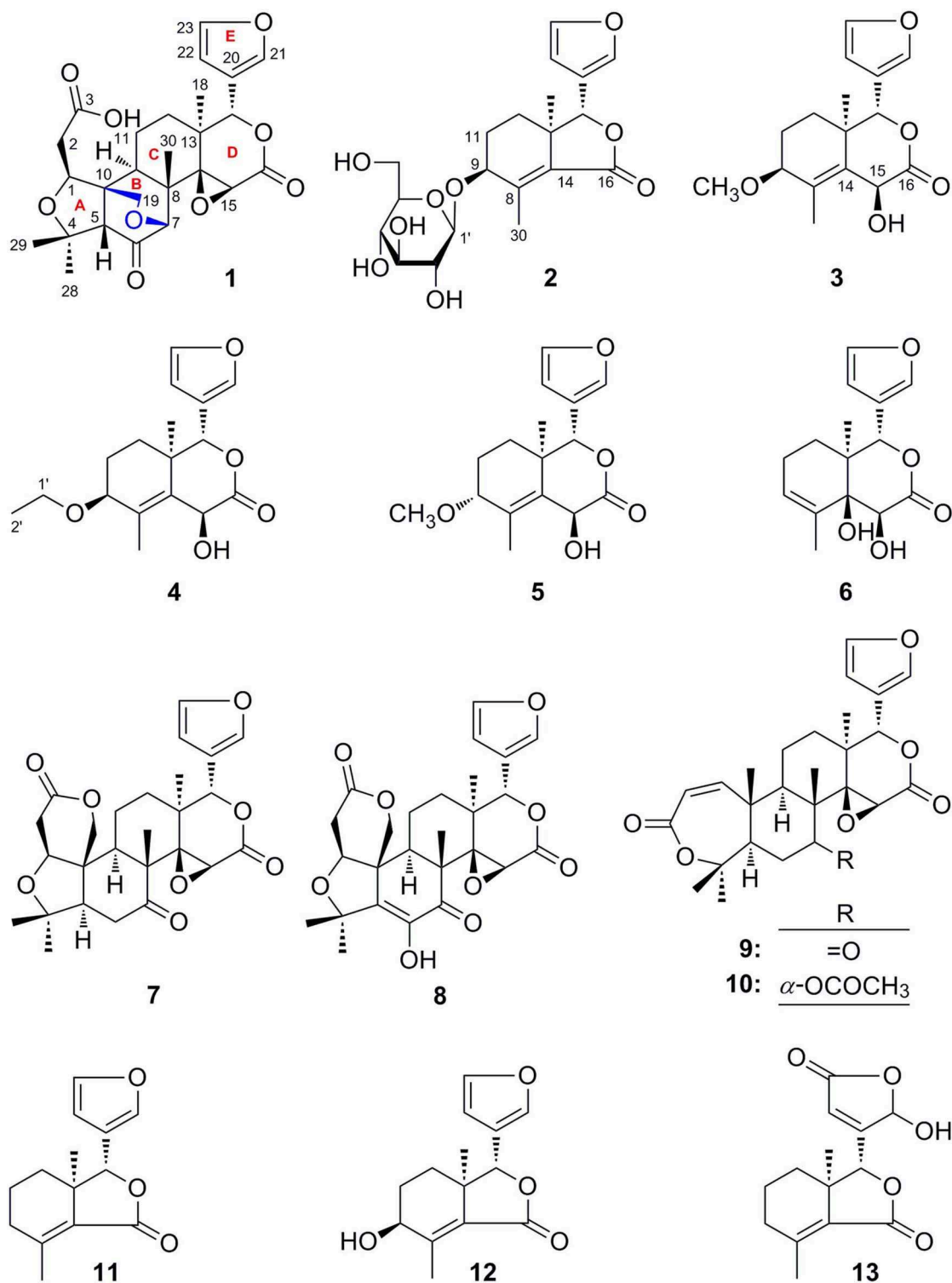
FIGURE 1 | The structures of compounds **1–13** isolated from *Cortex Dictamni*.

to C-8, C-14; H-15 to C-8, C-13, C-14, C-16; H-17 to C-14, C-20–22; H$_3$-18 to C-12–14, C-17; H$_3$-30 to C-8, C-9, C-14; 9-OCH$_3$ to C-9 were observed in its HMBC spectrum, and its planar structure was elucidated. Moreover, the NOE correlations

(**Figure 3**) between δ_H 0.95 (H$_3$-18) and δ_H 4.90 (H-15), 6.40 (H-22), 7.45 (H-21) revealed that 13-methyl, 17-furan ring, as well as H-15 presented α-orientation, and the correlations between δ_H 0.95 (H$_3$-18) and δ_H 1.73 (H-11α); δ_H 1.98 (H-11β); and δ_H

TABLE 1 | ^{1}H and ^{13}C NMR data for **1** in C_5D_5N.

No.	δ_C	δ_H (*J* in Hz)	No.	δ_C	δ_H (*J* in Hz)
1	83.6	4.61 (dd, 2.5, 2.5)	13	38.2	
2	36.8	3.10 (dd, 2.5, 16.0)	14	66.7	
		3.19 (dd, 2.5, 16.0)	15	52.1	4.72 (s)
3	170.9		16	167.7	
4	82.5		17	78.4	5.76 (s)
5	65.1	3.40 (s)	18	21.2	1.40 (s)
6	208.0		19	70.6	4.50, 4.62 (both d, 12.5)
7	83.2	4.72 (s)	20	121.1	
8	46.6		21	142.0	7.77 (t like, *ca*. 1)
9	46.8	2.89 (dd, 4.5, 10.0)	22	110.7	6.60 (t like, *ca*. 1)
10	49.7		23	143.8	7.68 (t like, *ca*. 1)
11	20.3	1.91 (m)	28	24.2	1.24 (s)
12	32.3	1.47 (m, overlapped)	29	29.1	1.48 (s)
		2.01 (m)	30	15.3	0.91 (s)

TABLE 2 | ^{1}H and ^{13}C NMR data for **2** in CD_3OD and DMSO-d_6.

No.	in CD_3OD		in DMSO-d_6	
	δ_C	δ_H (*J* in Hz)	δ_C	δ_H (*J* in Hz)
8	147.1		145.4	
9	78.1	4.11 (br. d, *ca*. 4)	75.9	4.01 (br. d, *ca*. 4)
11	27.4	1.91 (m)	25.7	1.80 (tt like, *ca*. 4, 14)
		2.39 (m)		2.27 (dt like, *ca*. 4, 14)
12	28.2	1.58 (dt like, *ca*. 4, 13)	26.6	1.50 (dt like, *ca*. 4, 13)
		1.78 (dt like, *ca*. 3, 13)		1.63 (dt like, *ca*. 2, 13)
13	44.6		42.7	
14	131.9		129.9	
16	171.8		169.0	
17	84.8	4.97 (br. s)	82.1	5.01 (br. s)
18	19.4	0.84 (s)	18.7	0.77 (s)
20	121.7		120.1	
21	141.4	7.55 (m, overlapped)	140.2	7.72 (m, overlapped)
22	109.8	6.44 (br. s)	109.0	6.52 (br. s)
23	145.0	7.55 (m, overlapped)	143.8	7.72 (m, overlapped)
30	15.9	2.25 (s)	15.0	2.18 (s)
1′	107.0	4.53 (d, 7.5)	105.8	4.40 (d, 8.0)
2′	75.5	3.21 (dd, 7.5, 8.5)	73.7	2.98 (m)
3′	78.0	3.38 (dd, 8.5, 8.5)	76.7	3.15 (m)
4′	71.5	3.31 (m, overlapped)	70.0	3.06 (m)
5′	77.9	3.31 (m, overlapped)	76.7	3.17 (m)
6′	62.7	3.69 (dd, 5.0, 12.0)	61.1	3.46 (m)
		3.88 (br. d, *ca*. 12)		3.69 (m)

3.41 (9-OCH$_3$), along with the coupling constant of H-9 (*ca. J* = 4 Hz), suggested that 9-OCH$_3$ presented β-orientation. The calculated ECD spectrum of **3** (**Figure 4C**) was identical to the experimental one, which indicated that its absolute configuration was 9*S*,13*R*,15*S*,17*R*. Then, the structure of dictamlimonol C (**3**) was elucidated.

Dictamlimonol D (**4**) was a white powder with negative optical rotation [[α]$_D^{25}$ −68.0, MeOH]. Its molecular formula, $C_{17}H_{22}O_5$, was determined by its quasi-molecular ion peak at *m/z* 351.14261 [M + COOH]$^-$ (calcd for $C_{18}H_{23}O_7$, 351.14383) in the negative ESI-Q-Orbitrap MS experiment, which was 14 amu greater than that of **3**. The ^{1}H and ^{13}C NMR (**Table 4**, CDCl$_3$) signals of **4** were similar to those of **3** except for C-9. The 9-methoxy in the structure of **3** has changed into an ethoxy in **4** at δ_H 1.25 (3H, t, *J* = 7.0 Hz, H$_3$-2′), 3.47, 3.70 (1H each, both m, H$_2$-1′), which was consistent with the mass spectrometry data as well. In addition, in its HMBC spectra, the long-range correlation from H$_2$-1′ to C-9 was observed, which verified that the ethoxyl connected to the C-9 position. Meanwhile, the optical rotation, NOE correaltions (**Figure 3**), and ECD spectra (**Figure 4D**) of **4** and **3** were also basically consistent. Consequently, the structure of dictamlimonol D (**4**) was deduced.

Dictamlimonol E (**5**) was a white powder, too. It also had negative optical rotation [[α]$_D^{25}$ −9.1, MeOH]. The ESI-Q-Orbitrap MS experiment results indicated that the molecular fomula of **5** was the same as that of **3**, $C_{16}H_{20}O_5$ (*m/z* 337.12818 [M + COOH]$^-$; calcd for $C_{17}H_{21}O_7$, 337.12818). The same planar structure of **5** and **3** was revealed by the ^{1}H, ^{13}C NMR (**Table 5**, CDCl$_3$), ^{1}H ^{1}H COZY, HSQC, and HMBC spectra. Meanwhile, the chemical shifts of C-9, 11, 12, 14, and 30 were different between these two compounds, which suggested they might be the C-9 epimers. In the NOESY spectrum of **5**, NOE correlations (**Figure 3**) were observed between the following proton and proton pairs: δ_H 1.14 (H$_3$-18) and δ_H 1.76 (H-11α), 4.98 (H-15), 6.41 (H-22), δ_H 1.47 (H-12β) and δ_H 3.79 (H-9), 5.44 (H-17). As a result, the relative configuration of 9-OCH$_3$ was deduced to be α. Finally, the absolute configuration

of dictamlimonol E (**5**) was determined to be 9*R*,13*R*,15*S*,17*R* by ECD spectra (**Figure 4E**) comparison between experimental and calculated data.

Dictamlimonol F (**6**) was a white powder with negative optical rotation [[α]$_D^{25}$ −18.5, MeOH]. Its molecular formula, $C_{15}H_{18}O_5$, was deduced by the ion peak at *m/z* 323.11221 [M + COOH]$^-$ (calcd for $C_{16}H_{19}O_7$, 323.11253). The aglycone of **6** was suggested to be similar to those of **3**–**5** by the comparison of their ^{1}H, ^{13}C NMR spectra. The differences were as follows: the substituent of C-9 disappeared; $\Delta^{8,14}$ had changed into $\Delta^{8,9}$; and there was one more oxygenated quaternary carbon at δ_C 75.4 (C-14) in **6**. The presence of "–C=CH–CH$_2$-CH$_2$-" and "–CH=CH–O–" moieties was determined by the observation of its ^{1}H ^{1}H COZY spectrum. Moreover, the long-range correlations from H-9 to C-8, C-14; H-15 to C-13, C-14, C-16; H-17 to C-16, C-20–22; H$_3$-18 to C-12–14, C-17; H$_3$-30 to C-8, C-9, C-14 were observed in the HMBC spectrum. As a result, the planar structure of **6** was deduced. The NOE correlations (**Figure 3**) between H$_3$-18 and H-12α, H-15, H-22; H-17 and H-12β were observed in its NOESY experiment. Moreover, Chem3D modeling was used to disclose the relative configuration of it (total energy of MM2 optimized calculation results: 33.9 kcal/mol for 14α-OH; 28.1 kcal/mol for 14β-OH). According to the relative stability, the relative configuration of **6** was speculated. The absolute configuration, 13*S*,14*S*,15*S*,17*S*, was clarified by comparing the experimental ECD spectrum (**Figure 4F**) with that of the calculated one.

FIGURE 2 | The main ^{1}H ^{1}H COZY and HMBC correlations of **1–6**.

Meanwhile, comparing the NMR data reported in the literatures, the structures of seven known compounds (**7–13**) were determined.

NO is closely associated with inflammation. Agents that block NO production might be beneficial for the treatment of inflammatory responses. The LPS-stimulated RAW 264.7 cells were used as a potential *in vitro* anti-inflammatory activity screening model to investigate the NO production inhibitory effect of limonoids **1–13** at a final concentration of 20 μM. Compared to the LPS group, compounds **5**, **7–11**, and **13** exhibited potential *in vitro* anti-inflammatory activities at 20 μM (**Table 7**).

Within the active compounds, **5**, **11**, and **13** were selected for further research. It was found they inhibited NO release from RAW 264.7 cells in a concentration-dependent manner at 5, 10, and 20 μM (**Figure 5**).

The structure–activity relationships on NO production in LPS-stimulated RAW 264.7 cells were summarized as follows: In compounds **2** and **11–13**, hydroxyl group or glucosyl group substitution at position 9 weakened the activity (**11** and **13** > **2** and **12**). Although the specimen was limited, carbonyl substitution at position 23 showed enhanced activity (**13** > **11**). In compounds **3–6**, α type alkoxy group substitution showed stronger inhibitory effects on NO production than β type (**5** > **3** and **4**).

LPS can stimulate the acute inflammatory response by increasing expression of tumor necrosis factor (TNF-α) and interleukin 6 (IL-6), inducible nitric oxide synthase (iNOS), nuclear factor kappa-light-chain-enhancer of activated B cells (NF-κB), and cyclooxygenase-2 (COX-2), successively (Ahujaa et al., 2019). In the process, the expressions of TNF-α, IL-6, iNOS/NO, NF-κB, as well as COX-2 will be upregulated, which will promote tissue damage and chronic disease. Therefore, the Western blot method was used to study the anti-inflammatory mechanism of compounds **5**, **11**, and **13** by determining the levels of these five proteins in LPS-stimulated RAW 264.7 cells.

Compared with the normal group, LPS treatment led to an obvious upregulation in the protein expressions of TNF-α, IL-6, NF-κB, iNOS, and COX-2. Compounds **5**, **11**, and **13** were found to inhibit the expression of the abovementioned proteins in a dose-dependent manner (**Figures 6–8**).

Among the anti-inflammatory active compounds, fraxinellone (**11**) had been found to inhibit LPS-induced NO production and reduce the LPS-induced expressions of iNOS and COX-2 at the mRNA and protein levels in a dose-dependent manner by regulating NF-κB in RAW 264.7 macrophage-like cells (Kim et al., 2009; Lee et al., 2009; Wu et al., 2014), which was identical to our experimental result, suggesting that our screening system was stable and suitable. Meanwhile, the effects and the mechanism of a new compound, dictamlimonol D (**5**), as well as the known compound, dasylactone A (**13**), in inflammation were
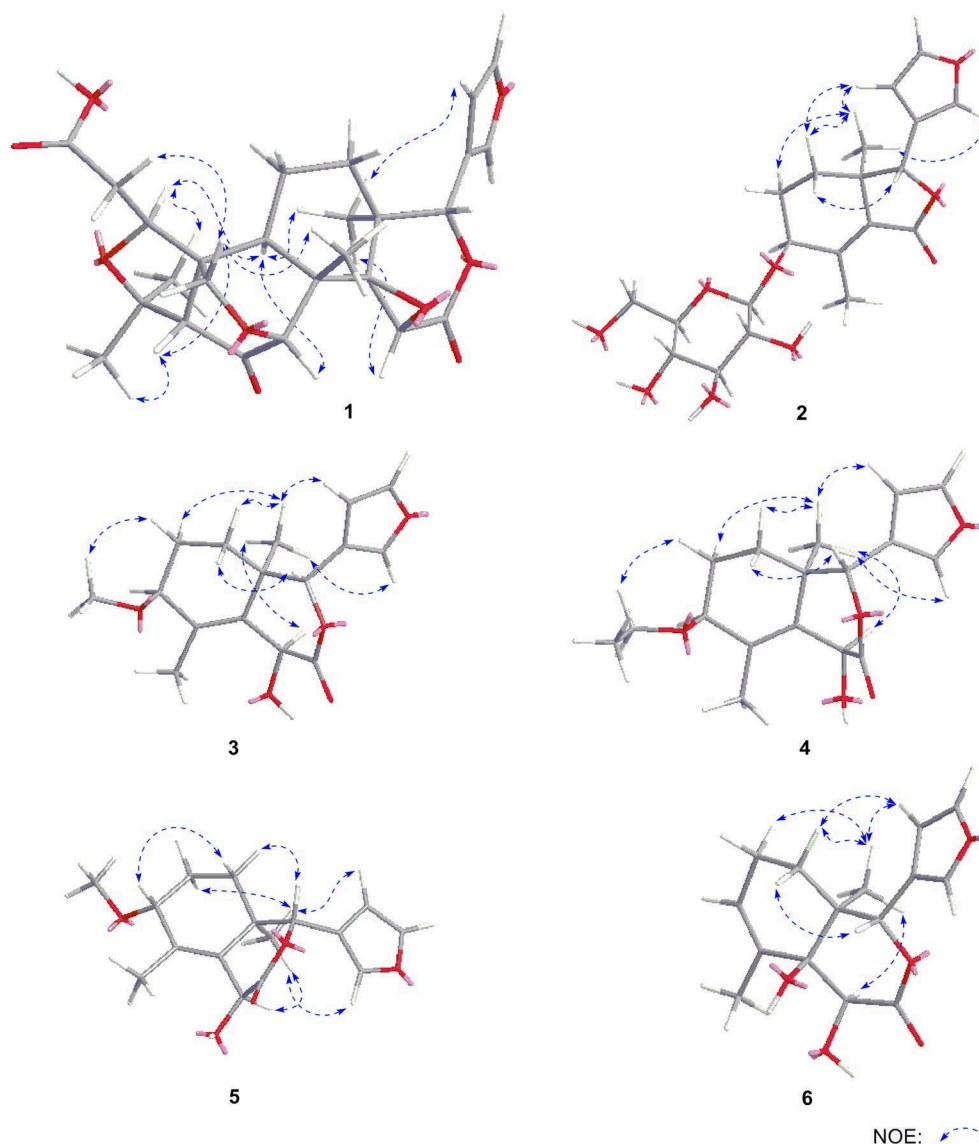
FIGURE 3 | The main NOE correlations of **1–6**.

characterized here firstly, which would provide new candidate drugs for inflammation-related diseases.

Since fraxinellone (**11**) is the main constituent in *Cortex Dictamni*, and the content of it is about 0.15% in *Cortex Dictamni*, we can predict that the anti-inflammatory activity of the plant is mainly derived from limonoids, especially fraxinellone. Further mechanism and clinical studies for it is necessary.

MATERIALS AND METHODS

Materials and Methods for Phytochemistry Research

General Experimental Procedures

Optical rotations were measured on a Rudolph Autopol® IV automatic polarimeter (l = 50 mm) (Rudolph Research

Analytical, Hackettstown NJ, USA). NMR spectra were determined on a Bruker 500-MHz NMR spectrometer (Bruker BioSpin AG Industriestrasse 26 CH-8117, Fällanden, Switzerland) at 500 MHz for ^{1}H and 125 MHz for ^{13}C NMR (internal standard: TMS). IR spectra were recorded on a Varian 640-IR FT-IR spectrophotometer (Varian Australia Pty Ltd., Mulgrave, Australia). Negative-ion mode ESI-Q-Orbitrap-MS was obtained on a Thermo ESI-Q-Orbitrap MS mass spectrometer connected with the UltiMate 3000 UHPLC instrument via ESI interface (Thermo Fisher Scientific, Inc., Waltham, MA, USA).

CC was performed on macroporous resin D101 (Haiguang Chemical Co., Ltd., Tianjin, China), silica gel (48–75 μm, Qingdao Haiyang Chemical Co., Ltd., Qingdao, China), and ODS (40–63 μm, YMC Co., Ltd., Tokyo, Japan). pHPLC columns,

FIGURE 4 | Calculated and experimental ECD spectra of **1**–**6 (A–F)** in acetonitrile.
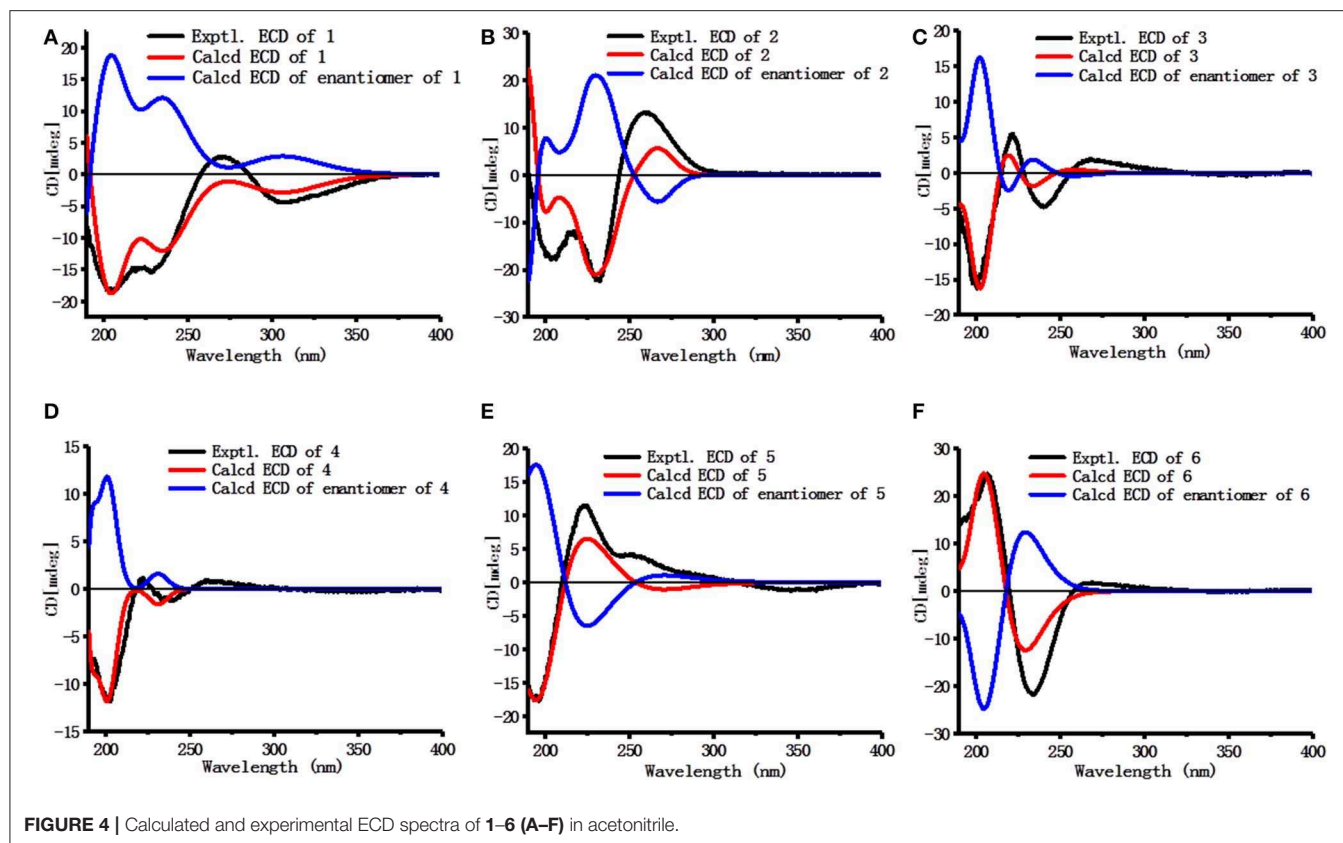
TABLE 3 | ^{1}H and ^{13}C NMR data for **3** in CDCl$_3$.

No.	δ_C	δ_H (J in Hz)	No.	δ_C	δ_H (J in Hz)
8	134.8		16	170.9	
9	77.1	3.46 (br. d, ca. 4)	17	79.5	5.47 (s)
11	21.6	1.73 (tt like, ca. 4, 15)	18	17.1	0.95 (s)
		1.98 (dt like, ca. 4, 15)	20	120.1	
12	27.3	1.09 (dt like, ca. 3, 15)	21	141.2	7.45 (t like, ca. 2)
		1.56 (dt like, ca. 4, 15)	22	110.0	6.40 (t like, ca. 2)
13	39.2		23	142.8	7.38 (t like, ca. 2)
14	136.7		30	17.0	1.90 (s)
15	66.9	4.90 (s)	9-OCH$_3$	57.3	3.41 (s)

TABLE 4 | ^{1}H and ^{13}C NMR data for **4** in CDCl$_3$.

No.	δ_C	δ_H (J in Hz)	No.	δ_C	δ_H (J in Hz)
8	134.9		17	79.4	5.48 (s)
9	75.3	3.56 (br. d, ca. 4)	18	17.2	0.95 (s)
11	22.6	1.75 (tt like, ca. 4, 15)	20	120.1	
		1.94 (m)	21	141.3	7.46 (t like, ca. 2)
12	27.4	1.08 (dt like, ca. 3, 13)	22	110.0	6.41 (t like, ca. 2)
		1.55 (dt like, ca. 3, 13)	23	142.8	7.37 (t like, ca. 2)
13	39.2		30	16.9	1.89 (s)
14	136.6		1′	65.2	3.47, 3.70 (both m)
15	66.9	4.91 (s)	2′	15.5	1.25 (t, 7.0)
16	170.9				

Cosmosil 5C$_{18}$-MS-II (20 mm i.d. ×250 mm, Nacalai Tesque, Inc., Kyoto, Japan), and Cosmosil PBr (20 mm i.d. ×250 mm, Nacalai Tesque, Inc., Kyoto, Japan) were used to separate the constituents.

Plant Material

Cortex Dictamni was purchased from the medicine market in Anguo city, Heibei province, China, and identified by Dr. Li Tianxiang (Experiment Teaching Department, Tianjin University of Traditional Chinese Medicine). The voucher specimen was deposited at the Academy of Traditional Chinese Medicine of Tianjin University of TCM.

Extraction and Isolation

Cortex Dictamni (9.0 kg) was refluxed with 70% EtOH-H$_2$O. The 70% EtOH extract (1725.3 g) was partitioned in an EtOAc-H$_2$O mixture (1:1, v/v). The H$_2$O layer (1253.8 g) was subjected to D101 macroporous resin CC (H$_2$O → 95% EtOH). Then, H$_2$O (1032.9 g) and 95% EtOH (123.4 g) eluates were obtained.

The 95% EtOH eluate (90.0 g) was subjected to silica gel CC [CHCl$_3$ → CHCl$_3$-MeOH (100:1 → 100:3 → 100:7, v/v) → CHCl$_3$-MeOH-H$_2$O (10:3:1 → 7:3:1 → 6:4:1, v/v/v, lower layer) → MeOH], and 12 fractions (Fr. 1–Fr. 12) were afforded. Fraction 7 (4.0 g) was isolated by ODS CC [MeOH-H$_2$O

TABLE 5 | ^{1}H and ^{13}C NMR data for **5** in CDCl$_3$.

No.	δ_C	δ_H (J in Hz)	No.	δ_C	δ_H (J in Hz)
8	137.7		16	170.8	
9	78.2	3.79 (dd, 8.0, 10.0)	17	79.9	5.44 (s)
11	23.3	1.76 (dddd, 4.0, 10.0, 13.5, 13.5)	18	18.4	1.14 (s)
		2.14 (m)	20	119.8	
12	31.2	1.32 (dt like, *ca*. 4, 14)	21	141.2	7.46 (t like, *ca*. 2)
		1.47 (dt like, *ca*. 4, 14)	22	109.9	6.41 (t like, *ca*. 2)
13	39.1		23	143.0	7.42 (t like, *ca*. 2)
14	134.9		30	14.6	1.86 (s)
15	67.3	4.98 (br. s)	9-OCH$_3$	56.0	3.37 (s)

TABLE 6 | ^{1}H and ^{13}C NMR data for **6** in C$_5$D$_5$N.

No.	δ_C	δ_H (J in Hz)	No.	δ_C	δ_H (J in Hz)
8	135.3		16	172.7	
9	128.8	5.90 (m)	17	80.3	6.36 (s)
11	21.8	2.03 (m)	18	18.3	1.18 (s)
12	33.7	1.64 (ddd, 3.5, 3.5, 13.0)	20	122.8	
		2.35 (m)	21	141.1	7.76 (t like, *ca*. 2)
13	40.8		22	111.0	6.71 (t like, *ca*., 2)
14	75.4		23	143.4	7.65 (t like, *ca*., 2)
15	74.7	5.15 (s)	30	18.4	2.03 (s)

TABLE 7 | Inhibitory effects of positive control and **1–13** on NO production in RAW 264.7 cells.

No.	NRC (%)	No.	NRC (%)	No.	NRC (%)
Normal	1.5 ± 0.5	**4**	102.2 ± 3.1	**10**	91.5 ± 2.6**
Control	100.0 ± 3.3	**5**	73.3 ± 2.6***	**11**	56.5 ± 3.5***
DEX	71.8 ± 0.9***	**6**	103.8 ± 3.0	**12**	97.4 ± 1.1
1	101.6 ± 3.7	**7**	90.4 ± 2.6**	**13**	10.5 ± 0.3***
2	99.2 ± 1.9	**8**	90.2 ± 0.7**		
3	99.9 ± 2.3	**9**	92.2 ± 2.4**		

*N, Unstimulated normal (negative control); C, Control group (stimulated by LPS); D, Dexamethasone (Dex, a positive control). Nitrite relative concentration (NRC): percentage of control group, which set as 100%. Values represent the mean ± SD of three determinations. **P < 0.01; ***P < 0.001 (differences between the compound-treated group and the control group). n = 4. Final concentration was 20 μM for **1–13**, and 1 μg/ml for Dex, respectively.*

$(10\% \rightarrow 20\% \rightarrow 30\% \rightarrow 40\% \rightarrow 50\% \rightarrow 60\% \rightarrow 100\%$, v/v)] to give nine fractions (Fr. 7-1–Fr. 7-9). Fraction 7-6 (923.7 mg) was separated by Sephadex LH-20 CC (MeOH), and three fractions (Fr. 7-6-1–Fr. 7-6-3) were obtained. Fraction 7-6-2 (526.5 mg) was purified by pHPLC [MeOH-H$_2$O (50:50, v/v), Cosmosil 5C$_{18}$-MS-II column] to gain dictamlimonoside B (**2**, 27.4 mg).

The EtOAc layer (175.0 g, E) was isolated by silica gel CC [hexane-EtOAc (100:1 $\rightarrow$ 20:1 $\rightarrow$ 10:1 $\rightarrow$ 5:1 $\rightarrow$ 3:1 $\rightarrow$ 1:1 $\rightarrow$ 0:1, v/v) $\rightarrow$ MeOH] to afford 10 fractions (Fr. E-1–Fr. E-10). Fraction E-4 (25.2 g) was separated by silica gel CC [hexane-EtOAc (1:1, v/v)] to gain fraxinellone (**11**, 8.0 g).

Fraction E-7 (3.2 g) was isolated by pHPLC [MeOH-H$_2$O (80:20, v/v), Cosmosil 5C$_{18}$-MS-II column], and nine fractions (Fr. E-7-1–Fr. E-7-9) were obtained. Fraction E-7-2 (278.5 mg) was purified by pHPLC [MeOH-H$_2$O (75:25, v/v), Cosmosil PBr column] to afford dictamlimonol D (**4**, 56.9 mg). Fraction E-8 (37.0 g) was centrifuged after dissolving in hexane, and two fractions (Fr. E-8-1–Fr. E-8-2) were gained. Fraction E-8-1 (70.0 mg) was isolated by pHPLC [MeOH-H$_2$O (50:50, v/v), Cosmosil 5C$_{18}$-MS-II column] to obtain dictamlimonol A (**1**, 8.7 mg) and limonin (**7**, 22.3 mg). Fraction E-8-2 (35.16 g) was subjected to silica gel CC [PE-EtOAc (5:1 $\rightarrow$ 3:1 $\rightarrow$ 2:1 $\rightarrow$ 1:1 $\rightarrow$ 0:1, v/v)], and nine fractions (Fr. E-8-2-1–Fr. 8-2-9) were afforded. Fraction E-8-2-5 (4.4 g) was separated by pHPLC [MeOH-H$_2$O (67:33, v/v), Cosmosil 5C$_{18}$-MS-II column] to provide nine fractions (Fr. E-8-2-5-1–Fr. E-8-2-5-9). Fraction E-8-2-5-1 (1396.6 mg) was subjected to pHPLC [MeOH-H$_2$O (65:35, v/v), Cosmosil PBr column], and eight fractions (Fr. E-8-2-5-1-1–Fr. E-8-2-5-1-8) were given. Fraction E-8-2-5-1-3 (190.9 mg) was purified by pHPLC [MeOH-H$_2$O (45:55, v/v), Cosmosil 5C$_{18}$-MS-II column] to afford dictamlimonol F (**6**, 22.1 mg) and 9β-hydroxyfraxinellone (**12**, 33.8 mg). Fraction E-8-2-5-1-4 (81.0 mg) was isolated by pHPLC [MeOH-H$_2$O (55:45, v/v), Cosmosil PBr column] to gain dictamlimonol E (**5**, 12.2 mg). Fraction E-8-2-5-1-6 (81.2 mg) was further subjected to pHPLC [MeOH-H$_2$O (65:35, v/v), Cosmosil PBr column], and dictamlimonol C (**3**, 63.1 mg) was afforded. Fraction E-8-2-6 (7.1 g) was separated by silica gel CC [PE-EtOAc (5:1 $\rightarrow$ 4:1 $\rightarrow$ 3:1 $\rightarrow$ 2:1 $\rightarrow$ 1:1 $\rightarrow$ 0:1, v/v) $\rightarrow$ MeOH] to afford eight fractions (Fr. E-8-2-6-1–Fr. E-8-2-6-8). Among them, fraction E-8-2-6-8 was identified as obacunon (**9**, 1380.0 mg). Fraction E-8-2-6-4 (3483.7 mg) was isolated by pHPLC [MeOH-H$_2$O (85:15, v/v), Cosmosil 5C$_{18}$-MS-II column], and 10 fractions (Fr. E-8-2-6-4-1–Fr. E-8-2-6-4-10) were obtained. Fraction E-8-2-6-4-1 (778.2 mg) was subjected to pHPLC [CH$_3$CN-H$_2$O (42:58, v/v), Cosmosil 5C$_{18}$-MS-II column] to provide six fractions (Fr. E-8-2-6-4-1-1–Fr. E-8-2-6-4-1-6). Fraction E-8-2-6-4-1-6 (70.5 mg) was purified by pHPLC [MeOH-H$_2$O (60:40, v/v), Cosmosil PBr column] to gain dasylactone A (**13**, 32.4 mg). Fraction E-8-2-6-4-2 (693.5 mg) was isolated by pHPLC [CH$_3$CN-H$_2$O (42:58, v/v), Cosmosil 5C$_{18}$-MS-II column] to afford five fractions (Fr. E-8-2-6-4-2-1–Fr. E-8-2-6-4-2-5). Fraction E-8-2-6-4-2-5 (50.8 mg) was further purified by pHPLC [MeOH-H$_2$O (70:30, v/v), Cosmosil 5C$_{18}$-MS-II column], and 7α-obacunyl acetate (**10**, 9.6 mg) was obtained. Fraction E-8-2-7 (3.1 g) was separated by pHPLC [MeOH-H$_2$O (62:38, v/v), Cosmosil 5C$_{18}$-MS-II column] to obtain seven fractions (Fr. E-8-2-7-1–Fr. E-8-2-7-7). Fraction E-8-2-7-3 (80.6 mg) was purified by pHPLC [MeOH-H$_2$O (57:43, v/v), Cosmosil 5C$_{18}$-MS-II column] to gain limonin diosphenol (**8**, 16.7 mg).

Dictamlimonol A (**1**). White powder; $[\alpha]_D^{25}$ −100.0 (*conc* 0.10, MeOH); UV λ_{max} (MeOH) nm (log ε): 204 (4.05), 280 (3.35); CD (*conc.* 0.002 M, CH$_3$CN) mdeg (λ_{nm}): −18.3 (223), −14.8 (223), −15.3 (228), +2.7 (271), −4.1 (307); IR ν_{max} (KBr) cm^{-1}: 3,515, 3,243, 2,985, 2,951, 1,746, 1,708, 1,652, 1,458, 1,390, 1,368, 1,281, 1,220, 1,176, 1,131, 1,105, 1,058, 1,023, 960, 898, 884, 828, 796; ^{1}H NMR (C$_5$D$_5$N, 500 MHz), ^{13}C NMR (C$_5$D$_5$N, 125 MHz); see **Table 1**. ESI-Q-Orbitrap MS Negative-ion mode
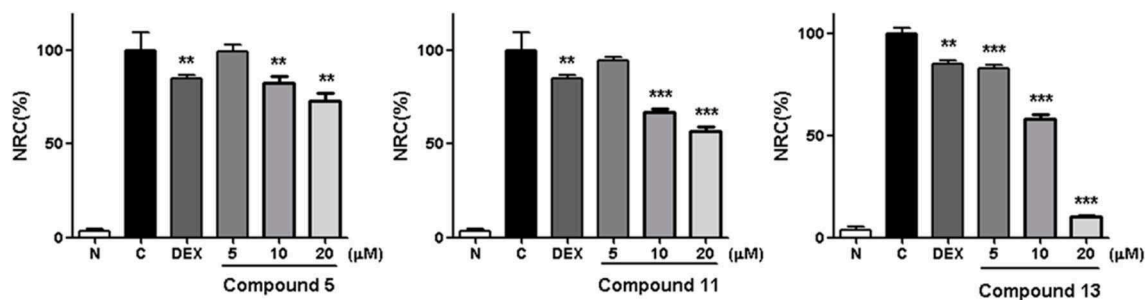
FIGURE 5 | Inhibitory effects of **5**, **11**, and **13** in the concentration of 5, 10 and 20 μM on NO production in RAW 264.7 cells. N, normal group without LPS, DEX, and other tested samples. C, control group with LPS. Nitrite relative concentration (NRC): percentage of control group, set as 100%. Values represent the mean ± SD of three determinations. **$P < 0.01$; ***$P < 0.001$ (differences between the compound-treated group and the control group). $N = 4$. Final concentration was 5, 10, and 20 μM for **5**, **11**, and **13**, respectively.
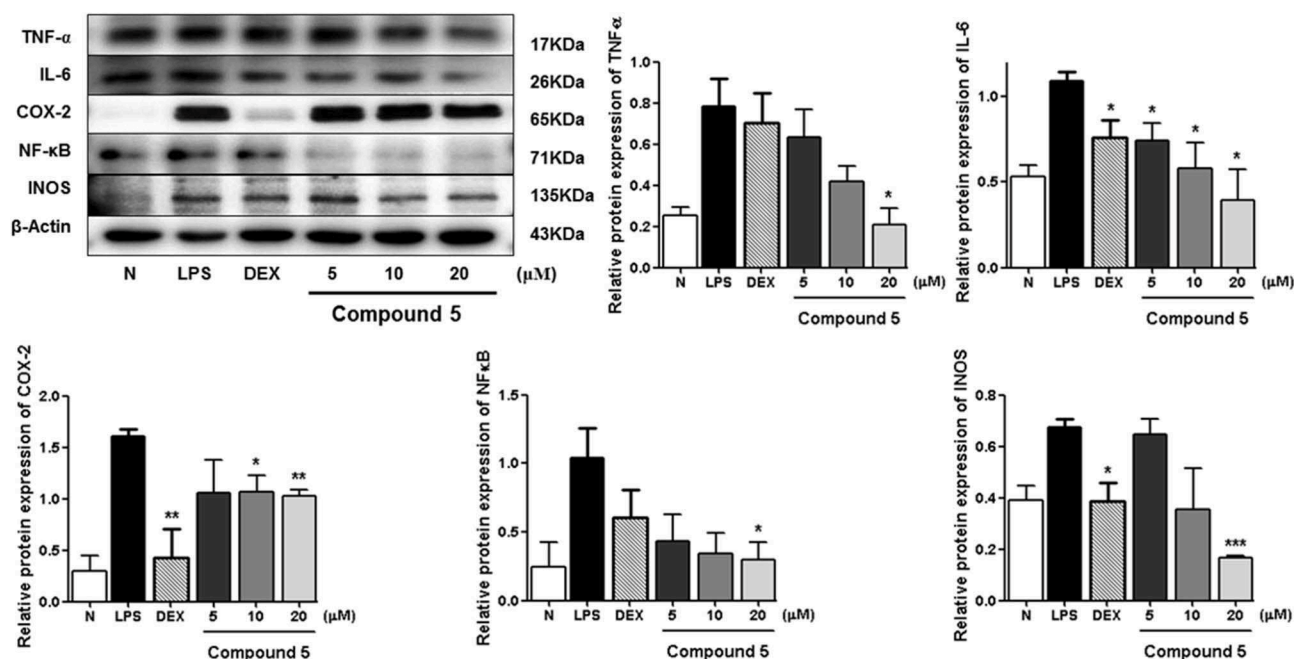
FIGURE 6 | Inhibitory effects of **5** on the protein expression of TNF-α, IL-6, COX-2, NF-κB, and iNOS in RAW 264.7 cells. N, normal group without LPS, DEX, and other tested samples. Values represent the mean ± SEM of three determinations. *$P < 0.05$; **$P < 0.01$; ***$P < 0.001$ (differences between the compound-treated group and the control group) $N = 3$.

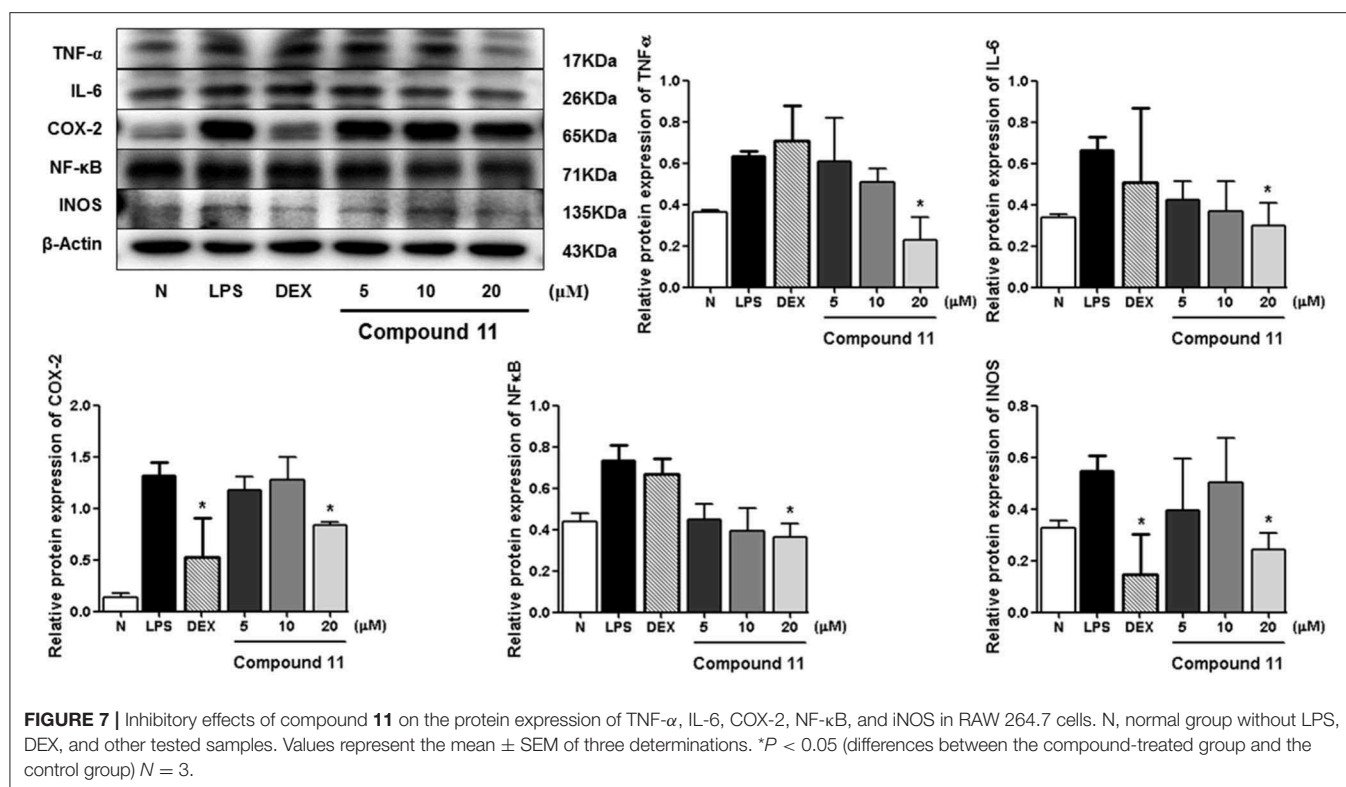m/z 485.17969 $[M - H]^-$ (calcd for $C_{26}H_{29}O_9$, 485.18061) (**Figures S1–S8**).

Dictamlimonoside B (**2**). White powder; $[\alpha]_D^{25}$ −72.1 (*conc* 0.61, MeOH); UV λ_{max} (MeOH) nm (log ε): 213 (4.20); CD (*conc.* 0.002 M, CH$_3$CN) mdeg (λ_{nm}): −17.5 (204), −12.4 (216), −21.8 (231), +13.0 (259); IR ν_{max} (KBr) cm^{-1}: 3,359, 2,931, 2,876, 1,755, 1,678, 1,504, 1,448, 1,406, 1,378, 1,344, 1,289, 1,226, 1,209, 1,161, 1,077, 1,048; ^{1}H NMR (CD$_3$OD/DMSO-d_6, 500 MHz), ^{13}C NMR (CD$_3$OD/DMSO-d_6, 125 MHz); see **Table 2**. ESI-Q-Orbitrap MS Negative-ion mode m/z 455.15375 $[M + COOH]^-$ (calcd for $C_{21}H_{27}O_{11}$, 455.15479) (**Figures S9–S19**).

Dictamlimonol C (**3**). White powder; $[\alpha]_D^{25}$ −74.6 (*conc* 0.81, MeOH); UV λ_{max} (MeOH) nm (log ε): 206 (4.10); CD

(*conc.* 0.002 M, CH$_3$CN) mdeg (λ_{nm}): −15.4 (200), +4.9 (222), −4.7 (240), +1.8 (268), −0.2 (355); IR ν_{max} (KBr) cm^{-1}: 3,445, 3,152, 2,973, 2,941, 2,863, 2,825, 1,748, 1,653, 1,505, 1,458, 1,381, 1,350, 1,327, 1,278, 1,192, 1,162, 1,133, 1,109, 1,070, 1,025, 994, 907, 874, 800, 764, 732; ^{1}H NMR (CDCl$_3$, 500 MHz), ^{13}C NMR (CDCl$_3$, 125 MHz); see **Table 3**. ESI-Q-Orbitrap MS Negative-ion mode m/z 337.12790 $[M + COOH]^-$ (calcd for $C_{17}H_{21}O_7$, 337.12818) (**Figures S20–S27**).

Dictamlimonol D (**4**). White powder; $[\alpha]_D^{25}$ −68.0 (*conc* 0.88, MeOH); UV λ_{max} (MeOH) nm (log ε): 206 (4.10), 239 (3.51, sh); CD (*conc.* 0.002 M, CH$_3$CN) mdeg (λ_{nm}): −11.3 (201), +0.8 (223), −1.1 (240), +0.8 (262), −0.2 (350); IR ν_{max} (KBr) cm^{-1}: 3,383, 3,147, 2,973, 2,941, 2,869, 1,750, 1,653, 1,506,

FIGURE 7 | Inhibitory effects of compound **11** on the protein expression of TNF-α, IL-6, COX-2, NF-κB, and iNOS in RAW 264.7 cells. N, normal group without LPS, DEX, and other tested samples. Values represent the mean ± SEM of three determinations. *$P < 0.05$ (differences between the compound-treated group and the control group) $N = 3$.

1,457, 1,380, 1,345, 1,325, 1,278, 1,265, 1,198, 1,162, 1,064, 1,024, 1,001, 911, 875, 800, 765, 731; ^{1}H NMR (CDCl$_3$, 500 MHz), ^{13}C NMR (CDCl$_3$, 125 MHz); see **Table 4**. ESI-Q-Orbitrap MS Negative-ion mode *m/z* 351.14261 [M + COOH]$^-$ (calcd for C$_{18}$H$_{23}$O$_7$, 351.14383) (**Figures S28–S35**).

Dictamlimonol E (**5**). White powder; [α]$_D^{25}$ −9.1 (*conc* 0.35, MeOH); UV λ_{max} (MeOH) nm (log ε): 208 (3.94), 253 (3.04, sh); CD (*conc.* 0.001 M, CH$_3$CN) mdeg (λ_{nm}): −17.3 (195), +11.3 (224), +4.1 (251), −1.1 (347); IR ν_{max} (KBr) cm^{-1}: 3,481, 3,148, 2,943, 2,876, 2,823, 1,749, 1,653, 1,506, 1,456, 1,380, 1,353, 1,282, 1,222, 1,163, 1,093, 1,023, 996, 911, 877, 802, 765, 731; ^{1}H NMR (CDCl$_3$, 500 MHz), ^{13}C NMR (CDCl$_3$, 125 MHz); see **Table 5**. ESI-Q-Orbitrap MS Negative-ion mode *m/z* 337.12818 [M + COOH]$^-$ (calcd for C$_{17}$H$_{21}$O$_7$, 337.12818) (**Figures S36–S43**).

Dictamlimonol F (**6**). White powder; [α]$_D^{25}$ −18.5 (*conc* 0.52, MeOH); UV λ_{max} (MeOH) nm (log ε): 203 (4.01), 249 (3.06, sh); CD (*conc.* 0.002 M, CH$_3$CN) mdeg (λ_{nm}): +23.9 (207), −21.4 (234), +1.7 (266); IR ν_{max} (KBr) cm^{-1}: 3,447, 3,149, 2,972, 2,944, 2,889, 1,745, 1,668, 1,550, 1,504, 1,450, 1,384, 1,305, 1,278, 1,160, 1,143, 1,023, 992, 970, 875, 806, 771, 758, 719; ^{1}H NMR (C$_5$D$_5$N, 500 MHz), ^{13}C NMR (C$_5$D$_5$N, 125 MHz); see **Table 6**. ESI-Q-Orbitrap MS Negative-ion mode *m/z* 323.11221 [M + COOH]$^-$ (calcd for C$_{16}$H$_{19}$O$_7$, 323.11253) (**Figures S44–S51**).

Enzymatic Hydrolysis of 2 With β-Glucosidase

Compound **2** (10.0 mg) was hydrolyzed with β-glucosidase (10.0 mg) in H$_2$O (1.0 ml) at 37°C for 5 h. After cooling, the reaction mixture was partitioned with EtOAc. The EtOAc layer was separated by silica gel CC [Hexane-EtOAc (3:2, v/v)] to yield 9β-hydroxyfraxinellone (**12**, 5.1 mg, 84.3%).

Acid Hydrolysis of 2

Acid hydrolysis reaction was performed by using a similar method to our previously reported one (Zhang et al., 2015), and D-glucose (12.6 min, positive optical rotation) from **2** was identified by comparison of its retention time and optical rotation with that of the authentic sample.

ECD Calculation

The calculations for ECD spectra were conducted as published previously (Shi et al., 2019).

Materials and Methods for Anti-inflammatory Assay
Materials

The materials for anti-inflammatory assay were similar to those reported by us (Ruan et al., 2019).

Cell Culture

RAW 264.7 macrophage-like cells were cultured by the method reported previously (Ruan et al., 2019).

Cell Viability Assay

Cell viability of RAW 264.7 macrophage-like cells was performed by MTT colorimetric assay (result shown in **Figure S52**) (Ruan et al., 2019).

Measurement of NO Levels

After pretreating compounds **1–13** to cells for 1 h, the cells were stimulated with LPS (1 μg/ml) for 18 h. Each culture medium (50 μl) was mixed with an equal volume of Griess reagent after incubation. An ELISA plate reader was used to determine the

FIGURE 8 | Inhibitory effects of compound **13** on the protein expression of TNF-α, IL-6, COX-2, NF-κB, and iNOS in RAW 264.7 cells. N, normal group without LPS, DEX, and other tested samples. Values represent the mean $\pm$ SEM of three determinations. *$P < 0.05$; **$P < 0.01$; ***$P < 0.001$ (differences between the compound-treated group and the control group) $N = 3$.
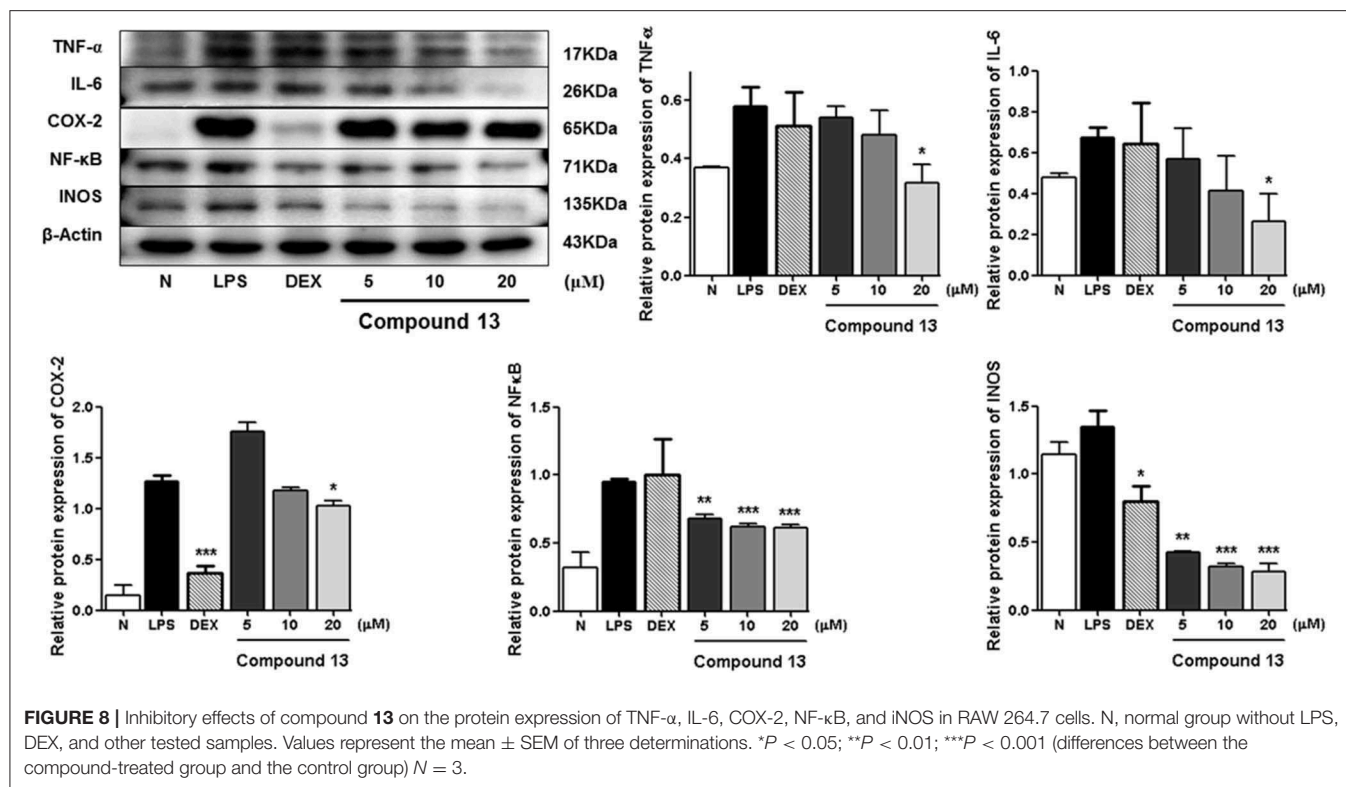
nitrite level (a major stable product of NO) at 540 nm, and the concentrations were calculated by referring to a NaNO$_2$ standard calibration curve.

Western Blot Analysis

Western blot method was used to study the anti-inflammatory mechanism of compounds **5**, **11**, and **13** by determining the levels of these five proteins (TNF-α, IL-6, COX-2, NF-κB, and iNOS) in LPS-stimulated RAW 264.7 cells as previously reported (He et al., 2018; Ruan et al., 2019). The raw quantification data were displayed in **Figures S53–S55**.

Statistical Analysis

Values were statistically analyzed by using SPSS 17.0 software. $P < 0.05$ was considered to indicate statistical significance. One-way analysis of variance (ANOVA) and Tukey's Studentized range test were used for the evaluation of the significant differences between means and *post hoc*, respectively.

CONCLUSION

In this study, 13 limonoids including 6 new ones, named dictamlimonol A (**1**), dictamlimonoside B (**2**), and dictamlimonols C–F (**3**–**6**), along with 7 known ones (**7**–**13**) were isolated from *Cortex Dictamni* by various chromatographies and identified by spectroscopies and chemical reactions. Among them, compound **1** was a first 7,19-epoxy limonoid found in natural products. Activity evaluation research showed several kinds of limonoids reduce expression of TNF-α, IL-6, iNOS,

NF-κB, and COX-2 in LPS-stimulated RAW 264.7 cells. These findings support the idea that the administration of *Cortex Dictamni* may be beneficial for inflammation.

DATA AVAILABILITY STATEMENT

The datasets generated for this study are available on request to the corresponding author.

AUTHOR CONTRIBUTIONS

YiZ and TW designed the research and wrote the manuscript. JR and YC performed the activity research. FS, SY, YinZ, and JY contributed to the isolation, purification, and characterization of all compounds. HW and YG performed the ECD calculation. HY perfected the language. All authors discussed, edited, and approved the final version.

FUNDING

SUPPLEMENTARY MATERIAL

The Supplementary Material for this article can be found online at: https://www.frontiersin.org/articles/10.3389/fchem.2020.00073/full#supplementary-material

REFERENCES

Ahujaa, A., Kim, M. Y., and Cho, J. Y. (2019). *Protium javanicum* burm. Methanol extract attenuates LPS-induced inflammatory activities in macrophage-like RAW264.7 cells. *Evid. Based Compl. Alter. Med.* 2019:2910278. doi: 10.1155/2019/2910278

Akihisa, T., Nishimoto, Y., Ogihara, E., Matsumoto, M., Zhang, J., and Abe, M. (2017). Nitric oxide production-inhibitory activity of limonoids from *Azadirachta indica* and *Melia azedarach*. *Chem. Biodivers.* 14:e1600468. doi: 10.1002/cbdv.201600468

Bennett, R. D., and Hasegawa, S. (1982). 7α-Oxygenated limonoids from the *Rutaceae*. *Phytochemistry* 21, 2349–2354. doi: 10.1016/0031-9422(82)85203-5

D'Ambrosio, M., and Guerriero, A. (2002). Degraded limonoids from *Melia azedarach* and biogenetic implications. *Phytochemistry* 60, 419–424. doi: 10.1016/S0031-9422(02)00107-3

Dong, L., Liu, X., Li, Z., Yin, M., and Qiu, M. (2010). Studies on chemical constituents from fruits of *Citrus medica* L. *Jingxi Huagong* 27, 982–986. doi: 10.13550/j.jxhg.2010.10.020

Du, C., Yang, X., and Tu, P. (2005). Studies on chemical constituents in bark of *Dictamnus dasycarpus*. *Zhongguo. Zhongyao. Zazhi.* 30, 1663–1666.

Frisch, M. J., Trucks, G. W., Schlegel, H. B., Scuseria, G. E., Robb, M. A., Cheeseman, J. R., et al. (2009). *Gaussian 09, Revision A. 02.* Wallingford, CT: Gaussian, Inc.

Guo, L. N. (2011). *Studies on the constituents from dictamnus dasycarpus and rehmannia glutinosa* (doctoral dissertation). Shenyang Pharmaceutical University, Shenyang, China.

He, W., Li, Y., Liu, M., Yu, H., Chen, Q., Chen, Y., et al. (2018). Citrus aurantium L. and its flavonoids regulate TNBS-induced inflammatory bowel disease through anti-inflammation and suppressing isolated jejunum contraction. *Inter. Int. J. Mol. Sci.* 19:E3057. doi: 10.3390/ijms19103057

Hu, Y., Heng, L., Xu, R., Li, J., Wei, S., Xu, D., et al. (2018). Meliacarpinin-type limonoids from the bark of *Melia toosendan*. *Molecules* 23:E2590. doi: 10.3390/molecules23102590

Kim, J. H., Park, Y. M., Shin, J. S., Park, S. J., Choi, J. H., Jung, H. J., et al. (2009). Fraxinellone inhibits lipopolysaccharide-induced inducible nitric oxide synthase and cyclooxygenase-2 expression by negatively regulating nuclear factor-kappa B in RAW 264.7 macrophages cells. *Biol. Pharm. Bull.* 32, 1062–1068. doi: 10.1248/bpb.32.1062

Lee, C. S., Won, C., Yoo, H., Yi, E. H., Cho, Y., Maeng, J. W., et al. (2009). Inhibition of double-stranded RNA-induced inducible nitric oxide synthase expression by fraxinellone and sauchinone in murine microglia. *Biol. Pharm. Bull.* 32, 1870–1874. doi: 10.1248/bpb.32.1870

Lv, M., Xu, P., Tian, Y., Liang, J., Gao, Y., Xu, F., et al. (2015). Medicinal uses, phytochemistry and pharmacology of the genus Dictamnus (*Rutaceae*). *J. Ethnopharmacol.* 171, 247–263. doi: 10.1016/j.jep.2015.05.053

Ruan, J., Li, Z., Zhang, Y., Chen, Y., Liu, M., Han, L., et al. (2019). Bioactive constituents from the roots of *Eurycoma longifolia*. *Molecules* 24:E3157. doi: 10.3390/molecules24173157

Shi, W., Ruan, J., Guo, Y., Ding, Z., Yan, J., Qu, L., et al. (2019). Bioactive constituents study of *Pugionium cornutum* L. Gaertn on intestinal motility. *Fitoterapia* 138:104291. doi: 10.1016/j.fitote.2019.104291

Sun, Y. P., Jin, W. F., Wang, Y. Y., Wang, G., Morris-Natschke, S. L., Liu, J. S., et al. (2018). Chemical structures and biological activities of limonoids from the *Genus Swietenia* (*Meliaceae*). *Molecules* 23:E1588. doi: 10.3390/molecules23071588

Wang, M., Zhang, J., Qian, Y., Li, J., and Ji, Z. (2006). The study on fungicidal activity of *Dictamnus dasycarpus*. *Nongyao* 45, 739–741.

Wu, X. F., Ouyang, Z. J., Feng, L. L., Chen, G., Guo, W. J., Shen, Y., et al. (2014). Suppression of NF-κB signaling and NLRP3 inflammasome activation in macrophages is responsible for the amelioration of experimental murine colitis by the natural compound fraxinellone. *Toxicol. Appl. Pharmacol.* 281, 146–156. doi: 10.1016/j.taap.2014.10.002

Yang, B., Lee, H. B., Kim, S., Park, Y. C., Kim, K., and Kim, H. (2017). Decoction of *Dictamnus Dasycarpus* Turcz. root bark ameliorates skin lesions and inhibits inflammatory reactions in mice with contact dermatitis. *Pharmacogn. Mag.* 13, 483–487. doi: 10.4103/0973-1296.211034

Yang, J. L., Liu, L. L., and Shi, Y. P. (2011). Limonoids and quinoline alkaloids from *Dictamnus dasycarpus*. *Planta Med.* 77, 271–276. doi: 10.1055/s-0030-1250344

Yang, S., Li, Z., Wang, J., Ruan, J., Zheng, C., Huang, P., et al. (2018). Eudesmane-type sesquiterpene glycosides from *Dictamnus dasycarpus* Turcz. *Molecules* 23:E642. doi: 10.3390/molecules23030642

Zhang, Y., Jin, L., Chen, Q., Wu, Z., Dong, Y., Han, L., et al. (2015). Hypoglycemic activity evaluation and chemical study on hollyhock flowers. *Fitoterapia* 102, 7–14. doi: 10.1016/j.fitote.2015.02.001

An Improved and Practical Method for Synthesizing of α-Sanshools and Spilanthol

Akira Nakamura, Kazuki Mimaki, Ken-ichi Tanigami and Tomohiro Maegawa*

School of Pharmaceutical Sciences, Kindai University, Osaka, Japan

An efficient and practical route for the synthesis of α-sanshools and spilanthol is described herein. Several modifications of an existing method enabled the preparation of the (2*E*,6*Z*,8*E*,10*E*)-tetraene precursor of hydroxy-α-sanshool in good yield. A highly selective Wittig reaction employing newly synthesized phosphonium salt with low deliquescence and long-term stability yielded the desired *Z*-form tetraene. This improved methodology was shown to be applicable to the efficient synthesis of α-sanshool and spilanthol.

Keywords: sanshool, stereoselective synthesis, Wittig reaction, polyene, natural products

INTRODUCTION

Sanshools are a family of polyunsaturated fatty acid amides, differing in the length and double bond geometry of the polyunsaturated (**Figure 1**), found in various *Zanthoxylum* species (Jang et al., 2008; Devkota et al., 2012; Greger, 2016). The various biological activities of hydroxy-α-sanshool **1** have attracted a great deal of interest in the scientific community (Koo et al., 2007; Bautista et al., 2008; Yang, 2008; Munekage et al., 2013; Tang et al., 2014; Kubota et al., 2015). However, the inherent instability of their conjugated (6*Z*,8*E*,10*E*)-triene structures, which are prone to isomerization, oxidation, polymerization, and/or photo-degradation, make sanshools difficult to isolate from natural products (Yang, 2008).

The synthesis of **1** has been reported previously by two independent research groups. Igarashi and co-workers developed two stereoselective approaches to hydroxyl-α-sanshool synthesis, both employing several metal reagents and requiring precise operations (Aoki et al., 2012; Igarashi et al., 2012). Toy and co-workers constructed a (6*Z*,8*E*,10*E*)-conjugated triene precursor moiety with moderate selectivity (6*Z*:6*E* = 2:1) using the Wittig reaction; a pure stereoisomer was isolated by recrystallization (Wu et al., 2012). The purpose of the current study was to produce high-purity hydroxy-α-sanshool **1**. Among the three existing synthesis methods, Toy's is the simplest due to the use of more conventional reagents and procedures. Our synthesis of **1** via Toy's method, however, proved difficult when following the literature, and resulted in reduced yields due to the instability or deliquescence of intermediate species. Therefore, we set out to enhance the general practicality and robustness of Toy's method of sanshool synthesis.

RESULTS AND DISCUSSION

Our synthesis of hydroxy-α-sanshool began with the oxidation of 4-bromobutan-1-ol with PCC, which was poorly reproducible on the gram scale. A more effective strategy was catalytic oxidation using commercially available AZADOL as the catalyst and sodium hypochlorite pentahydrate (NaClO·5H$_2$O) as a co-oxidant (**Scheme 1**) (Okada et al., 2014). The desired 4-bromobutanal **2** was
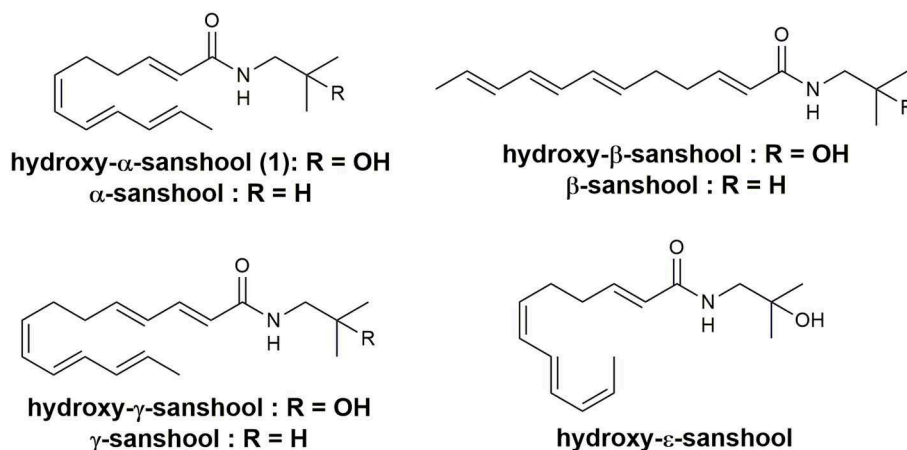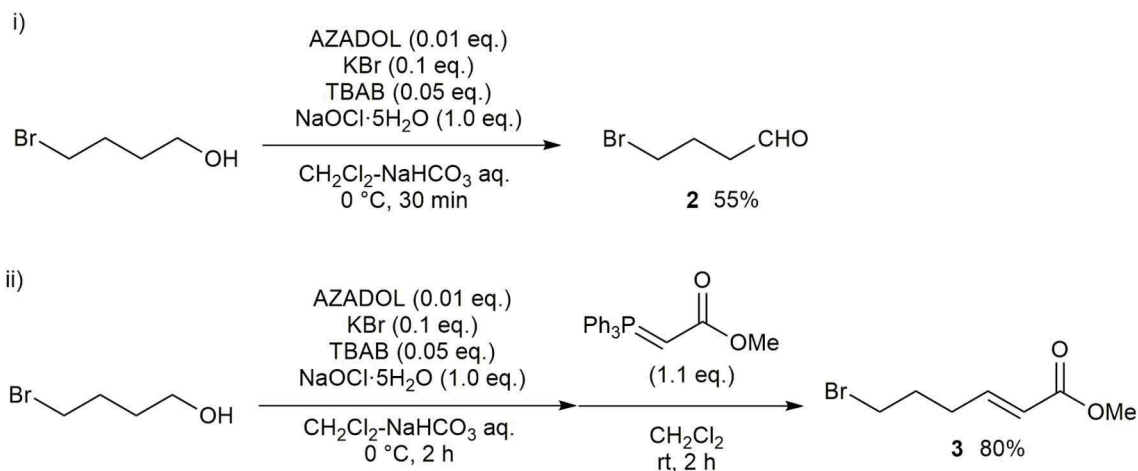
FIGURE 1 | Sanshool compounds.

SCHEME 1 | Synthesis of ester **3**.

produced in 55% yield together with small amounts of 4-bromobutanoic acid. These results were reproducible even on the gram scale (**Scheme 1**, i). Other nitroxyl radical catalysts did not improve the yield of **2**. Note that partial decomposition of **2** during purification resulting in moderate overall yields. Then, the Horner–Wadsworth–Emmons (HWE) reaction was conducted, resulting in ester **3** in 80% yield (**Scheme 1**, ii).

In an effort to improve the selectivity of the Wittig reaction (6*Z*:6*E* = 2:1), we converted ester **3** to its corresponding phosphonium salt **4a** with PPh₃ according to Toy's synthesis method. However, this reaction suffered from low reproducibility due to the high deliquescence of **4a**. We therefore evaluated several methods to create a phosphonium salt **4** with lower hygroscopicity (**Scheme 2**). First, ester **3** was hydrolyzed to carboxylic acid **5** and the phosphonium salt **4b** was obtained in good yield by the reaction with PPh₃. Unfortunately, **4b** exhibited deliquescence similar to that of **4a**. To determine the influence of the phosphonium salt counter anion on deliquescence, we

prepared the iodonium salt **4c** using the corresponding alkyl iodide **6**. However, this also resulted in a compound with high deliquescence. We found that the combination of counter anion and functional group is important in determining the deliquescence of phosphonium salts, and obtained the non-deliquescent iodine salt **4d** from the iodo ester **7**.

We next examined the stereoselective synthesis of tetraene **8** with **4d**. The results of the Wittig reaction of (2*E*,4*E*)-2,4-hexadienal **9** with phosphonium salt **4d** under various reaction conditions are summarized in **Table 1**. When *t*-BuOK or NaH was used as a base, tetraene **8** was obtained in moderate yields and 6*Z*/6*E* stereoselectivity (entries 1 and 2). The use of potassium bis(trimethylsilyl)amide (KHMDS) as a base afforded the best results. The use of KHMDS at −40°C improved the stereoselectivity of the product to 12:1, but with a slight decrease in yield (Entry 3). Conducting the reaction at −78°C failed to yield the desired product **8** (Entry 4). However, gradually increasing the temperature to −40°C from

SCHEME 2 | Investigation of phosphonium salt.
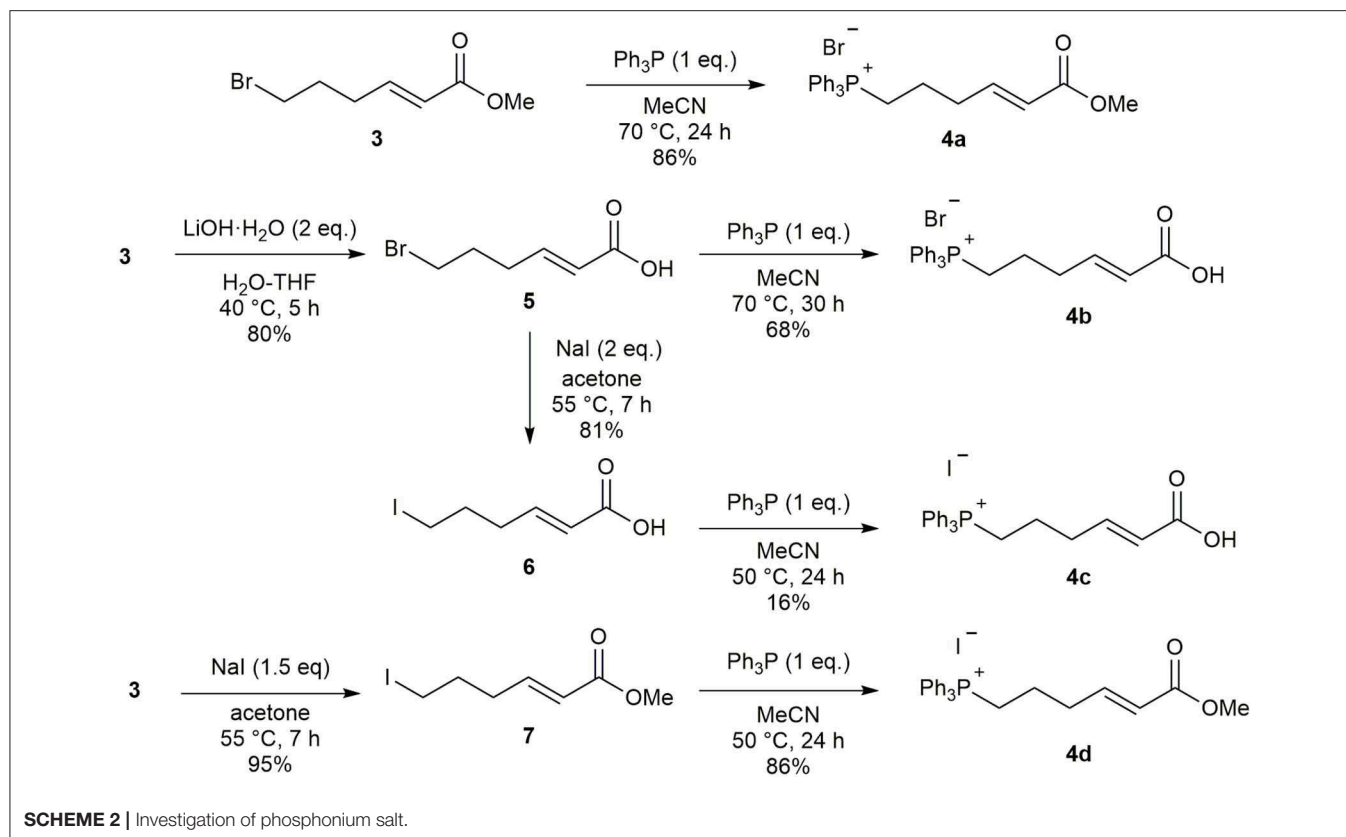
TABLE 1 | Optimization of Wittig reaction.

Entry	Base	Conditions	Yield (%)	6Z:6E[a]
1	t-BuOK	0°C, 12 h	52	5:1
2	NaH	rt, 3 h	60	4.5:1
3	KHMDS	−40°C, 2 h	43	12:1
4	KHMDS	−78°C, 6 h	–	–
5	KHMDS	−78°C, 0.5 h to −40°C, 2 h	83	>20:1

[a] The ratio of stereoisomers was determined by ^1H NMR analysis.

−78°C, after the addition of **9** to the ylide generated from **4d**, resulted in tetraene **8** in high yield and high 6Z/6E selectivity (Entry 5) (Uchiyama et al., 2017). However, other tetraene isomers, derived from small amounts of stereoisomers contained in commercially available (2E,4E)-2,4-hexadienal **9**, were still observed. We finally succeeded in obtaining (2E,6Z,8E,10E)-tetraene **8** as a single isomer in 83% yield by using pure (2E,4E)-2,4-hexadienal **9** prepared from (2E,4E)-2,4-hexadien-1-ol with manganese oxide.

Then, following Toy's method, ester **8** was converted to carboxylic acid **10** in 83% yield (**Scheme 3**). Amide formation,

via the coupling of **10** and the appropriate amine using HBTU and Et₃N, afforded hydroxy-α-sanshool **1** and α-sanshool **11** in 88% and 92% yields, respectively (please see **Supplementary Material**).

The developed method was applied to the synthesis of the biologically active compound spilanthol (Sharma et al., 2011; Barbosa et al., 2016), also known as affinin, which contains a (2E,6Z,8E)-decatrienamide moiety (**Scheme 4**). Several synthetic methods for spilanthol have been reported (Crombie et al., 1963; Ikeda et al., 1984, Ikeda et al., 1987). A recent short step synthesis by Pastre provided high stereoselectivity, but suffered from a relatively low overall yield of 18% (Alonso et al., 2018). Our synthesis, starting from the Wittig reaction of the ylide generated from **4d** and crotonaldehyde to afford ester **12**, resulted in a 95% yield of the (2E,6Z,8E)-single stereoisomer. Saponification of **12** gave carboxylic acid **13** in 91% yield. Spilanthol was then synthesized in 84% yield using the coupling reaction employed in the α-sanshool synthesis. Thus, the efficient and stereoselective synthesis of spilanthol was achieved from 4-bromobutanol in six steps with an overall yield of 47%.

CONCLUSION

We developed a practical and reproducible method for the synthesis of hydroxy-α-sanshool and α-sanshool. Notably, modifications of the Wittig reaction using a newly synthesized,
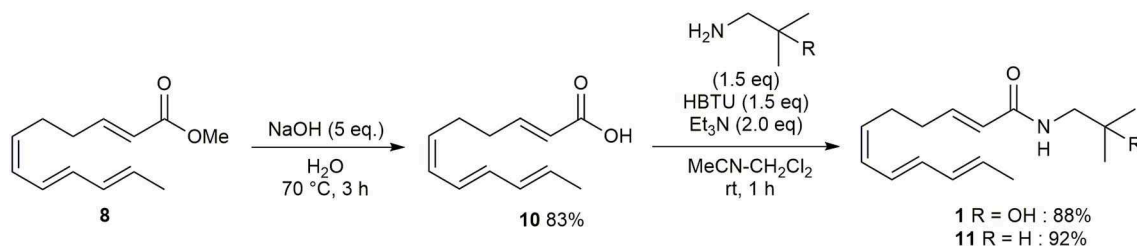
SCHEME 3 | Synthesis of hydroxy-α-sanshool **1** and α-sanshool **11**.
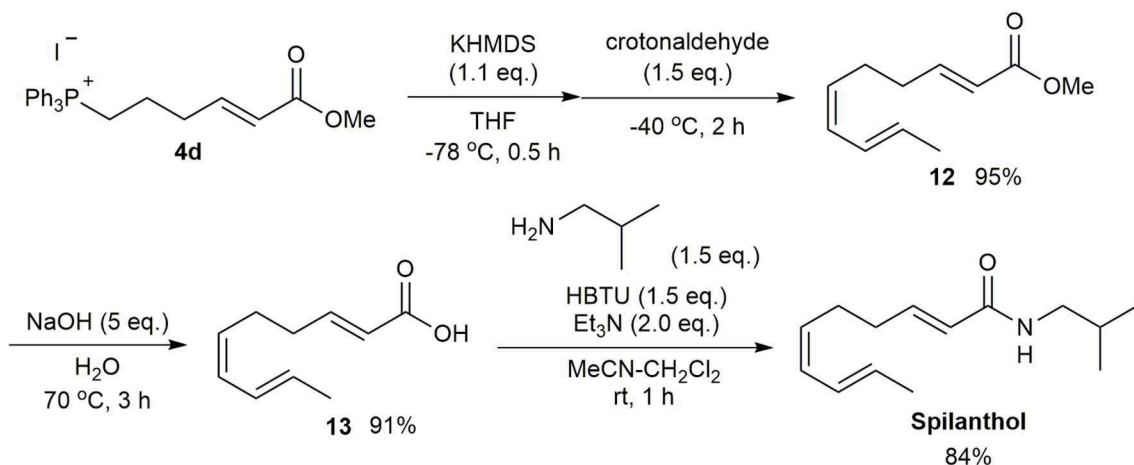
SCHEME 4 | Synthesis of spilanthol.

non-deliquescent phosphonium salt under low-temperature conditions succeeded in forming single stereoisomers of (2E,6Z,8E,10E)-tetraene and (2E,6Z,8E)-triene moieties in good yields. This method was shown to be applicable to the synthesis of spilanthol in six steps, resulting in an overall yield of 47%. Further studies on the synthesis of other sanshool derivatives are ongoing.

DATA AVAILABILITY STATEMENT

All datasets generated for this study are included in the article/**Supplementary Material**.

AUTHOR CONTRIBUTIONS

AN, KM, and KT performed the experiments. AN and TM wrote the manuscript. All authors designed the experiments and were involved in the data analysis. All authors designed

the experiments, were involved in the data analysis, and have expressed approval of the final version of the manuscript.

SUPPLEMENTARY MATERIAL

The Supplementary Material for this article can be found online at: https://www.frontiersin.org/articles/10.3389/fchem.2020.00187/full#supplementary-material

REFERENCES

Alonso, I. G., Yamane, L. T., de Freitas-Blanco, V. S., Novaes, L. F. T., Franz-Montan, M., de Paula, E., et al. (2018). A new approach for the total synthesis of spilanthol and analogue with improved anesthetic activity. *Tetrahedron* 74, 5192–5199. doi: 10.1016/j.tet.2018.06.034

Aoki, K., Igarashi, Y., Nishimura, H., Morishita, I., and Usui, K. (2012). Application of iron carbonyl complexation to the selective total synthesis of sanshools. *Tetrahedron Lett*. 53, 6000–6003. doi: 10.1016/j.tetlet.2012.08.135

Barbosa, A. F., de Carvalho, M. G., Smith, R. E., and Sabaa-Srur, A. U. O. (2016). Spilanthol: occurrence, extraction, chemistry and biological activities. *Rev. Bras. Farmacogn*. 26, 128–133. doi: 10.1016/j.bjp.2015.07.024

Bautista, D. M., Sigal, Y. M., Milstein, A. D., Garrison, J. L., Zorn, J. A., Tsuruda, P. R., et al. (2008). Pungent agents from Szechuan peppers excite sensory neurons by inhibiting two-pore potassium channels. *Nat. Neurosci.* 11, 772–779. doi: 10.1038/nn.2143

Crombie, L., Krasinski, A. H. A., and Manzoor-i-Khuda, M. (1963). Amides of vegetable origin. Part X. The stereohemistry and synthesis of affinin. *J. Chem. Soc.* 4970–4976. doi: 10.1039/JR9630004970

Devkota, K. P., Wilson, J., Henrich, C. J., McMahon, J. B., Reilly, K. M., and Beutler, J. A. (2012). Isobutylhydroxyamides from the pericarp of Nepalese Zanthoxylum armatum inhibit NF1-defective tumor cell line growth. *J. Nat. Prod.* 76, 59–63. doi: 10.1039/C7NP00044H

Greger, H. (2016). Alkamides: a critical reconsideration of a multifunctional class of unsaturated fatty acid amides. *Phytochem. Rev.* 15, 729–770. doi: 10.1007/s11101-015-9418-0

Igarashi, Y., Aoki, K., Nishimura, H., Morishita, I., and Usui, K. (2012). Total synthesis of hydroxy-α- and hydroxy-β-sanshool using Suzuki–Miyaura coupling. *Chem. Pharm. Bull.* 60, 1088–1091. doi: 10.1248/cpb.c12-00382

Ikeda, Y., Ukai, J., Ikeda, N., and Yamamoto, H. (1984). Facile routes to natural acyclic polyenes syntheses of spilanthol and trail pheromone for termite. *Tetrahedron Lett.* 25, 5177–5180. doi: 10.1016/S0040-4039(01)81556-2

Ikeda, Y., Ukai, J., Ikeda, N., and Yamamoto, H. (1987). Stereoselective synthesis of 1,4-disubstituted 1,3-diene from aldehyde using organotitanium reagent. *Tetrahedron* 43, 731–741. doi: 10.1016/S0040-4020(01)90007-9

Jang, K. H., Chang, Y. H., Kim, D.-D., Oh, K.-B., Oh, U., and Shin, J. (2008). New polyunsaturated fatty acid amides isolated from the seeds of Zanthoxylum piperitum. *Arch. Pharm. Res.* 31, 569–572. doi: 10.1007/s12272-001-1194-5

Koo, J. Y., Jang, Y., Cho, H., Lee, C. H., Jang, K. H., Chang, Y. H., et al. (2007). Hydroxy-alpha-sanshool activates TRPV1 and TRPA1 in sensory neurons. *Eur. J. Neurosci.* 26, 1139–1147. doi: 10.1111/j.1460-9568.2007.05743.x

Kubota, K., Ohtake, N., Ohbuchi, K., Mase, A., Imamura, S., Sudo, Y., et al. (2015). Hydroxy-α-sanshool induces colonic motor activity in rat proximal colon: a possible involvement of KCNK9. *Am. J. Physiol. Gastrointest. Liver Physiol.* 308, G579–G590. doi: 10.1152/ajpgi.00114.2014

Munekage, M., Ichikawa, K., Kitagawa, H., Ishihara, K., Uehara, H., Watanabe, J., et al. (2013). Population pharmacokinetic analysis of daikenchuto, a traditional Japanese medicine (Kampo) in Japanese and US health volunteers. *Drug Metab. Dispos.* 41, 1256–1263. doi: 10.1124/dmd.112.050112

Okada, T., Asawa, T., Sugiyama, Y., Kirihara, M., Iwai, T., and Kimura, Y. (2014). Sodium hypochlorite pentahydrate (NaOCl·5H$_2$O) crystals as an extraordinary oxidant for primary and secondary alcohols. *Synlett* 25, 596–598. doi: 10.1055/s-0033-1340483

Sharma, V., Boonen, J., Chauhan, N. S., Thakur, M., de Spiegeleer, B., and Dixit, V. K. (2011). Spilanthes acmella ethanolic flower extract: LC–MS alkylamide profiling and its effects on sexual behavior in male rats. *Phytomedicine* 18, 1161–1168. doi: 10.1016/j.phymed.2011.06.001

Tang, X., Zhou, X., Wu, J., Li, J., and Bai, L. (2014). A novel function of sanshools: the alleviation of injury from metolachlor in rice seedlings. *Pestic. Biochem. Physiol.* 110, 44–49. doi: 10.1016/j.pestbp.2014.02.006

Uchiyama, Y., Ohtsuki, T., Murakami, R., Shibata, M., and Sugimoto, J. (2017). (*E*)-Selective Wittig reactions between a nonstabilized phosphonium ylide bearing a phosphastibatriptycene skeleton and benzaldehydes. *Eur. J. Org. Chem.* 1, 159–174. doi: 10.1002/ejoc.201601098

Wu, B., Kun, L., and Toy, P. H. (2012). Synthesis of hydroxy-α-sanshool. *Synlett* 23, 2564–2566. doi: 10.1055/s-0032-1317172

Yang, X. (2008). Aroma constituents and alkylamides of red and green Huajiao (*Zanthoxylum bungeanum* and *Zanthoxylum schinifolium*). *J. Agric. Food Chem.* 56, 1689–1696. doi: 10.1021/jf0728101

![frontiers in Chemistry]

Geranylated Coumarins From Thai Medicinal Plant *Mammea siamensis* With Testosterone 5α-Reductase Inhibitory Activity

Toshio Morikawa[1]*, Fenglin Luo[1], Yoshiaki Manse[1], Hidemi Sugita[1], Shunsuke Saeki[1], Saowanee Chaipech[1,2], Yutana Pongpiriyadacha[3], Osamu Muraoka[1] and Kiyofumi Ninomiya[1]

[1] Pharmaceutical Research and Technology Institute, Kindai University, Osaka, Japan, [2] Faculty of Agro-Industry, Rajamangala University of Technology Srivijaya, Nakhon Si Thammarat, Thailand, [3] Faculty of Science and Technology, Rajamangala University of Technology Srivijaya, Nakhon Si Thammarat, Thailand

Geranylated coumarin constituents, kayeassamin I (**1**) and mammeasins E (**2**) and F (**3**) were newly isolated from the methanol extract of the flowers of *Mammea siamensis* (Calophyllaceae) originating in Thailand, along with five known isolates, such as mammea E/BC (**23**), deacetylmammea E/AA cyclo D (**31**), deacetylmammea E/BB cyclo D (**32**), mammea A/AA cyclo F (**34**), and mammea A/AC cyclo F (**35**). These compounds (**1–3**) were obtained as an inseparable mixture (*ca.* 1:1 ratio) of the 3″R and 3″S forms, respectively. Among the isolated coumarins from the extract, mammeasins E (**2**, 22.6 μM), A (**4**, 19.0 μM), and B (**5**, 24.0 μM), kayeassamins E (**9**, 33.8 μM), F (**10**, 15.9 μM), and G (**11**, 17.7 μM), surangin C (**13**, 5.9 μM), and mammeas A/AA (**17**, 19.5 μM), E/BB (**22**, 16.8 μM), and A/AA cyclo F (**34**, 23.6 μM), were found to inhibit testosterone 5α-reductase.

Keywords: *Mammea siamensis*, mammeasin, 5α-reductase inhibitor, geranylated coumarin, calophyllaceae

INTRODUCTION

The Calophyllaceae plant *Mammea siamensis* (Miq.) T. Anders. is a small evergreen tree distributed in Thailand (locally called "Sarapi" or "Saraphi"), Laos, Cambodia, Vietnam, and Myanmar. The flowers of this plant have traditionally been used as a heart tonic, fever-lowering, and enhancement of appetite in Thailand (Morikawa et al., 2012; Tung et al., 2013; Ninomiya et al., 2016; Sangkaruk et al., 2017). Previous chemical studies on the flowers (Kaweetripob et al., 2000; Prachyawarakorn et al., 2000, 2006a; Mahidol et al., 2002; Morikawa et al., 2012; Ninomiya et al., 2016), seeds (Laphookhieo et al., 2006, 2007), twigs (Poobrasert et al., 1998; Prachyawarakorn et al., 2006a,b), and bark (Ngo et al., 2010) of *M. siamensis* reported on the isolation of several coumarins and xanthones, etc. With regard to the biological studies on *M. siamensis* and its constituents, cytotoxicity, antiproliferative, and apoptotic effects against several tumor and cancer cell lines (Ngo et al., 2010; Tung et al., 2013; Noysang et al., 2014; Uto et al., 2016; Sangkaruk et al., 2017), suppressive effects on inducible nitric oxide synthase expression in RAW264.7 cells (Morikawa et al., 2012), and aromatase inhibitory activity (Ninomiya et al., 2016; Tanabe et al., 2017) have been reported. Further separation of the constituents in the extract resulted in the isolation of three geranylated coumarins, kayeassamin I (**1**) and mammeasins E (**2**) and F (**3**). Here, we conducted the isolation and structural verification of **1–3**, as well as examined the testosterone 5α-reductase

inhibitory activity of its coumarin constituents (**1–35**), including five new isolates, such as mammea E/BC (**23**), deacetylmammea E/AA cyclo D (**31**), deacetylmammea E/BB cyclo D (**32**), mammea A/AA cyclo F (**34**), and mammea A/AC cyclo F (**35**).

MATERIALS AND METHODS

General Experimental Procedures

The following instruments were used to obtain physical data: a SEPA-300 digital polarimeter (Horiba Ltd., Kyoto, Japan, $l = 5$ cm) for specific rotations; an UV-1600 spectrometer (Shimadzu Co., Kyoto, Japan) to record UV spectra; a FTIR-8100 spectrometer (Shimadzu Co.) to measure IR spectra; a JNM-ECA800 (800 MHz), JNM-ECA700 (700 MHz), JNM-ECA500 (500 MHz), and JNM-ECS400 and JNM-AL400 (400 MHz) spectrometers (JEOL Ltd., Tokyo, Japan) to determine ^{1}H NMR spectra; JNM-ECA800 (200 MHz), JNM-ECA700 (175 MHz), JNM-ECA500 (125 MHz), and JNM-ECS400 and JNM-AL-400 (100 MHz) spectrometers (JEOL Ltd.) to record ^{13}C NMR spectra in CDCl$_3$ at room temperature (25°C) with tetramethylsilane as an internal standard; an Exactive Plus Orbitrap mass spectrometer (Thermo Fisher Scientific Inc., Waltham, MA, USA) to measure ESIMS and HRESIMS; an HPLC detector, SPD-10A*vp* UV-Vis (Shimadzu Co.); and Cosmosil 5C$_{18}$-MS-II (Nacalai Tesque, Inc., Kyoto, Japan) HPLC columns (4.6 mm i.d. × 250 mm and 20 mm i.d. × 250 mm) for analytical and preparative purposes, respectively.

The following materials and experimental conditions were used for the column chromatography (CC): normal-phase silica gel CC, silica gel 60N (Kanto Chemical Co., Ltd., Tokyo, Japan; 63–210 mesh, spherical, neutral); reversed-phase ODS CC, Chromatorex ODS DM1020T (Fuji Silysia Chemical, Ltd., Aichi, Japan; 100–200 mesh); TLC, pre-coated TLC plates with silica gel 60F$_{254}$ (Merck, Darmstadt, Germany, 0.25 mm, normal-phase) and silica gel RP-18 WF$_{254S}$ (Merck, Darmstadt, Germany, 0.25 mm, reversed-phase); reversed-phase HPTLC, pre-coated TLC plates with silica gel RP-18 WF$_{254S}$ (Merck, 0.25 mm); detection was performed by spraying 1% Ce(SO$_4$)$_2$-10% aqueous H$_2$SO$_4$, followed by heating.

Plant Material

The flowers of *Mammea siamensis* were collected from the Nakhonsithammarat Province, Thailand, in September 2006, as described previously (Morikawa et al., 2012; Ninomiya et al., 2016). The plant material was identified by one of the authors (Y. P.). A voucher specimen (2006.09. Raj-04) for this plant has been deposited in our laboratory.

Extraction and Isolation

Dried flowers of *M. siamensis* (1.8 kg) were extracted three times with MeOH under reflux for 3 h. Evaporation of the combined extracts under reduced pressure afforded the MeOH extract (463.7 g, 25.66%). An aliquot (413.7 g) of the extract was partitioned into an EtOAc–H$_2$O (1:1, v/v) mixture to furnish an EtOAc-soluble fraction (110.34 g, 6.84%) and an aqueous phase. An aliquot (89.45 g) of the EtOAc-soluble fraction was subjected to normal-phase silica gel CC [3.0 kg, *n*-hexane–EtOAc

(10:1 → 7:1 → 5:1, v/v) → EtOAc → MeOH] to give 11 fractions [Fr. 1 (3.05 g), Fr. 2 (2.86 g), Fr. 3 (11.71 g), Fr. 4 (1.62 g), Fr. 5 (4.15 g), Fr. 6 (6.29 g), Fr. 7 (2.21 g), Fr. 8 (2.94 g), Fr. 9 (10.23 g), Fr. 10 (11.17 g), and Fr. 11 (21.35 g)]. Fraction 5 (4.15 g) was subjected to reversed-phase silica gel CC [120 g, MeOH–H$_2$O (80:20 → 85:15, v/v) → MeOH → acetone] to afford six fractions [Fr. 5-1 (115.7 mg), Fr. 5-2 (2789.8 mg), Fr. 5-3 (515.4 mg), Fr. 5-4 (430.0 mg), Fr. 5-5 (119.2 mg), and Fr. 5-6 (110.0 mg)] as reported previously (Ninomiya et al., 2016). Fraction 5-2 (517.0 mg) was purified by HPLC [Cosmosil 5C$_{18}$-MS-II, MeOH−1% aqueous AcOH (85:15, v/v)] to give mammea A/AC cyclo F (**35**, 4.6 mg, 0.0019%) (Morel et al., 1999; Prachyawarakorn et al., 2000; Guilet et al., 2001) together with mammeas A/AA (**17**, 101.2 mg, 0.0418%), A/AC (**19**, 112.9 mg, 0.0466%), A/AA cyclo D (**24**, 2.7 mg, 0.0011%), E/BC cyclo D (**29**, 14.0 mg, 0.0058%), and E/BD cyclo D (**30**, 1.8 mg, 0.0015%) (Mahidol et al., 2002). Fraction 5-3 (515.4 mg) was purified by HPLC [Cosmosil 5C$_{18}$-MS-II, MeOH−1% aqueous AcOH (85:15, v/v)] to give mammea A/AA cyclo F (**34**, 13.2 mg, 0.0010%) (Prachyawarakorn et al., 2000; Guilet et al., 2001) together with **19** (45.6 mg, 0.0035%), **24** (14.9 mg, 0.0011%), mammeas A/AB cyclo D (**25**, 46.4 mg, 0.0035%) and A/AC cyclo D (**26**, 30.1 mg, 0.0023%). Fraction 6 (6.29 g) was subjected to reversed-phase silica gel CC [200 g, MeOH–H$_2$O (80:20 → 90:10 → 95:5, v/v) → MeOH → acetone] to afford 10 fractions [Fr. 6-1 (44.7 mg), Fr. 6-2 (157.2 mg), Fr. 6-3 (928.8 mg), Fr. 6-4 (3117.0 mg), Fr. 6-5 (128.8 mg), Fr. 6-6 (487.1 mg), Fr. 6-7 (230.8 mg), Fr. 6-8 (280.5 mg), Fr. 6-9 (102.9 mg), and Fr. 6-10 (96.5 mg)] as reported previously (Morikawa et al., 2012; Ninomiya et al., 2016). Fraction 6-4 (536.2 mg) was purified by HPLC [Cosmosil 5C$_{18}$-MS-II, MeOH−1% aqueous AcOH (90:10, v/v)] to give kayeassamin I (**1**, 7.2 mg, 0.0032%) (Win et al., 2008b), mammeasin E (**2**, 16.5 mg, 0.0073%), and **35** (11.0 mg, 0.0049%) together with mammeasins A (**4**, 65.8 mg, 0.0293%) and B (**5**, 21.6 mg, 0.0096%), surangin B (**12**, 58.2 mg, 0.0259%), **17** (17.0 mg, 0.0076%), mammea A/AB (**18**, 10.7 mg, 0.0048%), and **19** (112.6 mg, 0.0501%). Fraction 7 (2.21 g) was subjected to reversed-phase ODS CC [47.0 g, MeOH-H$_2$O (60:40 → 80:20 → 90:10, v/v) → MeOH → acetone] to afford five fractions [Fr. 7-1 (187.3 mg), Fr. 7-2 (912.0 mg), Fr. 7-3 (275.2 mg), Fr. 7-4 (30.0 mg), and Fr. 7-5 (44.0 mg)]. Fraction 7-2 (912.0 mg) was purified by HPLC [column: Cosmosil 5C$_{18}$-MS-II, detection: UV (230 nm), mobile phase: MeOH-1% aqueous H$_2$O (85:15, v/v)] to give mammeasin E/BC (**23**, 99.0 mg, 0.0076%) (Yang et al., 2005). Fraction 7-3 (275.2 mg) was purified by HPLC [Cosmosil 5C$_{18}$-MS-II, UV (230 nm), MeOH-1% aqueous AcOH 85:15, v/v] to give **1** (52.1 mg, 0.0040%), **2** (34.1 mg, 0.0026%), and mammeasin F (**3**, 19.5 mg, 0.0015%). Fraction 9 (10.23 g) was subjected to reversed-phase silica gel CC [300 g, MeOH–H$_2$O (80:20 → 90:10, v/v) → MeOH → acetone] to afford five fractions [Fr. 9-1 (2809.0 mg), Fr. 9-2 (5678.0 mg), Fr. 9-3 (385.9 mg), Fr. 9-4 (422.0 mg), and Fr. 9-5 (51.9 mg)] as reported previously (Morikawa et al., 2012; Ninomiya et al., 2016). Fraction 9-1 (544.5 mg) was purified by HPLC [Cosmosil 5C$_{18}$-MS-II, MeOH−1% aqueous AcOH (85:15, v/v)] to give deacetylmammeas E/AA cyclo D (**31**, 1.3 mg, 0.0005%) (Mahidol et al., 2007) and E/BB cyclo D (**32**, 6.1 mg,

0.0023%) (Mahidol et al., 2007) together with kayeassamins E (**9**, 28.6 mg, 0.0113%), F (**10**, 98.7 mg, 0.0390%), and G (**11**, 43.4 mg, 0.0171%), deacetylmammea E/BC cyclo D (**33**, 18.6 mg, 0.0073%), and benzoic acid (10.9 mg, 0.0043%).

Kayeassamin I (1)

Pale yellow oil; $[\alpha]_D^{25}$ −50.4 (*c* 0.63, CHCl₃) {$[\alpha]_D^{23}$ −35.52 (*c* 0.90, CHCl₃) (Win et al., 2008a)}; ^{1}H and ^{13}C NMR spectroscopic data (see **Table 1**); Negative-ion ESIMS *m/z* 439 [M – H]⁻; HRESIMS *m/z* 439.2116 (calcd for $C_{26}H_{31}O_6$, 439.2115) (**Figures S3–S7**).

Mammeasin E (2)

Pale yellow oil; $[\alpha]_D^{25}$ −58.9 (*c* 0.12, CHCl₃); UV (MeOH) λ_{max} nm (log ε): 223 (4.01), 278 (4.12), 302 (4.12); IR (KBr) ν_{max} cm⁻¹: 1,740, 1,713, 1,613, 1,454, 1,408, 1,284, 1,126, 1,049; ^{1}H and ^{13}C NMR spectroscopic data (see **Table 2**); Negative-ion ESIMS *m/z* 453 [M – H]⁻; HRESIMS *m/z* 453.2272 (calcd for $C_{27}H_{33}O_6$, 453.2272) (**Figures S8–S12**).

Mammeasin F (3)

Pale yellow oil; $[\alpha]_D^{25}$ −42.1 (*c* 0.45, CHCl₃); UV (MeOH) λ_{max} nm (log ε): 224 (3.89), 298 (3.82); IR (KBr) ν_{max} cm⁻¹: 1,732, 1,713, 1,605, 1,454, 1,381, 1,261, 1,126, 1,049; ^{1}H and ^{13}C NMR spectroscopic data (see **Table 2**); Negative-ion ESIMS *m/z* 453 [M – H]⁻; HRESIMS *m/z* 453.2287 (calcd for $C_{27}H_{33}O_6$, 453.2272) (**Figures S13–S17**).

DDQ Oxidation of Kayeassamin A (8) and Surangins C (13) and D (14)

A solution of kayeassamin A (**8**, 9.0 mg) in dry-toluene (2.0 mL) was treated with 2,3-dichloro-5,6-dicyano-*p*-benzoquinone (DDQ, 10.0 mg) and the solution stirred at room temperature (25°C) for 4 h. The aqueous solution was saturated with sodium hydrogen carbonate (NaHCO₃) and extracted with EtOAc. The EtOAc extract was washed with brine then dried over anhydrous magnesium sulfate (MgSO₄) and filtered. Removal of the solvent under reduced pressure gave a residue, which was purified by HPLC [Cosmosil 5C₁₈-MS-II, MeOH−1% aqueous AcOH (85:15, v/v)] to give kayeassamin I (**1**, 3.8 mg, 46%). Through the similar procedure, mammeasin E (**2**, 3.3 mg, 38%) and mammeasin F (**3**, 2.0 mg, 17%) were obtained from surangins D (**14**, 9.6 mg) and C (**13**, 12.7 mg), respectively.

Assay for Testosterone 5α-Reductase Inhibitory Activity

The experiment was performed in accordance with previously reported methods (Matsuda et al., 2001; Lee et al., 2012; Koseki et al., 2015) with slight modifications. In brief, the assay was performed in 48-well microplates (Sumitomo Bakelite Co., Ltd., Tokyo, Japan). The reaction solution was pre-incubated with or without a test sample (5 μL/well, dissolved in DMSO), in a potassium phosphate buffer (40 mM, pH 6.5, 490 μL/well) containing substrate (0.35 nmol of testosterone, Tokyo Chemical Industry Co., Ltd., Tokyo, Japan) and NADPH (10 nmol, Oriental Yeast Co., Ltd., Tokyo, Japan) at room temperature (25°C) for 20 min. The enzymatic reaction was initiated by the addition of rat liver S9 fractions (10 μL/well, dissolved in

the phosphate buffer, 20.6 μg/well, Oriental Yeast Co., Ltd., Tokyo, Japan, lot no. 109031513) at 37°C for 30 min. After incubation, the reaction mixture was immediately heated in boiling water for 2 min to stop the reaction. Then the reaction solution of each well was transferred to a microtube and extracted with 500 μL of EtOAc. After the microtube was centrifuged (10,000 rpm, 5 min), an aliquot of each EtOAc phase (300 μL) was transferred into another tube. The solvent in the tube was evaporated and the residue was dissolved in 30 μL of acetonitrile containing an internal standard (I.S.) fludrocortisone acetate (20 μg/mL, Sigma-Aldrich, Co., LLC, St. Louis, USA). An aliquot of 2 μL was injected into the HPLC under the following conditions [Instrument: a series LC-20A Prominence HPLC system (Shimadzu Co., Kyoto, Japan); Detection: UV (254 nm); Column: Cosmosil 5C₁₈-MS-II (Nakalai Tesque Inc., Kyoto, Japan, 5 μm particle size, 2.0 mm i.d. × 150 mm); Column temperature: 40°C; Mobile phase: MeOH–H₂O (60:40, v/v); Flow rate: 0.2 mL/min; retention time: 13.5 min for testosterone and 8.0 min for I.S. A similar procedure that described above was carried out for the control tubes. The 5α-reductase inhibitory activity was determined from the following equation using the peak area ratios (*r* = testosterone/I.S.). Experiments were performed in triplicate or quadruple, and IC₅₀ values were determined graphically. The 5α-reductase inhibitor finasteride (Tokyo Chemical Industry Co., Ltd., Tokyo, Japan) was used as a reference compound.

$$\text{Inhibition}(\%) = [r(\text{T}) − r(\text{C})/r(\text{B}) − r(\text{C})] \times 100$$

Control (C): enzyme (+), test sample (−); Test (T): enzyme (+), test sample (+); Blank (B): enzyme (−), test sample (+).

Statistics

Values are expressed as mean ± S.E.M. One-way analysis of variance (ANOVA), followed by Dunnett's test, was used for statistical analysis. Probability (*p*) values <0.05 were considered significant.

RESULTS AND DISCUSSION

Effects of the Methanol Extract From the Flowers of *M. siamensis* on Testosterone 5α-Reductase

The male sex hormones, androgens, play a crucial role in the development, growth and function of the prostate, and other androgen-sensitive peripheral tissues. In the prostate gland, androgens are involved in benign prostatic hyperplasia and prostate cancer, as well as in skin disorders, such as acne, seborrhea, androgenic alopecia, and hirsutism. Among the androgens, testosterone is the most abundant in serum and secreted primarily by the testicles and ovaries. The enzyme steroid 5α-reductase catalyzes the conversion of testosterone to the most potent natural androgen, 5α-dihydrotestosterone (Yamana et al., 2010; Yao et al., 2011; Azzouni et al., 2012). Therefore, inhibition of testosterone 5α-reductase could be useful for the treatment of the above diseases. To date, three types

TABLE 1 | ^{1}H and ^{13}C NMR spectroscopic data (CDCl$_3$) for kayeassamin I (**1**).

Position	1a[a]		1b[a]		1[b]	
	δ_H	δ_C	δ_H	δ_C	δ_H	δ_C
2		159.6		159.6		159.6
3	6.60 (br s)	107.0	6.61 (d, 0.9)	107.2	6.61 (s)	107.0
4		160.6		160.6		160.6
4a		101.0		101.1		101.0
5		155.9		155.9		155.9
6		105.8		106.0		105.8
7		162.9		162.9		162.9
8		104.5		104.6		104.5
8a		157.2		157.2		157.3
1′	5.43 (br t, *ca.* 8)	71.8	5.43 (br t, *ca.* 8)	71.7	5.43 (d, 8.1)	71.8
2′	1.51, 1.95 (both m)	30.7	1.53, 1.96 (both m)	30.5	1.50, 1.97 (both m)	30.7
3′	1.11 (3H, t, 7.4)	10.2	1.09 (3H, t. 7.4)	10.1	1.13 (3H, t, 7.4)	10.2
2″		83.0		83.1		83.0
3″	5.53 (d, 10.2)	125.0	5.55 (d, 10.2)	124.8	5.54 (d, 10.0)	124.9
4″	6.78 (d, 10.2)	116.5	6.79 (d, 10.2)	116.6	6.79 (d, 10.0)	116.5
5″	1.71, 1.91 (both m)	41.6	1.71, 1.91 (both m)	41.9	1.90 (2H, m)	41.6
6″	2.09 (2H, m)	23.0	2.09 (2H, m)	23.2	2.09 (2H, m)	23.0
7″	5.06 (qt, 0.9, 7.1)	123.1	5.06 (qt, 0.9, 7.1)	123.0	5.07 (t, 7.1)	123.1
8″		132.6		132.6		132.6
9″	1.64 (3H, d, 0.9)	25.6	1.67 (3H, d, 0.9)	25.6	1.64 (3H, s)	25.6
10″	1.55 (3H, s)	17.6	1.57 (3H, s)	17.7	1.55 (3H, s)	17.7
1‴		206.4		206.4		206.4
2‴	3.26 (2H, t, 7.1)	46.7	3.26 (2H, t, 7.1)	46.7	3.27 (2H, t, 7.1)	46.7
3‴	1.78 (2H, qt, 7.4, 7.1)	18.0	1.78 (2H, qt, 7.4, 7.1)	18.0	1.79 (2H, m)	18.1
4‴	1.04 (3H, t, 7.4)	13.8	1.03 (3H, t, 7.4)	13.8	1.05 (3H, m)	13.8
2″-CH$_3$	1.52 (3H, s)	27.2	1.48 (3H, s)	27.5	1.51 (3H, s)	27.3
7–OH	14.47 (s)		14.47 (s)		14.48 (brs)	

[a]*Measured by 800 MHz for ^{1}H NMR and 200 MHz for ^{13}C NMR.*
[b]*Reported in Win et al. (2008b) by 400 MHz for ^{1}H NMR and 100 MHz for ^{13}C NMR.*

of 5α-reductases, chronologically named types 1, 2, and 3 5α-reductases, have been described (Yamana et al., 2010; Azzouni et al., 2012; Titus et al., 2014). A type 2 and 3 5α-reductase inhibitor, finasteride, is currently marketed worldwide as a drug for benign prostatic hyperplasia and is also used in the treatment of hair loss (Heinzl, 1999; Tosti and Piraccini, 2000) and in the prevention of prostate cancer (Coltman et al., 1999). Therefore, 5α-reductase is considered a useful therapeutic target in the treatment and prevention of the above deceases. In particular, many heterocyclic compounds based on oxygen and nitrogen atoms often have good antiproliferative activity against a variety of solid tumor cell lines and are expected to be seeds of new anticancer agents (Sharma et al., 2018; Petel et al., 2019).

During our characterization studies on bioactive constituents from Thai natural medicines (Manse et al., 2017; Morikawa et al., 2018; Tanabe et al., 2018; Kobayashi et al., 2019), a methanol extract of the flowers of *M. siamensis* was found to inhibit 5α-reductase activity (IC$_{50}$ = 2.4 μg/mL). In order to investigate new 5α-reductase inhibitors, we conducted a search for the bioactive constituents from the flowers of *M. siamensis*.

Isolation

In our previous report we described the isolation of 26 coumarins: mammeasins A (**4**, 0.0293%), B (**5**, 0.0115%), C (**6**, 0.0008%), and D (**7**, 0.0047%), kayeassamins A (**8**, 0.0578%), E (**9**, 0.0113%), F (**10**, 0.0390%), and G (**11**, 0.0171%), surangins B (**12**, 0.0271%), C (**13**, 0.0571%), and D (**14**, 0.0632%), 8-hydroxy-5-methyl-7-(3,7-dimethyl-octa-2,6-dienyl)-9-(2-methyl-1-oxobutyl)-4,5-dihydropyrano[4,3,2-*de*]chromen-2-one (**15**, 0.0015%), 8-hydroxy-5-methyl-7-(3,7-dimethyl-octa-2,6-dienyl)-9-(3-methyl-1-oxobutyl)-4,5-dihydropyrano[4,3,2-*de*]chromen-2-one (**16**, 0.0012%), mammeas A/AA (**17**, 0.0494%), A/AB (**18**, 0.0048%), A/AC (**19**, 0.1056%), A/AD (**20**, 0.0022%), E/BA (**21**, 0.0045%), E/BB (**22**, 0.0194%), A/AA cyclo D (**24**, 0.0035%), A/AB cyclo D (**25**, 0.0097%), A/AC cyclo D (**26**, 0.0109%), B/AB cyclo D (**27**, 0.0016%), B/AC cyclo D (**28**, 0.0062%), E/BC cyclo D (**29**, 0.0058%), and deacetylmammea E/BC cyclo D (**33**, 0.0073%), as described previously (Morikawa et al., 2012; Ninomiya et al., 2016). In the present study, we additionally isolated kayeassamin I (**1**, 0.0072%) and mammeasins E (**2**, 0.0099%) and F (**3**, 0.0015%),

TABLE 2 | ^{1}H and ^{13}C NMR spectroscopic data (CDCl$_3$) for mammeasins E (**2**) and F (**3**).

Position	2a[a]		2b[a]		3a[b]		3b[b]	
	δ_H	δ_C	δ_H	δ_C	δ_H	δ_C	δ_H	δ_C
2		159.6		159.6		159.5		159.5
3	6.61 (d, 0.9)	107.0	6.59 (d, 1.0)	107.1	6.62 (d, 1.0)	107.1	6.61 (d, 1.0)	107.2
4		160.7		160.7		160.6		1560.5
4a		101.0		101.1		101.0		101.2
5		156.0		156.0		155.8		155.8
6		105.8		106.0		105.9		106.1
7		163.0		163.0		163.1		163.1
8		104.5		104.6		104.3		104.3
8a		157.1		157.1		157.0		156.9
1′	5.40 (br t, *ca.* 8)	71.8	5.40 (br t, *ca.*8)	71.7	5.43 (m)	71.8	5.43 (m)	71.8
2′	1.53, 1.96 (both m)	30.7	1.53, 1.96 (both m)	30.6	1.52, 1.96 (both m)	30.7	1.52, 1.96 (both m)	30.6
3′	1.12 (3H, t, 7.3)	10.2	1.09 (3H, t, 7.1)	10.1	1.12 (3H, t, 7.1)	10.2	1.10 (3H, t, 7.1)	10.1
2″		83.0		83.1		83.0		83.1
3″	5.53 (d, 10.2)	125.0	5.54 (d, 10.2)	124.9	5.54 (d, 10.2)	124.9	5.54 (d, 10.2)	124.8
4″	6.79 (d, 10.2)	116.5	6.78 (d, 10.2)	116.5	6.79 (d, 10.2)	116.6	6.79 (d, 10.2)	116.6
5″	1.71, 1.90 (both m)	41.6	1.71, 1.90 (both m)	41.8	1.71, 1.91 (both m)	41.7	1.71, 1.91 (both m)	41.9
6″	2.08 (2H, m)	23.0	2.08 (2H, m)	23.2	2.09 (2H, m)	23.0	2.09 (2H, m)	23.3
7″	5.06 (qt, 1.0, 7.1)	123.1	5.06 (qt, 1.0, 7.1)	123.0	5.06 (dt, 1.3, 7.1)	123.1	5.06 (qt, 1.3, 7.1)	123.0
8″		132.6		132.5		132.6		132.6
9″	1.64 (3H, d, 1.0)	25.5	1.67 (3H, d, 1.0)	25.6	1.64 (3H, br s)	25.6	1.67 (3H, br s)	25.6
10″	1.52 (3H, s)	17.6	1.54 (3H, s)	17.7	1.57 (3H, s)	17.6	1.57 (3H, s)	17.7
1‴		206.2		206.2		210.7		210.7
2‴	3.14 (2H, d, 6.7)	53.6	3.14 (2H, d, 6.7)	53.6	3.89 (m)	47.0	3.89 (m)	47.0
3‴	2.27 (m)	25.6	2.27 (m)	25.5	1.25 (3H, d, 6.7)	16.6	1.26 (3H, d, 6.7)	16.6
4‴	1.03 (3H, d, 6.6)	22.6	1.03 (3H, d, 6.6)	22.6	1.46, 1.89 (both m)	27.2	1.46, 1.89 (each m)	27.2
5‴	1.03 (3H, d, 6.6)	22.6	1.03 (3H, d, 6.6)	22.6	0.98 (3H, t, 7.5)	11.7	0.98 (3H, t, 7.5)	11.7
2‴-CH$_3$	1.51 (3H, s)	27.3	1.48 (3H, s)	27.5	1.52 (3H, br s)	27.3	1.47 (3H, br s)	27.5
7-OH	14.51 (s)		14.51 (s)		14.44 (s)		14.44 (s)	

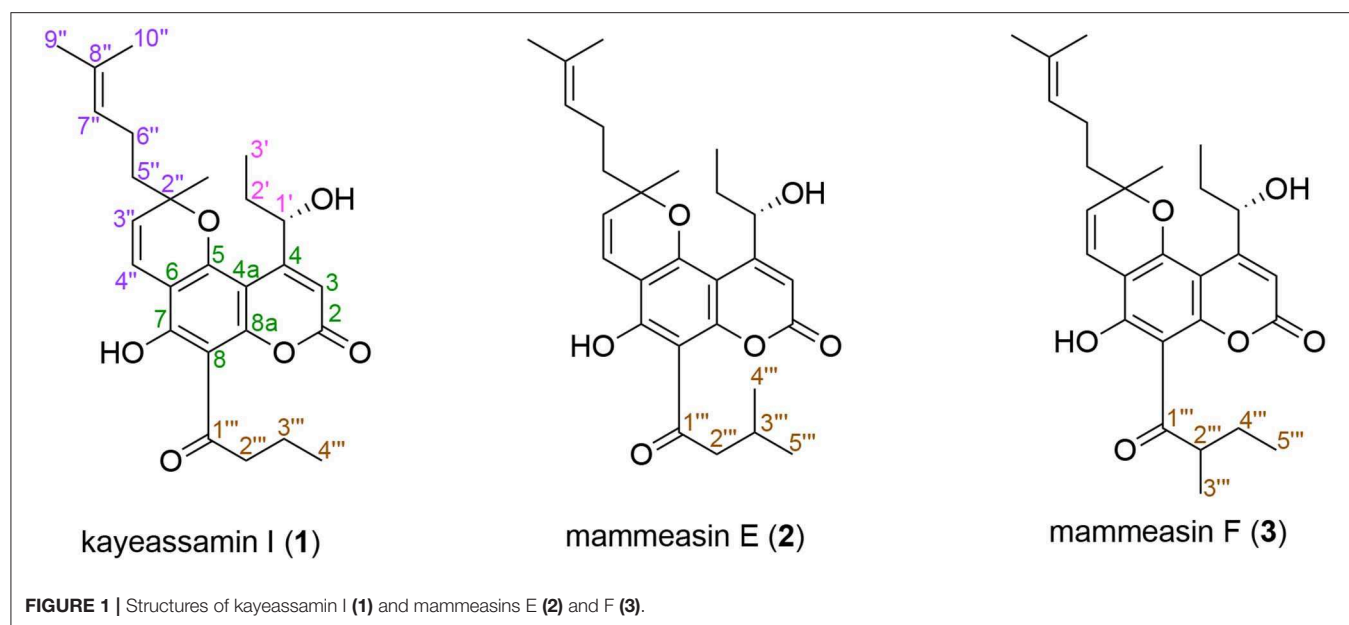[a]*Measured by 700 MHz for ^{1}H NMR and 175 MHz for ^{13}C NMR.*
[b]*Measured by 800 MHz for ^{1}H NMR and 200 MHz for ^{13}C NMR.*

from the methanol extract of *M. siamensis* flowers as shown in **Figure 1**, together with six coumarins: mammeas E/BC (**23**, 0.0076%) and E/BD cyclo D (**30**, 0.0015%), deacetylmammeas E/AA cyclo D (**31**, 0.0005%) and E/BB cyclo D (**32**, 0.0023%), and mammeas A/AA cyclo F (**34**, 0.0010%) and A/AC cyclo F (**35**, 0.0068%), using normal-phase silica gel and reversed-phase ODS column chromatographic purification steps, and finally by HPLC (**Figure 2**).

Structures of Kayeassamin I (1) and Mammeasins E (2) and F (3)

Compound **1** was obtained as pale yellow oil with a negative optical rotation ($[\alpha]_D^{25}$ −50.4 in CHCl$_3$), and its molecular formula was deduced to be C$_{26}$H$_{32}$O$_6$ by high-resolution ESIMS (HRESIMS) measurement. As shown in **Figure 3**, the HPLC analysis suggested that **1** was obtained as an inseparable mixture (*ca.* 1:1 ratio). The ^{1}H and ^{13}C NMR spectra spectroscopic properties (**Table 1**, CDCl$_3$) of **1**, which were assigned with the aid of DEPT, DQF-COSY, HSQC, and HMBC experiments,

were in accordance with those of kayeassamin I except for the observation of duplicate signals (**1a** and **1b**) measured by high resolution 800 MHz NMR spectrometer: two primary, a tertiary, and two vinyl methyls [**1a**: δ 1.04 (3H, t, $J = 7.4$ Hz, H$_3$-4‴), 1.11 (3H, t, $J = 7.4$ Hz, H$_3$-3′), 1.52 (3H, s, 2″-CH$_3$), 1.55 (3H, s, H$_3$-10″), 1.64 (3H, d, $J = 0.9$ Hz, H$_3$-9″); **1b**: δ 1.03 (3H, t, $J = 7.4$ Hz, H$_3$-4‴), 1.09 (3H, t, $J = 7.4$ Hz, H$_3$-3′), 1.48 (3H, s, 2″-CH$_3$), 1.57 (3H, s, H$_3$-10″), 1.67 (3H, d, $J = 0.9$ Hz, H$_3$-9″)], five methylenes [**1a**: δ 1.51, 1.95 (1H each, both m, H$_2$-2′), 1.71, 1.91 (1H each, both m, H$_2$-5″), 1.78 (2H, qt, $J = 7.4$, 7.1 Hz, H$_2$-3‴), 2.09 (2H, m, H$_2$-6″), 3.26 (2H, t, $J = 7.1$ Hz, H$_2$-2‴); **1b**: δ 1.53, 1.96 (1H each, both m, H$_2$-2′), 1.71, 1.91 (1H each, both m, H$_2$-5″), 1.78 (2H, qt, $J = 7.4$, 7.1 Hz, H$_2$-3‴), 2.09 (2H, m, H$_2$-6″), 3.26 (2H, t, $J = 7.1$ Hz, H$_2$-2‴)], a methine bearing an oxygen function [**1a**: δ 5.43 (1H, br t, $J = ca.$ 8 Hz, H-1′); **1b**: δ 5.43 (1H, br t, $J = ca.$ 8 Hz, H-1′)], four olefinic protons [**1a**: δ 5.06 (1H, qt, $J = 0.9$, 7.1 Hz, H-7″), 5.53 (1H, d, $J = 10.2$ Hz, H-3″), 6.60 (1H, br s, H-3), 6.78 (1H, d, $J = 10.2$ Hz, H-4″); **1b**: δ 5.06 (1H, qt, $J = 0.9$, 7.1 Hz, H-7″),

FIGURE 1 | Structures of kayeassamin I **(1)** and mammeasins E **(2)** and F **(3)**.

5.55 (1H, d, $J = 10.2$ Hz, H-3″), 6.61 (1H, d, $J = 0.9$ Hz, H-3), 6.79 (1H, d, $J = 10.2$ Hz, H-4″)], and a hydrogen-bonded hydroxy proton [**1a**: δ 14.47 (1H, s, 7-OH); **1b**: δ 14.47 (1H, s, 7-OH)]. This evidence allowed us to revise the structure of kayeassamin I as a mixture (**1a** and **1b**) of *ca.* 1:1 inseparable stereoisomers in the 2″ position. The absolute configuration of the 1′-position in **1** has been assumed to be *S* by comparison of the optical rotation with that of similar compounds (Win et al., 2008b). To confirm the stereochemistry, we carried out chemical correlation between **1** and kayeassamin A (**8**), which has been reported to be in the 1′*S* form by the modified Mosher's method (Win et al., 2008a). Thus, oxidation of **8** with 2,3-dichloro-5,6-dicyano-*p*-benzoquinone (DDQ) gave **1**. Consequently, the absolute configuration in the 1′ position of **1** was confirmed to be *S*.
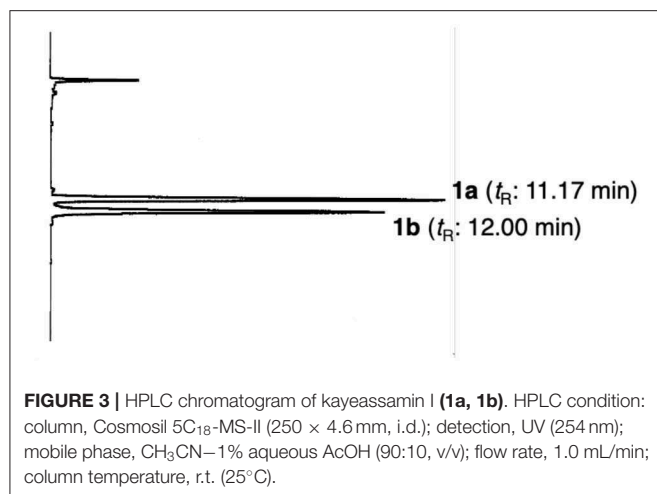
Mammeasin E (**2**) was also obtained as an inseparable mixture (*ca.* 1:1 ratio, **Figure S1**) with a negative optical rotation ($[\alpha]_D^{25}$ −58.9 in CHCl₃). In the negative-ion ESIMS of **2**, a quasimolecular ion peak was observed at m/z 453 [M − H]⁻, and HRESIMS analysis indicated the molecular formula was $C_{27}H_{34}O_6$. The ¹H and ¹³C NMR spectra (**Table 2**, CDCl₃) of **2** were similar to those of **1**, except for the signals due to the 3-methyl-1-oxobutyl moiety in the 8-position [**2a**: δ 1.03 (6H, d, $J = 6.6$ Hz, H₃-4‴ and H₃-5‴), 2.27 (1H, m, H-3‴), 3.14 (2H, d, $J = 6.7$ Hz, H₂-2‴); **2b**: δ 1.03 (6H, d, $J = 6.6$ Hz, H₃-4‴ and H₃-5‴), 2.27 (1H, m, H-3‴), 3.14 (2H, d, $J = 6.7$ Hz, H₂-2‴)] instead of the 1-oxobutyl moiety of **1**. As shown in **Figure S2**, the connectivity of the quaternary carbons in **2** were elucidated on the basis of DQF-COSY and HMBC experiments. Thus, the DQF-COSY experiment on **2** indicated the presence of the following partial structures: C-1′-C-3′; C-3″-C-4″; C-5″-C-7″; and C-2‴–C-5‴ shown in bold lines. In the HMBC experiment, long-range correlations were observed between the

following proton and carbon pairs: H-3 [**2a**: δ 6.61 (1H, d, $J = 0.9$ Hz); **2b**: δ 6.59 (1H, d, $J = 1.0$ Hz)] and C-2 (**2a**: δ_C 159.6; **2b**: δ_C 159.6), C-4a (**2a**: δ_C 101.0; **2b**: δ_C 101.1); the hydrogen-bonded hydroxy proton [**2a**: δ 14.51 (1H, s); **2b**: δ 14.51 (1H, s)] and C-6 (**2a**: δ_C 105.8; **2b**: δ_C 106.0), C-7 (**2a**: δ_C 163.0; **2b**: δ_C 163.0), C-8 (**2a**: δ_C 104.5; **2b**: δ_C 104.6); H-1′ [**2a**: δ 5.40 (1H, br t, $J = ca.$ 8 Hz); **2b**: δ 5.40 (1H, br t, $J = ca.$ 8 Hz)] and C-3 (**2a**: δ_C 107.0; **2b**: δ_C 107.1), C-4a; H-3‴ [**2a**: δ 5.53 (1H, d, $J = 10.2$ Hz); **2b**: δ 5.54 (1H, d, $J = 10.2$ Hz)] and C-6, C-2″ (**2a**: δ_C 83.0; **2b**: δ_C 83.1), 2″-CH₃ (**2a**: δ_C 27.3; **2b**: δ_C 27.5); H-4″ [**2a**: δ 6.79 (1H, d, $J = 10.2$ Hz); **2b**: δ 6.78 (1H, d, $J = 10.2$ Hz)] and C-5 (**2a**: δ_C 156.0; **2b**: δ_C 156.0), C-6; H₂-5″ [**2a**: δ 1.71, 1.90 (1H each, both m); **2b**: δ 1.71, 1.90 (1H each, both m)] and C-2″, 2″-CH₃; H-7″ [**2a**: δ 5.06 (1H, qt, $J = 1.0, 7.1$ Hz); **2b**: δ 5.06 (1H, qt, $J = 1.0, 7.1$ Hz)] and C-9″ (**2a**: δ_C 25.5; **2b**: δ_C 25.6), C-10″ (**2a**: δ_C 17.6; **2b**: δ_C 17.7); H-9″ [**2a**: δ 1.64 (3H, d, $J = 1.0$ Hz); **2b**: δ 1.67 (3H, d, $J = 1.0$ Hz)] and C-7″ (**2a**: δ_C 123.1; **2b**: δ_C 123.0), C-8″ (**2a**: δ_C 132.6; **2b**: δ_C 132.5), C-10″; H-10″ [**2a**: δ 1.52 (3H, s); **2b**: δ 1.54 (3H, s)] and C-7″-9″; and H₂-2‴ and C-1‴ (**2a**: δ_C 206.2; **2b**: δ_C 206.2). On the other hand, the molecular formula of mammeasin F (**3**) was determined to be the same as that of **2**, $C_{27}H_{34}O_6$, by HRESIMS measurement. The ¹H and ¹³C NMR spectroscopic properties (**Table 2**, CDCl₃) of **3**, which were observed to be duplicate signals caused by its inseparable mixture (*ca.* 1: 1 ratio, **Figure S1**), were quite similar to those of **2** except for the signals due to the 2-methyl-1-oxobutyl moiety in the 8-position [**3a**: δ 0.98 (3H, t, $J = 7.5$ Hz, H₃-5‴), 1.25 (3H, d, $J = 6.7$ Hz, H₃-3‴), 1.46, 1.89 (each 1H, both m, H₂-4‴), 3.89 (1H, m, H₂-2‴); **3b**: δ 0.98 (3H, t, $J = 7.5$ Hz, H₃-5‴), 1.26 (3H, d, $J = 6.7$ Hz, H₃-3‴), 1.46, 1.89 (each 1H, both m, H₂-4‴), 3.89 (1H, m, H₂-2‴)]. Finally, **2** and **3** were derived by DDQ oxidation of surangins D (**14**) (Ngo et al., 2010) and C (**13**) (Verotta et al., 2004; Yagi et al., 2006), respectively. Based on this
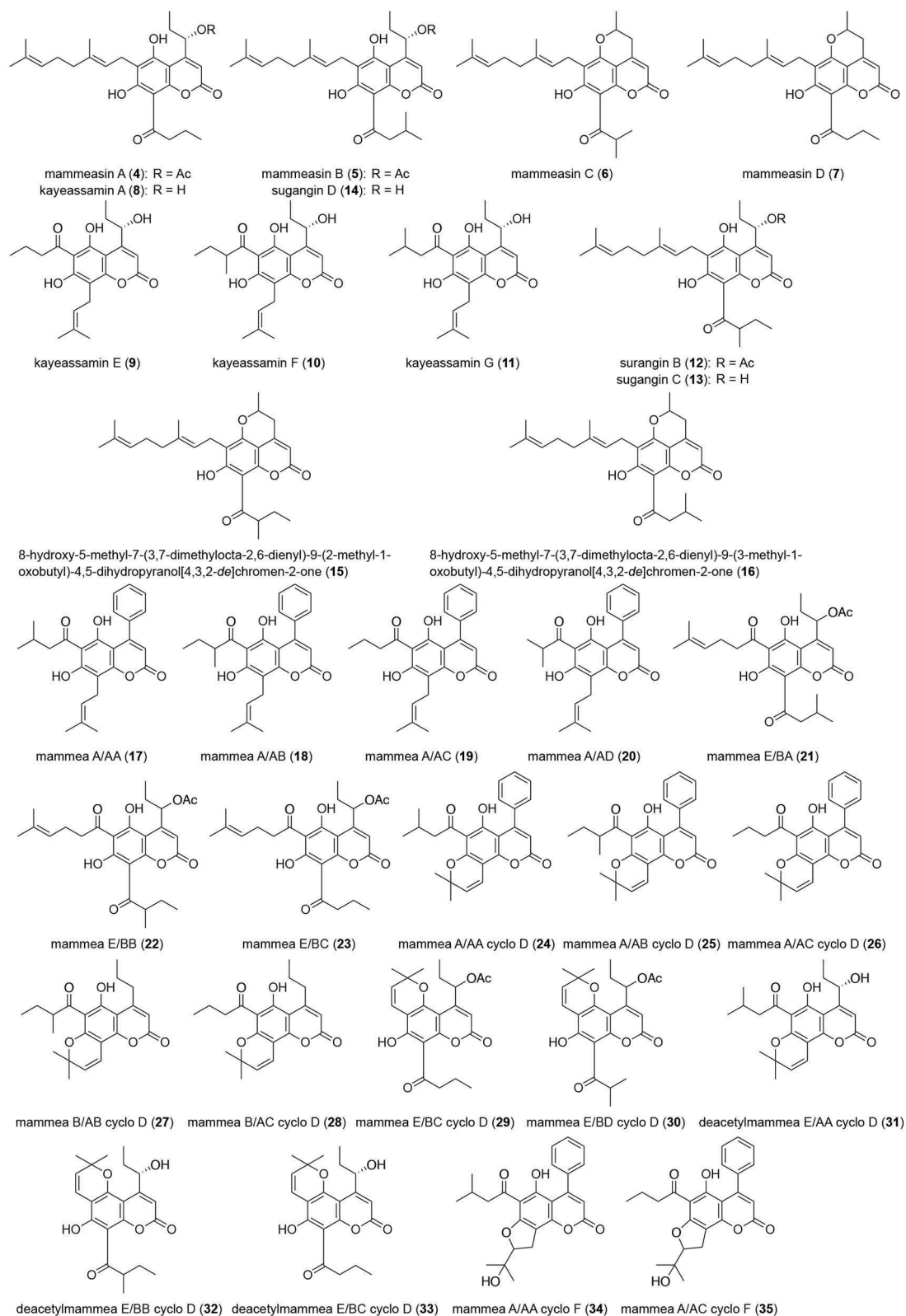
FIGURE 2 | Coumarin constituents **(4–35)** from the flowers of *M. siamensis*.

FIGURE 3 | HPLC chromatogram of kayeassamin I (**1a, 1b**). HPLC condition: column, Cosmosil 5C$_{18}$-MS-II (250 × 4.6 mm, i.d.); detection, UV (254 nm); mobile phase, CH$_3$CN−1% aqueous AcOH (90:10, v/v); flow rate, 1.0 mL/min; column temperature, r.t. (25°C).

evidence, the stereostructures of **2** and **3** were determined to be as shown.

Effects of Coumarin Constituents of the Flowers of *M. siamensis* on Testosterone 5α-Reductase

To characterize the active constituents of this plant material, the inhibitory effects of 30 isolates (**1–13, 17–20, 22–29, 31–35**) against 5α-reductase were examined. As shown in **Table 3**, mammeasins E (**2**, 22.6 μM), A (**4**, 19.0 μM), and B (**5**, 24.0 μM), kayeassamins E (**9**, 33.8 μM), F (**10**, 15.9 μM), and G (**11**, 17.7 μM), surangin C (**13**, 5.9 μM), and mammeas A/AA (**17**, 19.5 μM), E/BB (**22**, 16.8 μM), and A/AA cyclo F (**34**, 23.6 μM), were found to inhibit testosterone 5α-reductase (**Table S1**).

CONCLUSIONS

The structures of geranylated coumarin constituents, kayeassamin I (**1**) and mammeasins E (**2**) and F (**3**), newly isolated from the methanol extract of the flowers of *M. siamensis*, were determined. Of the isolated coumarins, mammeasins E (**2**, 22.6 μM), A (**4**, 19.0 μM), and B (**5**, 24.0 μM), kayeassamins E (**9**, 33.8 μM), F (**10**, 15.9 μM), and G (**11**, 17.7 μM), surangin C (**13**, 5.9 μM), and mammeas A/AA (**17**, 19.5 μM), E/BB (**22**, 16.8 μM), and A/AA cyclo F (**34**, 23.6 μM) were active 5α-reductase inhibitors. Although the intensity of the 5α-reductase inhibitory activity of these coumarins is moderate compared to a positive control having a steroid skeleton finasteride, to the best of our knowledge, there are few reports of the 5α-reductase inhibitors with non-steroidal skeletons (Dörsam and Altwein, 2009; Aggarwal et al., 2010; Chaudhary and Turner, 2010; Wu and Kapoor, 2013). Therefore, these active coumarins may be useful candidates for seed compounds of new non-steroidal 5α-reductase inhibitors. Further studies are required to elucidate the detailed structure activity relationships as well as the

TABLE 3 | IC$_{50}$ values of coumarin constituents from *M. siamensis* on testosterone 5α-reductase.

	IC$_{50}$ (μM)
Kayeassamin I (**1**)	>100 (37.5)[a]
Mammeasin E (**2**)	22.6
Mammeasin F (**3**)	>100 (14.9)[a]
Mammeasin A (**4**)	19.0
Mammeasin B (**5**)	24.0
Mammeasin C (**6**)	91.9
Mammeasin D (**7**)	>100 (16.4)[a]
Kayeassamin A (**8**)	>100 (20.2)[a]
Kayeassamin E (**9**)	33.8
Kayeassamin F (**10**)	15.9
Kayeassamin G (**11**)	17.7
Surangin B (**12**)	>100 (38.5)[a]
Surangin C (**13**)	5.9
Mammea A/AA (**17**)	19.5
Mammea A/AB (**18**)	>100 (23.3)[a]
Mammea A/AC (**19**)	>100 (41.5)[a]
Mammea A/AD (**20**)	>100 (30.3)[a]
Mammea E/BB (**22**)	16.8
Mammea E/BC (**23**)	>100 (19.1)[a]
Mammea A/AA cyclo D (**24**)	>100 (38.3)[a]
Mammea A/AB cyclo D (**25**)	>100 (6.7)
Mammea A/AC cyclo D (**26**)	>100 (32.0)[a]
Mammea B/AB cyclo D (**27**)	>100 (40.7)[a]
Mammea B/AC cyclo D (**28**)	>100 (27.3)[a]
Mammea E/BC cyclo D (**29**)	>100 (31.9)[a]
Deacetylmammea E/AA cyclo D (**31**)	>100 (37.1)[a]
Deacetylmammea E/BB cyclo D (**32**)	>100 (31.9)[a]
Deacetylmammea E/BC cyclo D (**33**)	>100 (40.8)[a]
Mammea A/AA cyclo F (**34**)	23.6
Mammea A/AC cyclo F (**35**)	83.8
Finasteride[b]	0.12

Each value represents the mean ± S.E.M. (N = 3–4).
[a]*Values in parentheses present of control of cell viability at 100 μM.*
[b]*Commercial finasteride was purchased from Sigma-Aldrich Co. LLC (St. Louis, USA).*

mode of action including the enzymatic inhibitory activity of these coumarins.

AUTHOR CONTRIBUTIONS

TM, FL, YM, HS, SS, and KN performed the experiments. TM, OM, and KN conceived and designed the experiments. SC and YP collected and identified the plant material. TM and FL wrote the paper. All authors have approved the final version of the manuscript.

FUNDING

ACKNOWLEDGMENTS

SUPPLEMENTARY MATERIAL

The Supplementary Material for this article can be found online at: https://www.frontiersin.org/articles/10.3389/fchem.2020.00199/full#supplementary-material

These data include HPLC chromatograms of mammeasins E (**2a**, **2b**) and F (**3a**, **3b**) (**Figure S1**), ^{1}H–^{1}H COSY and HMBC correlations of **2** and **3** (**Figure S2**), 1D and 2D NMR spectra of **1**–**3** (**Figures S3**–**S17**), and inhibitory effects of coumarin constituents (**1**–**35**) from *M. siamensis* on testosterone 5α-reductase (**Table S1**).

REFERENCES

Aggarwal, S., Thareja, S., Verma, A., Bhardwaj, T. R., and Kumar, M. (2010). An overview on 5 alpha-reductase inhibitors. *Steroids* 75, 109–153. doi: 10.1016/j.steroids.2009.10.005

Azzouni, F., Godoy, A., Li, Y., and Mohler, J. (2012). The 5 alpha-reductase isozyme family: a review of basic biology and their role in human diseases. *Adv. Urol.* 2012:530121. doi: 10.1155/2012/530121

Chaudhary, U. B., and Turner, J. S. (2010). Finasteride. *Expert Opin. Drug Metab. Toxicol.* 6, 873–881. doi: 10.1517/17425255.2010.495944

Coltman, C. A. Jr., Thompson, I. M. Jr., and Feigl, P. (1999). Prostate cancer prevention trial (PCPT) update. *Eur. Urol.* 35, 544-547. doi: 10.1159/000019895

Dörsam, J., and Altwein, J. (2009). 5α-Reductase inhibitor treatment of prostatic diseases: background and practical implications. *Prostate Cancer Prostatic. Dis.* 12, 130–136. doi: 10.1038/pcan.2008.56

Guilet, D., Hélesbeux, J.-J., Séraphin, D., Sévenet, T., Richomme, P., and Bruneton, J. (2001). Novel cytotoxic 4-phenylfuranocoumarins from *Calophyllum dispar*. *J. Nat. Prod.* 64, 563–568. doi: 10.1021/np000517o

Heinzl, S. (1999). Androgenetic alopecia: finasteride treated hair loss. *Med. Monatsschr. Pharm.* 22, 124–127.

Kaweetripob, W., Mahidol, C., Prawat, H., and Ruchirawat, S. (2000). Chemical investigation of *Mammea siamensis*. *Pharm. Biol.* 38, 55–57. doi: 10.1076/phbi.38.6.55.5954

Kobayashi, M., Akaki, J., Yamaguchi, Y., Yamasaki, H., Ninomiya, K., Pongpiriyadacha, Y., et al. (2019). *Salacia chinensis* stem extract and its thiosugar sulfonium constituent, neokotalanol, improves HbA1c levels in ob/ob mice. *J. Nat. Med.* 73, 584–588. doi: 10.1007/s11418-019-01311-w

Koseki, J., Matsumoto, T., Matsubara, Y., Tsuchiya, K., Mizuhara, Y., Sekiguchi, K., et al. (2015). Inhibition of rat 5α-reductase activity and testosterone-induced sebum synthesis in hamster sebocytes by an extract of *Quercus acutissima* cortex. *Evid. Based Complement. Alternat. Med.* 2015:853846. doi: 10.1155/2015/853846

Laphookhieo, S., Maneerat, W., and Kiattansakul, R. (2006). Phenolic compounds from *Mammea siamensis* seeds. *Can. J. Chem.* 84, 1546–1549. doi: 10.1139/v06-157

Laphookhieo, S., Promnart, P., Syers, J. K., Kanjana-Opas, A., Ponglimanont, C., and Karalai, C. (2007). Coumarins and xanthones from the seeds of *Mammea siamensis*. *J. Braz. Chem. Soc.* 18, 1077–1080. doi: 10.1590/S0103-50532007000500031

Lee, S. H., Lee, D.-H., Lee, J., Lee, W.-Y., Chung, B. C., and Choi, M. H. (2012). Comparative GC-MS based *in vitro* assays of 5α-reductase activity using rat liver S9 fraction. *Mass Spectrom. Lett.* 3, 21–24. doi: 10.5478/MSL.2012.3.1.021

Mahidol, C., Kaweetripob, W., Prawat, H., and Ruchirawat, S. (2002). Mammea coumarins from the flowers of *Mammea siamensis*. *J. Nat. Prod.* 65, 757–760. doi: 10.1021/np010579u

Mahidol, C., Prawat, H., Kaweetripob, W., and Ruchirawat, S. (2007). Regioisomers of acylcoumarins from the flowers of *Mammea siamensis*. *Nat. Prod. Commun.* 2, 557–564. doi: 10.1177/1934578X0700200509

Manse, Y., Ninomiya, K., Nishi, R., Hashimoto, Y., Chaipech, S., Muraoka, O., et al. (2017). Labdane-type diterpenes, galangalditerpenes A–C, with melanogenesis inhibitory activity from the fruit of *Alpinia galanga*. *Molecules* 22:2279. doi: 10.3390/molecules22122279

Matsuda, H., Sato, N., Yamazaki, M., Naruto, S., and Kubo, M. (2001). Tastosterone 5α-reductase inhibitory active constituents from Anemarrhenae Rhizoma. *Biol. Pharm. Bull* 24, 586–587. doi: 10.1248/bpb.24.586

Morel, C., Guilet, D., Oger, J.-M., Séraphin, D., Sévenet, T., Wiart, C., et al. (1999). 6-Acylcoumarins from *Mesua racemose*. *Phytochemistry* 50, 1243–1247. doi: 10.1016/S0031-9422(98)00688-8

Morikawa, T., Manse, Y., Koda, M., Chaipech, S., Pongpiriyadacha, Y., Muraoka, O., et al. (2018). Two new aromatic glycosides, elengiosides A and B, from the flowers of *Mimusops elengi*. *J. Nat. Med.* 72, 542–550. doi: 10.1007/s11418-017-1160-z

Morikawa, T., Sueyoshi, M., Chaipech, S., Matsuda, H., Nomura, Y., Yabe, M., et al. (2012). Suppressive effects of coumarins from *Mammea siamensis* on inducible nitric oxide synthase expression in RAW264.7 cells. *Bioorg. Med. Chem.* 20, 4968–4977. doi: 10.1016/j.bmc.2012.06.031

Ngo, N. T. N., Nguyen, V. T., Vo, H. V., Vang, O., Duus, F., and Ho, T.-D. H. (2010). Cytotoxic coumarins from the bark of *Mammea siamensis*. *Chem. Pharm. Bull.* 58, 1487–1491. doi: 10.1248/cpb.58.1487

Ninomiya, K., Shibatani, K., Sueyoshi, M., Chaipech, S., Pongpiriyadacha, Y., Hayakawa, T., et al. (2016). Aromatase inhibitory activity of geranylated coumarins, mammeasins C and D, isolated from the flowers of *Mammea siamensis*. *Chem. Pharm. Bull.* 64, 880-−885. doi: 10.1248/cpb.c16-00218

Noysang, C., Mahringer, A., Zeino, M., Saeed, M., Luanratana, O., Fricker, G., et al. (2014). Cytotoxicity and inhibition of P-glycoprotein by selected medicinal plants from Thailand. *J. Ethnopharmacol.* 155, 633–641. doi: 10.1016/j.jep.2014.06.001

Petel, D. M., Sharma, M. G., Vala, R. M., Lagunes, I., Puerta, A., Padrón, J. M., et al. (2019). Hydroxyl alkyl ammonium ionic liquid assisted green and one-pot regioselective access to functionalized pyrazolodihydropyridine core and their pharmacological evaluation. *Bioorg. Chem.* 86, 137–150. doi: 10.1016/j.bioorg.2019.01.029

Poobrasert, O., Constant, H. L., Beecher, C. W. W., Farnsworth, N. R., Kinghorn, A. D., Pezzuto, J. M., et al. (1998). Xanthones from the twigs of *Mammea siamensis*. *Phytochemistry* 47, 1661–1663. doi: 10.1016/S0031-9422(97)00820-0

Prachyawarakorn, V., Mahidol, C., and Ruchirawat, S. (2000). NMR study of seven coumarins from *Mammea siamensis*. *Pharm Biol.* 38, 58–62. doi: 10.1076/phbi.38.6.58.5962

Prachyawarakorn, V., Mahidol, C., and Ruchirawat, S. (2006a). Siamenols A–D, four new coumarins from *Mammea siamensis*. *Chem. Pharm. Bull* 54, 884–886. doi: 10.1248/cpb.54.884

Prachyawarakorn, V., Mahidol, C., and Ruchirawat, S. (2006b). Pyranocoumarins from the twigs of *Mammea siamensis*. *Phytochemistry* 67, 924–928. doi: 10.1016/j.phytochem.2006.02.006

Sangkaruk, R., Rungrojsakul, M., Tima, S., and Anuchapreeda, S. (2017). Effect of Thai saraphi flower extracts on WT1 and Bcr/Abl protein expression in leukemic cell lines. *Afr. J. Tradit. Complement. Altern. Med.* 14, 16–24. doi: 10.21010/ajtcam.v14i2.3

Sharma, M. G., Vala, R. M., Patel, D. M., Lagunes, I., Fernandes, M. X., Padrón, J. M., et al. (2018). Anti-proliferative 1,4-dihydropyridine and pyridine derivatives synthesized through a catalyst-free, one-pot multi-component reaction. *ChemistrySelect* 3, 12163–12168. doi: 10.1002/slct.201802537

Tanabe, G., Manse, Y., Ogawa, T., Sonoda, N., Marumoto, S., Ishikawa, F., et al. (2018). Total synthesis of γ-alkylidenebutenolides, potent melanogenesis

inhibitors from Thai medicinal plant *Melodorum fruticosum. J. Org. Chem.* 83, 8250–8264. doi: 10.1021/acs.joc.8b00986

Tanabe, G., Tsutsui, N., Shibatani, K., Marumoto, S., Ishikawa, F., Ninomiya, K., et al. (2017). Total synthesis of the aromatase inhibitors, mammeasins C and D, from Thai medicinal plant *Mammea siamensis. Tetrahedron* 73, 4481–4486. doi: 10.1016/j.tet.2017.06.016

Titus, M. A., Li, Y., Kozyreva, O. G., Maher, V., Godoy, A., Smith, G. J., et al. (2014). 5α-Reductase type 3 enzyme in benign and malignant prostate. *Prostate* 74, 235–249. doi: 10.1002/pros.22745

Tosti, A., and Piraccini, B. M. (2000). Finasteride and hair cycle. *J. Am. Acad. Dermatol.* 42, 848–849. doi: 10.1067/mjd.2000.103272

Tung, N. H., Uto, T., Sakamoto, A., Hayashida, Y., Hidaka, Y., Morinaga, O., et al. (2013). Antiproliferative and apoptotic effects of compounds from the flower of *Mammea siamensis* (Miq.) T Anders. on human cancer cell lines. *Bioorg. Med. Chem. Lett.* 23, 158–162. doi: 10.1016/j.bmcl.2012.10.127

Uto, T., Tung, N. H., Thongjankaew, P., Lhieochaiphant, S., and Shoyama, Y. (2016). Kayeassamin a isolated from the flower of *Mammea siamensis* triggers apoptosis by activation caspase-3/-8 in HL-60 human leukemia cells. *Pharmacog. Res.* 8, 244–248. doi: 10.4103/0974-8490. 188884

Verotta, L., Lovaglio, E., Vidari, G., Finzi, P. V., Neri, M. G., Raimondi, A., et al. (2004). 4-Alkyl- and 4-phenylcoumarins from *Mesua ferrea* as promising multidrug resistant antibacterials. *Phytochemistry* 65, 2867–2879. doi: 10.1016/j.phytochem.2004.07.001

Win, N. N., Awale, S., Esumi, H., Tezuka, Y., and Kadota, S. (2008a). Novel anticancer agents, kayeassamins A and B from the flower of *Kayea assamica* of Myanmar. *Bioorg. Med. Chem. Lett.* 18, 4688–4691. doi: 10.1016/j.bmcl.2008.07.001

Win, N. N., Awale, S., Esumi, H., Tezuka, Y., and Kadota, S. (2008b). Novel anticancer agents, kayeassamins C–I from the flower of *Kayea assamica*

of Myanmar. *Bioorg. Med. Chem.* 16, 8653–8660. doi: 10.1016/j.bmc.2008. 07.091

Wu, C., and Kapoor, A. (2013). Dutasteride for the treatment of benign prostatic hyperplasma. *Expert Opin. Phamacother.* 14, 1399–1408. doi: 10.1517/14656566.2013.797965

Yagi, N., Ohkubo, K., Okuno, Y., Oda, Y., and Miyazawa, M. (2006). Antimutagenic compound from yellow batai (*Peltophorum dasyrachis*). *J. Oleo Sci.* 55, 173–180. doi: 10.5650/jos.55.173

Yamana, K., Labrie, F., and Luu-The, V. (2010). Human type 3 5α-reductase is expressed in peripheral tissues at higher levels that types 1 and 2 and its activity is potently inhibited by finasteride and dutasteride. *Horm. Mol. Biol. Clin. Invest.* 2, 293–299. doi: 10.1515/hmbci.2010.035

Yang, H., Protiva, P., Jiang, B., Baggett, S., Reynertson, K. A., Weinstein, I. B., et al. (2005). Antioxidant and cytotoxic isoprenylated coumarins from *Mammea Americana. Planta Med.* 71, 852–860. doi: 10.1055/s-2005-871257

Yao, Z., Xu, Y., Zhang, M., Jiang, S., Nicklaus, M. C., and Liao, C. (2011). Discovery of a novel hybrid from finasteride and episteride as 5α-reductase inhibitor. *Bioorg. Med. Chem. Lett.* 21, 475–478. doi: 10.1016/j.bmcl.2010.10.112

Chemistry and Neurotrophic Activities of (–)-Talaumidin and Its Derivatives

Kenichi Harada*, Miwa Kubo* and Yoshiyasu Fukuyama

Faculty of Pharmaceutical Sciences, Tokushima Bunri University, Tokushima, Japan

(–)-Talaumidin (**1**), a 2,5-biaryl-3,4-dimethyltetrahydrofuran lignan isolated from Aristolochia arcuata Masters, exhibits significant neurite-outgrowth promotion and neuroprotection in primary cultured rat cortical neurons and in NGF-differentiated PC12 cells. The first enantioselective total synthesis of **1** was achieved by a flexible and reliable synthetic pathway involving an Evans asymmetric aldol reaction, as well as a stereocontrolled hydroboration and Friedel–Crafts arylation, to construct the four contiguous chiral centers on the tetrahydrofuran (THF) ring of **1**. In order to investigate the stereochemistry–activity relationship of **1**, a systematic synthesis of all diastereomers of **1** was accomplished by applying the synthetic strategy used for natural product **1**. The evaluation of neurite-outgrowth promotion by all of the synthesized diastereomers indicated that the (–)-(1S,2R,3S,4R)-isomer **1e** was significantly more active than naturally occurring **1**. Additionally, we established a synthetic methodology for talaumidin derivatives that could be used to prepare a variety of analogs in a few steps and on a large scale. The synthesized racemic analog rac-**1e** (**56a**) exhibited neurite-outgrowth promoting activity in NGF-differentiated PC12 cells to the same degree as the optically active (–)-**1e**, revealing that a relative configuration bearing all-cis- substituents is important for potent neurotrophic activity, whilst the absolute configuration does not affect activity. Fourteen analogs based on (±)-**56a** were prepared via the same synthetic methodology. Among them, **56b** with a methylenedioxy group on both benzene rings was found to exhibit the most significant neurite outgrowth promotion. In addition, **56a** and **56b** induced regeneration of the mouse optic nerve in vivo, and their activity was higher than that of talaumidin, as well as their in vitro measured activity. Furthermore, the structure–activity relationship of **56b** indicated that the two benzene rings were essential structures, and that the methyl groups on the THF ring could enhance the neurotrophic activity. This result suggests that the two benzene rings of the talaumidin derivatives are essential structures for neurotrophic activity, while the two methyl groups on the THF ring can enhance neurite-outgrowth activity. Finally, it was observed that 1 and derivatives **56a** and **56b** exhibited potent regenerative activity in the injured mouse optic nerve in vivo.

Keywords: talaumidin, neurotrophic activities, PC12, regenerative activity, primary cultured rat cortical neurons

INTRODUCTION

Neurotrophins (NGF, BDNF, NT3, and NT4/5) are known to play essential roles in neuron survival, process outgrowth, and synaptic connectivity during development and nervous system plasticity in adults. Hence, they have a potential to become useful agents for neurodegeneration (Pardridge, 2002). Although, these polypeptide cannot cross the brain–blood barrier because of their high molecular weight and easily metabolize by peptidases under physiological conditions (Pardridge, 2002; Thoenen and Sendtner, 2002). Therefore, small molecules that can mimic the functions of neurotrophic factors might be promising alternatives for the treatment of neurodegenerative diseases (Xie and Longo, 2000; Massa et al., 2002). Neurotrophins also are able to promote process outgrowth and survival neuronal cells *in vitro*. Thus, we have been investigating neurotrophin-mimic small molecules from natural products based on rat cortical neuron cultures and PC12 cells, resulting in the discovery of interesting neurotrophic compounds (Huang et al., 2000, 2001; Fukuyama et al., 2002; Yokoyama et al., 2002; Kubo et al., 2009, 2010, 2012, 2013, 2015; Matsui et al., 2012).

Talaumidin (**1**) is a 2,5-diaryl-3,4-dimethyltetrahydrofuran lignan (**Figure 1**), first isolated from the bark of *Talauma hodgsonii* Hook. f. and Thoms (Vieira et al., 1998). Talaumidin is categorized tetrahydrofuran lignans which are widely distributed in higher plants. Tertrahydrofuran lignans have attracted considerable attention due to their biological activities as cytotoxic activities (Vučković et al., 2007; Lin et al., 2010), DPPH-radical-scavenging activity (Mei et al., 2009), antioxidant

activity (Piao et al., 2008), superoxide anion scavenging activities (Sasaki et al., 2013), growth and differentiation of osteoblastic MC3T3-E1 (Kiem et al., 2008), *anti*-HIV-1 activities (Zhang et al., 2007; Warashima et al., 2008), downregulate cyclooxygenase-2 (COX-2), inducible nitric oxide synthase (iNOS), and interleukin-1b (IL-1b) gene expressions in a dose-dependent manner in LPS-elicited mouse macrophages (Ma et al., 2007), inhibited NO production (Kim et al., 2014), *anti*-inflammatory activity (Wu et al., 2005), antimicrobial activities (Ding et al., 2014), antiproliferative activities against human cancer cell lines (Kim et al., 2011), and neurite-outgrowth promoting activity on PC12 cells (Kuroyanagi et al., 2008). On the other hands, biological activity of **1** has been documented as antiplasmodial activity (Abrantes et al., 2008) except for our reports, to date.

In our continuing studies on neurotrophic compounds, we isolated **1** from Blazilian plant *Aristolochia arcuata*. In addition to significant neurite-outgrowth promotion in primary cultured rat cortical neurons, we found that **1** and its analogs also exhibited neuroprotections against cell death induced by several insults (Zhai et al., 2004, 2005). Furthermore, **1**, belonging to a diaryltetrahydrofuran-type lignan, possesses a tetrahydrofuran ring bearing four contiguous stereogenic centers. These promising biological activities and the prospective selective preparation of the possible stereoisomers with regard to the four stereogenic centers of **1** make it an attractive synthetic target. In this review, we focus and summarize neurite-outgrowth promotion activities in primary cultured rat cortical neurons (Zhai et al., 2004) and in NGF-differentiated PC12 cells. Additionally, we describe the synthesis of **1** and all
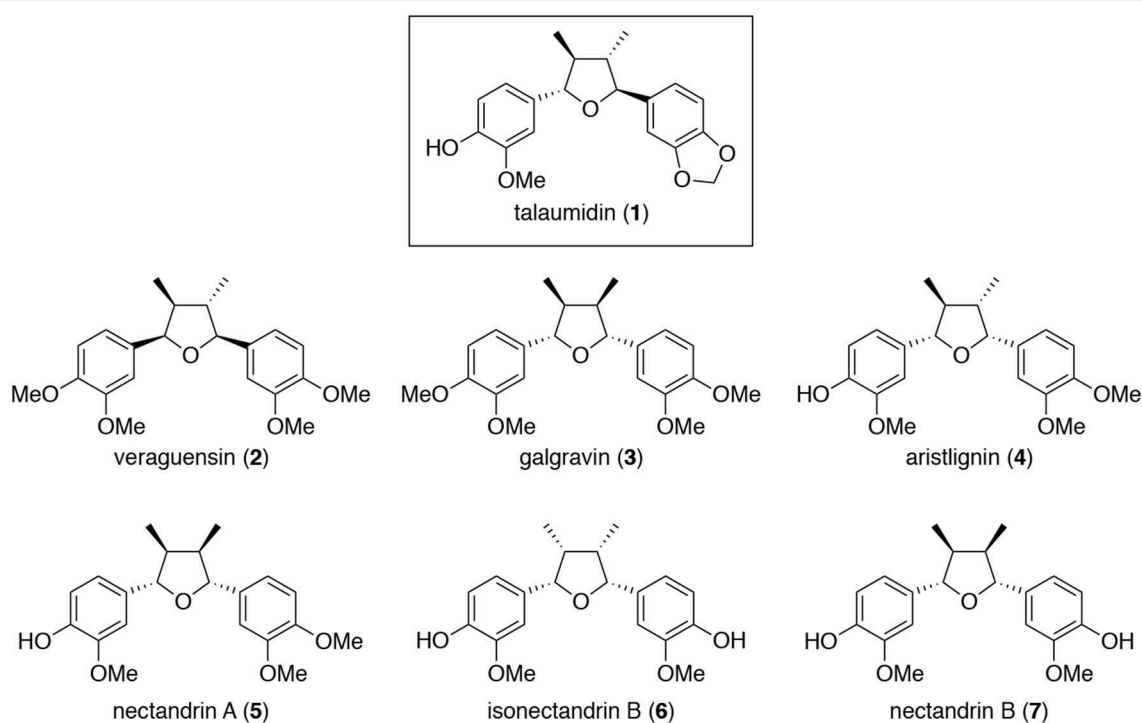
FIGURE 1 | Structures of talaumidin (**1**) and analogs **2–7** (Zhai et al., 2005).

stereoisomers of **1** (Esumi et al., 2006; Fukuyama et al., 2008), and discuss structure–activity relationships between **1** and its analogs on PC12 cells (Harada et al., 2015). Furthermore, we report their regenerative activity toward mouse optic nerves as a neurotrophic activity *in vivo,* reinforcing their potential as therapeutic agents for neurodegenerative disease (Harada et al., 2018).

RESULTS AND DISCUSSION

Talaumidin (**1**) (Vieira et al., 1998) and its analogs, veraguensin (**2**) (Barata et al., 1978), galgravin (**3**) (Urzúa et al., 1987), aristlignin (**4**) (Urzúa et al., 1987), nectandrin A (**5**) (Le Quesne et al., 1980), isonectandrin B (**6**) (Le Quesne et al., 1980), and nectandrin B (**7**) (Le Quesne et al., 1980), were isolated from a methanol extract of the root of *A. arcuata* (*Aristolochiaceae*) by consecutive silica gel column chromatographies (Zhai et al., 2005).

Neurite-Outgrowth Promoting Activity of Talaumidin in PC12 Cells

Rat pheochromocytoma PC12 cells have been widely used as a model cells of neurons (Vaudry et al., 2002). When PC12 cells are stimulated with NGF, they cease growth and begin to grow neurites, eventually differentiating into a neuron-like phenotype. In the absence of NGF, talaumidin had no morphological effects on PC12 cells. In the presence of 20 ng/mL NGF, however, talaumidin promoted neurite outgrowth dose-dependently at concentrations of 1–30 μM, inducing longer average neurite length, as well as a higher percentage of neurite-bearing cells (**Figure 2**). These effects were validated through morphological observations (**Figures 2C** vs. **2B**) and quantitative analysis of neurites (**Figure 2D**).

Neurotrophic Effects of Talaumidin in Primary Cultured Rat Cortical Neurons

In tissue sections and cell cultures, the *anti*-MAP2 antibody can stain neuronal cell bodies and dendrites but cannot use for efficient recognition of axons (Kaufmann et al., 1997). Alternatively, the *anti*-tau antibody reacts with tau proteins, which are distributed over the entire neuron surface, thus staining the cell body, dendrites as well as axons of neurons (Dotti et al., 1987). First, the morphological effects of talaumidin on cultured rat cortical neurons were evaluated by the *anti*-MAP2 staining method (**Figures 3A,B**). Talaumidin has been found to exhibit a significant promoting neurite outgrowth in the primary cultures of rat cortical neurons at concentration of 10 μmol/L. Measurements of each neuron stained by *anti*-MAP2
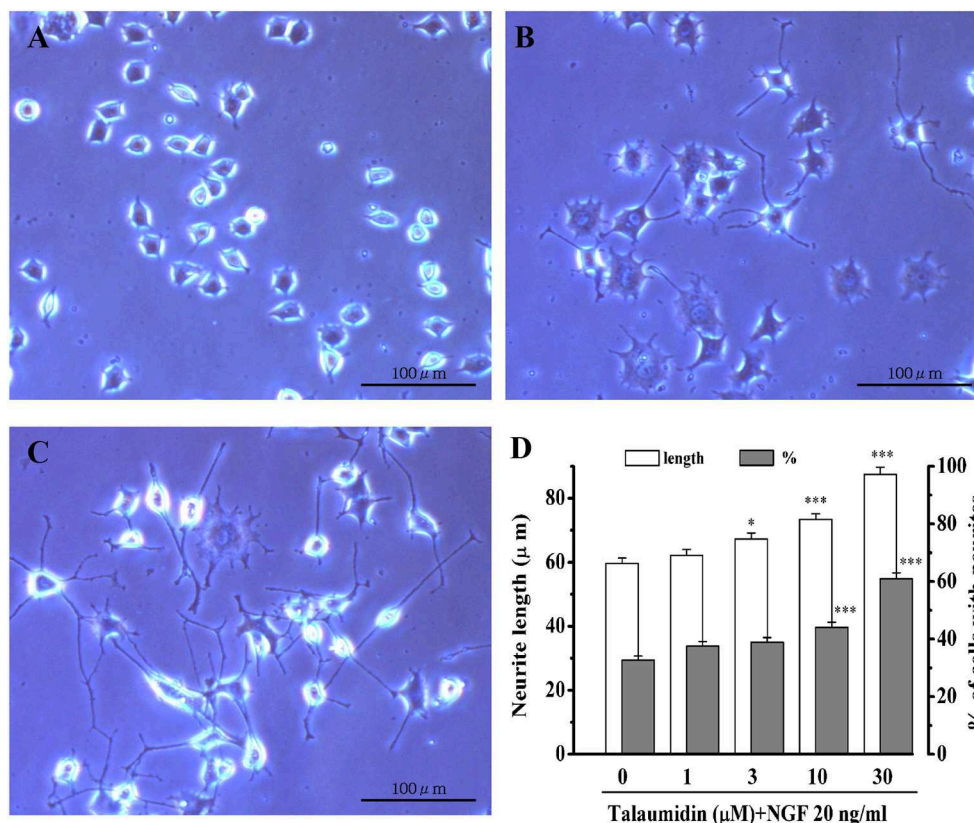
FIGURE 2 | Neurite outgrowth promoting activities of **1** in NGF-differentiated PC12 cells. **(A)** Vehicle control (0.5% ethanol), **(B)** NGF 20 ng/mL, **(C)** NGF 20 ng/mL + talaumidin 30 μM, **(D)** quantitative analysis of neurite length and percent of cells bearing neurites. *$P < 0.05$, ***$P < 0.001$ vs. NGF alone (0 μM talaumidin).

FIGURE 3 | Neurite outgrowth-promoting activity of **1** shown by *anti*-MAP2 and *anti*-tau immunohistochemical staining in primary cultured rat cortical neurons. **(A,D)** Morphology of neurons in control groups, **(B,E)** Morphology of neurons in 10 μM talaumidin groups, **(C,F)** quantitative analysis of dose-dependent manner. *P < 0.05, **P < 0.01, ***P < 0.001 compared with control (Ctrl) (Zhai et al., 2004).
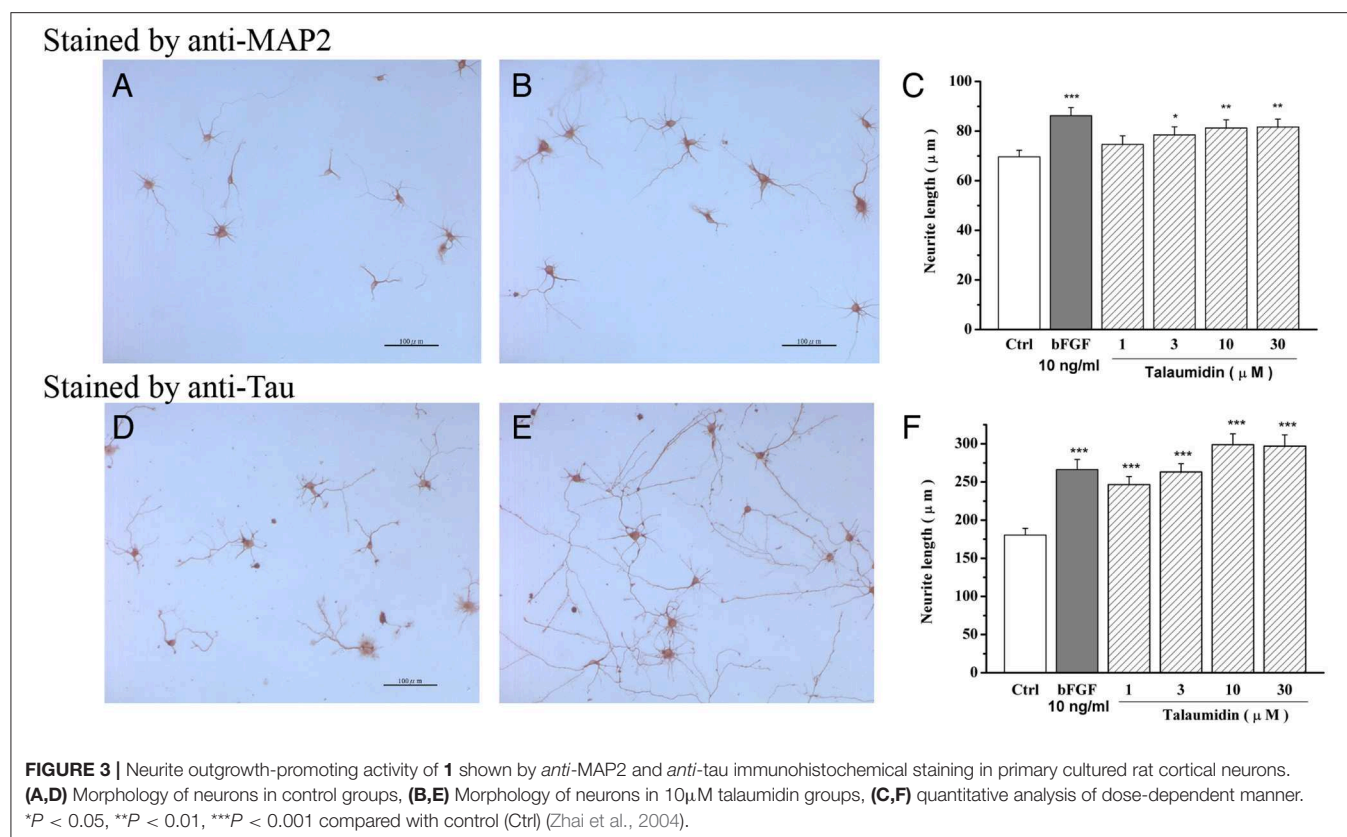
was performed by morphological analysis of process outgrowth brought on by talaumidin, and the quantitative results are shown in **Figure 3C**. It is obvious that talaumidin promotes process elongation dose-dependently at concentrations ranging from 3 to 30 μM. The longest processes stained with the *anti*-tau method are referred to as axon-like neurites, while others are referred to as dendrite-like neurites for clarity in the description of effects of **1** on neurite outgrowth. The morphological evaluation was carried out by *anti*-tau staining method (**Figures 3D,E**). According to expectations, **1** was observed to significantly promote dendrite-like processes, as well as axon-like processes at 10 μM. Quantitative analysis indicated that **1** enhanced process elongation in a dose-dependent manner at concentrations ranging from 1 to 30 μM (**Figure 3F**). Additionally, **1** also showed neuroprotective effects against serum deprivation-induced cell death in rat cortical neurons (Zhai et al., 2004).

Evaluation of Neurite-Outgrowth Promoting Activity of Talaumidin and Other 2,5-diaryl-3,4-dimethyltetrahydrofuran Neolignans

The neurotrophic effects of 2,5-diaryl-3,4-dimethyltetrahydrofuran neolignans (**2–7**) were compared with talaumidin (**1**) (Zhai et al., 2005). Comparison of the effects of compounds **1–7** in the neurite-outgrowth assay indicated that **5**, **6**, and **7** were similar to **1**, but **2** and **4** had fewer effects than **1** (**Figure 4**). Especially, all-*cis*-substituted -type **6** showed the

most potent neurite-outgrowth promoting activity at 30 μM. Furthermore, compounds **5** and **7**, whose stereochemistry are *trans-cis-trans* (4,5-*trans*, 3,4-*cis*, and 2,3-*trans*), presented similar activity of **1**. Curiously, *trans-cis-trans* **3** could not be attributed to effect. The above preliminary structure–activity analysis assumes that the stereochemistry of tetrahydrofuran ring and substituents on two benzene groups would make an important contribution to the enhancement of activity. It's very interesting challenge to investigate the relationship between stereochemistry and substituent and the neurotrophic activity of talaumidin.

Total Syntheses of (–)-Talaumidin

Due to its unique structure and potent neurotrophic activities, talaumidin has been the target of extensive synthetic efforts over the years. To date, six syntheses have been reported. In 2006, we reported the first total synthesis of (2S,3S,4S,5S)-talaumidin *via* a flexible and stereo-controlled synthetic strategy (Esumi et al., 2006; Fukuyama et al., 2008). In addition, we determined the absolute configuration of (–)-talaumidin to be (2S,3S,4S,5S) during the course of the synthetic study. In 2007, Hanessian et al. attained the synthesis of unnatural (+)-talaumidin along with four tetrahydrofuran analogs (Hanessian and Reddy, 2007). In the same year, Kim et al. disclosed the stereoselective reductive deoxygenation/epimerization of cyclic hemiacetals and the synthesis of (+)-talaumidin (Kim et al., 2007). Alternative syntheses of talaumidin have additionally been
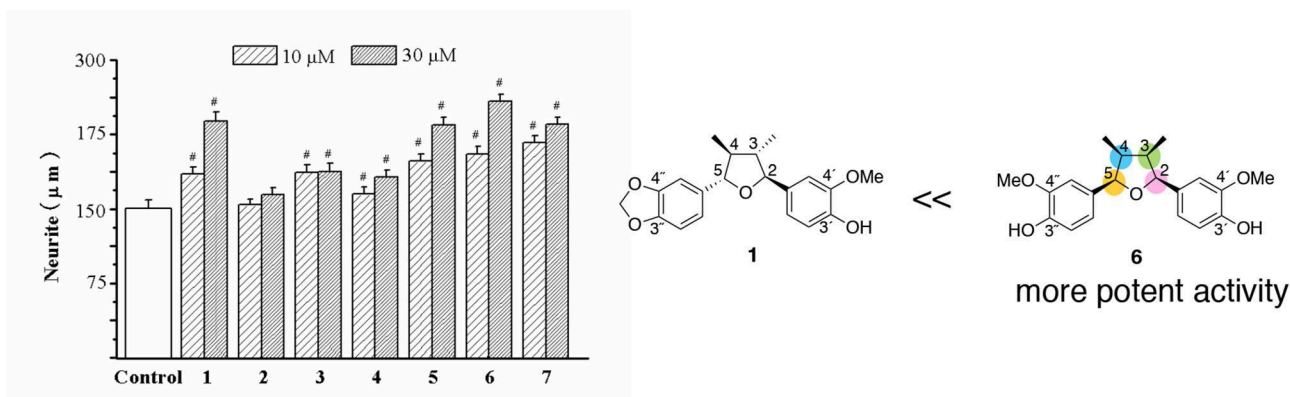
FIGURE 4 | Comparison of the effects of compounds **1–7** on neurite outgrowth in primary cultured rat cortical neurons. [#]$P < 0.001$ vs. control (Zhai et al., 2005).

SCHEME 1 | First synthesis of (–)-talaumidin by Fukuyama et al.
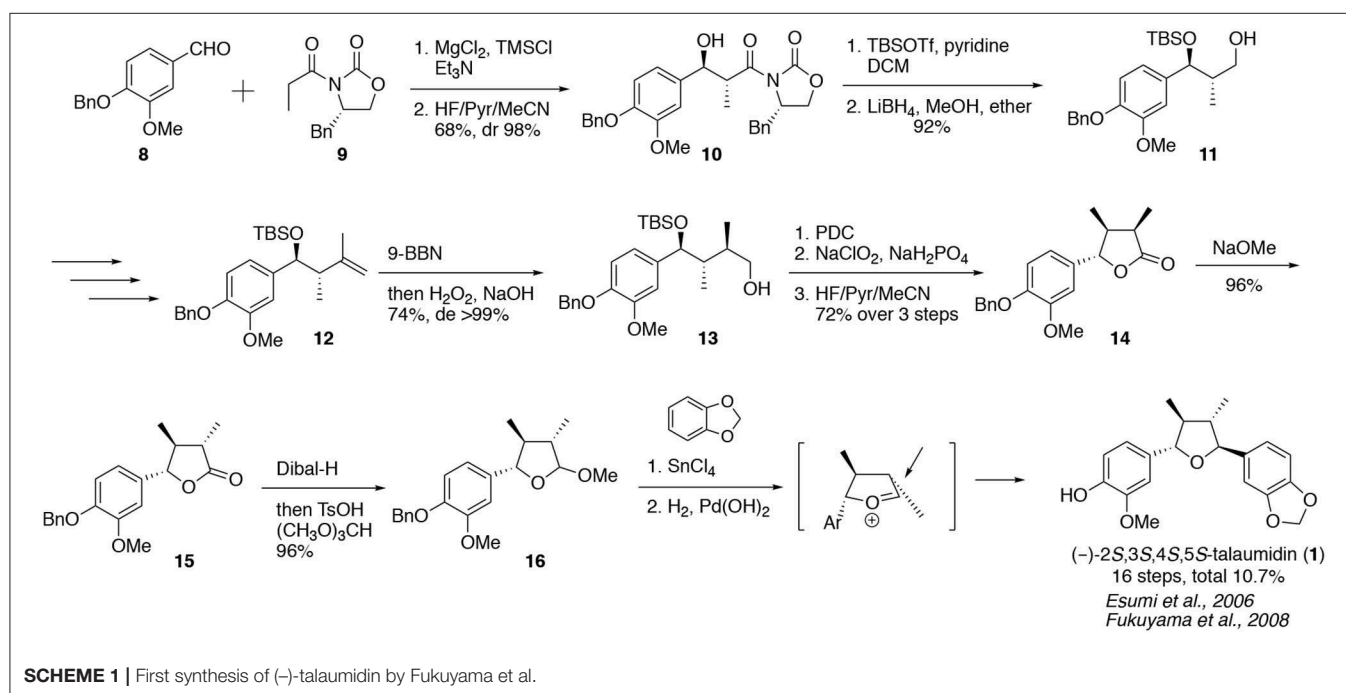
reported by Matcha and Ghosh (2008), Rye and Barker (2009), and Xue et al. (2009). Synthetic studies of tetrahydrofuran-type lignans are actively continuing worldwide.

Synthesis of Talaumidin by Fukuyama et al.

In 2006, we accomplished an enantioselective synthesis of (2S,3S,4S,5S)-talaumidin in advance of the other synthetic studies (**Scheme 1**) (Esumi et al., 2006; Fukuyama et al., 2008). The synthesis of **1** commenced with an *anti*-selective Evans asymmetric aldol reaction. The reaction of benzaldehyde **8** with chiral oxazolidinone **9** in the presence of MgCl$_2$, gave rise to (2S,3S)-aldol adduct **10** in 98% de (Evans et al., 2002). Following the conversion of alcohol **11** to the exomethylene **12**, diastereoselective hydroboration of **12** was examined. Using 9-BBN, the reaction proceeded in >99% de, in

accordance with the Cram rule (Houk et al., 1984). Although the generated chirality at C4 was opposite to the desired stereochemistry, the chiral center could be inverted to 4S-configuration by exposing lactone **14** to basic conditions. The last stage entailed a diastereoselective Friedel–Crafts arylation of cyclic acetal **16**, which afforded a single stereoisomer bearing the (2S,3S,4S,5S)-configuration. Finally, the total synthesis of (2S,3S,4S,5S)-**1** was completed by hydrogenolysis of the benzyl group. The first enantioselective synthesis of (2S,3S,4S,5S)-**1** was accomplished in 10.7% overall yield, over 16 steps. All spectroscopic data, such as NMR, HR-MS, IR, CD, [α]$_D$ of synthesized (2S,3S,4S,5S)-talaumidin were identical to those of natural (–)-talaumidin. From these results, the absolute configuration of natural (–)-talaumidin was determined to be (2S,3S,4S,5S).

Synthesis of (+)-Talaumidin by Hanessian et al.

In 2007, Hanessian et al. reported a second synthesis of talaumidin, which was performed as part of a synthetic study on tetrahydrofuran-type lignan compounds (**Scheme 2**) (Hanessian and Reddy, 2007). The synthesis began with a chiral cyanohydrin **18**, in turn prepared by a catalytic asymmetric reaction of **17**, according to Belokon's protocol (Belokon et al., 2000). After Wittig olefination, 1,4-addition of **19** with dimethyllithium cuprate and TMSCl afforded

anti-configuration in 12:1 dr. Subsequent α-alkylation of the ester with MeI *via* an enolate provided **20** with high diastereoselectivity. Then, a Grignard reaction with the aldehyde in the presence of CeCl$_3$ provided **21** having the two (*R*)-hydroxy moieties. The key cycloetherification of **21** gave rise to the talaumidin skeleton in 90% yield through a quinone methide intermediate. Following deprotection, the total synthesis of (+)-talaumidin was attained in an overall yield of 12.7% over 16 steps.

SCHEME 2 | Total syntheses of talaumidin.
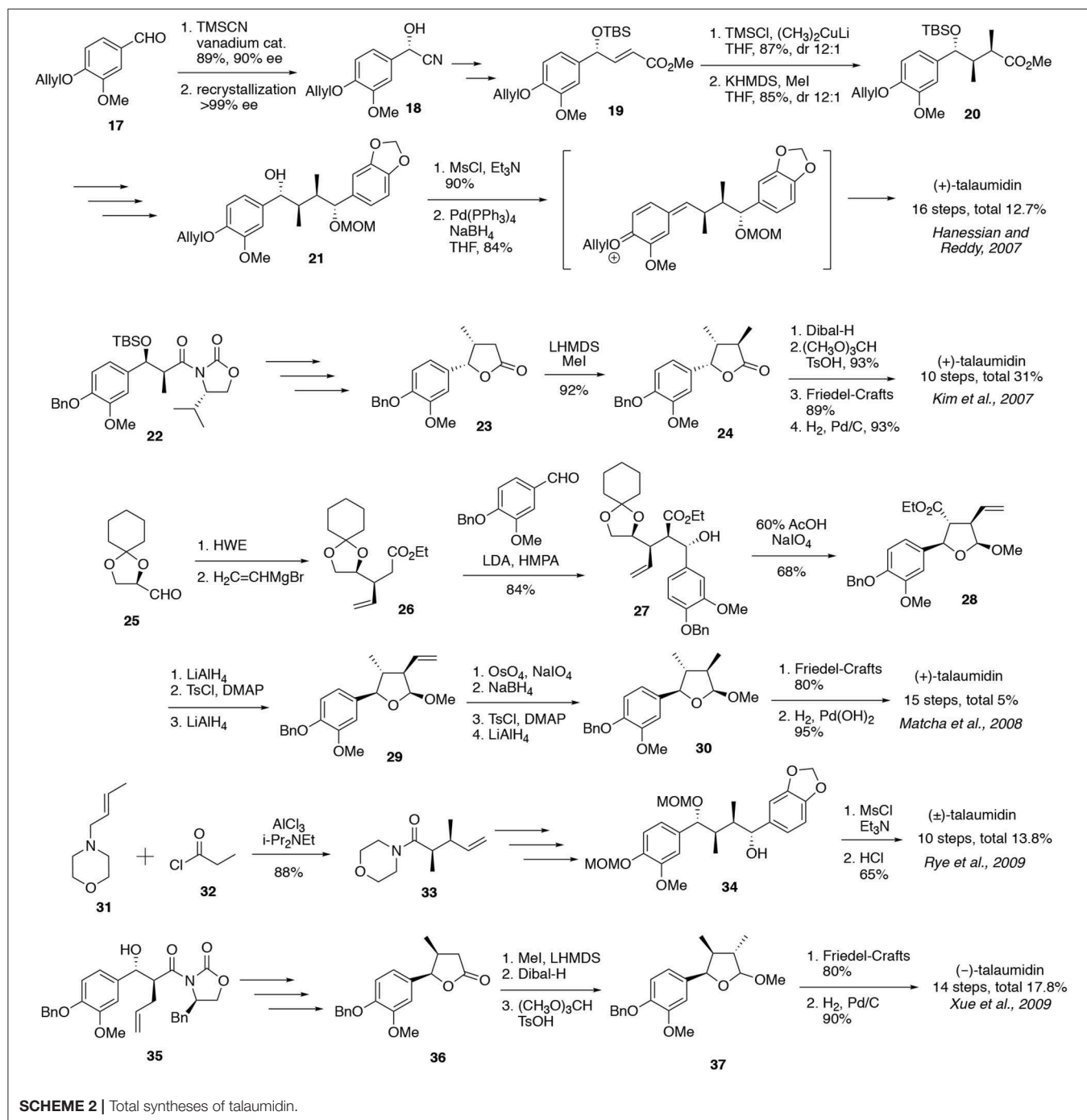
Synthesis of (+)-Talaumidin by Kim et al.

Kim et al. investigated synthetic methodologies for the assembly of tetrahydrofuran lignans and the total synthesis of (+)-talaumidin was accomplished as a part of these studies (Kim et al., 2007). Talaumidin was constructed utilizing the Evans aldol, anti-selective dimethylation, and Friedel–Crafts reactions as key transformations. In addition, they established a synthetic strategy featuring Lewis acid promoted deoxygenation followed by epimerization of a hemiacetal, and accomplished the synthesis of five tetrahydrofuran-type lignans. The efficiency of Kim's synthesis was showed by the short step and high overall yield of 31%.

Synthesis of (+)-Talaumidin by Matcha et al.

In 2008, Matcha et al. synthesized (–)-talaumidin and (–)-virgatusin using the chiral pool approach in 15 steps with 5.0% overall yield. The synthesis of 1 commenced with the chiral starting material (R)-(+)-2,3-di-O-cyclohexylidine glyceraldehyde (25) which was derived from the chirality of D-mannitol (Chattopadhyay, 1996; Banerjee et al., 2005). The key step was a diastereoselective aldol reaction of the enolate derived from 26 with benzaldehyde 8. The aldol 27 was obtained in 84% yield as a major product, accompanied by two diastereomers (dr 13:1.3:1). After several redox processes, a Friedel–Crafts arylation of acetal 30 followed by hydrogenolysis completed the synthesis of (–)-talaumidin. However, the indicated absolute configuration was not consistent with the optical rotation reported in other syntheses (Esumi et al., 2006; Hanessian and Reddy, 2007; Kim et al., 2007; Xue et al., 2009).

Synthesis of (±)-Talaumidin by Rye et al.

In 2009, Rye et al. reported a straightforward synthetic methodology for the preparation of tetra-substituted tetrahydrofuran lignans such as (±)-talaumidin and (±)-fragransin A$_2$. The synthetic pathway began with an acyl-Claisen rearrangement to construct two successive tertiary stereocenters. After the introduction of an aryl group, the intramolecular cyclization of monoprotected 1,4-diol 34 gave the talaumidin skeleton. Removal of the MOM group completed the total synthesis of racemic talaumidin in an overall yield of 13.8%. Its analog, racemic franransin A$_2$, was synthesized in the same manner, in an overall yield of 5.8%. Although it was a racemic synthesis, the economic synthesis of 1 was accomplished from inexpensive starting materials in 10 steps.

Synthesis of (–)-Talaumidin by Xue et al.

Xue et al. reported the total syntheses of (–)-talaumidin and (–)-galbergin. They combined Fukuyama's and Kim's strategies and applied the Evans aldol and Friedel–Crafts reactions to control the stereochemistry of successive four chiral centers. Overall yields of (–)-talaumidin and (–)-galbergin were 17.8 and 16.9%, respectively.

Stereoselective Construction of Tetrahydrofuran-Type Lignan Skeleton

In these syntheses, some common procedures were established in order to construct the four chiralities of talaumidin. Evans aldol reaction has been utilized by three research groups and proven to be an optimal procedure forming successive chiral centers at C2 and C3 of 1. On the other hand, the third chiral center at C4 was constructed by α-substitution of carbonyl group, except for Fukuyama's synthesis. Finally, Friedel–Crafts reaction or intramolecular etherification have been adopted for the control of chirality at C5. The both reactions are found to be appropriate to control the 4,5-trans-configuration. These procedures would be a standard strategy for the synthesis of tetrahydrofuran-type lignans.

The Relationship Between Stereochemistry and Neurite-Outgrowth Activity of Talaumidin (1)
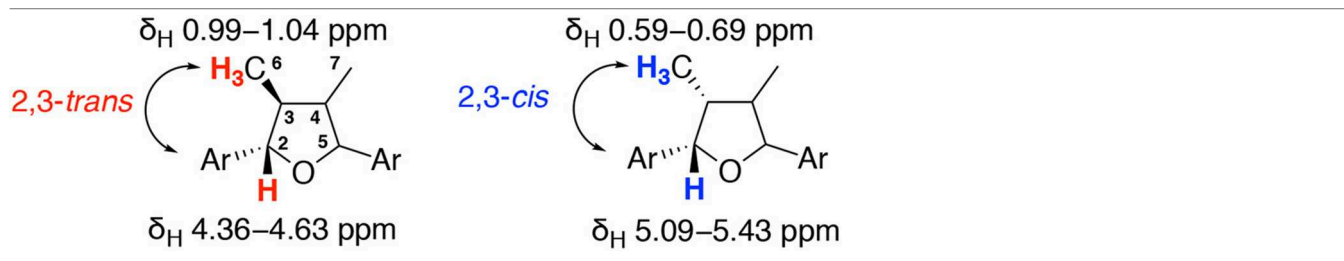
Following our asymmetric total synthesis of (–)-talaumidin, we embarked on structure–activity relationship (SAR) studies with the aim of potential drug discovery based on talaumidin. Initially, the relationship between stereochemistry and the neurotrophic activity of talaumidin was investigated. As 1 possesses four successive asymmetric carbons on the THF structure, seven diastereomers 1a–1g are possible, in addition to the enantiomer of each. The successful control of the four contiguous stereocenters in an asymmetric synthesis of all seven diastereomers would be crucial for the elucidation of the relationship between stereochemistry and neurotrophic activity, and likewise be an important achievement from the viewpoint of organic synthetic chemistry. In 2015, we published the systematic synthesis of talaumidin diastereomers and their evaluation of neurotrophic activity (Scheme 3) (Harada et al., 2015).

Diastereomers 1a–1c having (2S,3S)-configuration were synthesized from 13, which was an intermediate in the synthesis of 1 (Esumi et al., 2006; Fukuyama et al., 2008). After the introduction of the aryl group, the resulting ketone 38 was converted to dihydrofuran 39. The stereoselective hydrogenation of dihydrofuran 39 provided (2S,3S,4S,5R)-1a as a sole stereoisomer. Next, treatment of hemiacetal 40 with BF$_3$·OEt$_2$ followed by reduction with NaBH$_3$CN furnished (2S,3S,4R,5S)-1b. In this reductive sequence, the hydride nucleophile approaches from the opposite face to the adjacent methyl group. On the other hand, the synthesis of (2S,3S,4R,5R)-1c was attained by applying a Mitsunobu-type reaction with 1,4-diol 41 using DEAD and PPh$_3$. Noteworthy, the stereoselective cyclization proceeded with net retention of original configurations at C1 and C4. This surprising stereoselectivity was rationalized by preferential elimination of the PPh$_3$-activated hydroxy group over the normal substitution pathway, giving rise to quinone methide intermediates (Harada et al., 2011b). The steric hindrance between a methyl group and the adjacent aryl group forces the product to adopt the desired conformations, resulting in the construction of (2S,3S,4R,5R)-configuration.

Subsequently, the synthesis of stereoisomers 1d–1g with (2S,3R)-configuration was achieved via common intermediate 44. The (2S,3R)-configuration of 44 was constructed by syn-selective Evans aldol reaction between 8 and 9 in 80% yield with >99% de. According to the same synthetic procedure

SCHEME 3 | Systematic synthesis of seven diastereomers of (−)-talaumidin.
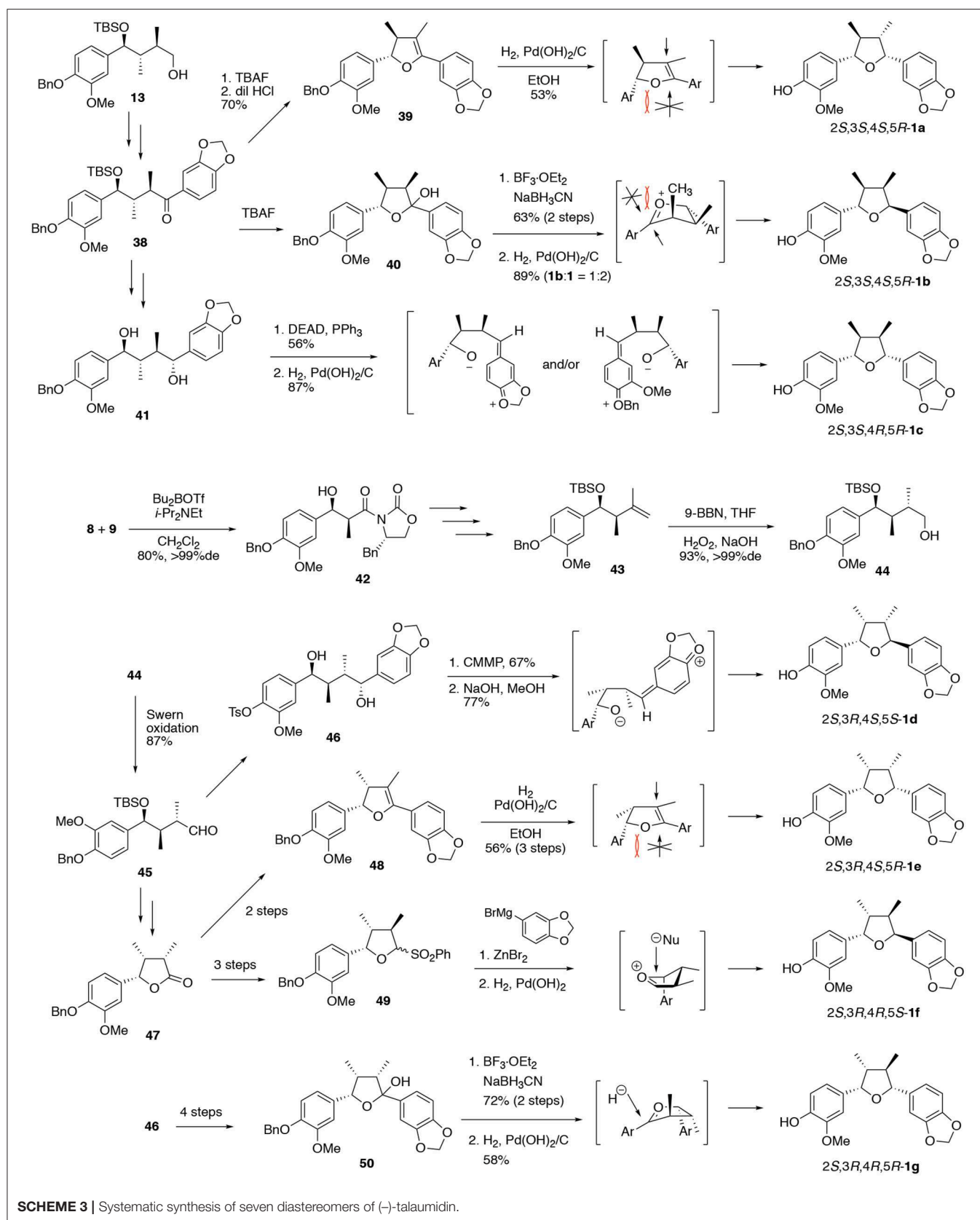
TABLE 1 | Characteristic ^{1}H NMR data (δ_H (J in Hz)) for talaumidin (**1**) and its diastereomers **1a–1g**.

2,3-*trans*: δ_H 0.99–1.04 ppm (H$_3$C), δ_H 4.36–4.63 ppm (H); 2,3-*cis*: δ_H 0.59–0.69 ppm (H$_3$C), δ_H 5.09–5.43 ppm (H)

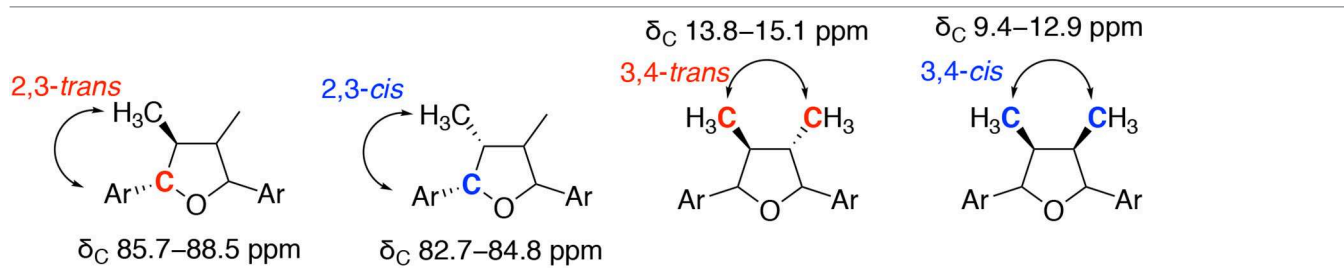| Positions	1	1a	1b	1c	1d	1e	1f	1g
6 and 7	1.02 (5.8)	0.67 (7.0)	0.62 (7.3)	1.02 (6.6)	0.61 (7.1)	0.59 (6.1)	0.68 (6.5)	0.65 (6.8)
	1.02 (5.8)	1.04 (6.6)	0.99 (6.2)	1.02 (6.6)	1.00 (6.6)	0.61 (6.1)	0.69 (6.5)	1.04 (6.6)
3 and 4	1.76 (m)	1.75 (m)	2.43 (m)	2.28 (m)	2.42 (m)	2.65 (m)	2.25 (m)	1.74 (m)
	1.76 (m)	2.23 (m)	2.43 (m)	2.28 (m)	2.42 (m)	2.65 (m)	2.25 (m)	2.21 (m)
2 and 5	4.61 (9.1)	4.36 (9.3)	4.63 (9.3)	4.45 (6.4)	4.62 (9.3)	5.09 (6.4)	5.40 (6.0)	4.36 (9.3)
	4.61 (9.1)	5.09 (8.8)	5.43 (4.0)	4.46 (6.7)	5.43 (4.4)	5.09 (6.4)	5.40 (6.0)	5.10 (8.5)

TABLE 2 | Characteristic ^{13}C NMR data (δ_C) for talaumidin (**1**) and its diastereomers **1a–1g**.

2,3-*trans*: δ_C 85.7–88.5 ppm; 2,3-*cis*: δ_C 82.7–84.8 ppm; 3,4-*trans*: δ_C 13.8–15.1 ppm; 3,4-*cis*: δ_C 9.4–12.9 ppm

Positions	1	1a	1b	1c	1d	1e	1f	1g
6 and 7	13.8	14.9	9.6	12.9	9.4	11.8	14.6	15.0
	13.8	15.1	11.9	12.9	11.8	11.8	14.7	15.1
3 and 4	50.9	46.0	43.5	44.5	43.5	41.5	43.8	45.9
	51.2	48.1	47.5	44.5	47.7	41.5	43.9	48.3
2 and 5	88.2	83.0	84.8	87.4	84.8	82.7	83.7	83.1
	88.5	87.5	85.8	87.5	85.7	82.8	83.7	87.4

for (–)-**1**, the key intermediate **44** was derived from **43** by hydroboration with 9-BBN. With **44** in hand, the synthesis of (2*S*,3*R*,4*S*,5*S*)-**1d** was firstly attained by a cyclization of diol **13** under conditions of Mitsunobu-type reaction (Harada et al., 2011a). In this case, the benzyl group was converted to a tosylate prior to cyclization, in order to enhance the selectivity eliminating the hydroxy group at C4. Next, hydrogenation of dihydrofuran **11b** gave all-*cis*-substituted (2*S*,3*R*,4*S*,5*R*)-**1e** with high diastereoselectivity. In addition, the C4 position of lactone **21** was epimerized, and then led to **23** by reduction of the lactone, followed by sulfonation. In accordance with Ley's method (Brown et al., 1989; Kim et al., 2007), a Grignard reaction with zinc bromide introduces the methylenedioxy benzene moiety from the β-face to avoid steric hindrance between the aryl groups (Harada et al., 2011a). Then, (2*S*,3*R*,4*R*,5*S*)-**1f** was synthesized

by removal of the benzyl group. Finally (2*S*,3*R*,4*R*,5*R*)-**1g** was synthesized by the reduction of **27** with NaBH$_3$CN/BF$_3$·OEt$_2$ conditions. Regarding this stereochemistry, the epimerization at C3 proceeded spontaneously in order to decrease the steric hindrance from the methyl group.

These synthetic studies provided useful information for the analysis of stereochemistries of tetrahydrofuran lignans. The characteristic ^{1}H and ^{13}C NMR data of **1** and **1a–1g** are summarized in **Tables 1**, **2**. Although coupling constants are indecisive, chemical shifts play a role in identifying relative stereochemistries on the THF ring. In the case of 2,3-*trans*- and/or 4,5-*trans*-configurations, the signal of methyl group appears at 0.99–1.04 ppm. In contrast, 2,3-*cis*- and/or 4,5-*cis*-oriented methyl groups are shielded by the adjacent aromatic ring to result in upfield shift of the signal at 0.59–0.69 ppm. Moreover,

the relative 2,3-stereochemistry is also able to be confirmed by ^{13}C NMR. The chemical shifts of benzylic carbon are at 85.7–88.5 ppm for 2,3-*trans* and at 82.7–84.8 ppm for 2,3-*cis*, respectively. On the other hand, the relative configuration of 3,4-dimethyl groups can be distinguished by the chemical shifts of ^{13}C NMR. The signal of 3,4-*trans*-dimethyl groups appears at 13.8–15.1 ppm, whereas 3,4-*cis*-dimethyl groups have lower chemical shifts around 9.4–12.9 ppm. These results of NMR experiments are consistent with those of natural products **2–7** and useful for the determination of relative stereochemistries of tetrahydrofuran type lignans.

Once the synthesis of all diastereomers was complete, their neurotrophic activity was compared with that of natural talaumidin (Harada et al., 2015). Talaumidin (**1**) and isomers **1a–1g** were assessed their neurite-outgrowth promoting activity together with enantiomer of (−)-talaumidin. Consequently, the enantiomer of (−)-talaumidin exhibited activity similar to the natural product, and all synthesized compounds induced neurite-outgrowth promotion. Particularly, **1e** having all-*cis*-configuration was found to show more potent activity than naturally occurring talaumidin (**Figure 5**). Furthermore, their neurite-outgrowth promoting activity of stereoisomers in primary cultured rat cortical neurons was evaluated at 0.01 μM. The results indicated that all-*cis*-substituted **1e** also exhibited the most significant neurite-outgrowth promotion among all of the stereoisomers (**Figure 5**).

Synthesis of Racemic Compound 56a and Relationship Between Substituents on the Benzene Ring and Neurotrophic Activity

(−)-Talaumidin and the stereoisomer (−)-**1e** were found to possess potent neurotrophic activity, however, preparative procedures of optically active (−)-talaumidin and (−)-**1e** required long synthetic steps and high cost. Therefore, drug discovery based on talaumidin necessitated a simplification of the structure and synthetic methodology for talaumidin derivatives. Then, we focused on the efficient synthetic methodology of talaumidin derivatives and exploration of new compounds that could be supplied on a large scale (Harada et al., 2018). In section The Relationship Between Stereochemistry and Neurite-Outgrowth Activity of Talaumidin (1), it was revealed that there are few difference in neurotrophic activity between both enantiomers of **1**. This result suggested that a racemic mixture of **1e** could have activity similar to optically active **1e**. Accordingly, racemic **1e** (**56a**) was decided on as the next target compound. The developed step-economic synthesis of *rac*-**1e** (**56a**) is shown in **Scheme 4**. The synthesis began with a Grignard reaction onto the commercially available benzaldehyde **8**, followed by a Dess–Martin oxidation. After bromination of **51**, the obtained bromide **52** was coupled with **53**, giving rise to a diketone **54** in 86% yield. Subsequently, Paal–Knorr furan synthesis of **54** under acidic conditions provided a furan compound **55** in good yield. At last, hydrogenation of the furan ring completed the synthesis of **56a** bearing all-*cis*-configuration. Consequently, the synthesis of racemic **1e** (**56a**) was accomplished in 6 steps with an overall

SCHEME 4 | Step-economic synthesis of talaumidin derivatives.
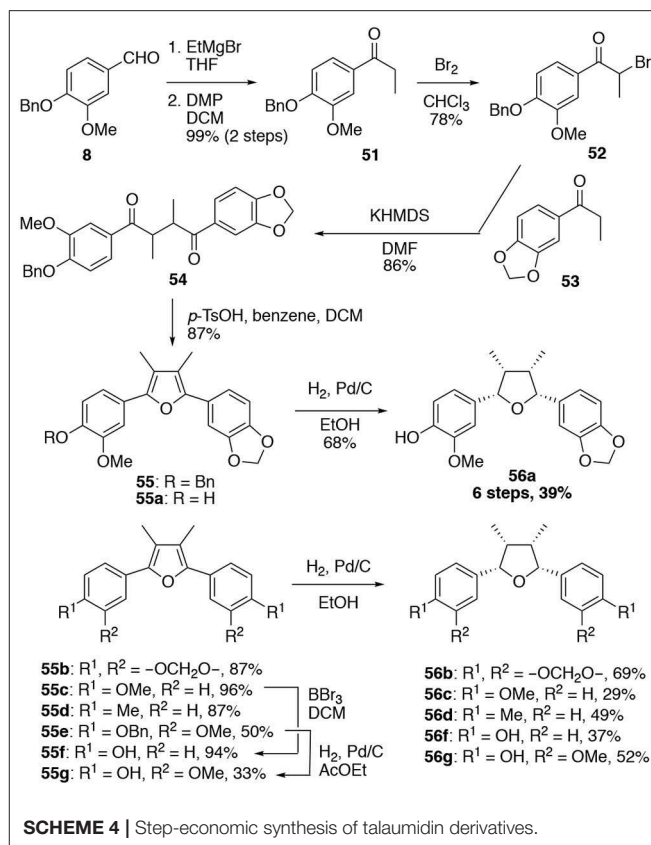
yield of 39%. In addition, five novel talaumidin derivatives were prepared by applying this synthetic methodology.

With six derivatives **56–ad**, **56f**, and **56g** and their precursor furan compounds **55–ad**, **55f**, and **55g** in hand, the neurite-outgrowth activity was evaluated in NGF-differentiated PC12 cells at 30 μM. As results, tetrahydrofuran compounds tended to promote neurite-outgrowth to a higher degree than furan-type compounds (**Figure 6**). Among the tetrahydrofuran compounds, **56b** having two methylenedioxyphenyl groups was found to exhibit the most significant activity. In addition, the step-economic synthesis of talaumidin derivatives allowed adequate quantities of samples to be prepared for *in vivo* experiments. Thus, we evaluated the optic nerve regenerating activity of talaumidin derivatives as an *in vivo* experiment. Remarkably, the all-*cis*-derivatives **56a** and **56b** showed high regenerative activity toward the injured optic nerve.

The Role of Dimethyl and Diaryl Groups on THF Ring of Talaumidin Derivatives

Furthermore, the role of the phenyl and methyl groups on the THF ring of **56b** was examined as part of the SAR study. In order to determine which moieties were necessary for neurotrophic properties, **57** lacking one benzene ring and **58** lacking two methyl groups were prepared, and their neurotrophic activity was assessed in NGF-differentiated PC12 cells (**Figure 7**). It was found that monophenyl analog **57** exhibited no activity
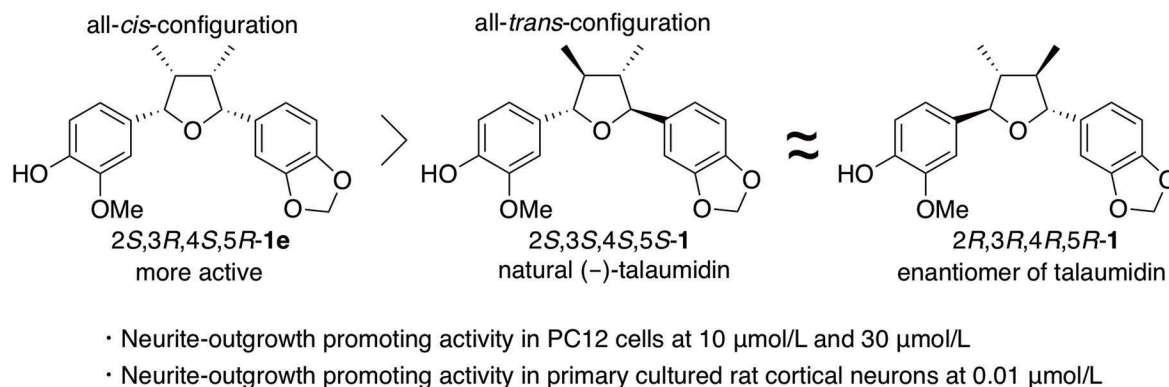
FIGURE 5 | Relationship between stereochemistries and neurotrophic activity of talaumidin.
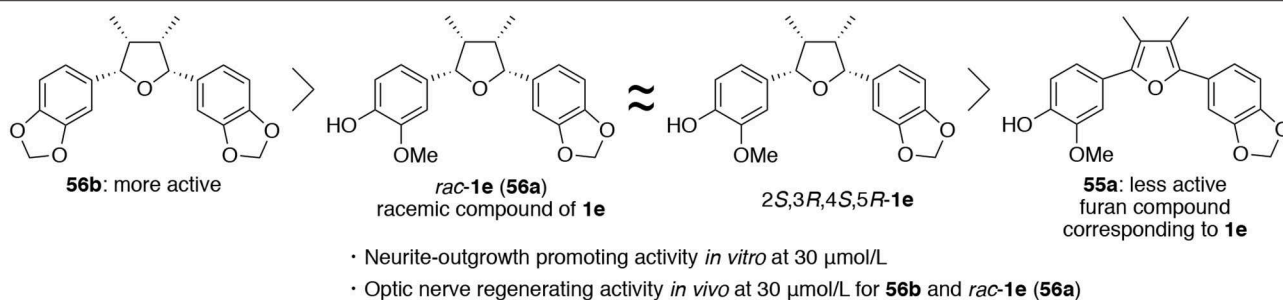
FIGURE 6 | Relationship between substituents on the benzene ring and neurotrophic activity of talaumidin derivatives.
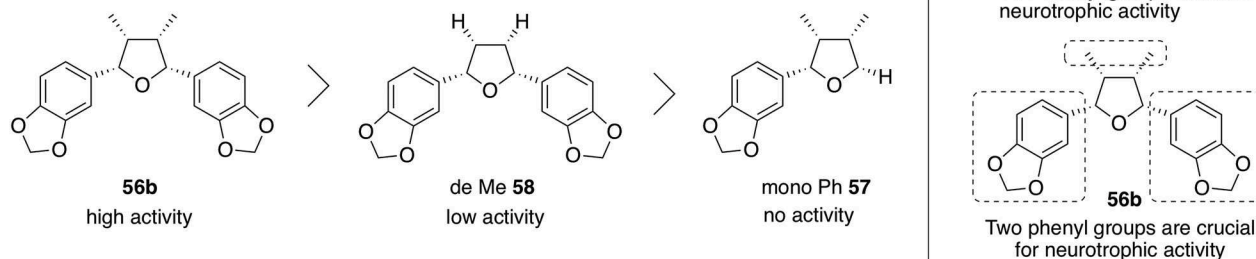
FIGURE 7 | Investigation of SAR of talaumidin derivative **56b**.

at all, whereas **58** had lower activity than **56b**. These results indicate that the two benzene rings of the talaumidin derivatives are essential structures for neurotrophic activity while the two methyl groups at C3 and C4 positions can increase the neurite-outgrowth activity.

Mechanistic Study on Neurite-Outgrowth Activity of Staurosporine-Differentiated RGC-5 Cells

In 2018, Koriyama et al. examined the neurite-outgrowth promotion of talaumidin in the neuroretinal cell line, RGC-5

(Koriyama et al., 2018). They assessed the neurite outgrowth effect and elucidated a mechanism of its neurotrophic action. At concentrations ranging from 1 to 10 μM, talaumidin promoted neurite outgrowth dose-dependently in differentiated RGC-5 cells. Its neurite-outgrowth promoting activity was not altered by PD98059, an extracellular signal-regulated kinase inhibitor. On the other hand, LY29002, a PI3K inhibitor, decreased the talaumidin-mediated neurite outgrowth. These results indicate that the PI3K-Akt signaling is involved in downstream pathway in talaumidin-induced neurite-outgrowth activity of RGC-5 cells.

CONCLUSION

In conclusion, the neurotrophic and protective activities of talaumidin have been found in several cellular models. Talaumidin can not only promote neurite outgrowth in NGF-differentiated PC12 cells but also enhance cell survival after NGF withdrawal in differentiated PC12 cells. These are coincident with the fact that talaumidin has neurotrophic effects on primary cultured rat cortical neurons. In addition, the neurotrophic activities of talaumidin are extended to neuroprotection, which are deleterious factors in Alzheimer's disease. Due to its interesting structure and neurotrophic activity, talaumidin have attracted considerable attentions from synthetic chemists. We achieved the first enantioselective synthesis of (−)-(2S,3S,4S,5S)-talaumidin using a Evans aldol reaction, hydroboration, and FriedelCrafts reaction. In addition, the systematic synthesis of all of the stereoisomers of (−)-talaumidin was accomplished, and their neurotrophic activity was evaluated. As results, the all-*cis*-substituted isomer **1e** showed more potent neurite-outgrowth promotion in NGF-differentiated PC12 cells than natural product talaumidin. Furthermore, we established a step-economic synthesis that could prepare a compound library based on talaumidin, and 14 derivatives were synthesized. As a result, compound **56b** having two methylenedioxyphenyl groups was found to show the most potent neurite-outgrowth promoting activity *in vitro*. Moreover, it was found that derivatives **56a** and **56b** could induce the regeneration of mouse optic nerve *in vivo*. These consequences indicate that talaumidin derivatives can be an innovative agent for neurodegenerative diseases such as glaucoma, depression, and Alzheimer's disease. Further mechanistic and pharmacological investigations of neurotrophic activities of talaumidin derivatives are currently ongoing.

AUTHOR CONTRIBUTIONS

ACKNOWLEDGMENTS

REFERENCES

Abrantes, M., Mil-Homens, T., Duarte, N., Lopes, D., Cravo, P., Madureira, M., et al. (2008). Antiplasmodial activity of lignans and extracts from *Pycnanthus angolensis. Planta Med.* 74, 1408–1412. doi: 10.1055/s-2008-1081317

Banerjee, S., Ghosh, S., Sinha, S., and Ghosh, S. (2005). Convenient route to both enantiomers of a highly functionalized trans-disubstituted cyclopentene. S-synthesis of the carbocyclic core of the nucleoside BCA. *J. Org. Chem.* 70, 4199–4202. doi: 10.1021/jo0502504

Barata, L. E. S., Baker, P. M., Gottlieb, O. R., and Rùveda, E. A. (1978). Neolignans of virola surinamensis. *Phytochemistry* 17, 783–786. doi: 10.1016/S0031-9422(00)94227-4

Belokon, Y. N., North, M., and Parsons, T. (2000). Vanadium-catalyzed asymmetric cyanohydrin synthesis. *Org. Lett.* 2, 1617–1619. doi: 10.1021/ol005893e

Brown, D. S., Bruno, M., Davenport, R. J., and Ley, S. V. (1989). Substitution reactions of 2-benzenesulphonyl cyclic ethers with carbon nucleophiles. *Tetrahedron* 45, 4293–4308. doi: 10.1016/S0040-4020(01)81323-5

Chattopadhyay, A. (1996). (R)-2,3-O-Cyclohexylideneglyceraldehyde, a versatile intermediate for asymmetric synthesis of homoallyl and homopropargyl alcohols in aqueous medium. *J. Org. Chem.* 61, 6104–6107. doi: 10.1021/jo9604696

Ding, J.-Y., Yuan, C.-M., Cao, M.-M., Liu, W.-W., Yu, C., Zhang, H.-Y., et al. (2014). Antimicrobial constituents of the mature carpels of *Manglietiastrum sinicum. J. Nat. Prod.* 77, 1800–1805. doi: 10.1021/np500187c

Dotti, C. G., Banker, G. A., and Binder, L. I. (1987). The expression and distribution of the microtubule-associated proteins tau and microtubule-associated protein 2 in hippocampal neurons in the rat *in situ* and in cell culture. *Neuroscience* 23, 121–130. doi: 10.1016/0306-4522(87)90276-4

Esumi, T., Hojyo, D., Zhai, H., and Fukuyama, Y. (2006). First enantioselective synthesis of (-)-talaumidin, a neurotrophic diaryltetrahydrofuran-type lignan. *Tetrahedron Lett.* 47, 3979–3983. doi: 10.1016/j.tetlet.2006.04.006

Evans, D. A., Tedrow, J. S., Shaw, J. T., and Downey, C. W. (2002). Diastereoselective magnesium halide-catalyzed anti-aldol reactions of chiral N-acyloxazolidinones. *J. Am. Chem. Soc.* 124, 392–393. doi: 10.1021/ja0119548

Fukuyama, Y., Harada, K., Esumi, T., Hojyo, D., Kujime, Y., Kubo, N., et al. (2008). Synthesis of (-)-talaumidin, a neurotrophic 2,5-biaryl-3,4-dimethyltetrahydrofuran lignan, and its stereoisomers. *Heterocycles* 76, 551–567. doi: 10.3987/COM-08-S(N)42

Fukuyama, Y., Nakade, K., Minoshima, Y., Yokoyama, R., Zhai, H., and Mitsumoto, Y. (2002). Neurotrophic activity of honokiol on the cultures of fetal rat cortical neurons. *Bioorg. Med. Chem. Lett.* 12, 1163–1166. doi: 10.1016/S0960-894X(02)00112-9

Hanessian, S., and Reddy, G. J. (2007). Total synthesis and stereochemical confirmation of 2,5-diaryl-3,4-dimethyl-tetrahydrofuran lignans: (+)-fragransin A2, (+)-galbelgin, (+)-talaumidin, (-)-saucernetin and (-)-verrucosin. *Synletter* 2007, 475–479. doi: 10.1055/s-2007-968019

Harada, K., Horiuchi, H., Tanabe, K., Carter, R. G., Esumi, T., Kubo, M., et al. (2011a). Asymmetric synthesis of (-)-chicanine using a highly regioselective intramolecular Mitsunobu reaction and revision of its absolute configuration. *Tetrahedron Lett.* 52, 3005–3008. doi: 10.1016/j.tetlet.2011.03.154

Harada, K., Kubo, M., Horiuchi, H., Ishii, A., Esumi, T., Hioki, H., et al. (2015). Systematic asymmetric synthesis of all diastereomers of (-)-talaumidin and their neurotrophic activity. *J. Org. Chem.* 80, 7076–7088. doi: 10.1021/acs.joc.5b00945

Harada, K., Kubo, N., Tanabe, K., Kubo, M., Esumi, T., Hioki, H., et al. (2011b). Asymmetric synthesis of (+)-machilin F by unusual stereoselective mitsunobu reaction. *Heterocycles* 82, 1127–1132. doi: 10.3987/COM-10-S(E)88

Harada, K., Zaha, K., Bando, R., Irimaziri, R., Kubo, M., Koriyama, Y., et al. (2018). Structure-activity relationships of talaumidin derivatives: their neurite-outgrowth promotion *in vitro* and optic nerve regeneration *in vivo*. *Eur. J. Med. Chem.* 148, 86–94. doi: 10.1016/j.ejmech.2018.02.014

Houk, K. N., Rondan, N. G., Wu, Y. D., Metz, J. T., and Paddon-Row, M. N. (1984). Theoretical studies of stereoselective hydroborations. *Tetrahedron* 40, 2257–2274. doi: 10.1016/0040-4020(84)80009-5

Huang, J.-M., Yokoyama, R., Yang, C.-S., and Fukuyama, Y. (2001). Structure and neurotrophic activity of *seco*-prezizaane-type sesquiterpenes from *Illicium merrillianum*. *J. Nat. Prod.* 64, 428–431. doi: 10.1021/np0005715

Huang, J. M., Yokoyama, R., Yang, C. S., and Fukuyama, Y. (2000). Merrilactone A, a novel neurotrophic sesquiterpene dilactone from *Illicium merrillianum*. *Tetrahedron Lett.* 41, 6111–6114. doi: 10.1016/S0040-4039(00)01023-6

Kaufmann, W. E., Taylor, C. V., and Lishaa, N. A. (1997). Immunoblotting patterns of cytoskeletal dendritic protein expression in human neocortex. *Mol. Chem. Neuropathol.* 31, 235–244. doi: 10.1007/BF02815127

Kiem, P. V., Tri, M. D., Tuong, L. V. D., Tung, N. H., Hanh, N. N., Quang, T. H., et al. (2008). Chemical constituents from the leaves of *Manglietia phuthoensis* and their effects on osteoblastic MC3T3-E1 cells. *Chem. Pharm. Bull.* 56, 1270–1275. doi: 10.1248/cpb.56.1270

Kim, H., Wooten, C. M., Park, Y., and Hong, J. (2007). Stereoselective synthesis of tetrahydrofuran lignans via BF$_3$·OEt$_2$-promoted reductive deoxygenation/epimerization of cyclic hemiketal: synthesis of (-)-odoratisol C, (-)-futokadsurin A, (-)-veraguensin, (+)-fragransin A2, (+)-galbelgin, and (+)-talaumidin. *Org. Lett.* 9, 3965–3968. doi: 10.1021/ol7016388

Kim, K. H., Kim, H. K., Choi, S. U., Moon, E., Kim, S. Y., and Lee, K. R. (2011). Bioactive lignans from the rhizomes of *Acorus gramineus*. *J. Nat. Prod.* 74, 2187–2192. doi: 10.1021/np200541m

Kim, K. H., Moon, E., Ha, S. K., Suh, W. S., Kim, H. K., Kim, S. Y., et al. (2014). Bioactive lignan constituents from the twigs of *Lindera glauca*. *Chem. Pharm. Bull.* 62, 1136–1140. doi: 10.1248/cpb.c15-00381

Koriyama, Y., Furukawa, A., Sugitani, K., Kubo, M., Harada, K., and Fukuyama, Y. (2018). Talaumidin promotes neurite outgrowth of staurosporine-differentiated RGC-5 cells through PI3K/Akt-dependent pathways. *Adv. Exp. Med. Biol.* 1074, 649–653. doi: 10.1007/978-3-319-75402-4_79

Kubo, M., Gima, M., Baba, K., Nakai, M., Harada, K., Suenaga, M., et al. (2015). Novel neurotrophic phenylbutenoids from Indonesian ginger bangle, *Zingiber Purpureum*. *Bioorg. Med. Chem. Lett.* 25, 1586–1591. doi: 10.1016/j.bmcl.2015.02.005

Kubo, M., Ishii, R., Ishino, Y., Harada, K., Matsui, N., Akagi, M., et al. (2013). Evaluation of constituents of *Piper Retrofractum* fruits on neurotrophic activity. *J. Nat. Prod.* 76, 769–773. doi: 10.1021/np300911b

Kubo, M., Kishimoto, Y., Harada, K., Hioki, H., and Fukuyama, Y. (2010). NGF-potentiating vibsane-type diterpenoids from *Viburnum sieboldii*. *Bioorg. Med. Chem. Lett.* 20, 2566–2571. doi: 10.1016/j.bmcl.2010.02.085

Kubo, M., Kobayashi, K., Huang, J.-M., Harada, K., and Fukuyama, Y. (2012). The first examples of *seco*-prezizaane-type norsesquiterpenoids with neurotrophic activity from *Illicium jiadifengpi*. *Tetrahedron Lett.* 53, 1231–1235. doi: 10.1016/j.tetlet.2011.12.107

Kubo, M., Okada, C., Huang, J.-M., Harada, K., Hioki, H., and Fukuyama, Y. (2009). Novel pentacyclic *seco*-prezizaane-type sesquiterpenoids with neurotrophic properties from *Illicium Jiadifengpi*. *Org. Lett.* 11, 5190–5193. doi: 10.1021/ol9021029

Kuroyanagi, M., Ikeda, R., Gao, H. Y., Muto, N., Otaki, K., Sano, T., et al. (2008). Neurite outgrowth-promoting active constituents of the Japanese cypress (*Chamaecyparis obtusa*). *Chem. Pharm. Bull.* 56, 60–63. doi: 10.1248/cpb.56.60

Le Quesne, P. W., Larrahondo, J. F., and Raffauf, R. F. (1980). Antitumor plants. X. constituents of *Nectandra rigida*. *J. Nat. Prod.* 43, 353–359. doi: 10.1021/np50009a006

Lin, S., Chen, T., Liu, X. H., Shen, Y. H., Li, H. L., Liu, R. H., et al. (2010). Iridoids and lignans from *Valeriana jatamansi*. *J. Nat. Prod.* 73, 632–638. doi: 10.1021/np900795

Ma, J., Dey, M., Yang, H., Poulev, A., Dorn, R., Lipsky, P. E., et al. (2007). Anti-inflammatory and immunosuppressive compounds from *Tripterygium wilfordii*. *Phytochemistry* 68, 1172–1178. doi: 10.1016/j.phytochem.2007.02.021

Massa, S. M., Xie, Y., and Longo, F. M. (2002). Alzheimer's therapeutics. *J. Mol. Neurosci.* 19, 107–111. doi: 10.1007/s12031-002-0019-1

Matcha, K., and Ghosh, S. (2008). A stereocontrolled approach for the synthesis of 2,5-diaryl-3,4-disubstituted furano lignans through a highly diastereoselective aldol condensation of an ester enolate with an α-chiral center: total syntheses of (-)-talaumidin and (-)-virgatusin. *Tetrahedron Lett.* 49, 3433–3436. doi: 10.1016/j.tetlet.2008.03.105

Matsui, N., Kido, Y., Okada, H., Kubo, M., Nakai, M., Fukuishi, N., et al. (2012). Phenylbutenoid dimers isolated from *Zingiber purpureum* exert neurotrophic effects on cultured neurons and enhance hippocampal neurogenesis in olfactory bulbectomized mice. *Neurosci. Lett.* 513, 72–77. doi: 10.1016/j.neulet.2012.02.010

Mei, R.-Q., Wang, Y.-H., Du, G.-H., Liu, G. M., Zhang, L., and Cheng, Y.-X. (2009). Antioxidant lignans from the fruits of *Broussonetia papyrifera*. *J. Nat. Prod.* 72, 621–625. doi: 10.1021/np800488p

Pardridge, W. M. (2002). Neurotrophins, neuroprotection and the blood-brain barrier. *Curr. Opin. Invest. Drugs* 3, 1753–1757.

Piao, X.-L., Jang, M. H., Cui, J., and Piao, X. (2008). Lignans fromt the fruits of *Forsyhia suspensa*. *Bioorg. Med. Chem. Lett.* 18, 1980–1984. doi: 10.1016/j.bmcl.2008.01.115

Rye, C. E., and Barker, D. (2009). An acyl-Claisen approach to tetrasubstituted tetrahydrofuran lignans: synthesis of fragransin A2, talaumidin, and lignan analogues. *Synlett*. 2009:3315–3319. doi: 10.1055/s-0029-1218363

Sasaki, T., Li, W., Zaike, S., Asada, Y., Li, Q., Ma, F., et al. (2013). Antioxidant lignoids from leaves of *Ribes nigrum*. *Phytochemistry* 95, 333–340. doi: 10.1016/j.phytochem.2013.07.022

Thoenen, H., and Sendtner, M. (2002). Neurotrophins: from enthusiastic expectations through sobering experiences to rational therapeutic approaches. *Nat. Neurosci.* 5, 1046–1050. doi: 10.1038/nn938

Urzúa, A., Freyer, A. J., and Shamma, M. (1987). 2,5-diaryl-3,4-dimethyltetrahydrofuranoid lignans. *Phytochemistry* 26, 1509–1511. doi: 10.1016/S0031-9422(00)81846-4

Vaudry, D., Stork, P. J. S., Lazarovici, P., and Eiden, L. E. (2002). Signaling pathways for PC12 cell differentiation: making the right connections. *Science* 296:1648. doi: 10.1126/science.1071552

Vieira, L. M., Kijioa, A., Silva, A. M. S., Mondranondra, I.-O., and Herz, W. (1998). 2,5-Diaryl-3,4-dimethyltetrahydrofuran lignans from *Talauma hodgsonii*. *Phytochemistry* 48, 1079–1081. doi: 10.1016/S0031-9422(97)01029-7

Vučković, I., Trajković, V., Macura, S., Tešević, V., Janaćković, P., and Milosavljević, S. (2007). A novel cytotoxic lignan from *Seseli Annuum* L. *Phytochem. Res.* 21, 790–792. doi: 10.1002/ptr.2152

Warashima, T., Shikata, K., Miyase, T., Fujii, S., and Noro, T. (2008). New cardenolide and acylated lignan glycosides from the aerial parts of *Asclepias Curassavica*. *Chem. Pharm. Bull.* 56, 1159–1163. doi: 10.1248/cpb.56.1159

Wu, J.-I., Li, N., Hasegawa, T., Sakai, J.-I., Kakuta, S., Tang, W., et al. (2005). Bioactive tetrahydrofuran lignans from *Peperomia Dindygulensis*. *J. Nat. Prod.* 68, 1656–1660. doi: 10.1021/np050283e

Xie, Y., and Longo, F. M. (2000). Neurotrophin small-molecule mimetics. *Prog. Brain Res.* 128, 333–347. doi: 10.1016/s0079-6123(00)28030-8

Xue, P., Wang, L.-P., Jiao, X.-Z., Jiang, Y.-J., Xiao, Q., Luo, Z.-G., et al. (2009). Total synthesis of (-)-talaumidin and (-)-galbelgin. *J. Asian Nat. Prod. Res.* 11, 281–287. doi: 10.1080/10286020802675191

Yokoyama, R., Huang, J.-M., Yang, C.-S., and Fukuyama, Y. (2002). New seco-prezizaane-type sesquiterpenes, jiadifenin with neurotrophic activity and 1,2-dehydroneomajucin from *Illicium Jiadifengpi*. *J. Nat. Prod.* 65, 527–531. doi: 10.1021/np010571k

Zhai, H., Inoue, T., Moriyama, M., Esumi, T., Mitsumoto, Y., and Fukuyama, Y. (2005). Neuroprotective effects of 2,5-diaryl-3,4-dimethyltetrahydrofuran neolignans. *Biol. Pharm. Bull.* 28, 289–293. doi: 10.1248/bpb. 28.289

Zhai, H., Nakatsukasa, M., Mitsumoto, Y., and Fukuyama, Y. (2004). Neurotrophic effects of talaumidin, a neolignan from *Aristolochia Arcuata*, in primary cultured rat cortical neurons. *Planta Med.* 70, 598–602. doi: 10.1055/s-2004-827179

Zhang, G. -L., Li, N., Wang, Y.-H., Zheng, Y.-T., Zhang, Z., and Wang, M.-W. (2007). Bioactive lignans from *Peperomia Heyneana*. *J. Nat. Prod.* 70, 662–664. doi: 10.1021/np0605236

frontiers
in Chemistry

Check for updates

Triterpenoids From *Alisma* Species: Phytochemistry, Structure Modification, and Bioactivities

Pengli Wang†, Tongxin Song†, Rui Shi, Mingshuai He, Rongrong Wang, Jialin Lv and Miaomiao Jiang*

Tianjin Key Laboratory of TCM Chemistry and Analysis, Institute of Traditional Chinese Medicine, Tianjin University of Traditional Chinese Medicine, Tianjin, China

Plants from *Alisma* species belong to the genus of *Alisma* Linn. in *Alismataceae* family. The tubers of *A. orientale* (Sam.) Juzep, also known as *Ze Xie* in Chinese and *Takusha* in Japanese, have been used in traditional medicine for a long history. Triterpenoids are the main secondary metabolites isolated from *Alisma* species, and reported with various bioactive properties, including anticancer, lipid-regulating, anti-inflammatory, antibacterial, antiviral and diuretic activities. In this brief review, we aimed to summarize the phytochemical and pharmacological characteristics of triterpenoids found in *Alisma*, and discuss their structure modification to enhance cytotoxicity as well.

Keywords: triterpenoids, *Alisma*, structure, anticancer, lipid-regulation

INTRODUCTION

Plants from the genus of *Alisma* Linn. (*Alismataceae*) are widely distributed in temperate regions and subtropics of the northern hemisphere, belonging to 11 species. Six species were found in China and Asia, including *A. canaliculatum*, *A. gramineum*, *A. nanum*, *A. orientale*, *A. plantago-aquatica* and *A. lanceolatum* (Flora of China Committee, 1992). The tubers of *A. orientale*, known as *Ze Xie* in Chinese or *Takusha* in Japanese, have been used as diuretic and detumescent medications for a long history (Chinese Pharmacopoeia Commission, 2015). It is also used to treat obesity, diabetes and hyperlipidemia nowadays.

Phytochemical studies have revealed that triterpenoids are dominant components in tubers of *Alisma* plants. A total of 118 triterpenoids have been isolated and identified from *Alisma* species so far. Most of them contain protostane tetracyclic aglycones, whereas glycosides are rarely found in other plants. These triterpenoids have been considered as chemotaxonomic markers of the genus (Zhao et al., 2007). A small amount of other kinds of compounds have also been isolated from A. orientale, including diterpenoids, sesquiterpenoids, polysaccharides, phytosterols, amino acids, flavonoids and fatty acids (Zhang et al., 2017). The presence of triterpenoids attributes to the bioactivities of A. orientales (Tian et al., 2014; Shu et al., 2016), such as alisol A 24-acatate (**2**), and alisol B 23-acetate (**47**) (Choi et al., 2019).

Alisols have shown a series of biological activities, such as anticancer (Law et al., 2010), lipid-regulating (Cang et al., 2017), anti-inflammatory (Kim et al., 2016), antibacterial (Jin et al., 2012), antiviral (Jiang et al., 2006), and diuretic activities (Zhang et al., 2017). Since alisol B 23-acetate (**47**) exhibits a significant anti-tumor activity, structure-based modification on alisol B 23-acetate (**47**) gives a profound change of activity.

This paper aims to systematically review triterpenoids from *Alisma* species, involving their phytochemical characteristics, biosynthesis, bioactivities and structure modification.

TRITERPENOIDS

Starting from 1968, triterpenoids have been isolated from *Alisma* genus successively (Murata et al., 1968). All these compounds contain protostane tetracyclic skeleton with the structural characteristics of *trans*-fusions for A/B, B/C and C/D rings, α-methyl submitted at C-8, β-methyl at C-10, β-methyl at C-14 and side chain at C-17. At present there are 101 protostane triterpenoids, 12 nor-protostanes, and 5 seco-protostanes reported from *Alisma*. According to the changes of side chains submitted at C-17, protostane triterpenoids from *Alisma* are divided into four classes, including open aliphatic chains, epoxy aliphatic chains, spiro hydrocarbon at C-17, and epoxy at C-16, C-23 or C-16, C-24. The individual triterpenoids were detailed in **Table 1**.

Protostanes With Open Aliphatic Chains at C-17

Forty-five protostanes with open aliphatic chains at C-17 (**1–45**) have been identified as shown in **Figure 1**. Alisol A (**1**) is a representative compound of this type. Hydroxyl groups may substitute at C-29 (**11**) (Wang et al., 2017b), disubstitute at C-23/C-24 (**19**) and C-23/C-25 (**43-45**) (Nakajma et al., 1994; Peng et al., 2002b), or trisubstitute at C-23, C-24, and C-25 (**41**, **42**). The hydroxyl group at C-23 or C-24 is easily acetylated. Moreover, double bond may form at C-25 and C-26 (**38**, **39**) (Han et al., 2013), or C-25 may be substituted by carboxyl group (**31**) (Zhao et al., 2013).

Carbonyl groups substitute at C-16 (**8**, **9**) (Zhao et al., 2015), disubstitute at C-7/C-16 (**41**) (Mai et al., 2015) or C-16/C-23 (**21**) (Yoshikawa et al., 1999), or substitute at C-24 (**37**) (Xu et al., 2012) or C-23 (**23**) (Yi et al., 2019). Hydroxymethyl groups substitute at C-16 (**18**) (Li et al., 2017) or disubstitute at C-16/C-25 (**19**).

Protostanes With Epoxy Aliphatic Chains at C-17

Thirty-six protostanes with epoxy aliphatic chains at C-17 (**46–81**) have been found in the genus of *Alisma* and their structures are listed in **Figure 2**. Alisol B 23-acetate (**47**) is a representative compound of this type. Epoxy group usually forms at C-24 and C-25 (**46–73**, **77–79**, **81**) (Fukuyama et al., 1988), and C-23 may be substituted by hydroxyl (**66**) or acetoxyl group (**67–71**).

Except for epoxy ring, tetrahydrofuran ring from C-20 to C-24 (**74**, **75**) and seven-membered peroxic ring from C-20 to C-25 (**76**) are also existed in the side chains at C-17.

Protostanes With Spiro Hydrocarbon at C-17

Eight protostanes with spiro hydrocarbon at C-17 (**82–89**) have been isolated from the genus of *Alisma* as shown in **Figure 3**. Oxaspiro-nonane moiety is generated between D ring and its side chain with C-17 as spiro hydrocarbon. Methyl group substituted at C-20 with α- (**82**) (Xin et al., 2016) or β- (**85**) (Jin et al., 2019) conformation. Alisol U (**83**) differs from alisol V (**84**) by forming an epoxy at C-24 and C-25.

Protostanes With Fused Ring at C-16 and C-17

Twelve protostanes with fused-ring at C-16 and C-17 (**90–101**) have been isolated from *Alisma* as shown in **Figure 4**. Tetrahydropyrane ring is fused at C-16 and C-17 (**90–98**) (Yoshikawa et al., 1993; Peng and Lou, 2001; Hu et al., 2008a,b; Chen et al., 2018). Oxacycloheptane ring is fused at C-16 and C-17 (**99–101**). Alismanol J (**101**) differs from alismaketone B-23-acetate (**99**) by forming an oxygen bridge between C-16 and C-23.

Nor- and seco-protostanes

Twelve nor-protostanes (**102–113**) have been found in *Alisma*, including two demethyl-protostanes (**102**, **103**) and ten tetranorprotostanes (**104–113**). Among C-2 may be submitted by carbanyl group (**109**) (Mai et al., 2015). The configuration of C-17 is determined (**107**, **108**) (Xin et al., 2018).

Only five seco-protostanes (**114–118**) have been known in *Alisma*, including two 13, 17-seco-protostanes (**114**, **115**) (Matsuda et al., 1999; Wang et al., 2017a) and three 2, 3-seco-protostanes (**116–118**) (Yoshikawa et al., 1997). Their structures were detailed in **Figure 5**.

BIOSYNTHESIS

Alisma triterpenoids is commonly biosynthesized through mevalonic aid (MVA) pathway (Zhang et al., 2018) as shown in **Figure 6**. Three molecules of acetyl-CoA are catalyzed by enzymes to form mevalonate acid (MVA) (Vinokur et al., 2014). It is catalyzed by mevalonate pyrophosphate decarboxylase to produce isopentyl pyrophosphate (IPP), which reacts with dimethylallyl pyrophosphate (DMAPP) to generate geranyl pyrophosphate (GPP) by farnesyl pyrophosphate synthase of A. orientale (AOFPPS) (Peng et al., 2018). Squalene is synthesized by squalene synyase of *A. orientale* (AOSS) (Shen et al., 2013), which is then catalyzed by squalene epoxidase of *A. orientale* (AOSE) to produce 2,3-oxidosqualeneand further to form protostane tetracyclic skeleton (Zhang et al., 2018). AOFPPS and AOSS are rate-limiting enzymes in *Alisma* triterpenoids biosynthesis pathway (Zhou et al., 2018).

Fresh materials of *A. orientalis* are naturally rich in alisol B 23-acetate (**47**) (Zhu and Peng, 2006), which can convert into alisol A 24-acetate (**2**), alisol A (**1**), and alisol B (**46**) after processing at high temperature (Zheng et al., 2006). Other triterpenoids, such as alisol A (**1**) (Peng et al., 2002a) and their derivatives, were formed during the drying process (Yoshikawa et al., 1994).

BIOACTIVITIES

Alisma orientale is traditionally used to treat oliguria, edema, gonorrhea with turbid urine, leukorrhea, diarrhea, dizziness and hyperlipidemia (Chinese Pharmacopoeia Commission, 2015). Modern pharmacological studies have demonstrated its diuretic and lipid-lowering efficiency, together with anticancer, lipid-regulating, anti-inflammatory, antibacterial, antiviral activities.

TABLE 1 | A total of 118 triterpenoids isolated and identified from *Alisma* genus.

No.	Name	Skeleton structure	R_1	R_2	R_3	R_4	R_5	R_6	Double bond position	Source	References
PROTOSTANES WITH OPEN ALIPHATIC CHAINS AT C-17											
1	alisol A	A	βOH	H	βOH	βOH	OH	H	$\Delta^{13(17)}$	*A. orientalis*	Peng et al., 2002a
2	alisol A 24-acetate	A	βOH	H	βOH	βOAc	OH	H	$\Delta^{13(17)}$	*A. orientalis*	Peng et al., 2002a
3	alisol A 23-acetate	A	βOH	H	βOAc	βOH	OH	H	$\Delta^{13(17)}$	*A. orientalis*	Peng et al., 2002a
4	11-deoxyalisol A	A	H	H	βOH	βOH	OH	H	$\Delta^{13(17)}$	*A. orientalis*	Peng et al., 2002b
5	23-o-methyl alisol A	A	βOH	H	βOMe	βOH	OH	H	$\Delta^{13(17)}$	*A. orientale*	Nakajma et al., 1994
6	25-o-methoxy-alisol A	A	βOH	H	βOH	βOH	OMe	H	$\Delta^{13(17)}$	*A. orientale*	Nakajma et al., 1994
7	16-oxo-alisol A	A	βOH	O	βOH	βOH	OH	H	$\Delta^{13(17)}$	*A. orientale*	Mai et al., 2015
8	16-oxo-alisol A-23-acetate	A	βOH	O	βOAc	βOH	OH	H	$\Delta^{13(17)}$	*A. orientale*	Zhao et al., 2015
9	16-oxo-alisol A-24-acetate	A	βOH	O	βOH	βOAc	OH	H	$\Delta^{13(17)}$	*A. orientale*	Zhao et al., 2015
10	16-oxo-11-deoxy- alisol A	A	H	O	βOH	βOH	OH	H	$\Delta^{13(17)}$	*A. orientale*	Mai et al., 2015
11	5β,29-dihydroxy alisol A	A (5βOH)	βOH	H	βOH	βOH	OH	OH	$\Delta^{13(17)}$	*A. plantago-aquatica*	Wang et al., 2017b
12	25-o-butyl alisol A	A	βOH	H	βOH	βOH	OBu	H	$\Delta^{13(17)}$	*A. orientalis*	Zhang et al., 2017
13	alisol E	A	βOH	H	βOH	αOH	OH	H	$\Delta^{13(17)}$	*A. orientale*	Yoshikawa et al., 1993
14	alisol E-23-acetate	A	βOH	H	βOAc	αOH	OH	H	$\Delta^{13(17)}$	*A. orientale*	Yoshikawa et al., 1993
15	alisol E-24-acetate	A	βOH	H	βOH	αOAc	OH	H	$\Delta^{13(17)}$	*A. orientale*	Yoshikawa et al., 1993
16	25-o-ethylalisol A	A	βOH	H	βOH	βOH	OEt	H	$\Delta^{13(17)}$	*A. orientale*	Mai et al., 2015
17	alisol H	A	H	O	O	H	OH	H	$\Delta^{13(17)}$	*A. orientale*	Yoshikawa et al., 1999
18	16β-methoxyalisol E	A	βOH	βOMe	βOH	αOH	OH	H	$\Delta^{13(17)}$	*A. orientale*	Li et al., 2017
19	16β,25-dimethoxyalisol E	A	βOH	βOMe	βOH	αOH	OMe	H	$\Delta^{13(17)}$	*A. orientale*	Li et al., 2017
20	16β-hydroperoxyalisol E	A	βOH	βOOH	βOH	αOH	OH	H	$\Delta^{13(17)}$	*A. orientale*	Li et al., 2017
21	11,24-dihydroxy-alisol H	A	βOH	O	O	βOH	OH	H	$\Delta^{13(17)}$	*A. orientale*	Yoshikawa et al., 1999
22	alisol T	A	βOH	βOMe	OH	H	OH	H	$\Delta^{13(17)}$	*A. orientale*	Li et al., 2017
23	alismanin I	A	βOH	H	O	OH	H	H	$\Delta^{13(17)}$	*A. orientale*	Yi et al., 2019
24	15,16-dihydroalisol A.	A	βOH	H	βOH	βOH	OH	H	$\Delta^{13(17),15(16)}$	*A. orientale*	Mai et al., 2015
25	alismanol D	A	H	H	H	αOH	OH	H	$\Delta^{9(11),12(13)}$	*A. orientale*	Mai et al., 2015
26	24-epi-alismanol D	A	H	H	H	βOH	OH	H	$\Delta^{9(11),12(13)}$	*A. orientalis*	Xin et al., 2018
27	alismanol A	A	H	O	O	αOH	OH	H	$\Delta^{11(12),13(17)}$	*A. orientale*	Mai et al., 2015
28	alismanol C	A	H	O	βOAc	αOH	OH	H	$\Delta^{11(12),13(17)}$	*A. orientale*	Mai et al., 2015
29	16-oxo-11-anhydro alisol A	A	H	O	βOH	βOH	OH	H	$\Delta^{11(12),13(17)}$	*A. orientale*	Mai et al., 2015
30	16-oxo-11-anhydroalisol A 24-acetate	A	H	O	βOH	βOAc	OH	H	$\Delta^{11(12),13(17)}$	*A. orientale*	Ma et al., 2016
31	3-oxo-11β,23-dihydroxy-24,24-dimethyl−26,27-dinorprotost-13(17)-en-25-oic-acid	A	βOH	O	H	βOH	COOH	H	$\Delta^{13(17)}$	*A. orientale*	Zhao et al., 2013
32	alismanin B	A	βOH	O	H	βOH	H	H	$\Delta^{13(17)}$	*A. orientale*	Wang et al., 2017a
33	25-anhydroalisol A	B	βOH	H	βOH	βOH			$\Delta^{13(17)}$	*A. orientalis*	Peng et al., 2002a
34	11-acetate-25-anhydroalisol A	B	βOAc	H	βOH	βOH			$\Delta^{13(17)}$	*A. orientalis*	Peng et al., 2002a
35	24-acetate-25-anhydroalisol A	B	βOH	H	βOH	βOAc			$\Delta^{13(17)}$	*A. orientalis*	Peng et al., 2002a
36	11-deoxy-25-anhydro-alisol E.	B	H	H	βOH	αOH			$\Delta^{13(17)}$	*A. orientale*	Mai et al., 2015
37	alisol X	B	βOH	H	H	O			$\Delta^{13(17)}$	*A. orientale*	Xu et al., 2012
38	23-acetate-25-anhydroalisol E	B	H	H	βOAc	αOH			$\Delta^{13(17)}$	*A. orientalis*	Han et al., 2013
39	24-acetate-25-anhydroalisol E	B	H	H	βOH	αOAc			$\Delta^{13(17)}$	*A. orientalis*	Han et al., 2013
40	alismanol B	B	H	O	βOH	αOH			$\Delta^{11(12),13(17)}$	*A. orientale*	Mai et al., 2015
41	7-oxo-16-oxo-11-anhydro alisol A	C								*A. orientale*	Mai et al., 2015
42	alismanol M	D								*A. orientale*	Xin et al., 2016
43	13,17-epo-alisol A	E	βOH	αOH						*A. orientalis*	Peng et al., 2002b
44	13,17-epoalisol A 24-acetate	E	βOH	αOAc						*A. orientalis*	Peng et al., 2002b
45	11-deoxy-13,17-epoxy-alisol A	E	H	βOH						*A. orientale*	Nakajma et al., 1994

(Continued)

TABLE 1 | Continued

No.	Name	Skeleton structure	R_1	R_2	R_3	R_4	R_5	R_6	Double bond position	Source	References
PROTOSTANES WITH EPOXY ALIPHATIC CHAINS AT C-17											
46	alisol B	F	βOH	H	H	H	αMe	βOH	$\Delta^{13(17)}$	*A. orientale*	Nakajma et al., 1994
47	alisol B 23-acetate	F	βOH	H	H	H	αMe	βOAc	$\Delta^{13(17)}$	*A. orientale*	Nakajma et al., 1994
48	11-deoxy-alisol B-23-acetate	F	H	H	H	H	βMe	βOAc	$\Delta^{13(17)}$	*A. orientale*	Nakajma et al., 1994
49	11-deoxy-alisol B	F	H	H	H	H	βMe	βOH	$\Delta^{13(17)}$	*A. orientale*	Nakajma et al., 1994
50	16β-acetoxy alisol B	F	βOH	H	βOAc	H	αMe	βOH	$\Delta^{13(17)}$	*A. orientalis*	Cang et al., 2017
51	16α-acetoxy alisol B	F	βOH	H	αOAc	H	αMe	βOH	$\Delta^{13(17)}$	*A. orientalis*	Cang et al., 2017
52	16β-hydroxyalisol B-23-acetate	F	βOH	H	βOH	H	αMe	βOAc	$\Delta^{13(17)}$	*A. orientalis*	Peng and Lou, 2001
53	16β-methoxyalisol B-23- acetate	F	βOH	H	βOMe	H	αMe	βOAc	$\Delta^{13(17)}$	*A. orientale*	Jin et al., 2012
54	16β-ethoxy alisol B 23-acetate	F	βOH	H	βOEt	H	αMe	βOAc	$\Delta^{13(17)}$	*A. orientalis*	Zhang et al., 2017
55	alisol C	F	βOH	H	O	H	αMe	βOH	$\Delta^{13(17)}$	*A. orientale*	Nakajma et al., 1994
56	11-deoxy-alisol C-23-acetate	F	H	H	O	H	αMe	βOAc	$\Delta^{13(17)}$	*A. orientale*	Nakajma et al., 1994
57	11-deoxy-alisol C	F	H	H	O	H	αMe	βOH	$\Delta^{13(17)}$	*A. plantago-aquatica*	Fukuyama et al., 1988
58	20-hydroxyalisol C	F	βOH	H	O	OH	αMe	βOH	$\Delta^{13(17)}$	*A. orientale*	Mai et al., 2015
59	alisol C 23-acetate	F	βOH	H	O	H	αMe	βOAc	$\Delta^{13(17)}$	*A. plantago-aquatica*	Fukuyama et al., 1988
60	alisol M-23-acetate	F	βOH	βOH	O	H	αMe	βOAc	$\Delta^{13(17)}$	*A. orientale*	Li et al., 2017
61	alisol N-23-acetate	F	βOH	βOH	H	H	αMe	βOAc	$\Delta^{13(17)}$	*A. orientale*	Li et al., 2017
62	16β-hydroperoxyalisol B	F	βOH	H	βOOH	H	αMe	βOH	$\Delta^{13(17)}$	*A. orientale*	Li et al., 2017
63	16β-hydroperoxyalisol B 23-acetate	F	βOH	H	βOOH	H	αMe	βOAc	$\Delta^{13(17)}$	*A. orientale*	Li et al., 2017
64	alisol L	F	H	H	O	H	αMe	βOH	$\Delta^{11(12),13(17)}$	*A. orientale*	Zhao et al., 2015
65	alisol L-23-acetate	F	H	H	O	H	αMe	βOAc	$\Delta^{11(12),13(17)}$	*A. orientale*	Yoshikawa et al., 1999
66	13β,17β-epoxy-alisol B	G	βOH	βOH						*A. orientale*	Nakajma et al., 1994
67	13β,17β-epoxy-23- acetate-alisol B	G	βOH	βOAc						*A. orientale*	Jin et al., 2012
68	11-deoxy-13β,17β-epoxy-alisol B 23-acetate	G	H	βOAc						*A. orientale*	Nakajma et al., 1994
69	alisol D	G	βOH	αOAc						*A. plantago-aquatica*	Fukuyama et al., 1988
70	alisol D 11-acetate	G	βOAc	αOAc						*A. plantago-aquatica*	Fukuyama et al., 1988
71	11-deoxyalisol D	G	H	αOAc						*A. orientale*	Yoshikawa et al., 1999
72	alisol J−23 acetate	H								*A. orientale*	Yoshikawa et al., 1999
73	alisol K-23-acetate	I								*A. orientale*	Yoshikawa et al., 1999
74	alismanol O	J	H							*A. orientale*	Xin et al., 2016
75	alismanol P	J	αOH							*A. orientale*	Xin et al., 2016
76	alisolide H	K								*A. plantago-aquatica*	Jin et al., 2019
77	alisolide G	L	O	αOAc						*A. plantago-aquatica*	Jin et al., 2019
78	alisol Q 23-acetate	L	O	βOAc						*A. orientale*	Jin et al., 2012
79	alisol S 23-acetate	L	βOH	βOAc						*A. orientale*	Li et al., 2017
80	alisolide I	M								*A. plantago-aquatica*	Jin et al., 2019
81	alismaketone A-23-acetate	N								*A. orientale*	Yoshikawa et al., 1997
PROTOSTANES WITH SPIRO HYDROCARBON AT C-17											
82	alismanol Q	O								*A. orientale*	Xin et al., 2016
83	alisol U	P								*A. orientale*	Li et al., 2017
84	alisol V	Q								*A. orientale*	Li et al., 2017
85	alisolide D	R								*A. plantago-aquatica*	Jin et al., 2019

(Continued)

TABLE 1 | Continued

| No.	Name	Skeleton structure	R₁	R₂	R₃	R₄	R₅	R₆	Double bond position	Source	References
86	alisolide E	S	βOH						$\Delta^{12(13)}$	*A. plantago-aquatica*	Jin et al., 2019
87	alisolide F	S	H						$\Delta^{9(11),12(13)}$	*A. plantago-aquatica*	Jin et al., 2019
88	neoalisol	T	βOH	βOH						*A. orientalis*	Peng et al., 2002a
89	neoalisol 11.24-diacetate	T	βOAc	βOAc						*A. orientalis*	Peng et al., 2002a
PROTOSTANES WITH FUSED RING AT C-16 AND C-17											
90	16,23-oxidoalisol B	U	βOH						$\Delta^{13(17)}$	*A. orientale*	Nakajma et al., 1994
91	alisol I	U	βH						$\Delta^{13(17)}$	*A. orientale*	Yoshikawa et al., 1999
92	alisol F	V	βOH	βOH	OH				$\Delta^{13(17)}$	*A. orientale*	Yoshikawa et al., 1993
93	alisol F-24-acetate	V	βOH	βOAc	OH				$\Delta^{13(17)}$	*A. orientalis*	Peng and Lou, 2001
94	25-o-methylalisol F	V	βOH	βOH	OMe				$\Delta^{13(17)}$	*A. orientalis*	Chen et al., 2018
95	11-anhydroalisol F	V	H	βOH	OH				$\Delta^{11(12),13(17)}$	*A. orientalis*	Hu et al., 2008a
96	alisol O	V	H	βOAc	OH				$\Delta^{11(12),13(17)}$	*A. plantago-aquatica*	Jiang et al., 2006
97	25-anhydroalisol F	W	βOH						$\Delta^{13(17)}$	*A. orientalis*	Hu et al., 2008a
98	11,25-anhydro-alisol F	W	H						$\Delta^{11(12),13(17)}$	*A. orientalis*	Hu et al., 2008b
99	alismaketone B-23-acetate	X	βOH	αOAc					$\Delta^{13(17)}$	*A. orientale*	Matsuda et al., 1999
100	alismanol E	X	H	O					$\Delta^{11(12),13(17)}$	*A. orientale*	Mai et al., 2015
101	alismanol J	Y								*A. orientalis*	Zhang et al., 2017
NOR-PROTOSTANES											
102	alismanol H	Z	H	Me						*A. orientalis*	Zhang et al., 2017
103	alismanin A	Z	C₆H₅	H						*A. orientale*	Wang et al., 2017a
104	alisolide A	a	O	βOH					C-17R	*A. plantago-aquatica*	Jin et al., 2019
105	alisolide B	a	O	βOOH					C-17S	*A. plantago-aquatica*	Jin et al., 2019
106	alisolide C	a	βOH	βOH					C-17S	*A. plantago-aquatica*	Jin et al., 2019
107	alisolide	b								*A. orientalis*	Xin et al., 2018
108	17-epi-alisolide	c								*A. orientalis*	Xin et al., 2018
109	alismanol F	d								*A. orientale*	Mai et al., 2015
110	alismanol G	e	H	O	Ac				$\Delta^{11(12),13(17)}$	*A. orientale*	Mai et al., 2015
111	alismanol I	e	βOH	O	OH				$\Delta^{13(17)}$	*A. orientalis*	Zhang et al., 2017
112	alisol R	e	βOH	H	O				$\Delta^{12(13)}$	*A. orientale*	Li et al., 2017
113	13β,17β-epoxy-24,25,26,27-tetranor-alisol A 23-oic acid	f								*A. orientale*	Zhao et al., 2007
SECO-PROTOSTANES											
114	alismanin C	g								*A. orientale*	Wang et al., 2017a
115	alismaketone C-23-acetate	h								*A. orientale*	Matsuda et al., 1999
116	alismalactone-23-acetate	i	H							*A. orientale*	Yoshikawa et al., 1997
117	3-methyl-alismalactone 23-acetate	i	Me							*A. orientale*	Yoshikawa et al., 1997
118	alisol P	j								*A. orientale*	Zhao et al., 2007

Anticancer Activities

Recently, the experiments *in vitro* highlight that alisols induce apoptosis and autophagy in human tumor cells, such as lung cancer (Wang et al., 2018), ovarian cancer (Zhang et al., 2016), and prostate cancer (Huang et al., 2006) cell lines. The cytotoxicities of alisol B 23-acetate (**47**), cancer cell lines, including L1210 and K562 leukemia alisol C 23-acetate (**59**), alisol B (**46**) and alisol A 24-acetate (**2**) are examined on several cells, B16-F10 melnoma cells, A549 lung adenocarcinoma cells, SK-OV3 ovarian cells, HT 1080 fibrosarcoma cells. The results show that alisol B 23-acetate (**47**), alisol C 23-acetate (**59**) and alisol A 24-acetate (**2**) have weaker inhibitory activities against all the tested cancer cells with ED₅₀ values in the range of 10∼20 μg/ml, while alisol B (**46**) exhibits significant effect on SK-OV3, B16-F10, and HT1080 with ED₅₀ values of 7.5, 7.5, and 4.9 μg/ml, respectively (Lee et al., 2001).
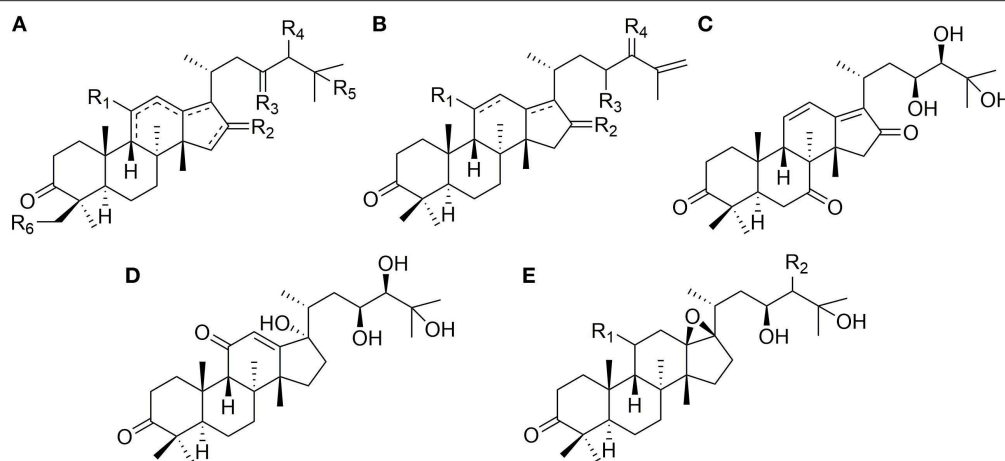
FIGURE 1 | Chemical structures of the protostanes with open aliphatic chains at C-17.
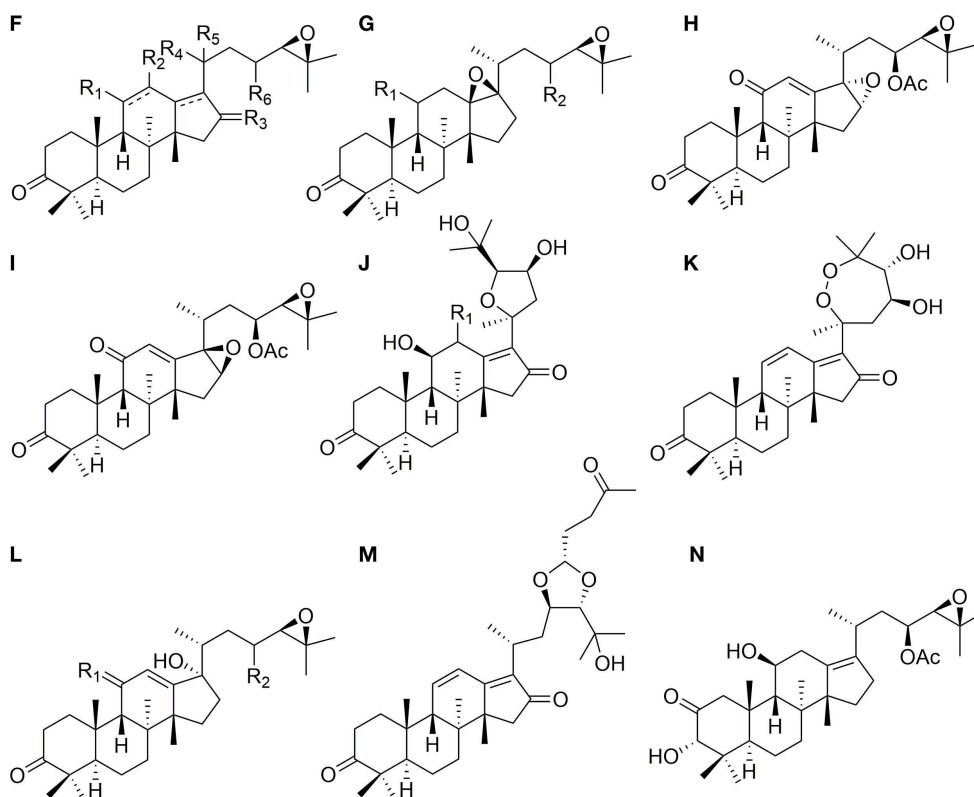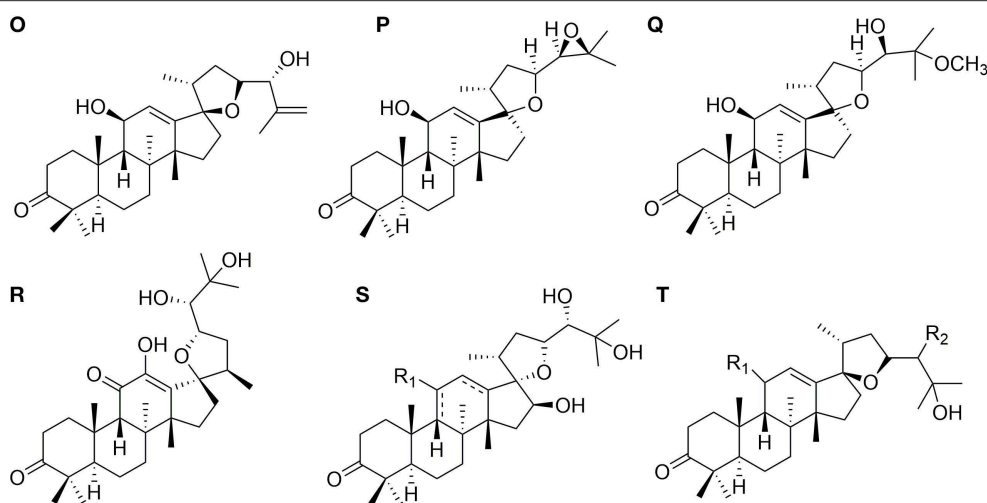

FIGURE 2 | Chemical structures of the protostanes with epoxy aliphatic chains at C-17.

Moreover, alisol F 24-acetate (**93**) and alisol B 23-acetate (**47**) are found inducing cell apoptosis via inhibiting P-glycoprotein mediation and reversing the multidrug resistance in cancer cell lines (Wang et al., 2004; Hyuga et al., 2012; Pan et al., 2016).

Alisol B (**46**) targets on Ca^{2+}-ATP enzymes in the sarcoplasmic reticulum or endoplasmic reticulum to induce autophagy of cancer cells (Law et al., 2010). This compound can also induce cell apoptosis by inhibiting the invasion and metastasis of SGC7901 cells (Xu et al., 2009).

Alisol B 23-acetate (**47**) can inhibit the proliferation of PC-3 prostate cancer (Huang et al., 2006), and induce the apoptosis of lung cancer A549 and NCI-H292 cells through the mitochondrial caspase pathway (Wang et al., 2018). Alisol B 23-acetate (**47**)

FIGURE 3 | Chemical structures of the protostanes with spiro hydrocarbon at C-17.
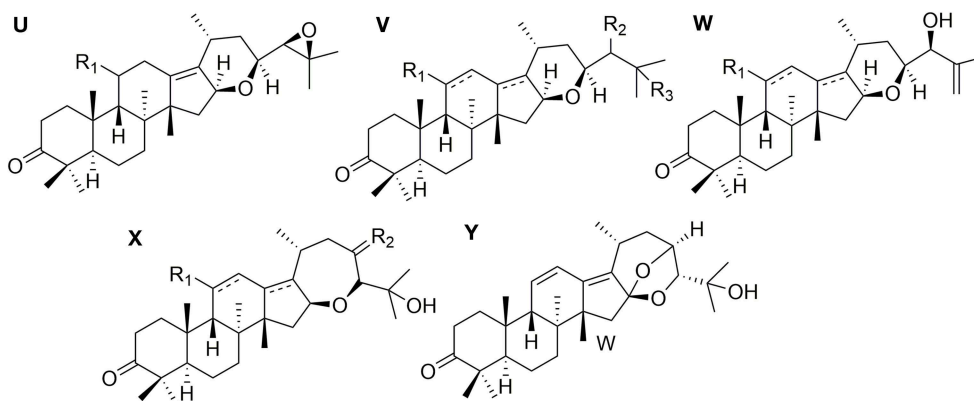
FIGURE 4 | Chemical structures of the protostanes with fused ring at C-16 and C-17.

obviously inhibits the proliferation, migration and invasion of ovarian cancer cell lines and induces accumulation of the G1 phase in a concentration-dependent manner. The protein levels of cleaved poly ADP-ribose polymerase (PARP) and the ratio of Bax/Bcl-2 are up-regulated, while the levels of CDK4, CDK6 and cyclin D1 are down-regulated after alisol B 23-acetate (**47**) treatment. Moreover, it can up-regulate the expression levels of IRE1α and Bip, and down regulate MMP-2 and MMP-9 in a dose- and time- dependent manner (Zhang et al., 2016). However, current studies of *Alisma* triterpenoids are limited into drug screening *in vitro*, and their anticancer activities need to be validated *in vivo*.

Lipid-Lowering Effects

One of *A. orientale* traditional effects is to treat hyperlipidemia. Studies have shown that the extracts of A. orientale tubers have potential effects on hyperlipidemia diseases (Park et al., 2014; Jang et al., 2015; Li et al., 2016; Miao et al., 2017). Alisol B

23-acetate (**47**) and alisol A 24-acetate (**2**) reduce the levels of TC and LDL-C in hyperlipidemia mice via inhibiting the activity of HMG-CoA reductase (Murata et al., 1970; Xu et al., 2016). According to the evaluations of alisols on inhibiting pancreatic lipase, the IC50 of alisol F 24-acetate (**93**) on pancreatic lipase was 45.5 μM (Cang et al., 2017). Studies results show that alisol B 23-acetate (**47**) can bound plasma protein (Xu et al., 2014).

Alisol A (**1**), alisol A 24-acetate (**2**) and alisol B (**46**) can decrease TG level in plasma by improving lipoprotein lipase (LPL) activity (Xu et al., 2018). The effects of alisols with epoxy aliphatic chain at C-17 on LPL are stronger than those with an open aliohatic chain at C-17. Hydroxyl groups submitted at C-14, C-22, C-28, C-30, and an acetyl group at C-29 are necessary for lipid-regulation action of alisols.

Anti-inflammatory

Alisol B 23-acetate (**47**) prevents the production of NO in RAW264.7 cells by inhibiting iNOS mRNA expression
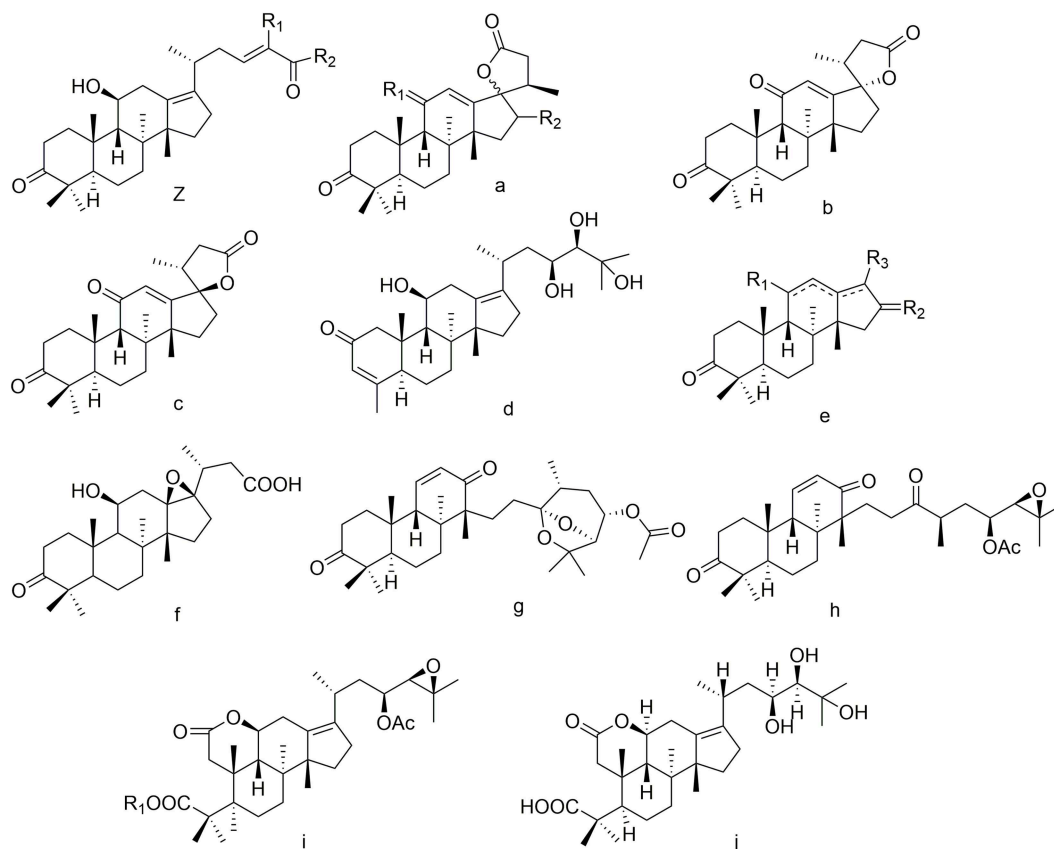
FIGURE 5 | Chemical structures of the nor- and seco-protostanes.

(Kim et al., 1999). Alisol A 24-acetate (**2**) effectively alleviates liver steatosis by down-regulating SREBP-1c, ACC, FAS genes and up-regulating CPT1 and ACOX1 genes to activate AMPK signaling pathway and inhibit inflammatory cytokines TNF-α, IL-6 levels (Zeng et al., 2016). In addition, alisol B (**46**) and alisol B 23-acetate (**47**) significantly inhibit the production of leukotriene and the release of β-hexosaminidase in the concentrations of 1–10 mM (Lee et al., 2012).

Antibacterial

Alisol B (**46**), alisol B 23-acetate (**47**), alisol C 23-acetate (**59**), and alisol A 24-acetate (**2**) have significant bacteriostatic actions on four gram positive and four gram negative antibiotic resistant strains with the MICs ranged from 5 to 10 µg/ml (Jin et al., 2012). In addition, alisol A (**1**), 25-o-ethylalisol A (**16**), 11-deoxyalisol A (**4**), alisol E 24-acetate (**15**) and 25-anhydroalisol F (**97**) fight off gram-positive strains of bacillus subtilis and staphylococcus aureus with MICs ranged from 12.5 to 100 mg/ml (Ma et al., 2016).

Antiviral

Studies have shown that alisols from A. orientale exhibit obvious anti-hepatitis b virus effect (Jiang et al., 2006). Alisol F (**92**) and alisol F 24-acetate (**93**) significantly inhibit the secretion of HBV surface antigen with an IC_{50} value of 7.7 and 0.6 µM, and

HBVe antigen secretion with an IC_{50} value of 5.1 and 8.5 µM, respectively. A series of derivatives of alisol A (**1**) obtained after structural modification also showed potential effect (Zhang et al., 2008, 2009).

STRUCTURE MODIFICATION

Alisol B 23-acetate can induce apoptosis and autophagy in cancer cell lines (Xu et al., 2015), and structure modification on alisol B 23-acetate (**47**) allows to obtain a diverse of derivatives (Lee et al., 2002). Alisol B 23-acetate (**47**) reacts with m-chloroperoxybenzoic acid (mCPBA) in CH_2Cl_2 at room temperature to gain 13β, 17β-epoxy-23-acetate-alisol B (**67**), and reacts with $NH_2OH\cdot HCl$ in pyridine and MeOH to achieve amination at C-3. Deacetylation of alisol B 23-acetate (**47**) by NaOH yields alisol B (**46**). Although there is no significant difference of inhibition effect on B16-F10 and HT1080 cell lines between 13β, 17β-epoxy-23-acetate-alisol B (**67**) (ED50 values of 17 and 18 µg/ml) and alisol B 23-acetate (**47**) (ED50 values of 20 µg/ml, respectively), alisol B (**46**) (B16-F10 and HT1080 with ED50 values of 5.2 and 3.1 ug/ml), amination at C-3 of alisol B 23-acetate (**47**) (with ED50 values of 7.5 and 5.1 ug/ml) show exhibited greater activation against B16-F10 and HT1080 cancer cells. It indicates that deacetylation of C-23 and amination at

FIGURE 6 | Biosynthesis pathway of *Alisma* triterpenoids.

C-3 significantly enhance the inhibition effect on B16-F10 and HT1080 cell lines.

Four hydroxyl groups of alisol A (**1**) are usually the target sites for modification by reacting with acetic anhydride in *N*, *N′*- dicyclohexylcarbodiimide and 4-dimethylamnopyridine. Alisol A (**1**) can also dehydrate by $SOCl_2$ in the presence of anhydrous pyridine. The assessments of anti-hepatitis B virus (HBV) activities suggest alisol A (**1**) analogs with acetoxyl groups at C-11, C-23, C-24 or the epoxy ring at C-13 and C-17 increase the effects on HBV. Dehydration at C-25/C-26 enhances its sensitivity on HBV (Zhang et al., 2008, 2009).

Biotransformation of alisol A (**1**) also derives a series of active compound by several bacteria strains, such as *C. elegans* AS 3.2028 and *P. janthinellum* AS 3.510. Alisol A (**1**) can inhibit the proliferation of HCE-2 cells on the IC_{50} of 99.65 ± 2.81 μM (Zhang et al., 2017). The activity screening results reveal hydroxylation at C-7 and C-12 increases the inhibiting effects of alisol A (**1**) on human carboxylesterase 2 (IC_{50} values of 7.39 ± 1.21 and 3.73 ± 0.76 μM) and the acetyl group at C-23 or C-24 also increases its inhibition effect on HCE-2 cells (IC_{50} values of 3.78 ± 0.21 and 6.11 ± 0.46 μM).

Taken together, epoxidation at C-13 and C-17, hydroxylation at C-23, C-7/C-12, amination at C-3, and dehydration at C-25/C-26 contribute to the activities of protostane tetracyclic skeleton of *A. orientale*, including anticancer activity, anti-hepatitis B virtus, and the inhibiting activity on human carboxylesterase 2.

CONCLUSION

The present work systematically summarized the information concerning the phytochemistry, bioactivities and structure modification of triterpenoids in *Alisma* species. To date, more than 100 protostane-type terterpenoids have been isolated and identified. Alisols are reported with anticancer, lipid-regulating, anti-inflammatory, antibacterial, and antiviral activities. Structure modification might contribute to the investigation of the therapeutic potential of alisols.

AUTHOR CONTRIBUTIONS

MJ designed the review and was responsible for the study conception. PW and MJ wrote the paper. PW, TS, and RS contributed to summarizing the phytochemistry and structure modification studies on triterpenoids. MH, RW, and JL contributed to summarizing the bioactivity studies on triterpenoids.

FUNDING

REFERENCES

Cang, J., Wang, C., Huo, X. K., Tian, X. G., Sun, C. P., Deng, S., et al. (2017). Sesquiterpenes and triterpenoids from the rhzomes of *Alisma orientalis* and their pancreatic lipase inhibitory activities. *Phytochem. Lett.* 19, 83–88. doi: 10.1016/j.phytol.2016.12.017

Chen, H., Yang, T., Wang, M. C., Chen, D. Q., Yang, Y., and Zhao, Y. Y. (2018). Novel RAS inhibitor 25-O-methylalisol F attenuates epithelial-to-mesenchymal transition and tubulo-interstitial fibrosisi by selectively inhibiting TGF-β-mediated Smad3 phosphorylation. *Phytomedicine* 42, 207–218. doi: 10.1016/j.phymed.2018.03.034

Chinese Pharmacopoeia Commission (2015). *Pharmacopoeia of the People's Republic of China.* Beijing: China Medical Science.

Choi, E., Jang, E., and Lee, J. H. (2019). Pharmacological activities of *Alisma orientale* against nonalcoholic fatty liver disease and metabolic syndrome: literature review. *Evid. Based Comple. Alternat. Med.* 2019:2943162. doi: 10.1155/2019/2943162

Flora of China Committee (1992). *Flora of China.* Beijing: Science Press Beijing. 127–145.

Fukuyama, Y., Pei-Wu, G., Rei, W., Yamada, T., and Nakagawa, K. (1988). 11-deoxyalisol C and alisol D: new protostane-type triterpenoids from *Alisma plantago-aquatica*. *Planta Med.* 1988,445–447. doi: 10.1055/s-2006-962495

Han, C. W., Kwun, M. J., Kim, K. H., Choi, J. Y., Oh, S. R., Ahn, K. S., et al. (2013). Ethanol extract of alismatis rhizoma reduces acute lung inflammation by suppressing NF-κB and activating Nrf2. *J. Ethnopharmacol.* 146, 402–410. doi: 10.1016/j.jep.2013.01.010

Hu, X. Y., Guo, Y. Q., Gao, W. Y., Chen, H. X., and Zhang, T. J. (2008b). A new triterpenoid from *Alisma orientalis. Chin. Chem. Lett.* 19, 438–440. doi: 10.1016/j.cclet.2008.01.019

Hu, X. Y., Guo, Y. Q., Gao, W. Y., Zhang, T. J., and Chen, H. X. (2008a). Two new triterpenes from the rhizomes of *Alisma orientalis. J. Asian Nat. Prod. Res.* 10, 487–790. doi: 10.1080/10286020801948441

Huang, Y. T., Huang, D. M., Chueh, S. C., Teng, C. M., and Guh, J. H. (2006). Alisol B acetate, a triterpene from alismatis rhizoma, induces bax nuclear translocation and apoptosis in human hormone-resistant prostate cancer PC-3 cells. *Cancer Lett.* 231, 270–278. doi: 10.1016/j.canlet.2005.02.011

Hyuga, S., Shiraishi, M., Hori., A., Hyuga, M., and Hanawa, T. (2012). Effect of kampo medicines on MDR-1-mediated multidrug resistance in human hepatocellular carcinoma HuH-7/PTX cells. *Biol. Pharm. Bull.* 35, 1729–1739. doi: 10.1248/bpb.b12-00371

Jang, M. K., Han, Y. R., Nam, J. S., Han, C. W., Kim, B. J., Jeong, H. S., et al. (2015). Protective effect of *Alisma orientale* extract against hepatic steatosis via inhibition of endoplasmic reticulum stress. *Int. J. Mol. Sci.* 16, 26151–26165. doi: 10.3390/ijms161125944

Jiang, Z. Y., Zhang, X. M., Zhang, F. X., Liu, N., Zhao, F., Zhou, J., et al. (2006). A new triterpene and anti- hepatitis B virus active compounds from *Alisma orientalis. Plant Med.* 72, 951–954. doi: 10.1055/s-2006-947178

Jin, H. G., Jin, Q. L., Kim, A. R., Choi, H., Lee, J. H., Kim, Y. S., et al. (2012). A new triterpenoid from *Alisma orientale* and their antibacterial effect. *Arch. Pharm. Res.* 35, 1919–1926. doi: 10.1007/s12272-012-1108-5

Jin, Q. H., Zhang, J. Q., Hou, J. J., Lei, M., Liu, C., Wang, X., et al. (2019). Novel C-17 spirost protostane-type triterpenoids from *Alisma plantago-aquatica* with anti-inflammatory activity in Caco-2 cells. *Acta Pharm. Sin. B* 9, 809–818. doi: 10.1016/j.apsb.2019.04.002

Kim, K. H., Song, H. H., Ahn, K. S., Oh, S. R., Sadikot, R. T., and Joo, M. (2016). Ethanol extract of the tuber of *Alisma orientale* reduces the pathologic features in a chronic obstructive pulmonary disease mouse model. *J. Ethnopharmacol.* 188, 21–30. doi: 10.1016/j.jep.2016.05.004

Kim, N. Y., Kang, T. H., Pae, H. O., Choi, B. M., Chung, H. T., Myung, S. W., et al. (1999). *In vitro* inducible nitric oxide synthesis inhibitors from *Alismatis rhizoma. Biol. Pharm. Bull.* 22, 1147–1149. doi: 10.1248/bpb.22.1147

Law, B. Y. K., Wang, M. F., Ma, D. L., Al-Mousa, F., Michelangeli, F., Cheng, S. H., et al. (2010). Alisol B, a novel inhibitor of the

sarcoplasmic/endoplasmic reticulum Ca(2+) ATPase pump, induces autophagy, endoplasmic reticulum stress, and apoptosis. *Mol. Cancer Ther.* 9, 718–730. doi: 10.1158/1535-7163.MCT-09-0700

Lee, J. H., Kwon, O. S., Jin, H. G., Woo, E. R., Kim, Y. S., and Kim, H. P. (2012). The rhizomes of *Alisma orientale* and Alisol derivatives inhibit allergic response and experimental atopic dermatitis. *Biol. Pharm. Bull.* 35, 1581–1587. doi: 10.1248/bpb.b110689

Lee, S. M., Kho, Y. H., Min, B. S., Kim, J. H., Na, M. K., Kang, S. J., et al. (2001). Cytotoxic triterpenoides from *Alismatis rhizome. Arch. Pharm. Res.* 24, 524–526. doi: 10.1007/BF02975158

Lee, S. M., Min, B., and Bae, K. (2002). Chemical modification of alisol B 23-acetate and their cytotoxic activity. *Arch. Pharm. Res.* 25, 608–612. doi: 10.1007/BF02976929

Li, H. M., Chen, X. J., Luo, D., Fan, M., Zhang, Z. J., Peng, L. Y., et al. (2017). Protostane-type triterpenoids from *Alisma orientale. Chem. Biodivers.* 14:e1700452. doi: 10.1002/cbdv.201700452

Li, S., Jin, S. N., Song, C. W., Chen, C., Zhang, Y., Xiang, Y., et al. (2016). The metabolic change of serum lysophosphatidylcholines involved in the lipid lowering effect of triterpenes from *Alismatis rhizoma* on high-fat diet induced hyperlipidemia mice. *J. Ethnopharmacol.* 177, 10–18. doi: 10.1016/j.jep.2015.11.017

Ma, Q. J., Han, L., Bi, X. X., Wang, X. B., Mu, Y., Guan, P. P., et al. (2016). Structures and biological activities of the triterpenoids and sesquiteropenoids from *Alisma orientale. Phytochemistry* 131, 150–157. doi: 10.1016/j.phytochem.2016.08.015

Mai, Z. P., Zhou, K., Ge, G. B., Wang, C., Huo, X. K., Dong, P. P., et al. (2015). Protostane triterpenoids from the rhizome of *Alisma orientale* exhibit inhibitortory effects on human carboxylesterase2. *J. Nat. Prod.* 78, 2372–2380. doi: 10.1021/acs.jnatprod.5b00321

Matsuda, H., Kageura, T., Toguchida, I., Murakami, T., Kishi, A., and Yoshikawa, M. (1999). Effects of sesquiterpenes and triterpenes from the rhizome of *Alisma orientale* on nitric oxide production in lipopolysaccharide-activated macrophages: absolute stereostructures of alismaketones B 23-acetate and -C 23-acetate. *Bioorg. Med. Chem. Lett.* 9, 3081–3086. doi: 10.1016/S0960-894X(99)00536-3

Miao, H., Zhang, L., Chen, D. Q., Chen, H., Zhao, Y. Y., and Ma, S. C. (2017). Urinary biomarker and treatment mechanism of rhizoma alismatis on hyperlipidemia. *Biomed. Chromatograp.* 31:e3829. doi: 10.1002/bmc.3829

Murata, T., Shinohara, M., Hirata, T., Kamiya, K., Nishikawa, M., and Miyamoto, M. (1968). New triterpenes of *alisma plantago-aquatica* L. Var. *Orientale* samuels. *Tetrahedron Lett.* 9, 103–108. doi: 10.1016/S0040-4039(01)98735-0

Murata, T. Y., Imai, T., Hirata, T., and Miyamoto, M. (1970). Biological-active trieterpenes of Alismatis rhizoma.I. *isolation of the Alisols rhizoma. Chem. Pharm. Bull.* 18, 1347–1353. doi: 10.1248/cpb.18.1347

Nakajma, Y., Satoh, Y., Katsumata, M., Tsujiyama, K., Ida, Y., and Shoji, J. (1994). Terpenoids of *Alisma Orientale* rhizome and the crude drug *Alismatis Rhizoma. Phytochemistry* 36, 119–127. doi: 10.1016/S0031-9422(00)97024-9

Pan, G. X., Li, T. T., Zeng, Q. Q., Wang, X. M., and Zhu, Y. (2016). Alisol F 24 acetate enhances chemosensivity and apoptosis of MCF-7/DOX cell by inhibiting P-glycoprotein-mediated drug efflux. *Molecules* 21:183. doi: 10.3390/molecules21020183

Park, Y. J., Kim, M. S., Kim, H. R., Kim, J. M., Hwang, J. K., Yang, S. H., et al. (2014). *Ethanol extract of Alismatis rhizome inhibits adipocyte differentiation of OP9 cells. Evid. Based Comple. Alternt. Med.* 2014:415097. doi: 10.1155/2014/415097

Peng, B., Nielsen, L. K., Kampranis, S. C., and Vickers, C. E. (2018). Engineered protein degradation of farnesyl pyrophosphate synthase is an effective regulatory mechanism to increase monoterpene production in *Saccharomyces cerevisiae. Metab. Eng.* 47, 83–93. doi: 10.1016/j.ymben.2018.02.005

Peng, G. P., and Lou, F. C. (2001). Study on triterpenes in rhizoma alismatis from Sichuan. *Nat. Prod. Res. Dev.* 13, 1–4. doi: 10.1633/j.1001-6880.2001.04.001

Peng, G. P., Zhu, G. Y., and Lou, F. C. (2002a). Study on two new constituents of triterpenes from rhizoma alismatis II. *Nat. Prod. Res. Dev.* 14, 5–8. doi: 10.1633/j.10001-6880.2002.04.002

Peng, G. P., Zhu, G. Y., and Lou, F. C. (2002b). Study on triterpenes in rhizoma alismatis from Sichuan III. *Nat. Prod. Res. Dev.* 14, 7–10. doi: 10.16333/j.1001-6880.2002.06.003

Shen, X. Y., Gu, W., Zhou, J. J., Wu, Q. N., Xu, F., and Gao, J. (2013). Gene cloning of squalene synthase in *Alisma orientalis* and its bioinformatic analysis.

Chin. Trad. Herb. Drug. 44, 604–609. doi: 10.7501/j.issn.0253-2670.2013.05.021

Shu, Z. H., Pu, J., Chen, L., Zhang, Y. B., Rahman, K., Qin, L., et al. (2016). *Alisma orientale*: ethnopharmacology, phytochemistry and pharmacology of an important traditional chinese medicine. *Am. J. Chin. Med.* 2, 227–251. doi: 10.1142/S0192415X16500142

Tian, T., Chen, H., and Zhao, Y. Y. (2014). Traditional uses, phytochemistry, pharmacology, toxicology and quality control of *Alisma orientale* (Sam.) juzep: a review. *J. Ethnopharmacol.* 158, 373–387. doi: 10.1016/j.jep.2014.10.061

Vinokur, J. M., Korman, T. P., Cao, Z., and Bowie, J. U. (2014). Evidence of a novel mevalonate pathway in archaea. *Biochemistry* 25, 4161–4168. doi: 10.1021/bi500566q

Wang, C., Huo, X. K., Luan, Z. L., Cao, F., Tian, X. G., Zhao, X. Y., et al. (2017a). Alismanin A, a triterpenoid with a C34 skeleton from *Alisma orientale* as a natural agonist of human pregnane X receptor. *Org. Lett.* 19, 5645–5648. doi: 10.1021/acs.orglett.7b02738

Wang, C., Zhang, J. X., Shen, X. L., Wan, C. K., Tse, K. W., and Fong, W. F. (2004). Reversal of P-glycoprotein-mediated multidrug resistance by alisol B 23-acetate. *Biochem. Pharmacol.* 68, 843–855. doi: 10.1016/j.bcp.2004.05.021

Wang, J. X., Li, H. Z., Wang, X. N., Shen, T., Wang, S. Q., and Ren, D. M. (2018). Alisol B-23-acetate, a tetracyclic triterpenoid isolated from *Alisma orientale*, induces apoptosis in human lung cancer cells via the mitochondrial pathway. *Biochem. Biophys. Res. Commun.* 2018, 1015–1021. doi: 10.1016/j.bbrc.2018.10.022

Wang, Y. L., Zhao, J. C., Liang, J. H., Tian, X. G., Huo, X. K., Feng, L., et al. (2017b). A bioactive new protostane-type triterpenoid from *Alisma plantago-aquatica* subsp. *orientale (sam.) juzep. Nat. Prod. Res.* 11, 776–781. doi: 10.1080/14786419.2017.1408106

Xin, X. L., Mai, Z. P., Wang, X. C., Liang, D. S., and Zhang, B. (2016). Protostane alisol derivatives from the rhizome of *Alisma orientale. Phytochem. Lett.* 16, 8–11. doi: 10.1016/j.phytol.2016.02.008

Xin, X. L., Zhao, X. Y., Huo, X. K., Tian, X. G., Sun, C. P., Zhang, H. L., et al. (2018). Two new protostane-type triterpenoids from *Alisma orientalis. Nat. Prod. Res.* 32, 189–194. doi: 10.1080/14786419.2017.1344660

Xu, D., Zhang, H. D., and Xie, X. (2012). New triterpenoids from rhizoma alisma. *Chin. Trad. Herb. Drugs* 43, 841–843.

Xu, F., Lu, Q. A., Gu, W., Chen, J., Fang, F., Zhao, B., et al. (2018). Studies on the lipid-regulating mechanism of alisol-based compounds on lipoprotein lipase. *Bioorg. Chem.* 80, 347–360. doi: 10.1016/j.bioorg.2018.07.001

Xu, F., Wu, Q. N., Chen, J., Gu, W., Fang, F., Zhang, L. Q., et al. (2014). The binding mechanisms of plasma protein to active compounds in *Alisma orientale* rhizomes (*Alismatis Rhizoma*). *Bioorg. Med. Chem. Lett.* 24, 4099–4105. doi: 10.1016/j.bmcl.2014.07.065

Xu, F., Yu, H., Lu, C., Chen, J., and Gu, W. (2016). The cholesterol - lowering effect of alisol acetate based on HMG-CoA reductase and its molecular mechanism. *Evid. Based Complement. Altern. Med.* 2016:4753852. doi: 10.1155/2016/4753852

Xu, W., Li, T., Qiu, J. F., Wu, S. S., Huang, M. Q., Lin, L. G., et al. (2015). Anti-proliferative activities of terpenoid isolated from *Alisma orirntalis* and their structure activity relationships. *Anticancer Agents Med. Chem.* 15, 228–235. doi: 10.2174/1871520614666140601213514

Xu, Y. H., Zhao, L. J., and Li, Y. (2009). Alisol B acetate induces apoptosis of SGC7901 cells via mitochondrial and phosphatidylinositol 3-kinases/Akt signaling pathways. *World J. Gastroenterol.* 15, 2870–2877. doi: 10.3748/wjg.15.2870

Yi, J., Bai, R., An, Y., Liu, T. T., Liang, J. H., Tian, X. G., et al. (2019). A natural inhibitor from *Alisma orientale* against human carboxylesterase 2: kinetics, circular dichroism spectroscopic analysis, and docking simulation. *Int. J. Biol. Macromol.* 133, 184–189. doi: 10.1016/j.ijbiomac.2019.04.099

Yoshikawa, M., Hatakeyama, S., Tanaka, N., Fuhuda, Y., Yamahara, J., and Murakami, N. (1993). Crude drug from aquatic plants. I. on the constituents of *Alismatis Rhizoma*. (1). absolute stereostructures of Alisols E 23-acetate, F, and G, three new protostane-type triterpenes from Chinese *Alismatis Rhizoma. Chem. pharm. Bull.* 41, 1948–1954. doi: 10.1248/cpb.41.1948

Yoshikawa, M., Muraakami, T., Ikebata, A., Ishikado, A., Murakami, N., Yamahara, J., et al. (1997). Absolute stereostructures of Alismalactone

23-acetate and Alismaketone-A-23-acetate, new seco-protostane and protostane-type triterpenes with vasorelaxant effects from Chinese *Alismatis Rhizoma*. *Chem. Pharm. Bull.* 45, 756–758. doi: 10.1248/cpb. 45.756

Yoshikawa, M., Tomohro, N., Murakami, T., Ikebata, A., Matsude, H., Matsude, H., et al. (1999). Studies on *Alismatis Rhizoma*. III. stereostructures of new protostane-type triterpenes,aliaols H, I, J-23-acetate, K-23-acetate, L-23-acetata, M-23-acetate, and N-23-acetate, from the dried rhizome of *Alisma orientale*. *Chem. Pharm. Bull.* 147, 524–528. doi: 10.1248/cpb. 47.524

Yoshikawa, M., Yamaguchi, S., Chatani, N., Matsuoka, T., Yamahara, J., Murakami, N., et al. (1994). Crude drugs from aquaticplants. III. quantitative analysis of triterpene constituents in *Alismatis rhizoma* by means of high performance liquid chromatography on the chemical change of the constituents during *Alismatis rhizoma* processing. *Yakuqaku Zasshi.* 114, 241–247. doi: 10.1248/yakushi1947. 114.4_241

Zeng, L., Tang, W. J., Yin, J. J., Feng, L. J., Li, Y. B., Yao, X. R., et al. (2016). Alisol A 24-acetate prevents hepatic steatosis and metabolic disorders in HepG2 cells. *Cell. Physiol. Biochem.* 40, 453–464. doi: 10.1159/000452560

Zhang, L. L., Xu, Y. L., Tang, Z. H., Xu, X. H., Chen, X., Li, T., et al. (2016). Effects of alisol B 23-acetate on ovarian cancer cells: G1 phase cell cycle arrest, apoptosis, migration and invasion inhibition. *Phytomedicine* 23, 800–809. doi: 10.1016/j.phymed.2016.04.003

Zhang, Q., Jiang, Z. Y., Luo, J., Cheng, P., Ma, Y. B., Zhang, X. M., et al. (2008). Anti-HBV agents. part 1: synthesis of alisol A derivatives: a new class of hepatitis B virus inhibitors. *Bioorg. Med. Chem. Lett.* 18, 4647–4650. doi: 10.1016/j.bmcl.2008.07.012

Zhang, Q., Jiang, Z. Y., Luo, J., Liu, J. F., Ma, Y. B., Guo, R. H., et al. (2009). Anti-HBV agents. part 2: synthesis and *in vitro* anti-hepatitis B virus activities of alisol A derivatives. *Bioorg. Med. Chem. Lett.* 19, 2148–2153. doi: 10.1016/j.bmcl.2009.02.122

Zhang, T. J., Bai, G., Chen, C. Q., Xu, J., Han, Y. Q., and Long, S. X. (2018). Research pathways of Q-marker of compound Chinese medicine based on five principles. *Chin. Trad. Herb. Drugs* 49, 1–13. doi: 10.7501/j.issn.0253-2670.2018. 01.001

Zhang, Z. J., Huo, X. K., Tian, X. G., Feng, L., Ning, J., Zhao, X. Y., et al. (2017). Novel protostane-type triterpenoids with inhibitory human carboxylesterase 2 activities. *Rsc. Adv.* 7, 28702–28710. doi: 10.1039/C7RA04841F

Zhao, M., Godecke, T., Gunn, J., Duan, J. A., and Che, C. T. (2013). Protostane ang fusidane triterpenes: a mini- review. *Molecules* 18, 4054–4080. doi: 10.3390/molecules18044054

Zhao, M., Xu, L. J., and Che, C. T. (2007). Alisolide, alisols O and P from the *Alisma orientale*. *Phytochemistry* 69, 527–532. doi: 10.1016/j.phytochem.2007.06.014

Zhao, W. L., Huang, X. Q., Li, X. Y., Zhang, F. F., Chen, S. N., Ye, M., et al. (2015). Qualitative and quantitative analysis of major teiterpenoids in *Alismatis rhizome* by high performance liquid chromatography/diode-array detector/quadrupole-time-of-flight mass spectrometry and ultra-performance liquid chromatography/triple quadrupole mass spectrometry. *Molecules* 20, 13958–13981. doi: 10.3390/molecules200813958

Zheng, Y. F., Zhu, Y. L., and Peng, G. P. (2006). Transformation of alisol B 23-acetate in processing drug of *Alisma orientale*. *Chin. Trad. Herb. Drugs* 37, 1479–1482.

Zhou, C., Tian, R., Gu, W., Geng, C., Wu, Q. N., and Xu, F. (2018). Prokaryotic expression, functional verification and immunoassay of farnesyl pyrophosphate synthase of *Alisma orientale* (sam.) juzep. *Acta Pharm. Sin.* 53, 1571–1577. doi: 10.16438/j.0513-4870.2018-0401

Zhu, Y. L., and Peng, G. P. (2006). Progress in the study on chemical constituents of *Alisma orientalis*. *Nat. Prod. Res. Dev.* 18, 348–351. doi: 10.16333/j.1001-6880.2006.02.041

Structures of Cyclic Organosulfur Compounds From Garlic (*Allium sativum* L.) Leaves

Masashi Fukaya, Seikou Nakamura, Hitoshi Hayashida, Daisuke Noguchi, Souichi Nakashima, Taichi Yoneda and Hisashi Matsuda*

Department of Pharmacognosy, Kyoto Pharmaceutical University, Kyoto, Japan

Five new cyclic organosulfur compounds, foliogarlic disulfanes A_1 (**1**), A_2 (**2**), and A_3 (**3**) and foliogarlic trisulfane A_1 (**4**) and A_2 (**5**), were isolated from the leaves of *Allium sativum* (garlic). The chemical structures of these compounds were elucidated on the basis of physicochemical evidence including Nuclear Magnetic Resonance (NMR) and Mass Spectrometry (MS). Compounds **1–5** were obtained as complex compounds with disulfane or trisulfane and tetrahydro-2*H*-difuro[3,2-*b*:2′,3′-*c*]furan-5(5a*H*)-one. In addition, the hypothetical biosynthetic pathways of these compounds were suggested.

Keywords: *Allium sativum* L., garlic, organosulfur compound, foliogarlic disulfane, foliogarlic trisulfane

INTRODUCTION

Allium plants (Allieae), such as garlic, onion, and chives, have been cultivated as not only foodstuffs but also medicinal plants in the worldwide from ancient. For example, the extract of *Allium* plants, such as garlic, has shown anticancer, antidiabetic, and antibacterial effects. In addition, the National Cancer Institute in the United States had focused on *Allium* species as expecting cancer prevention (Theisen, 2001). *Allium* plants are well-known to have various cysteine sulfoxide derivatives such as alliin, methiin, and propiin (Rose et al., 2005). The type and contents of cysteine sulfoxides were also known to be different among *Allium* species (Fritsch and Keusgen, 2006). The cysteine sulfoxides change to thiosulfinates, such as allicin (Cavallito and Bailey, 1944; Cavallito et al., 1944), by the reaction with enzyme called alliinase (Ellmore and Feldberg, 1994) when the tissues of *Allium* plants are broken. Allicin has been reported to have several biological effects (Gebhardt et al., 1994; Briggs et al., 2000; Cañizares et al., 2004; Oommen et al., 2004; Arditti et al., 2005). However, unstable thiosulfinates including allicin are changed to organosulfur compounds, such as ajoene (Block et al., 1984), methyl 1-(methylthio)ethyl disulfane, and 5,7-diethyl-1,2,3,4,6-pentathiepane (Kuo et al., 1990). These compounds are also comparatively unstable and volatile. Although ajoene was known to have significantly anticancer effect, the application as medicines is difficult. On the other hand, several cyclic organosulfur compounds with anticancer effects isolated from the bulbs of the *Allium sativum* (garlic) have been reported by Nohara et al. (2012, 2013, 2014). Thus, cyclic organosulfur compounds are important on the development of medicines including anticancer effect. On the basis of this background, we have isolated several comparatively stable organosulfur compounds from *Allium fistulosum* (green onion and welsh onion) (Fukaya et al., 2018, 2019a) and *Allium schoenoprasum* var. *foliosum* (Japanese chive) (Fukaya et al., 2019b). In the course of our ongoing research program for discovery of bioactive organosulfur compounds, the constituents from the leaves of *Allium sativum* were examined. In this article, we discuss the isolation and the structure elucidation of cyclic organosulfur compounds, foliogarlic disulfanes A_1 (**1**), A_2 (**2**), and A_3 (**3**) and foliogarlic trisulfane A_1(**4**) and A_2 (**5**), from the leaves of *A. sativum* and the biosynthetic pathways.

RESULTS AND DISCUSSIONS

The fresh leaves of *A. sativum* (15.0 kg) were mixed with water. Then, acetone was added into the mixture to be 80% acetone solution. The solution was concentrated after standing for 4 days (96 h) at room temperature. The acetone extract was portioned between ethyl acetate (EtOAc) and water. The organic fraction was evaporated *in vacuo* and obtained EtOAc fraction as syrup (41.98 g, 0.27% from the plant). The EtOAc fraction was also subjected with the normal and reversed-phase column chromatography and high-performance liquid chromatography (HPLC) to give foliogarlic disulfanes A_1 (**1**, 0.00013%), A_2 (**2**, 0.00021%), and A_3 (**3**, 0.00009%) and foliogarlic trisulfanes A_1 (**4**, 0.00015%) and A_2 (**5**, 0.00008%) (**Figure 1**).

Foliogarlic disulfanes A_1 (**1**) was obtained as yellow oil and showed positive optical rotation (+160.9). In the Electrospray Ionization MS (ESIMS) measurement of **1**, a pseudomolecular ion peak $[M + Na]^+$ was observed at *m/z* 343.0282, and the molecular formula was determined as $C_{12}H_{16}O_6S_2$ on the basis of the High Resolution ESIMS (HRESIMS) peak and the ^{13}C NMR data. The ^{13}C NMR spectra of **1** showed signals corresponding to a secondary methyl group at δ_C 9.1 (6-CH$_3$), a methine at δ_C 48.1 (C-6), a diastereotopic oxygen-bearing methylene at δ_C 74.98 (C-3); an oxygen-bearing methine at δ_C 75.03 (C-2); two methines neighboring the electron-withdrawing atom at δ_C

90.4 (C-3a) and δ_C 103.2 (C-7); an oxygen-bearing quaternary carbon at δ_C 79.6 (C-5a); a two-oxygen–bearing quaternary carbon at δ_C 119.1 (C-8a); and a lactone carbonyl carbon at δ_C 175.4 (C-5) (**Table 1**, **Figure 2**, and **Supplementary Material**). The correlations of COSY double-quantum filter (DQF COSY) NMR spectroscopy were observed between 6-CH$_3$, H-6, and H-7 and between H-2, H-3, and H-3a (**Figure 2**). The heteronuclear multiple-bond correlation (HMBC) spectrum of **1** is shown in **Figure 2**. Namely, the correlation of H-2 to C-8a, H-7 to C-5a and H-3a to C-5a indicates acetal structure, the correlation of H-3a to C-5 and C-5a indicates a lactone, and the correlations of H-6 to C-5a and C-7, H-7 to C-5 and 6-CH$_3$, 6-CH$_3$ to C-5a, C-6, and C-7 indicate a secondary methyl moiety. These evidences indicate that compound **1** had a tetrahydro-2*H*-difuro[3,2-b:2′,3′-c]furan-5(5a*H*)-one skeleton. In addition, 1-propenyl disulfane structure at the side chain was confirmed by High Resolution MS (HRMS) and NMR (Nuclear Magnetic Resonance) data. Next, the NOESY spectrum of **1** showed key correlations between H-3a and H-6; and H-6 and H-7 (**Figure 2**). The results prove that the relative configurations among H-3, H-6, and H-7 were of the same orientation, respectively. Furthermore, the ^{1}H and ^{13}C NMR signals of **1** assigned to tetrahydro-2*H*-difuro[3,2-b:2′,3′-c]furan-5(5a*H*)-one skeleton were superimposable on those of known compound, kujounin A_3, except for 1-propenyl disulfane moiety (Fukaya et al., 2019a). All the evidences support that the chemical structure of **1**
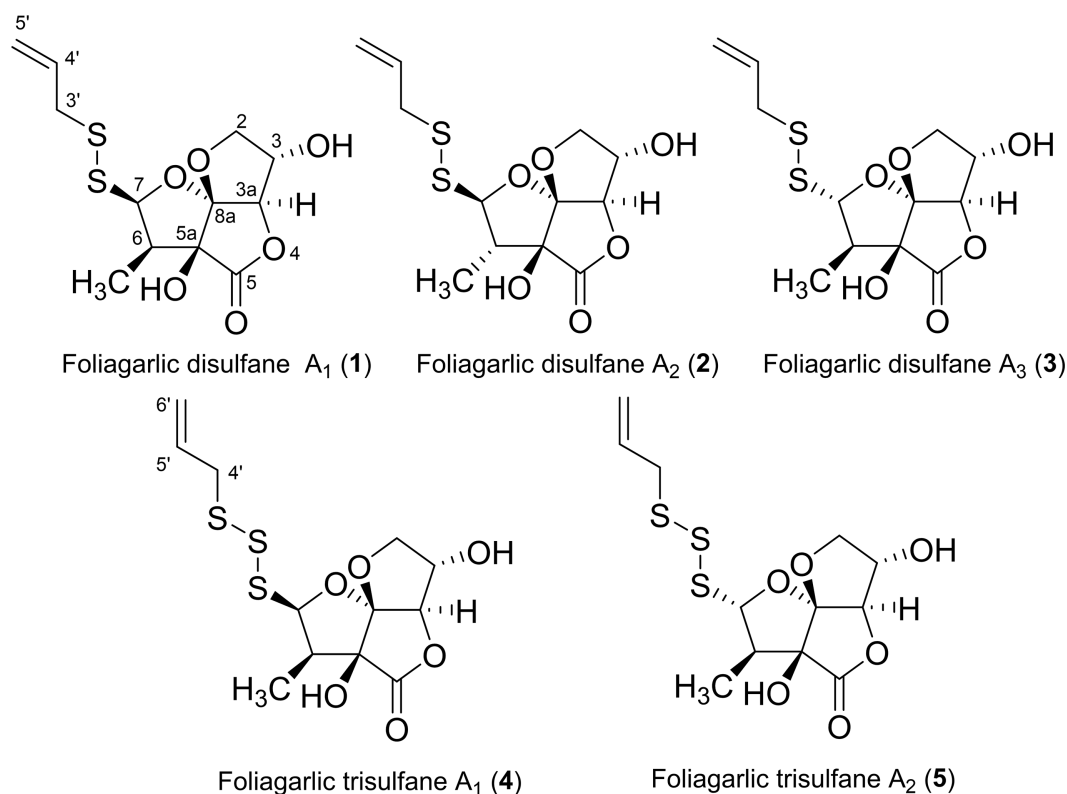
FIGURE 1 | Structures of new compounds **1-5** from the leaves of *A. sativum*.

TABLE 1 | ^{1}H NMR and ^{13}C NMR data of **1** and **2**.

Position	1		2		2	
	δ_H (J, Hz)^a	δ_C^{a}	δ_H (J, Hz)^a	δ_C^{a}	δ_H (J, Hz)^b	δ_C^{b}
2	4.05 (m)	75.03	4.00 (dd, J = 5.5, 7.5)	75.0	α 4.11 (dd, J = 4.8, 10.3)	74.2
			4.01 (dd, J = 5.5, 9.5)		β 4.23 (dd, J = 3.4, 10.3)	
3	4.30 (m)	74.98	4.30 (m)	75.5	4.44 (m)	74.4
3a	4.62 (d-like)	90.4	4.60 (d, J = 2.5)	90.4	4.64 (d, J = 1.3)	88.6
5		175.4		175.0		171.4
5a		79.6		82.3		81.6
6	2.91 (m)	48.1	2.63 (m)	49.8	2.75 (m)	49.7
7	5.55 (d, 7.0)	103.2	4.78 (d, J = 7.0)	94.5	5.00 (d, J = 3.5)	97.5
8a		119.1		117.0		117.0
3′	3.45 (m)	43.5	3.47 (d, J = 7.5)	43.8	3.48 (m)	42.7
4′	5.88 (m)	134.6	5.86 (m)	134.4	5.88 (m)	133.0
5′	5.09 (d like, 10.0)	118.9	5.12 (d-like, J = 9.5)	119.1	5.15 (d-like, J = 11.6)	120.0
	5.19 (d like, 17.0)		5.18 (d-like, J = 16.0)		5.20 (d-like, J = 16.4)	
6-CH$_3$	1.18 (d, 7.0)	9.1	1.13 (d, J = 7.5)	12.6	1.21 (d, J = 7.6)	14.0

^{a}^{1}H NMR, ^{13}C NMR (CD$_3$OD, 500 MHz).
^{b}^{1}H NMR, ^{13}C NMR (CDCl$_3$, 600 NMR).

was (3S*,3aR*,5aS*,6R*,7R*,8aR*)-3,5a-dihydroxy-6-methyl-7-(allyldisulfanyl)tetrahydro-2H-difuro[3,2-b:2′,3′-c]furan-5(5aH)-one.

Foliogarlic disulfanes A$_2$ (**2**) and A$_3$ (**3**) were isolated as yellow oil with positive specific rotations (**2**: $[\alpha]_D^{25}$ + 139.0° in MeOH) and negative specific rotations (**3**: $[\alpha]_D^{25}$ – 213.6° in MeOH). In the ESIMS spectra of **2** and **3**, the same quasi-molecular ion peaks (**2** and **3**: [M+Na]$^+$) were observed at m/z 343. The molecular formulas (**2** and **3**: C$_{12}$H$_{16}$O$_6$S$_2$) were determined on the basis of HRESIMS peaks at [**2**: m/z 343.0277, **3**: m/z 343.0282 (calcd. 343.0281)] and the ^{13}C NMR data. The ^{1}H and ^{13}C NMR spectrum of **2** and **3** showed signals corresponding to a secondary methyl group, a methine, a diastereotopic oxygen-bearing methylene, and an oxygen-bearing methine (**Tables 1**, **2** and **Figure 2**). On the basis of this evidence and detailed examination of DQF COSY and HMBC experiments, the planner structures of **2** and **3** were found to be the same as that of **1**. Next, the relative configurations of **2** and **3** were characterized by the detailed NOESY experiments. The NOESY spectrum of **2** showed key correlations between H-3a and 6-CH$_3$; and H-7 and 6-CH$_3$ (**Figure 2**). The NOESY spectrum of **3** showed key correlations between H-3a and H-6; and H-7 and 6-CH$_3$ (**Figure 2**). In addition, the ^{1}H and ^{13}C NMR signals of **2** and **3** were superimposable on those of known compounds, kujounin A$_1$ and A$_2$, respectively, except for 1-propenyl disulfane structure (Fukaya et al., 2018). Consequently, the chemical structures of foliogarlic disulfanes A$_2$ (**2**) and A$_3$ (**3**) were determined as (3S*,3aR*,5aS*,6S*,7R*,8aR*)-3,5a-dihydroxy-6-methyl-7-(allyldisulfanyl)tetrahydro-2H-difuro[3,2-b:2′,3′-c]furan-5(5aH)-one and (3S*,3aR*,5aS*,6R*,7S*,8aR*)-3,5a-dihydroxy-6-methyl-7-(allyldisulfanyl)tetrahydro-2H-difuro[3,2-b:2′,3′-c]furan-5(5aH)-one, respectively.

Foliogarlic trisulfanes A$_1$ (**4**) and A$_2$ (**5**) were isolated as yellow oil with positive specific rotations (**4**: $[\alpha]_D^{25}$ +124.6°

in MeOH) and negative specific rotations (**5**: $[\alpha]_D^{25}$ −119.8° in MeOH). In the ESIMS spectra of **4** and **5**, the same quasi-molecular ion peaks (**4** and **5**: [M+Na]$^+$) were observed at m/z 375. The molecular formulas (**4** and **5**: C$_{12}$H$_{16}$O$_6$S$_3$) were determined on the basis of HRESIMS peaks at [**4**: m/z 374.9998, **3**: m/z 374.0003 (calcd. 374.0001)], and the ^{13}C NMR data. On the basis of the detailed analysis of the ^{1}H and ^{13}C NMR, 2D-NMR (DQF COSY, HMBC, NOESY) spectrum of **4** and **5**, the relative structures of tetrahydro-2H-difuro[3,2-b:2′,3′-c]furan-5(5aH)-one skeleton on **4** and **5** were found to be the same as those of **1** and **3**, respectively (**Tables 3**, **4** and **Figure 3**). Next, the ^{1}H and ^{13}C NMR spectrum at the side chain showed signals corresponding to an allyl group, as well as those of compounds **1**–**3**. The determination of the sulfur linkage was confirmed by the HRMS spectrum. Namely, the pseudomolecular formula was established as C$_{12}$H$_{16}$O$_6$S$_3$Na. Therefore, compounds **4** and **5** were found to have a trisulfane bridge. Finally, the relative configurations of **4** and **5** were characterized by the comparison of ^{13}C NMR data with **1** and **3** and the NOESY experiments. The ^{13}C NMR signals of **4** and **5** were superimposable on those of **1** and **3**. All the evidences supported that the chemical structures of **4** and **5** were (3S*,3aR*,5aS*,6R*,7R*,8aR*)-3,5a-dihydroxy-6-methyl-7-(allyltrisulfanyl)tetrahydro-2H-difuro[3,2-b:2′,3′-c]furan-5(5aH)-one and (3S*,3aR*,5aS*,6R*,7S*,8aR*)-3,5a-dihydroxy-6-methyl-7-(allyltrisulfanyl)tetrahydro-2H-difuro[3,2-b:2′,3′-c]furan-5(5aH)-one, respectively.

The biological synthetic pathways for compounds **1**–**5** are presumed. At first, allicin is generated from alliin by alliinase when plant tissues of A. sativum are broken. Next, allicin is decomposed into intermediates (a), (b), and (c) by hydrolysis and is reconstructed to disulfane (d) and trisulfane (e) (Jacob, 2006). Finally, the structure of tetrahydro-2H-difuro[3,2-b:2′,3′-c]furan-5(5aH)-one
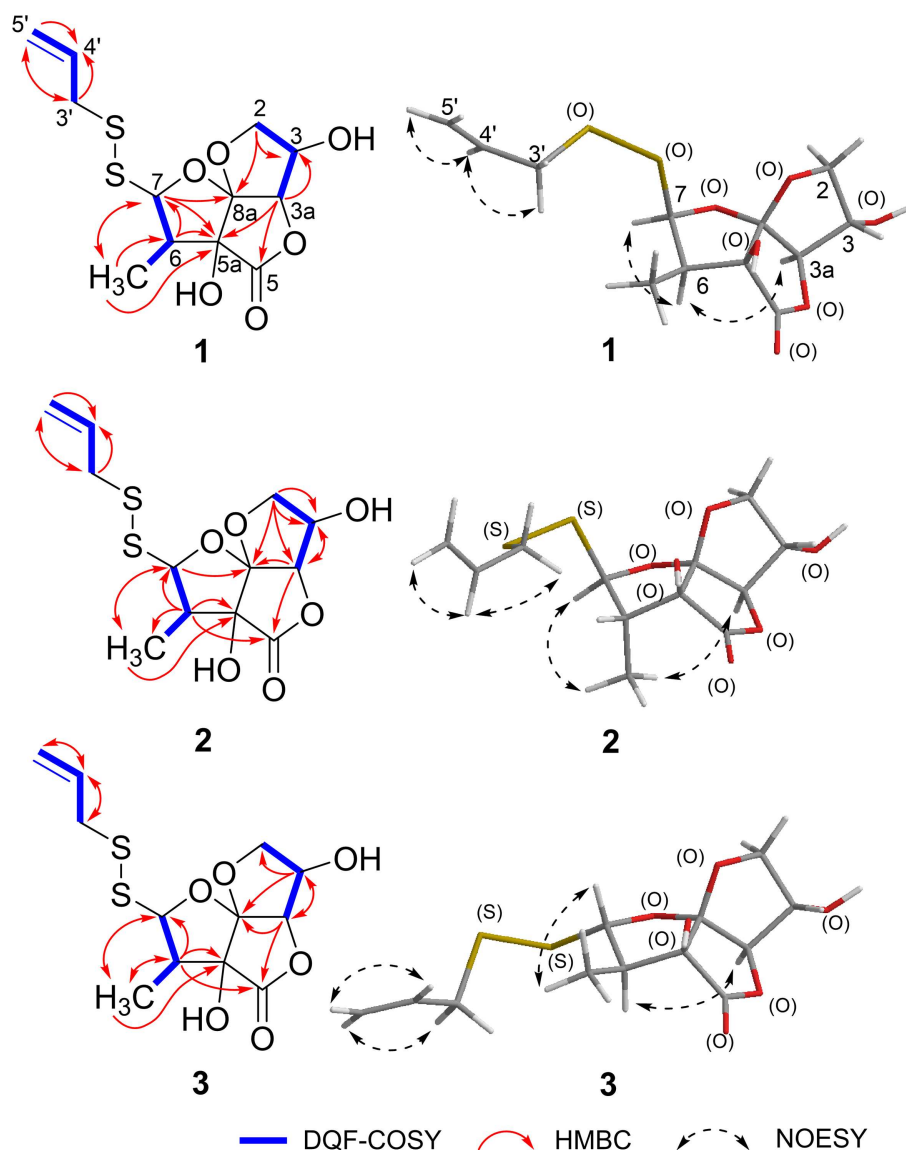
FIGURE 2 | Key-correlations of 2D NMR and NOESY of **1–3**.

skeleton is formed from semidehydroascorbate by cyclization and sulfane formation with the intermediates d and e. Consequently, compounds **1–5** were presumed to be obtained (**Figure 4**).

CONCLUSION

Five new organosulfur compounds, foliogarlic disulfanes **1–3** and foliogarlic trisulfanes **4** and **5**, were isolated from the leaves of *A. sativum*. These compounds **1–5** have a tetrahydro-2*H*-difuro[3,2-*b*:2′,3′-*c*]furan-5(5a*H*)-one skeleton with methyl group at 6-position and 2-propenyl disulfane or 2-propenyl trisulfane group at 7-position. Particularly, foliogarlic trisulfanes **4** and **5** with a trisulfane moiety are a

rare compound derived from medicinal plants. The biological effects of these cyclic organosulfur compounds should be studied further.

EXPERIMENTAL

General

The following instruments were used to obtain physical data: specific rotations, a Horiba (Kyoto, Japan) SEPA-300 digital polarimeter ($l = 5$ cm); IR spectra, JASCO (Tokyo, Japan) FT/IR-4600 Fourier Transform Infrared Spectrometer; ESIMS, Agilent Technologies (CA, US) Quadrupole LC/MS 6130; HRESIMS, SHIMADZU LCMS-IT-TOF; ^{1}H NMR spectra, JEOL (Tokyo, Japan) JNM-LA 500 (500 MHz) spectrometer; ^{13}C-NMR spectra,

TABLE 2 | ^{1}H NMR and ^{13}C NMR data of **3**.

Position	3			
	δ_H (J, Hz)^a	δ_C^{a}	δ_H (J, Hz)^b	δ_C^{b}
2	4.04 (dd, J = 4.5, 10.0)	75.9	α 4.11 (dd, J = 4.1, 10.3)	75.4
	4.07 (dd, J = 3.0, 10.0)		β 4.27 (dd, J = 1.4, 10.3)	
3	4.29 (m)	74.7	4.48 (m)	73.9
3a	4.75 (s-like)	89.9	4.85 (s-like)	87.5
5		174.9		172.2
5a		80.0		78.4
6	2.69 (m)	47.9	2.71 (m)	46.5
7	5.11 (d, J = 10.0)	96.3	5.16 (d, J = 9.6)	95.5
8a		119.1		117.2
3′	3.46 (d, J = 7.5)	44.1	3.44 (d, J = 7.6)	43.2
4′	5.85 (m)	134.3	5.85 (m)	132.5
5′	5.14 (d like, J = 10.0)	119.4	5.19 (d like, J = 10.3)	119.5
	5.20 (d like, J = 16.5)		5.22 (d like, J = 15.8)	
6-CH$_3$	1.09 (d, J = 6.5)	8.4	1.19 (d, J = 6.8)	7.9

^{a}^{1}H NMR, ^{13}C NMR (CD$_3$OD, 500 MHz).
^{b}^{1}H NMR, ^{13}C NMR (CDCl$_3$, 600 NMR).

TABLE 3 | ^{1}H NMR and ^{13}C NMR data of **4**.

Position	4			
	δ_H (J, Hz)^a	δ_C^{a}	δ_H (J, Hz)^b	δ_C^{b}
2	4.07 (m)	75.7	4.28 (m)	75.0
3	4.26 (m)	75.0	4.42 (m)	73.9
3a	4.66 (d, J = 1.5)	90.6	4.68 (s-like)	88.5
5		175.1		170.2
5a		79.5		78.0
6	2.97 (m)	48.0	2.83 (m)	47.0
7	5.68 (d, J = 7.0)	102.3	5.71 (d, J = 6.9)	99.5
8a		119.1		119.0
3′	3.59 (dd, J = 6.5, 13.0)	42.3	3.49 (m)	42.6
	3.63 (dd, J = 7.5, 13.0)			
4′	5.86 (m)	134.3	5.86 (m)	132.5
5′	5.17 (d-like, J = 10.0)	119.5	5.16 (d-like, J = 9.6)	119.6
	5.22 (d-like, J = 17.0)		5.21 (J = 16.5)	
6-CH$_3$	1.16 (d, J = 7.0)	9.2	1.28 (d, J = 6.9)	8.6

^{a}^{1}H NMR, ^{13}C NMR (CD$_3$OD, 500 MHz).
^{b}^{1}H NMR, ^{13}C NMR (CDCl$_3$, 600 NMR).

JEOL JNM-LA 500 (125 MHz) spectrometer; NOESY spectra, JNM-ECA 600 (600 MHz) spectrometer; HPLC, a Shimadzu (Kyoto, Japan) SPD-20AVP UV-VIS detector. YMC-triart C18 (250 × 4.6 mm i.d. and 250 × 10 mm i.d.) and YMC-triart PFP (250 × 4.6 mm i.d. and 250 × 10 mm i.d.) columns were used for analytical and preparative purposes. The following experimental materials were used for chromatography: normal-phase silica gel column chromatography, silica gel BW-200 (Fuji Silysia Chemical, Ltd. (Aichi, Japan), 150–350 mesh); reversed-phase silica gel column chromatography, Cosmosil 140C$_{18}$-OPN

TABLE 4 | ^{1}H NMR and ^{13}C NMR data of **5**.

Position	5	
	δ_H (J, Hz)^a	δ_C^{a}
2	4.02 (m)	75.6
3	4.25 (m)	75.1
3a	4.71 (d, J = 1.5)	90.2
5		175.0
5a		80.1
6	2.63 (m)	48.2
7	5.23 (d, J = 9.5)	96.6
8a		118.8
3′	3.56 (m)	42.7
4′	5.82 (m)	134.0
5′	5.15 (d like, J = 10.0)	119.9
	5.21 (d like, J = 16.5)	
6-CH$_3$	1.11 (d, J = 6.5)	8.7

^{a}^{1}H NMR, ^{13}C NMR (CD$_3$OD, 500 MHz).

[Nacalai Tesque (Kyoto, Japan)], TLC, precoated TLC plates with silica gel 60F$_{254}$ [Merck (NJ, US), 0.25 mm] (ordinary phase), and silica gel RP-18 F$_{254S}$ (Merck, 0.25 mm) (reversed phase); reversed-phase HPTLC, precoated TLC plates with silica gel RP-18 WF$_{254S}$. Detection was achieved by spraying with 1% Ce (SO$_4$) 2–10% aqueous H$_2$SO$_4$ followed by heating.

Plant Material

Fresh leaves of *A. sativum* cultivated in Kochi prefecture, Japan, were obtained as commercial products purchased from Japan Agricultural Cooperatives (JA) farmers' market (Kochi, Japan) in April 2017. The plants were identified by the authors (H.M. and S.N.).

Extraction and Isolation

The fresh leaves of *A. sativum* (15.2 kg) were chopped and mixed with water, and then acetone was added to the mixture to be 80% acetone solution. The mixture was soaked for 4 days (96 h) at room temperature. Evaporation of the filtrate under reduced pressure provided acetone extract (1,500.37 g, 9.87%). The extract was partitioned between EtOAc and H$_2$O (1:1, vol/vol) to obtain EtOAc fraction (41.98 g, 0.27%) and aqueous phase. The EtOAc-soluble fraction (41.98 g) was subjected to normal phase silica gel column chromatography [1,260 g, CHCl$_3$-MeOH (1:0→ 100:1→ 50:1→ 30:1→ 10:1→ 0:1, vol/vol)] to give nine fractions {Fr.1 (1,471.6 mg), Fr.2 (715.5 mg), Fr.3 (7,193.2 mg), Fr.4 (8,339.2 mg), Fr.5 (4,085.8 mg), Fr.6 (1,334.9 mg), Fr.7 (4,367.0 mg), Fr.8 (617.7 mg), Fr.9 (5,841.2 mg)}. r. 5 (4,085.8 mg) was further separated by reversed-phase silica gel column chromatography [200 g, MeOH-H$_2$O (2:8→ 4:6→ 6:4→ 8:2→ 1:0, vol/vol)] to give 13 fractions {Fr.5-1 (52.3 mg), Fr.5-2 (21.0 mg), Fr.5-3 (31.0 mg), Fr.5-4 (19.1 mg), Fr.5-5 (84.4 mg), Fr.5-6 (281.7 mg), Fr.5-7 (43.5 mg), Fr.5-8 (26.3 mg), Fr.5-9 (67.9 mg), Fr.5-10 (482.9 mg), Fr.5-11 (2,637.7 mg), Fr.5-12 (178.7 mg), Fr.5-13 (16.9 mg)}. Fr.5-5 (84.4 mg) was

FIGURE 3 | Key-correlations of 2D NMR and NOESY of **4** and **5**.
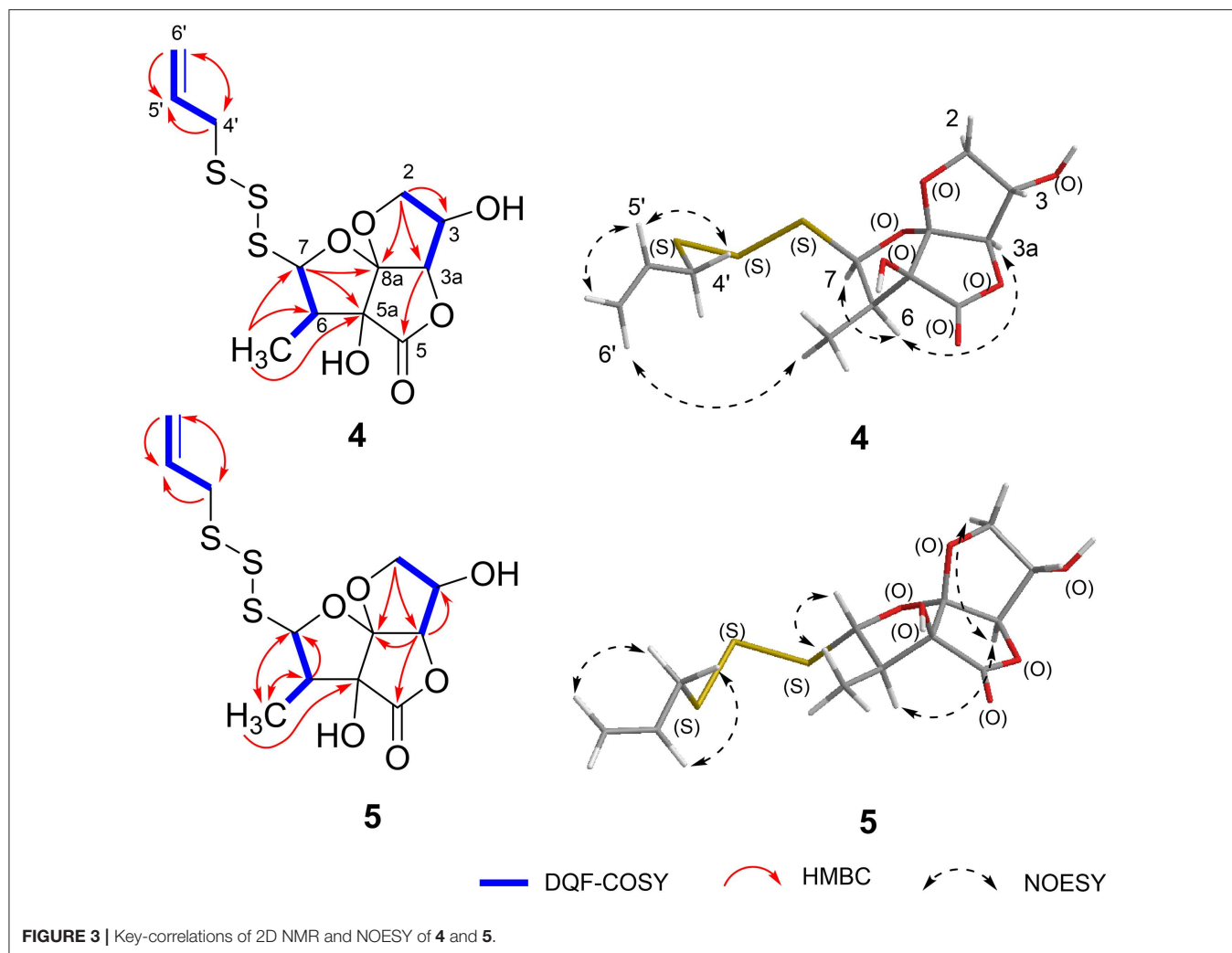
purified by HPLC {mobile phase: MeOH-H$_2$O (35:65, vol/vol) [YMC-triart PFP (250 × 10 mm i.d.)]} to give **1** (6.0 mg) and **2** (16.3 mg). Fr.5-6 (281.7 mg) was purified by HPLC {mobile phase: MeOH-H$_2$O (50:50, vol/vol) [YMC-triart C18 (250 × 10 mm i.d.)]} to give **1** (14.6 mg), **2** (16.0 mg), **4** (24.2 mg), and **5** (12.3 mg). Fr.5-6-5 (37.1 mg) was purified by HPLC {mobile phase: MeOH-H$_2$O (45:55, vol/vol) [YMC-triart C18 (250 × 10 mm i.d.)]} to give **3** (14.7 mg) and **4** (4.5 mg).

Foliogarlic Disulfane A$_1$ (1)
Yellow oil; $[\alpha]_D^{25}$ +160.9 (MeOH); HRESIMS: calcd for C$_{12}$H$_{16}$O$_6$S$_2$Na (M+Na)$^+$: 343.0281, found: 343.0282; IR(ATR): 3,400, 2,975, 1,782 cm^{-1}; ^{1}H NMR (CD$_3$OD), ^{13}C NMR (CD$_3$OD, 500 MHz): given in **Table 1**.

Foliogarlic Disulfane A$_2$ (2)
Yellow oil; $[\alpha]_D^{25}$ +139.0 (MeOH); HRESIMS: calcd for C$_{12}$H$_{16}$O$_6$S$_2$Na (M+Na)$^+$: 343.0281, found: 343.0277; IR(ATR): 3,400, 2,970, 1,785 cm^{-1}; ^{1}H NMR (CD$_3$OD, CDCl$_3$), ^{13}C NMR (CD$_3$OD, CDCl$_3$): given in **Table 1**.

Foliogarlic Disulfane A$_3$ (3)
Yellow oil; $[\alpha]_D^{25}$ −213.6 (MeOH); HRESIMS: calcd for C$_{12}$H$_{16}$O$_6$S$_2$Na (M+Na)$^+$: 343.0281, found: 343.0282; IR(ATR): 3,400, 2,981, 1,785 cm^{-1}; ^{1}H NMR (CD$_3$OD, CDCl$_3$), ^{13}C NMR (CD$_3$OD, CDCl$_3$): given in **Table 2**.

Foliogarlic Trisulfane A$_1$ (4)
Yellow oil; $[\alpha]_D^{25}$ +124.6 (MeOH); HRESIMS: calcd for C$_{12}$H$_{16}$O$_6$S$_3$Na (M+Na)$^+$: 375.0001, found: 374.9998; IR(ATR): 3,400, 2,975, 1,780 cm^{-1}; ^{1}H NMR (CD$_3$OD, CDCl$_3$), ^{13}C NMR (CD$_3$OD, CDCl$_3$): given in **Table 3**.

Foliogarlic Trisulfane A$_2$ (5)
Yellow oil; $[\alpha]_D^{25}$ −119.8 (MeOH); HRESIMS: calcd for C$_{12}$H$_{16}$O$_6$S$_3$Na (M+Na)$^+$: 375.0001, found: 375.0003; IR(ATR): 3,400, 2,931, 1,789 cm^{-1}; ^{1}H NMR (CD$_3$OD), ^{13}C NMR (CD$_3$OD): given in **Table 4**.
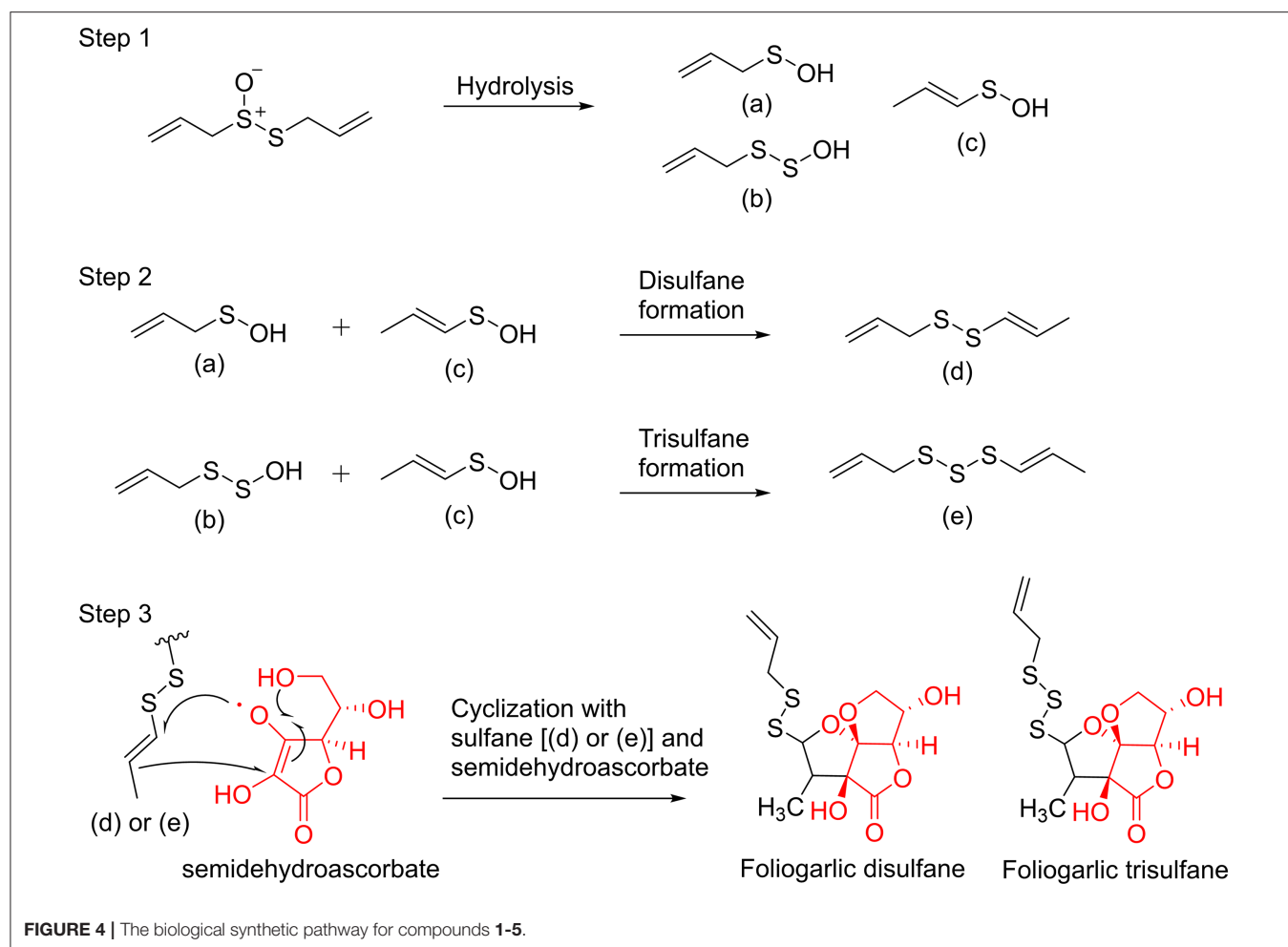
FIGURE 4 | The biological synthetic pathway for compounds **1-5**.

DATA AVAILABILITY STATEMENT

All datasets generated for this study are included in the article/**Supplementary Material**.

AUTHOR CONTRIBUTIONS

MF: isolation of constituents and Structure elucidation of new compounds. SeiN: Structure elucidation of new compounds and overall supervision in this study. HH and DN: isolation of constituents. SouN: Preparation of plant extracts and overall supervision in this study. TY: Structure elucidation of new compounds. HM: overall supervision in this study.

FUNDING

SUPPLEMENTARY MATERIAL

The Supplementary Material for this article can be found online at: https://www.frontiersin.org/articles/10.3389/fchem.2020.00282/full#supplementary-material

REFERENCES

Arditti, F. D., Rabinkov, A., Miron, T., Reisner, Y., Berrebi, A., Wilcheck, M., et al. (2005). Apoptotic killing of B-chronic lymphocytic leukemia tumor cells by allicin generated *in situ* using a rituximab-alliinase conjugate. *Mol. Cancer Ther.* 4, 325–331.

Block, E., Ahmad, S., Jain, M. K., Crecely, R. W., Apitz-Castro, R., and Cruz, M. R. (1984). The chemistry of alkyl thiosulfate esters. 8. (E,Z)-Ajoene: a

potent antithrombotic agent from garlic. *J. Am. Chem. Soc.* 106, 8295–8296. doi: 10.1021/ja00338a049

Briggs, W. H., Xiao, H., Parkin, K. L., Shen, C., and Goldman, I. L. (2000). Differential inhibition of human platelet aggregation by selected allium thiosulfinates. *J. Agric. Food Chem.* 48, 5731–5735. doi: 10.1021/jf0004412

Cañizares, P., Gracia, I., Gómez, L. A., Argila, C. M., Boixeda, D., García, A., et al. (2004). Allyl-thiosulfinates, the bacteriostatic compounds of garlic against *Helicobacter pylori*. *Biotechnol. Prog.* 20, 397–401. doi: 10.1021/bp034143b

Cavallito, C. J., and Bailey, J. H. (1944). Allicin, the antibacterial principle of *Allium sativum*. I. isolation, physical properties and antibacterial action. *J. Am. Chem. Soc.* 66, 1950–1951. doi: 10.1021/ja01239a048

Cavallito, C. J., Buck, J. S., and Suter, C. M. (1944). Allicin, the antibacterial principle of *Allium sativum*. II. determination of the chemical structure. *J. Am. Chem. Soc.* 66, 1952–1954. doi: 10.1021/ja01239a049

Ellmore, G. S., and Feldberg, R. S. (1994). Alliin lyase localization in bundle sheaths of the garlic clove (*Allium sativum*). *Am. J. Bot.* 81, 89–94. doi: 10.1002/j.1537-2197.1994.tb15413.x

Fritsch, M. R., and Keusgen, M. (2006). Occurrence and taxonomic significance of cysteine sulphoxides in the genus *Allium* L. (alliaceae). *Phytochemistry* 67, 1127–1135. doi: 10.1016/j.phytochem.2006.03.006

Fukaya, M., Nakamura, S., Kyoku, Y., Nakashima, S., Yoneda, T., and Matsuda, H. (2019b). Cyclic sulfur metabolites from *Allium schoenoprasum* var. *foliosum*. *Phytochem. Lett.* 29, 125–128. doi: 10.1016/j.phytol.2018.11.018

Fukaya, M., Nakamura, S., Nakagawa, R., Kinka, M., Nakashima, S., and Matsuda, H. (2019a). Cyclic sulfur-containing compounds from *Allium fistulosum* 'Kujou'. *J. Nat. Med.* 73, 397–403. doi: 10.1007/s11418-018-1272-0

Fukaya, M., Nakamura, S., Nakagawa, R., Nakashima, S., Yamashita, M., and Matsuda, H. (2018). Rare sulfur-containing compounds, kujounins A_1 and A_2 and allium sulfoxide A_1, from *Allium fistulosum* 'Kujou'. *Org. Lett.* 20, 28–31. doi: 10.1021/acs.orglett.7b03234

Gebhardt, R., Beck, H., and Wagner, K. G. (1994). Inhibition of cholesterol biosynthesis by allicin and ajoene in rat hepatocytes and $HepG_2$ cells. *Biochim. Biophys. Acta Lipids Lipid. Metab.* 1213, 57–62. doi: 10.1016/0005-2760(94)90222-4

Jacob, C. (2006). A scent of therapy: pharmacological implications of natural products containing redox-active sulfur atoms. *Nat. Prod. Rep.* 23, 851–863. doi: 10.1039/b609523m

Kuo, M. C., Chien, M., and Ho, C. T. (1990). Novel polysulfides identified in the volatile components from welsh onions (*Allium fistulosum* L. var. maichuon)

and scallions (*Allium fistulosum* L. var. *caespitosum*). *J. Agric. Food Chem.* 38, 1378–1381. doi: 10.1021/jf00096a017

Nohara, T., Fujiwara, Y., Ikeda, T., Murakami, K., Ono, M., Nakano, D., et al. (2013). Cyclic sulfoxides garlicnins B_2, B_3, B_4, C_2, and C_3 from *Allium sativum*. *Chem. Pharm. Bull.* 61, 695–699. doi: 10.1248/cpb.c13-00082

Nohara, T., Fujiwara, Y., Ikeda, T., Yamaguchi, K., Manabe, H., Murakami, K., et al. (2014). Acyclic sulfides, garlicnins L-1–L-4, E, and F, from *Allium sativum*. *Chem. Pharm. Bull.* 62, 477–482. doi: 10.1248/cpb.c14-00003

Nohara, T., Kitaya, Y., Sakamoto, T., Manabe, H., Ono, M., Ikeda, T., et al. (2012). Garlicnins B_1, C_1, and D, from the fraction regulating macrophage activation of *Allium sativum*. *Chem. Pharm. Bull.* 60, 747–751. doi: 10.1248/cpb.60.747

Oommen, S., Anto, R. J., Srinivas, G., and Karunagaran, D. (2004). Allicin (from garlic) induces caspase-mediated apoptosis in cancer cells. *Eur. J. Pharmacol.* 485, 97–103. doi: 10.1016/j.ejphar.2003.11.059

Rose, P., Whiteman, M., Moore, P. K., and Zhu, Y. Z. (2005). Bioactive S-alk(en)yl cysteine sulfoxide metabolites in the genus allium: the chemistry of potential therapeutic agents. *Nat. Prod. Rep.* 22, 351–368. doi: 10.1039/b417639c

Theisen, C. (2001). What ever happened to looking back 10 years. *J. Natl. Cancer Inst.* 93, 1049–1050. doi: 10.1093/jnci/93.14.1049

Advantages of publishing in Frontiers

OPEN ACCESS
Articles are free to read
for greatest visibility
and readership

FAST PUBLICATION
Around 90 days
from submission
to decision

HIGH QUALITY PEER-REVIEW
Rigorous, collaborative,
and constructive
peer-review

TRANSPARENT PEER-REVIEW
Editors and reviewers
acknowledged by name
on published articles

Frontiers
Avenue du Tribunal-Fédéral 34
1005 Lausanne | Switzerland

Visit us: www.frontiersin.org
Contact us: info@frontiersin.org | +41 21 510 17 00

REPRODUCIBILITY OF RESEARCH
Support open data
and methods to enhance
research reproducibility

DIGITAL PUBLISHING
Articles designed
for optimal readership
across devices

FOLLOW US
@frontiersin

IMPACT METRICS
Advanced article metrics
track visibility across
digital media

EXTENSIVE PROMOTION
Marketing
and promotion
of impactful research

LOOP RESEARCH NETWORK
Our network
increases your
article's readership